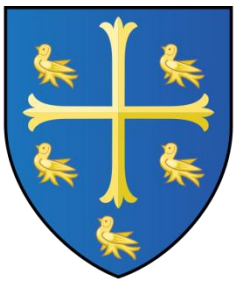
EXPLORING THE REACTIVITY PATTERNS OF CATIONIC AND NEUTRAL RHODIUM *BIS*-PHOSPHINE SPECIES WITH AMINE-BORANES

Laura J. Sewell

A thesis submitted in partial fulfilment of the requirements for the degree of Doctor of Philosophy at the University of Oxford





University College

February 2013

The work presented in this thesis was carried out between October 2009 and February 2013 under the supervision of Professor Andrew S. Weller. All of the work is my own, unless otherwise stated and has not been submitted previously for any other degree at this, or any other, university.

Laura J. Sewell

February 2013

ACKNOWLEDGEMENTS

Firstly, I would like to thank Prof. Andrew S. Weller for giving me the opportunity to study at Oxford, and for his continuous support, motivation and advice throughout my project. His sense of humour, abundance of lycra and the many "interesting" stories will not be forgotten.

To the various incarnations of the Weller group, thanks (and massive hugs obviously) for making the past three and a half years excellent fun. I shall miss your company, the various UC trips (but not the disgusting drinks), paella/fondue/pizza nights, tea breaks, Christmas parties, research day out, what NOT to put in a Schlenk, Phil Collins Fridays and Sash-athons.

To the post-docs who've passed through the Weller group over the past 3 years: Dr. Adrian B. Chaplin, Dr. Miguel A. Huertos, Dr. Rowan A. Young and Dr. Thomas N. Hooper, thanks for all your help and advice. A special thanks to ABC for inventing some truly disgusting pink drinks, fondue, partiality for tight black clothing, crystal structure solving and being the Weller group's I.C.S. To Miguel/Manuel/Yes Man, thanks for being an excellent lab dad and more recently for your time spent solving my crystal structures.

To my fellow DPhils, Maeo, Bex, Indreka, Sebby, Hevz and Amit, you have truly made the experience for me. I could not have asked for a better bunch of fellow DPhils for entertainment in/out of the lab. Specifically: to Maeo/Dr. Love (Dr. Romaeo Dallanegra) thanks for constantly being so helpful (generally to the detriment of your own work), always smelling nice, having ridiculously soft earlobes and teaching us all how to moan. To Bex (Dr. Rebekah J. Pawley) thanks for being an awesome housemate, cooking yummy food, being a fellow fan of the ESC and enthusiastic Maeo molester despite the never ending sporting commitments. To the Pump Man/Dunkirk/Kendrick/Indreka (Indrek Pernik) thank you (I think) for expanding my knowledge on speedos, saunas and Estonian "salad". Thanks also for being an entertaining desk buddy and showing the group how to lunge. To Sebby Webby/Seb^{n} (Sebastian D. Pike) thanks for taking over Maeo's role as the group's grumpy old man (with hair to match), providing hugs on request and cooking scrummy pizzas (despite being very busy). To Hevz (Heather C. Johnson), thanks for being a brilliant inaugural

Part II (Andy matched us well!), showing us all how to rant, drunken striding and for excellent Daily Mail and dog chats – I hope "our Max" is okay. But please remember you *really* don't have to drink that Hevz.

A huge thanks to the many Part IIs who have been a big part of the Weller group during my time. Despite changing each year you've all fitted in/adapted to the lab and bought your own unique(!) contributions: CJ (queen of the T.C.), Woolfy (spectacular shapes), Will (revealing a little too much), Georgie (shrieking), Timmy (not so subtle updates on your night-time activities). To this year's cohort: Becky, Mark and Rosie, thanks for providing entertainment during the much needed breaks from thesis writing. A special mention to the Mozzatron, my second Part II, for not being too disgusted by the lab (I tried to make sure it wasn't too vile), and for equalling mine and Hevz's love of dogs and the Daily Mail.

Thanks to the various CRL support staff especially Colin Sparrow (Mass Spectrometry), Alan Roper and Jude Nettleton (Workshop). Particular thanks must go to Dr. Nick Rees (NMR) for all his help with NMR and also for broadening my musical horizons!

To Prof. Guy C. Lloyd-Jones (University of Bristol) thank you for all the advice and help with Chapter 3, and in particular for doing the kinetic simulations. Also, thanks to Prof. Stuart A. Macgregor (Heriot-Watt University) for the initial computational results reported in Chapter 2.

Finally, a huge thanks to all my friends and family for their support.

ABBREVIATIONS

Å	Angstrom (1×10^{-10} metres)
AB	ammonia-borane
atm	atmospheres
$[BAr^{F}{}_4]^-$	$[B\{3,5\text{-}C_6H_3(CF_3)_2\}_4]^-$
$[BAr^{Cl}{}_4]^-$	$[B\{3,5\text{-}C_6H_3Cl_2\}_4]^-$
Bu	butyl
calc.	calculated
cat.	catalyst
COD	cyclooctadiene
COE	cyclooctene
Cp	cyclopentadienyl
Cp*	(pentamethyl)-cyclopentadienyl
Cy	cyclohexyl
δ	chemical shift
ΔG	change in Gibb's free energy
ΔH	change in enthalpy
ΔS	change in entropy
DCM	dichloromethane
dcype	1,2-*bis*(dicyclohexylphosphino)ethane
DIMER	$[H_2BNMe_2]_2$
Dipp	2,6-di-isopropylphenyl
DMAB	dimethylamine-borane
ESI-MS	Electrospray Ionisation Mass Spectrometry
Et	ethyl
FLP	frustrated Lewis pair
HBCat	catecholborane
Hz	Hertz
IMes	*N,N-bis*(2,4,6-trimethylphenyl)imidazol-2-ylidene
IPE	isotopic perturbation of equilibrium
IPR	isotopic perturbation of resonance
IR	infrared

J	coupling constant
K_{eq}	equilibrium constant
LUMO	lowest unoccupied molecular orbital
M	mol dm^{-3}
Me	methyl
Mes	mesityl
MMAB	monomethylamine-borane
MON	$H_2B{=}NMe_2$
m/z	mass to charge ratio
NBA	norbornane
NBD	norbornadiene
NHC	*N*-heterocyclic carbene
NMR	Nuclear Magnetic Resonance
OLIG	$H_3B{\cdot}NMe_2BH_2{\cdot}NMe_2H$
OTf	triflate (trifluoromethanesulfonate, $CF_3SO_3^-$)
Ph	phenyl
Phephos	1,2-*bis*(diphenylphosphino)-1-phenylethane
POCOP	κ^3-1,3-$(OP^tBu_2)_2C_6H_3$
PONOP	2,6-$(^tBu_2PO)_2C_5H_3N$
ppm	parts per million
Pr	propyl
RDS	rate determining step
σ-CAM	sigma Complex Assisted Metathesis
solv	solvent
$t_{½}$	half life
TBE	*tert*-butylethylene
TEM	Transmission Electron Microscopy
THF	tetrahydrofuran
TMAB	trimethylamine-borane
TOF	turnover frequency
TON	turnover number
UV	ultraviolet

ABSTRACT

This thesis details the synthesis of novel Rh(I) and Rh(III) *bis*-phosphine fragments, and their use, along with other known rhodium species, to investigate the reactivity of amine-boranes, with a particular focus on the dehydrocoupling of the secondary amine-borane $H_3B{\cdot}NMe_2H$ (DMAB).

Chapter 2 utilises the new mixed phosphine, $P^tBu^iBu_2$, to investigate the role of the phosphine with regard to the corresponding low-coordinate organometallic species isolated. Their coordination and reactivity with amine-boranes is studied, leading to the development of a mechanism for an alkene hydroboration catalyst that employs $H_3B{\cdot}NMe_3$ (TMAB). The final section of the chapter studies several fluxional processes pertinent to rhodium and iridium complexes of the model amine-borane TMAB using H/D exchange and low temperature NMR experiments.

In Chapter 3, the mechanism of dehydrocoupling of DMAB is investigated in detail, employing catalysts based on the cationic *bis*-phosphine Rh fragment, $\{Rh(PCy_3)_2L_n\}^+$. A series of stoichiometric and catalytic reactions are probed using NMR spectroscopy and mass spectrometry, revealing a complex mechanistic landscape. Subtleties include: the product of dehydrocoupling, $[H_2BNMe_2]_2$, acting in an autocatalytic role; and parallel dehydrogenation of DMAB by a neutral catalyst present in a low but constant concentration. The mechanism was additionally interrogated through kinetic simulations conducted by Prof. Guy C. Lloyd-Jones (University of Bristol). From this, a generic mechanistic scheme has been suggested, aspects of which can be applied to transition metal and main group systems reported to catalyse the dehydrocoupling of DMAB.

The final chapter moves on from cationic rhodium fragments to investigate the reactivity of the neutral rhodium species, $Rh(H)_2(PCy_3)_2Cl$ and $[Rh(PCy_3)_2Cl]_2$, with amine-boranes. The mechanism by which $Rh(H)_2(PCy_3)_2Cl$ catalyses the dehydrogenation of DMAB has been investigated through initial rate and H/D exchange experiments, leading to the proposal of a reaction scheme. Additionally, the formation and characterisation of a base-stabilised boryl species has been reported resulting from the reactivity of an amino-borane with $[Rh(PCy_3)_2Cl]_2$.

CONTENTS

Declaration i

Acknowledgements ii

Abbreviations iv

Abstract vi

Contents vii

1 Introduction 1

1.1 Low-coordinate complexes 1

1.2 Latent low-coordinate complexes 2

1.2.1 Solvent interactions 3

1.2.2 Anions interactions 4

1.2.3 σ-interactions 5

1.2.3.1 Dihydrogen σ-complexes 7

1.2.3.2 Borane σ-complexes 9

1.2.3.3 Alkane σ-complexes 12

1.2.3.4 Agostic interactions 15

1.3 B-H and C-H activation processes 16

1.3.1 C-H activation 17

1.3.1.1 Intramolecular C-H activation 18

1.3.2 B-H activation 21

1.3.2.1 Hydroboration 21

1.3.2.2 Hydrido-boryl compounds 24

1.4 Dehydrogenation and dehydrocoupling of amine-boranes 26

1.4.1 Introduction 26

1.4.2 Early examples of dehydrocoupling 29

1.4.3 Mechanistic studies 30

1.4.3.1 Heterogeneous *vs.* homogeneous dehydrocoupling 31

1.4.3.2 Amine- and amino-borane σ-complexes 33

1.4.3.3 Proposed mechanisms of dehydrocoupling (homogeneous) 41

1.5 Phosphine ligands 56

1.5.1 Structure and bonding 56

1.5.2 Electronic and steric properties 57
1.6 Summary 58
1.7 References 59
2 B-H and C-H Activation Processes 65
2.1 Introduction 65
2.2 Synthesis of a low-coordinate rhodium complex 65
2.2.1 Reactivity of **2-4** 74
2.2.1.1 Reactivity of **2-4** with TMAB 77
2.3 Hydroboration 81
2.3.1 Hydroboration by TMAB 81
2.3.2 Tandem hydroboration and dehydrogenation 93
2.3.3 Post functionalisation of linear diborazane, OLIG 95
2.4 Investigation of fluxional processes in amine-borane σ-complexes 97
2.4.1 B-H bridging/terminal exchange 99
2.4.2 M-H and B-H exchange 106
2.5 Conclusions 115
2.6 References 117
3 Mechanistic Insights into the Dehydrocoupling of DMAB using Cationic Rhodium Complexes 120
3.1 Introduction 120
3.2 Choice of catalyst system 121
3.3 Synthesis of new complexes and their reactivity 125
3.3.1 Reactivity with TMAB 125
3.3.2 Reactivity with DMAB (**A**) 132
3.3.3 Reactivity with linear diborazane (**B**) 136
3.3.4 Reactivity with cyclic dimer (**C**) 142
3.4 Catalytic activity 145
3.4.1 Open system 145
3.4.1.1 Dehydrocoupling of DMAB (**A**) 145
3.4.1.2 Dehydrocoupling of linear diborazane (**B**) 149
3.4.1.3 Dehydrocoupling in the presence of excess cyclic dimer (**C**) 150
3.4.2 Closed system 153
3.5 Kinetic simulations 157

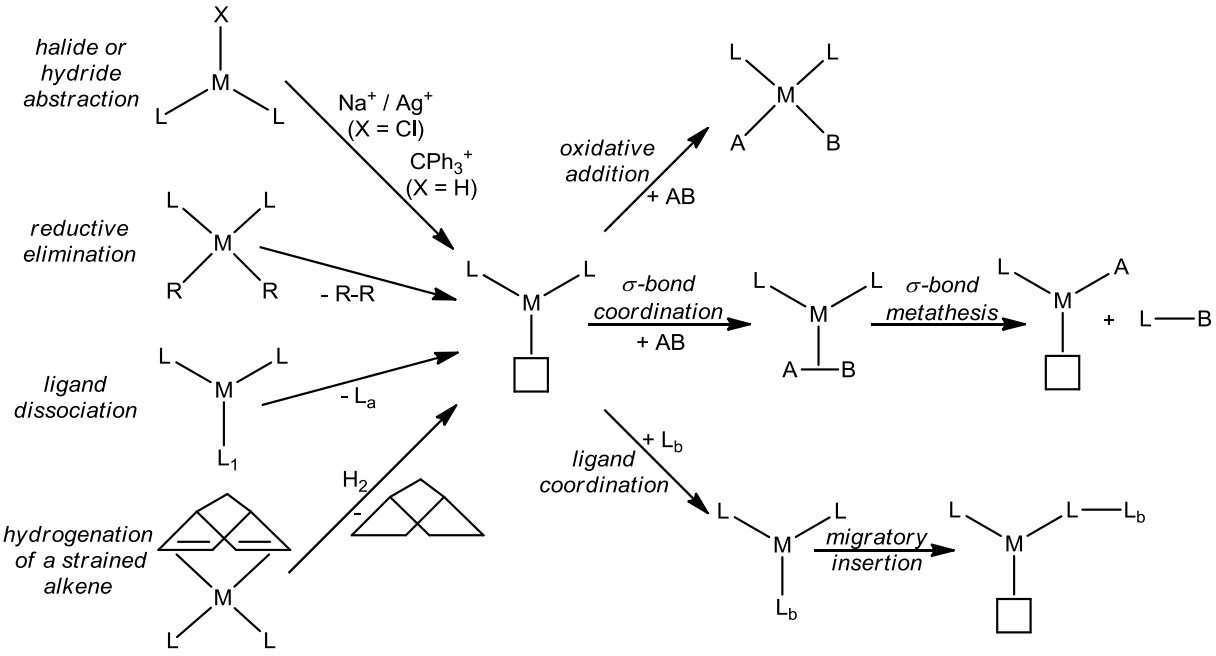
3.6 Second active catalyst 162
3.7 Mechanistic insights 163
3.8 Conclusions and future work 169
3.9 References 170
4 Investigating the Reactivity of Neutral Rhodium Complexes with Amine-Boranes 173
4.1 Introduction 173
4.2 Chloride-bridged adduct 174
4.2.1 Synthesis and characterisation 174
4.2.2 Reactivity 178
4.3 Neutral rhodium(III) complex 180
4.3.1 Catalysis 181
4.3.1.1 Catalytic dehydrocoupling of $H_3B{\cdot}NMe_2H$ (**A**) 181
4.3.1.2 Catalytic dehydrocoupling of $H_3B{\cdot}NMe_2BH_2{\cdot}NMe_2H$ (**B**) 188
4.3.1.3 Initial rates 189
4.3.1.4 Probing B-H and N-H activation 196
4.3.2 Proposed catalytic cycle 201
4.4 Neutral rhodium(I) complex 204
4.4.1 Catalysis 204
4.4.2 Stoichiometric reactivity 205
4.4.2.1 Reactivity with $H_3B{\cdot}NMe_2H$ (**A**) 206
4.4.2.2 Reactivity with TMAB 206
4.4.2.3 Reactivity with $H_2B{=}N^iPr_2$ 209
4.4.2.4 Reactivity with $H_3B{\cdot}NMe_2BH_2{\cdot}NMe_2H$ (**B**) 211
4.4.2.5 Reactivity with cyclic dimer (**C**) 213
4.5 Conclusions and future work 214
4.6 References 215
5 Experimental 218
5.1 Experimental techniques 218
5.1.1 General 218
5.1.2 Hydrogenation 218
5.1.3 Nuclear Magnetic Resonance spectroscopy 219
5.1.4 Mass Spectrometry 219

5.1.5 X-ray crystallography....219
5.2 Synthesis and characterisation....220
5.2.1 Starting materials....220
5.2.2 Synthesis of new complexes....220
5.3 Catalysis....236
5.3.1 Hydroboration....236
5.3.1.1 General method for TMAB....236
5.3.2 Dehydrocoupling....237
5.3.2.1 General method, open system....237
5.3.2.2 General method, sealed system (cationic)....237
5.3.2.3 General method, sealed system (neutral)....238
5.4 Kinetic simulations (Chapter 3)....238
5.4.1 General comments....238
5.4.2 Procedure....238
5.5 Computational (Chapter 2)....241
5.6 References....241
6 Appendices....242
6.1 Crystallographic data....242
6.2 Publications....244

1 Introduction

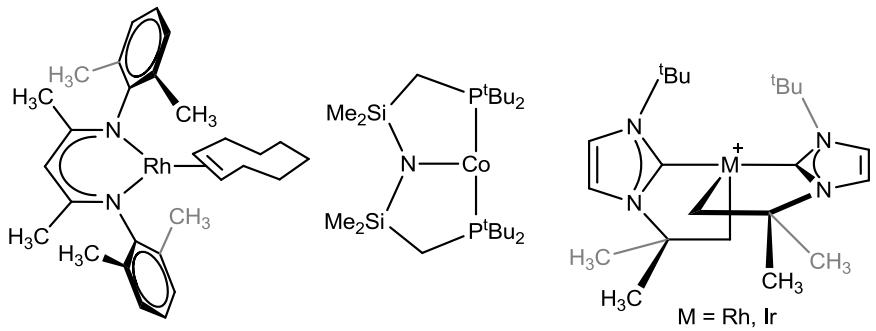
1.1 Low-coordinate complexes

Many catalytic processes require the generation and stabilisation of vacant coordination sites at metal centres.[1] These can be generated by a variety of routes, as outlined in Scheme 1.1. The isolation and characterisation of such electronically and coordinatively unsaturated metal complexes is thus of fundamental importance in helping to understand the mechanism of these processes and aid future catalyst design with respect to activity, selectivity and attenuating decomposition.[2, 3]



Scheme 1.1 Formation of and reactivity at low-coordinate metal centres.

They are by their nature, highly reactive, and as such only a relatively small number of well characterised examples of genuinely low-coordinate complexes of late transition metals exist.[4-12] Those that do all have several key features in common; sterically bulky ligands and, for cationic species, non-coordinating anions. Examples of low-coordinate group 9 complexes are shown in Figure 1.1.



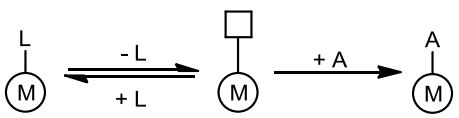
i-1 **i-2** **i-3**

Figure 1.1 Examples of genuinely low-coordinate complexes. Anions not shown.

Examples of low-coordinate complexes with weak stabilising interactions from counterions, solvent or σ-interactions[13] (both intra- and intermolecular) are much more common and shall be discussed in the next section.

1.2 Latent low-coordinate complexes

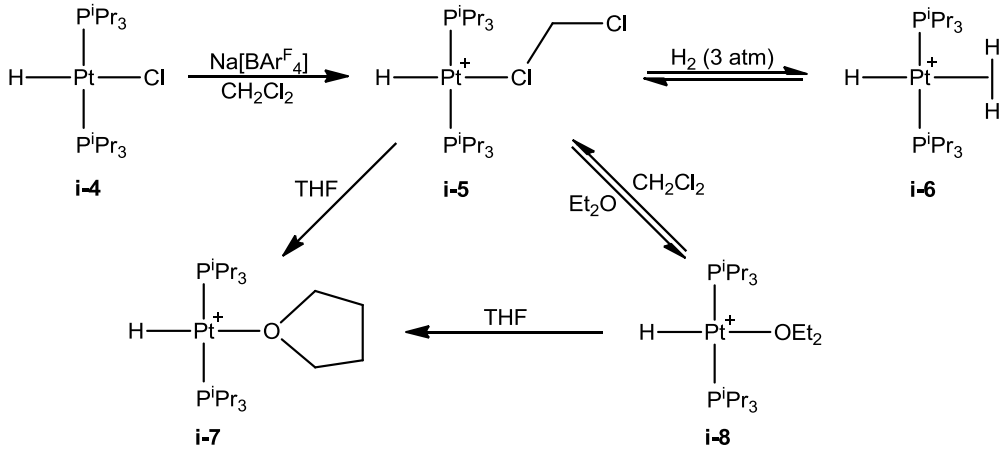
Complexes featuring weak stabilising interactions are termed "latent low-coordinate complexes". The interactions occupy vacant sites in the coordination sphere of the metal and stabilise the complex with respect to decomposition through the donation of electron density to the metal centre, often through a sigma bonding interaction. Well-characterised examples of latent low-coordinate complexes provide valuable insight into how molecules approach, coordinate and react at unsaturated metal centres. Utilisation of this understanding may allow catalyst design for reactions that are challenging, for example C-H activation. To function as a catalyst, the interactions need to be weak enough to allow dissociation and subsequent reactivity with the substrate (Scheme 1.2).



Scheme 1.2 Formation of a vacant site from a latent low-coordinate complex. L = weakly coordinating ligand, A = substrate.

1.2.1 Solvent interactions

The choice of solvent is extremely important; a strongly coordinating solvent will block the vacant site and prevent further reaction, whilst weakly bound solvents will stabilise the low-coordinate metal centre but can be easily displaced to allow further reaction.



Scheme 1.3 Et_2O and CH_2Cl_2 act as weakly coordinating solvents. $[BAr^F_4]^-$ anions not shown.

Kubas and co-workers reported the first fully characterised example of dichloromethane coordination to a transition metal complex in 1996 (Scheme 1.3).[14] Addition of $Na[BAr^F]_4$ (Ar^F = 3,5-$C_6H_3(CF_3)_2$) to $[Pt(P^iPr_3)_2(H)Cl]$ (**i-4**) in CH_2Cl_2 abstracts the chloride and generates $[Pt(P^iPr_3)_2(H)(CH_2Cl_2)][BAr^F_4]$ (**i-5**). Addition of H_2 or Et_2O to **i-5** forms $[Pt(P^iPr_3)_2(H)(\eta^2\text{-}H_2)][BAr^F_4]$ (**i-6**) or $[Pt(P^iPr_3)_2(H)(OEt_2)][BAr^F_4]$ (**i-8**) respectively, demonstrating the lability of the CH_2Cl_2 ligand. More strongly coordinating solvents such as THF can block the vacant site and prevent further reaction as demonstrated by the addition of THF to **i-5** and **i-8**, which leads to the formation of $[Pt(P^iPr_3)_2(H)(THF)][BAr^F_4]$ (**i-7**).

Arene solvents are also able to coordinate to transition metals through a variety of different binding modes (*e.g.* η^2, η^4 and η^6). However, they frequently form strong bonds which are not easily displaced.[2] Recent work from the Weller group using group 9 metals has shown that the introduction of electron withdrawing groups to the aryl ring (*e.g.* C_6H_5F and 1,2-$C_6H_4F_2$) reduces the strength of the interaction allowing the arene to act as a labile ligand.[15-18] Alkane solvents are generally non-coordinating, but many metal complexes, especially cationic ones, have poor solubility in such non polar mediums. The coordination of alkanes to metal centres will be discussed in more detail in Section 1.2.3.3.

1.2.2 Anion interactions

To allow the isolation of low-coordinate complexes, the correct anion with a low binding strength needs to be chosen. Weakly coordinating anions generally have the negative charge delocalised over a large area of non-nucleophilic and chemically robust species.[19] Borate-based anions have been one of the main areas of research into weakly coordinating anions. Early research focused on $[BPh_4]^-$, however this was prone to hydrolysis and strong coordination to metal centres.[20, 21] Fluorination of the aryl groups overcame these problems yielding $[B(C_6F_5)]^-$ and $[BAr^F_4]^-$ which are now commonly used in homogeneous catalysis.[22, 23] The CF_3 groups of $[BAr^F_4]^-$ frequently suffer from rotational disorder, which can potentially hamper the accurate structural determination of the resulting complexes in the solid state; the use of $[BAr^{Cl}_4]^-$ (Ar^{Cl} = 3,5-$C_6H_3Cl_2$) can be a solution to this problem.[24] Other commonly used weakly coordinating anions include $[Al\{OC(CF_3)_3\}_4]^-$ and [*closo*-$CB_{11}H_6Cl_6]^-$, and derivatives thereof.[25-28]

Despite the weakly coordinating nature of these anions, examples are known where $[BAr^F_4]^-$ is coordinated to a metal centre. Powell *et al.* have reported examples showing η^3 (**i-10**, Figure 1.2) and η^4 coordination to silver complexes and η^6 coordination to a rhodium cation, which were characterised by X-ray diffraction.[29] Recent examples of η^6 coordination to rhodium centres have been reported by the Weller group, characterised both by X-ray diffraction and NMR spectroscopy (**i-9**, Figure 1.2).[17, 30] Besides coordination, B-C bond cleavage by Pt,[31] Rh,[32] and most recently Au[33] complexes has also been noted.

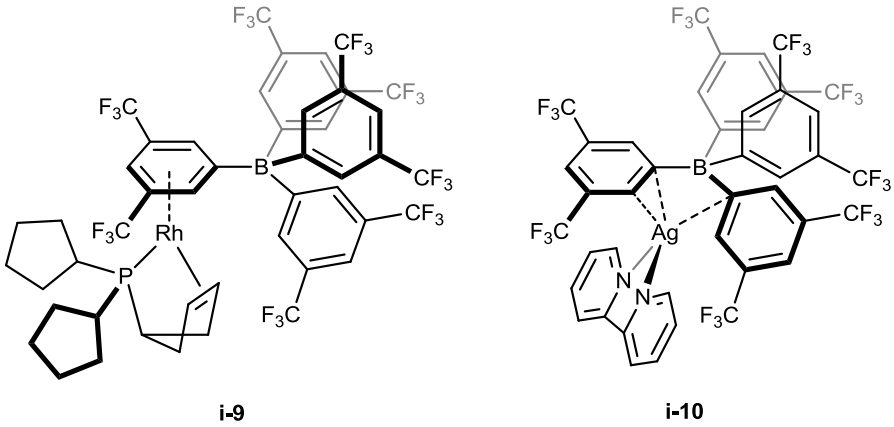


Figure 1.2 Coordination of $[BAr^F_4]^-$ to rhodium (η^6) (**i-9**) and silver (η^3) (**i-10**).

1.2.3 σ-interactions

In theory, favourable steric and electronic factors can allow a sigma interaction[13] to occur between any A-X bond and a metal centre, but examples are only known where A-X is H-H,[34] B-H,[35] Si-H,[36] Si-Si,[37] C-C,[38] C-H,[39] Ge-H[40] and Sn-H.[13] Such complexes, featuring a 3-centre 2-electron bond, have been studied extensively and many hundreds of examples now exist in the literature.

The bonding in σ-complexes relies on two principal interactions; a donation from the A-X bonding σ-orbital into an empty d-orbital on the metal, and backdonation from a

filled metal d-orbital into the antibonding A-X σ*-orbital (Figure 1.3). This bonding is analogous to the Dewar-Chatt-Duncanson model for metal-olefin π-coordination. The exact ratio of ligand donation to metal donation is dependent on the nature of the A-X bond, the metal and its ancillary ligands.[13]

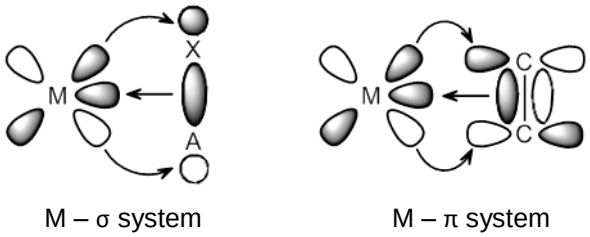


Figure 1.3 Comparison of M-A-X bonding in a σ-complex (left) with the Dewar-Chatt-Duncanson model for metal-alkene π-bonding (right).

No stable σ-complexes exist for d^0 metals illustrating the importance of the backdonation from the metal. However, a delicate balance between σ-donation and backdonation is needed to achieve an isolable σ-complex; increased backdonation into the A-X anti-bonding orbital can weaken the A-X bond to such an extent that oxidative cleavage occurs (Figure 1.4).[13]

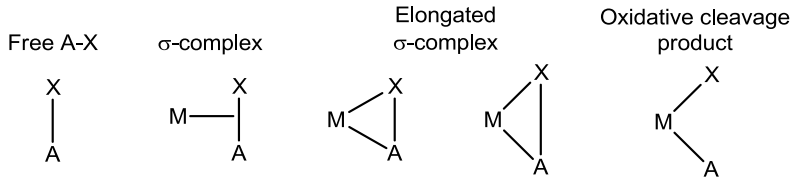
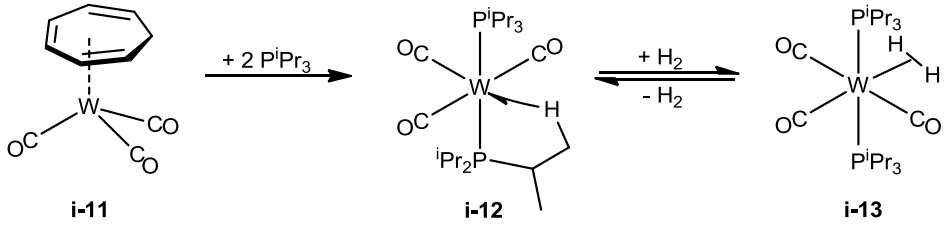


Figure 1.4 Coordination, elongation and oxidative cleavage of an A-X bond to a metal centre.

While σ-interactions can help to stabilise low-coordinate metal centres, they are also key in many catalytic processes. The coordination of a substrate to a metal centre *via* a σ-bond is thought to often be the first step in the catalytic cycle of many reactions prior to oxidative cleavage.[41] Examples of dihydrogen, borane, alkane and agostic σ-complexes are discussed in the following sections.

1.2.3.1 Dihydrogen σ-complexes

The simplest type of σ-interaction is a metal-dihydrogen complex. In 1984 Kubas *et al.* reported the first examples of isolable transition metal complexes containing a dihydrogen ligand, $[M(\eta^2\text{-}H_2)(PR_3)_2(CO)_3]$ (M = Mo, W; PR_3 = P^iPr_3, PCy_3).[34] $[W(\eta^2\text{-}H_2)(P^iPr_3)_2(CO)_3]$ (**i-13**) was obtained by the reversible addition of hydrogen to $[W(P^iPr_3)_2(CO)_3L]$ (L = agostic interaction) (**i-12**) (Scheme 1.4). Many other examples are now known.[13, 42-44]



Scheme 1.4 Formation of $[W(\eta^2\text{-}H_2)(P^iPr_3)_2(CO)_3]$ (**i-13**).

Backdonation into the hydrogen antibonding orbital results in the weakening of the dihydrogen bond. This causes a lengthening of the dihydrogen bond compared with that observed in free dihydrogen (0.74 Å) (Figure 1.5). Extensive backdonation results in oxidative cleavage of the dihydrogen ligand to form a metal dihydride.

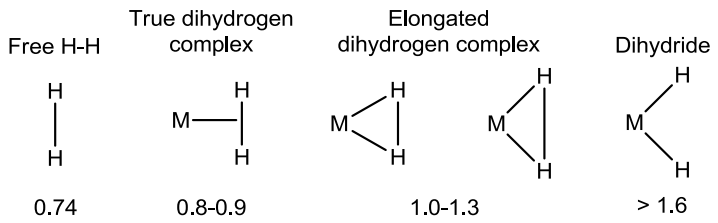


Figure 1.5 Elongation and cleavage of an H-H bond by increased backdonation from the metal. H-H bond lengths in Å.

Down a triad in the period table, there is a tendency to go from a dihydrogen complex to a classical dihydride as demonstrated by $[M(H)_2(PR_3)_3(\eta^2\text{-}H_2)]$ (M = Fe, PR_3 = $PEtPh_2$, PH_3, **i-14**; M = Ru, PR_3 = PPh_3, PH_3, **i-15**) and $[Os(H)_4(PR_3)_2]$ (PR_3 = PPh_3, PH_3,

PMe_2Ph, **i-16**).[2, 45-47] This is further shown by the report of the rhodium(III) hydride/dihydrogen complex $[Rh(\eta^5\text{-}C_5Me_5)(PMe_3)(H)(\eta^2\text{-}H_2)][BAr^F{}_4]$ (**i-17**),[48] while its iridium analogue $[Ir(\eta^5\text{-}C_5Me_5)(PMe_3)(H)_3][BF_4]$ (**i-18**) is an Ir(V) trihydride complex.[49] These examples can be rationalised by the increased radial extension of the orbitals down a triad giving more effective overlap with the σ*-antibonding orbital leading to oxidative cleavage, in combination with the increased tendency for heavier members of a triad for higher oxidation states.[50] Across the transition metals, dihydrogen complexes become more common, especially for groups 8 to 10.[2]

Bis-dihydrogen complexes are rare.[51] Sabo-Etienne and co-workers reported the first crystallographically characterised example in 2000, $[Ru(H)_2(PCy_3)_2(\eta^2\text{-}H_2)_2]$ (**i-19**), [52] however the iridium analogue (**i-21**)[53] was first reported in 1985 (Figure 1.6). The rhodium congener (**i-20**) is of particular relevance to this work.[54]

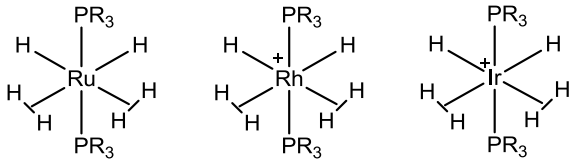


Figure 1.6 *Bis*-dihydrogen complexes of Ru, Rh and Ir. R = Cy. $[BAr^F{}_4]^-$ anions not shown.

The characterisation of a dihydrogen complex by standard techniques of NMR spectroscopy or X-ray crystallography is quite challenging. Hydrogen has only one electron, and as a result a very low X-ray scattering ability, a problem which is further exacerbated by the hydrogen's close proximity to the metal which has a much greater electron density and hence will dominate the scattering. Neutron diffraction allows accurate determination but is less available and more expensive while also requiring large crystals. As a result T_1 relaxation measurements and the observation of H-D

coupling from solution ^{1}H NMR spectroscopy are some of the most informative methods as they allow for interrogation by readily available solution techniques.

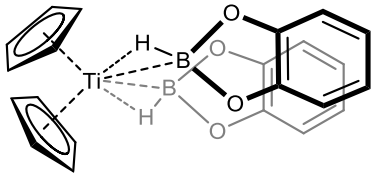
T_1 measurements give the relaxation time of the nuclear spin with the rate of relaxation being affected by nearby nuclei through the dipole-dipole mechanism. This ability to affect the relaxation rate diminishes rapidly (r^{-6}) with the internuclear distance (r). The distance between the two nuclei in a dihydrogen ligand or two hydrides is different (Figure 1.5) and as such they have different T_1 values helping to distinguish between the two bonding modes. The generally accepted T_1 value for a dihydrogen ligand is <50 ms (at 400 MHz), with a T_1>150 ms (at 400 MHz) representative of a dihydride.[53, 55]

1.2.3.2 Borane σ-complexes

For a wide variety of metal-mediated organic transformations such as the hydroboration of olefins, borane compounds such as pinacolborane are key reagents. Coordination of these borane compounds to the metal centre is often the step prior to activation and as such σ-borane complexes have received much interest in recent years.[13, 56, 57]

The first example of a structurally characterised σ-borane complex was reported by Hartwig *et al.* in 1996 (Figure 1.7).[58] $TiCp_2(HBcat)_2$ (**i-22**) (HBcat = catecholborane) is an 18 electron complex with two HBcat ligands acting as 2 electron donors and is an example of a true σ-borane complex with the ligands bound in an η^2 side-on coordination mode. σ-donation occurs from the σ-bonding orbital of the B-H into an empty metal d-orbital. Backbonding into the σ*-antibonding orbital of the B-H is prevented owing to its high energy, but backdonation into the free p-orbital of the

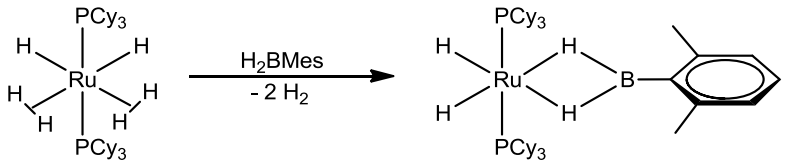
boron is highly efficient and responsible for the side-on coordination.[59] Hartwig *et al.* have since expanded their range of σ-borane complexes for Ti, Nb, Mn and Re in an area which is still receiving interest.[41, 60]



i-22

Figure 1.7 First example of a transition metal σ-borane complex by Hartwig, $TiCp_2(HBcat)_2$ (**i-22**).

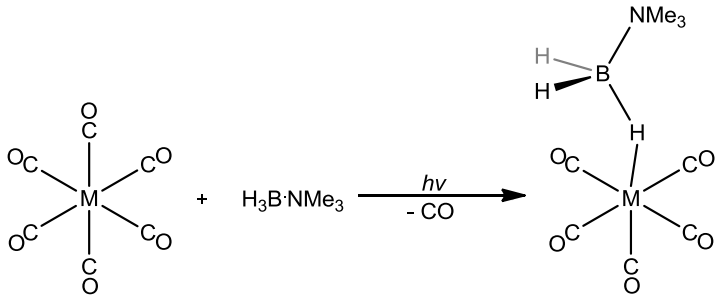
In 2007, Alcaraz *et al.* reported an unprecedented coordination mode of a tricoordinated borane.[61] Addition of mesitylborane (H_2BMes) to **i-19** leads to the formation of $[Ru(H)_2(PCy_3)_2(\eta^2\text{-}H_2BMes)]$ (**i-23**), which represents the first example of one borane bound to a metal centre through two σ B-H bonds (Scheme 1.5). **i-23** is structurally similar to coordinated amino-boranes, discussed in Section 1.4.3.2.



i-19 **i-23**

Scheme 1.5 Synthesis of $[Ru(PCy_3)_2(H)_2(\eta^2\text{-}H_2BMes)]$ (**i-23**).

To further investigate borane coordination, Shimoi and co-workers prepared a series of neutral σ-borane complexes featuring $H_3B{\cdot}L$ ligands (L = NMe_3, PMe_3, PPh_3) (Scheme 1.6).[62] These were the first reported metal complexes of neutral monoborane-Lewis base adducts featuring an unsupported M-H-B bond. Of particular relevance to this thesis is $[M(CO)_5(\eta^1\text{-}H_3B{\cdot}NMe_3)]$ (**i-27**, M = Cr; **i-28**, M = Mo; **i-29**, M = W) which is the first reported example of an amine-borane coordinated to a transition metal.



i-24 M = Cr
i-25 M = Mo
i-26 M = W

i-27 M = Cr
i-28 M = Mo
i-29 M = W

Scheme 1.6 Synthesis of neutral σ-borane complexes featuring end-on coordination.

In contrast to the σ-borane complexes prepared by Hartwig (Figure 1.7), the Shimoi-type complexes feature an amine-borane bound in an η^1 end-on coordination mode, due to the lack of an empty p-orbital on the boron, with the hydrogen lying nearly *trans* to the CO ligand in the solid state. In a closed system (NMR tube), displacement of the $H_3B{\cdot}L$ ligand by CO is observed along with the concomitant precipitation of $[M(CO)_6]$ demonstrating the reversibility of the reaction. Similar behaviour is observed for analogous alkane complexes (*vide infra*).[63] The weakly coordinating nature of $H_3B{\cdot}L$ is evident in solution with signals corresponding to free $H_3B{\cdot}L$ seen to grow in the NMR spectra with time. The M-H-B linkage primarily results from electron donation from the B-H σ-bonding orbital with negligible backdonation into the σ*-antibonding orbital. The complexes are fluxional on the NMR timescale with rapid exchange occurring between the terminal and bound B-H atoms, even at low temperatures. Shimoi and co-workers have since extended this work to manganese[64] and ruthenium[65] systems, both of which demonstrate end-on binding. The manganese complex, $[CpMn(CO)_2(\eta^1\text{-}H_3B{\cdot}NMe_3)]$ (**i-30**), was generated by a comparable method to Ball's Re-alkane complex (**i-35**, Scheme 1.7) *via* the photolysis of $[CpMn(CO)_3]$ (**i-31**) in the presence of excess $H_3B{\cdot}NMe_3$. As amine-boranes are isoelectronic with

alkanes, complexes such as **i-30** aid understanding of the coordination chemistry of alkanes.

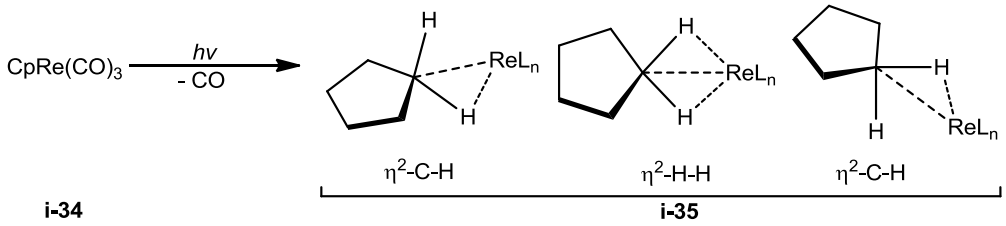
Amine-boranes have received considerable interest in the past decade due to their potential for chemical hydrogen storage.[66, 67] Although they release hydrogen on heating (>120 °C for $H_3B{\cdot}NH_3$), the use of metal catalysts allows dehydrogenation to occur at room temperature.[68, 69] A postulated first step in the transition-metal catalysed dehydrogenation of amine-boranes is the formation of a σ-complex, and as such σ-complexes of amine-boranes have received much attention. Amine-borane σ-complexes will be discussed in more detail, in the context of dehydrocoupling, in Section 1.4.3.2.

1.2.3.3 Alkane σ-complexes

The term transition metal σ-alkane complex refers to an intermolecular interaction between an alkane C-H bond and a transition metal complex.[13, 70, 71] Such complexes are key intermediates in the activation of C-H bonds, but their full characterisation has proved problematic due to the inert (non-polar) nature of the C-H bond and subsequent poor transition metal coordination capability.[72-74] The first reported evidence for an alkane σ-complex was in 1975 by Perutz *et al.* who characterised $[Cr(CO)_5(CH_4)]$ (**i-32**) and $[Fe(CO)_4(CH_4)]$ (**i-33**) by UV-spectroscopy using matrix isolation techniques at low temperatures.[75]

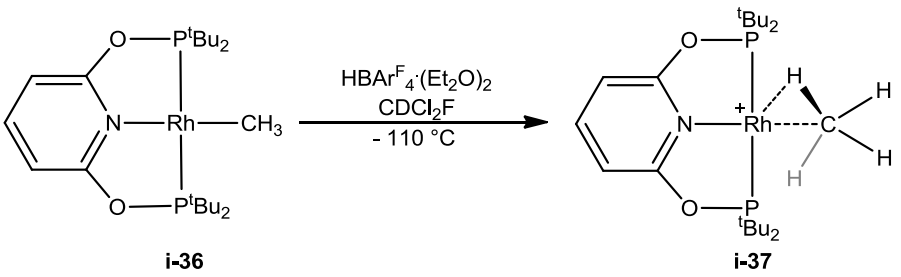
In 1998, Ball and Geftakis reported the solution NMR characterisation of a Re-cyclopentane complex (**i-35**) generated by the irradiation of $[CpRe(CO)_3]$ (**i-34**) in cyclopentane at temperatures below -80 °C (Scheme 1.7). Proton NMR data indicated that both protons attached to the same carbon were involved in binding to the metal

centre. The equivalence of the two protons of the methylene group was postulated to result from rapid exchange of the two C-H bonds interacting individually and alternately with the rhenium centre in an η^2-C-H σ-type interaction, with the η^2-H-H binding mode acting as a low-energy transition state for their interconversion (Scheme 1.7).



Scheme 1.7 Irradiation of $CpRe(CO)_3$ to form a Re-alkane complex (**i-35**). Different possible binding modes are shown. $ReL_n = CpRe(CO)_2$.

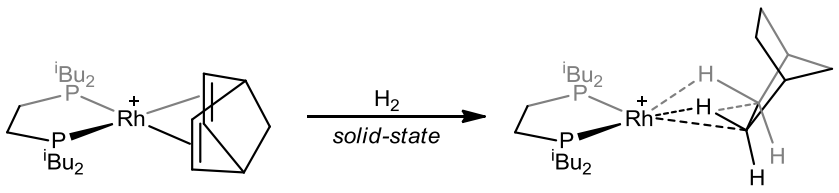
Recently there have been several important advances in the characterisation of σ-alkane complexes. In 2009, Brookhart and co-workers reported the full NMR characterisation of a methane σ-complex at a d^8-rhodium(I) centre formed by the direct protonation of a Rh-CH_3 bond (Scheme 1.8).[39] $[(PONOP)Rh(\eta^2\text{-}CH_4)][BAr^F]_4$ (PONOP = 2,6-$(^tBu_2PO)_2C_5H_3N$) (**i-37**) is only stable at -110 °C in $CDCl_2F$, at which temperature all four hydrogen atoms are undergoing exchange. Above this temperature the complex is unstable with methane dissociation occurring ($t_{1/2}$ = 83 minutes at -87 °C). Since then σ-alkane complexes in solution have been observed using IR and NMR spectroscopic methods for Mn and Re metal fragments.[76, 77] Previous studies have also used time-resolved infrared spectroscopy to observe σ-alkane complexes in solution.[63, 78]



i-36 i-37

Scheme 1.8 Formation of a transition metal σ-methane complex (**i-137**), characterised by NMR spectroscopy. [BAr$^F_4$]$^-$ anion not shown.

Two solid-state structures of transition metal σ-alkane complexes have been reported prior to 2012: heptane interacting with an iron(II)-porphyrin complex (**i-38**)[79] and methylcyclohexane coordinated to a uranium(III) complex (**i-39**).[80] However, they have been subject to debate as to whether they are *true* σ-complexes due to the possibility of host-guest effects as well as discussion over the nature of the direct C-H···M bond interaction. In both cases, the alkane ligands are not retained in solution. In 2012, Weller and co-workers reported the synthesis of an alkane σ-complex which was characterised by X-ray diffraction (Scheme 1.9).[30] [Rh(^{i}Bu$_2$PCH$_2$CH$_2$P^{i}Bu$_2$)(η^{2}η^2-C$_7$H$_{12}$)][BAr$^F_4$] (**i-41**) was produced *via* a gas-solid reaction through solid-state hydrogenation of the strained alkene precursor (**i-40**). No evidence for a bound alkane complex was seen at -100 °C in CDCl$_2$F but free NBA (norbornane, C$_7$H$_{12}$) was observed confirming its formation in the solid state.



i-40 i-41

Scheme 1.9 Formation of [Rh(^{i}Bu$_2$PCH$_2$CH$_2$P^{i}Bu$_2$)(η^{2}η^2-C$_7$H$_{12}$)][BAr$^F_4$] (**i-41**). [BAr$^F_4$]$^-$ anions not shown.

1.2.3.4 Agostic interactions

The term "agostic interaction" was coined by Brookhart and Green in 1983 as an attractive interaction between a metal and a proximal C-H bond of a ligand already bonded to the metal centre.[81, 82] Agostic interactions provide valuable insight into the M···H-C interaction, a key step in C-H activation. The first example of an agostic interaction was reported in 1968 by Trofimenko[83] and since then there have been many reported examples of low-coordinate transition metal centres stabilised by intramolecular α-, β- or γ- C-H interactions (Figure 1.8).[16, 84-86]

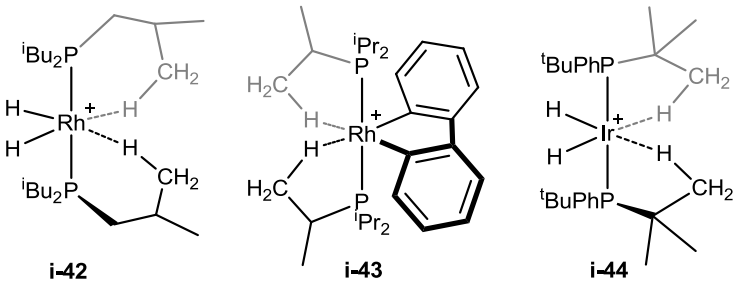


Figure 1.8 Examples of crystallographically characterised transition metal complexes featuring agostic interactions. Anions not shown.

In the solid state, agostic interactions are characterised by a short M-H distance (~ 1.8 – 2.3 Å) and a small M-H-C bond angle (~ 90 – 140°). In addition to agostic interactions, electrostatic "anagostic" M-H-C interactions have also been identified (Figure 1.9).[87] Anagostic interactions typically have a longer M-H distance (~ 2.3 – 2.9 Å) and a larger M-H-C bond angle (~ 110 - 170°). Agostic and anagostic interactions also show differences when studied in solution by ^{1}H NMR spectroscopy; agostic interactions show an upfield shift with a reduced coupling constant compared with the free ligand, while anagostic interactions experience a downfield shift.[88]

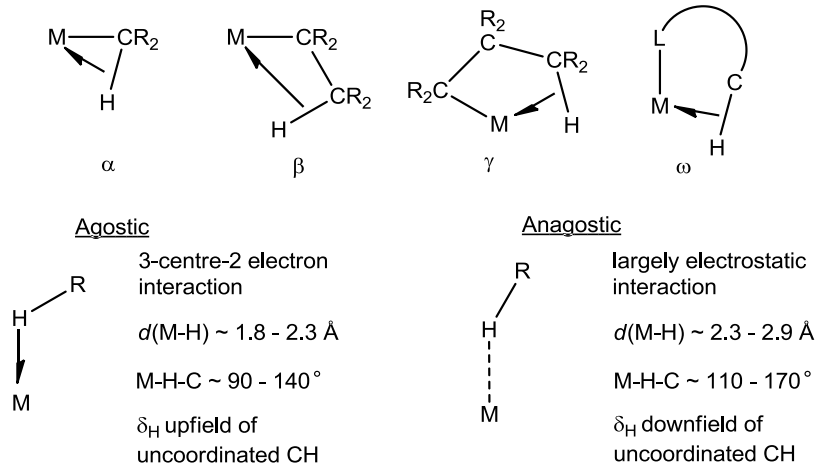
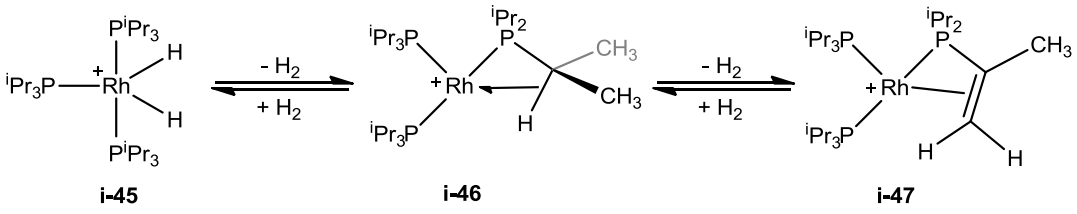


Figure 1.9 Classification and structural characteristics of agostic and anagostic interactions.

Although agostic interactions are implicated as intermediates in C-H activation processes, reported examples of both the agostic intermediate and the activated product are rare.[89-93] Crystallographically characterised examples are even rarer. The Weller group have reported one such example where C-H activation of the agostic intermediate (**i-46**) is followed by β-elimination, resulting in the dehydrogenation of the isopropylphosphine (**i-47**) (Scheme 1.10). A further example by Nolan[4] will be discussed in Section 1.3.1.1.



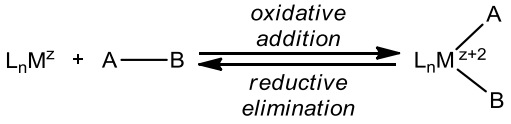
i-45 **i-46** **i-47**

Scheme 1.10 Dehydrogenation of an *iso*propylphosphine ligand *via* a β-H agostic complex. Anions not shown.

1.3 B-H and C-H activation processes

Oxidative addition, a reaction of great importance in synthesis and catalysis, involves the formation of new metal-ligand bonds *via* the cleavage of a bond in a reagent or

coordinated ligand (Scheme 1.11).[2] The reverse reaction, reductive elimination, leads to the extrusion of an A-B molecule and is often the product forming step of catalysis. In the forward reaction, to give the higher oxidation state, valence electron count and coordination number of the metal all increase by two.



Scheme 1.11 General scheme for oxidative addition and reductive elimination.

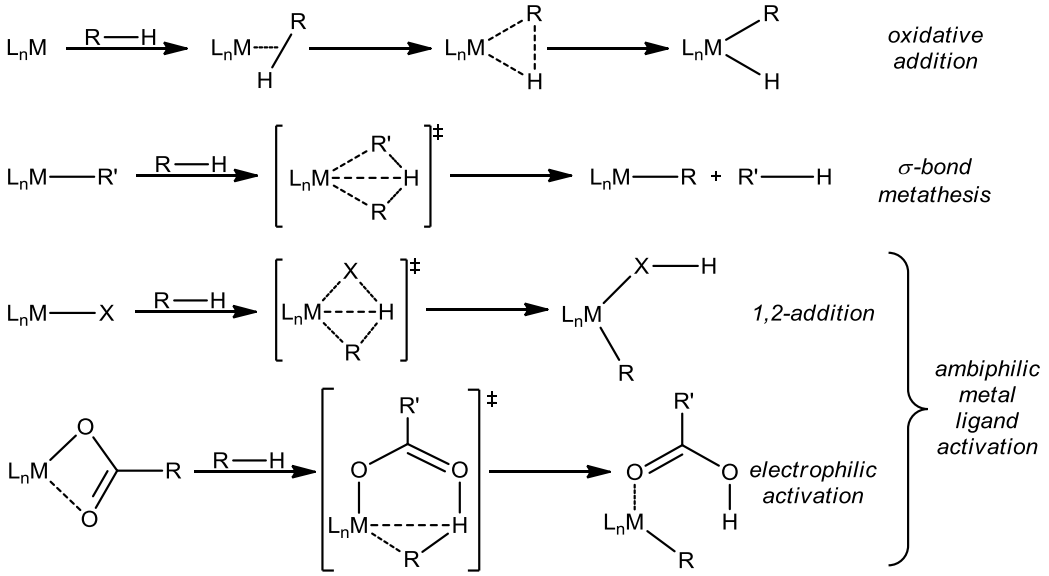
There is a general trend in the reactivity of metal complexes towards oxidative addition due to the change in oxidation state, coordination number and number of valence electrons of the metal complex. Oxidative addition is favoured by electron rich, less-hindered metal centres with a vacant site and fewer than 18 electrons (or the ability to form a 16 electron compound through ligand dissociation).[94]

There are several different possible mechanisms of oxidative addition; concerted, S_N2, radical and ionic mechanisms. The focus of this section will be the concerted pathway favoured by non-polar substrates; and in particular C-H and B-H activation.

1.3.1 C-H activation

The activation of the ubiquitous but inert C-H bond has received considerable recent attention as it can facilitate useful transformations of organic molecules.[72, 74, 95] There are several different possible mechanisms of C-H activation (Scheme 1.12). For the purpose of this work, which focuses on low valent rhodium, only the classical oxidative addition, requiring an electron rich metal centre such as Rh(I), will be discussed. The first step in oxidative addition is the coordination of the C-H bond to give an agostic or σ-complex as the transition state or intermediate, with the same

bonding interaction as described in Figure 1.3. The reaction may stop at this point to give an isolable agostic or σ-complex. If the degree of backdonation is sufficient, oxidative cleavage will occur generating a C-M-H complex with the ligands located *cis* to each other.[96]



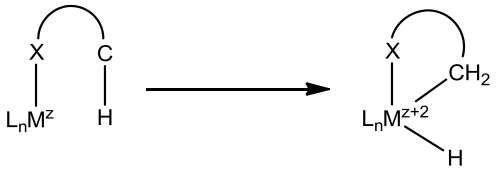
Scheme 1.12 Mechanisms of C-H activation.

Examples of C-H activation at a Rh(III) centre are relatively rare,[97] and it is unlikely to occur *via* oxidative addition which would involve a Rh(V) intermediate.[98] Alternatively, C-H activation can occur by σ-bond metathesis (Scheme 1.12); however distinguishing between the two can be problematic.[57, 99] Perutz and Sabo-Etienne have recently proposed the closely related σ-Complex Assisted Metathesis (σ-CAM) where a σ-bond metathesis transformation is preceded and followed by the formation of a stable σ-complex.[57, 100]

1.3.1.1 Intramolecular C-H activation

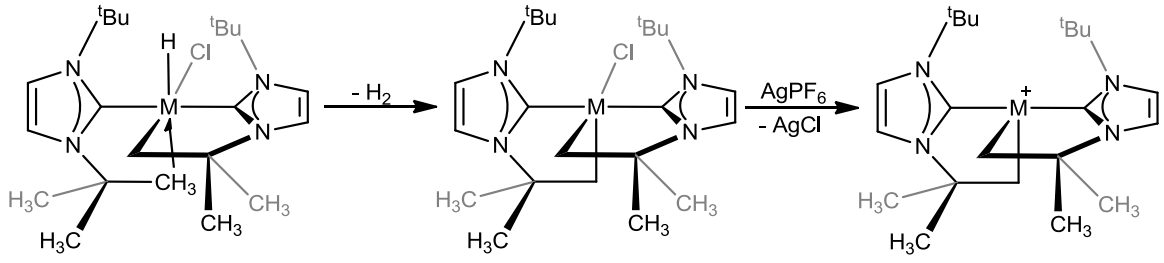
C-H activation can be assisted through chelation, by the coordination of a donor heteroatom such as N, O, P, S, Se and As, leading to intramolecular C-H activation

otherwise known as cyclometalation (Scheme 1.13).[97, 101] Intramolecular C-H activation occurs more readily than intermolecular C-H activation due to being both kinetically (reagents pre-organised) and thermodynamically (ΔS ~ 0) more favourable.



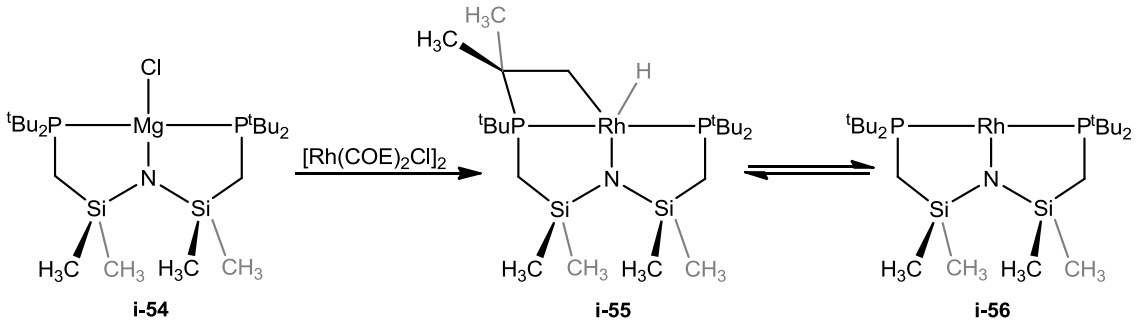
Scheme 1.13 Heteroatom (X) assisted intramolecular C-H activation.

There are many examples of heteroatom assisted C-H activation at rhodium centres which act as model systems for investigating oxidative addition reactions. Particularly prevalent are cyclometalations of aryl and alkyl C-H bonds of phosphine ligands which shall be the focus of this section.[97] Nolan and co-workers have reported a rare *bis*-cyclometalated M(III) complex (**i-50**, M = Rh; **i-51**, M = Ir) (Scheme 1.14).[4, 102] Addition of Ag[PF_6] abstracts the rhodium-bound chloride providing access to a 14 electron M(III) species (**i-52**, M = Rh; **i-53**, M = Ir). The isolation of **i-48** and **i-49,** the precursors to the second cyclometalation, which show a strong agostic interaction, provides a rare example where both the agostic intermediate and the C-H activated product (**i-50** and **i-51**) have been reported.



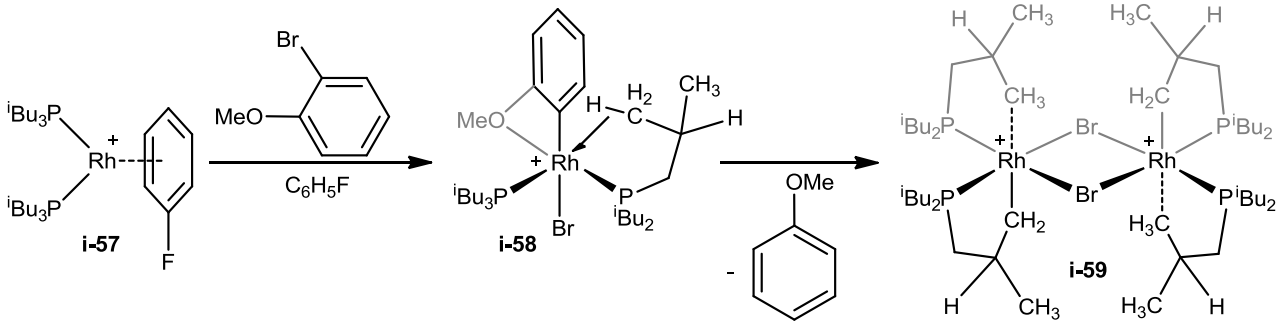
Scheme 1.14 A rare *bis*-cyclometalated Rh(III) complex. PF_6^- anion not shown.

In 2008 Caulton and co-workers reported a rhodium(III) metallacycle (**i-55**), which is in rapid equilibrium with the 14-electron Rh(I) complex [{(^{t}Bu$_2$PCH$_2$SiMe$_2$)$_2$N}Rh] (**i-56**) as indicated by variable-temperature NMR experiments (Scheme 1.15).[103] The metallacycle is rapidly opening and closing (10^3 s^{-1}) in a process which involves all twelve of the methyl groups of the four ^{t}Bu substituents.



Scheme 1.15 Oxidative C-H bond addition of a ^{t}Bu methyl group.

Rhodium(III) precursors have also been found to be active towards cyclometalation. Addition of *ortho*-bromo anisole to the arene adduct [Rh(P^{i}Bu$_3$)$_2$(η^6-C$_6$H$_5$F)][BAr$^F_4$] (**i-57**) immediately gave **i-58**, the product of C-Br activation (Scheme 1.16).[104] Over time (7 days) **i-58** evolved to generate the halide bridged dimer **i-59** and anisole. **i-59** features two cyclometalated alkyl groups resulting from the C-H activation of *iso*-butyl at the Rh(III) centre.



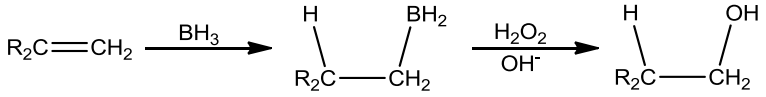
Scheme 1.16 Intramolecular C-H activation at a Rh(III) centre. [BAr$^F_4$]$^-$ anions not shown.

1.3.2 B-H activation

B-H activation has received much interest in recent years. Hydrido-boryl metal complexes resulting from B-H activation at a metal centre are probable intermediates in the transition metal-catalysed hydroboration of olefins.[105-107] Related (base-stabilised boryl) compounds are also likely to be involved in the dehydrocoupling of amine-boranes, which will be discussed in Section 1.4.

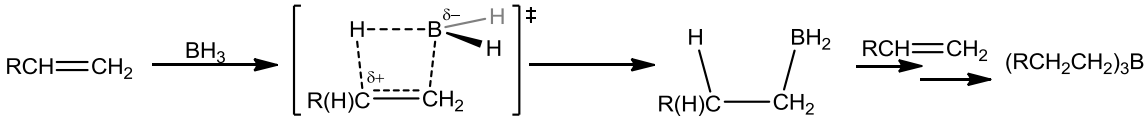
1.3.2.1 Hydroboration

Hydroboration refers to the addition of a B-H bond across an unsaturated C-C bond producing organoborane compounds, which are versatile building blocks in organic synthesis.[108] They can react with a variety of reagents to produce useful compounds such as alcohols *via* the hydroboration-oxidation reaction (Scheme 1.17).[109]



Scheme 1.17 The hydroboration-oxidation reaction.

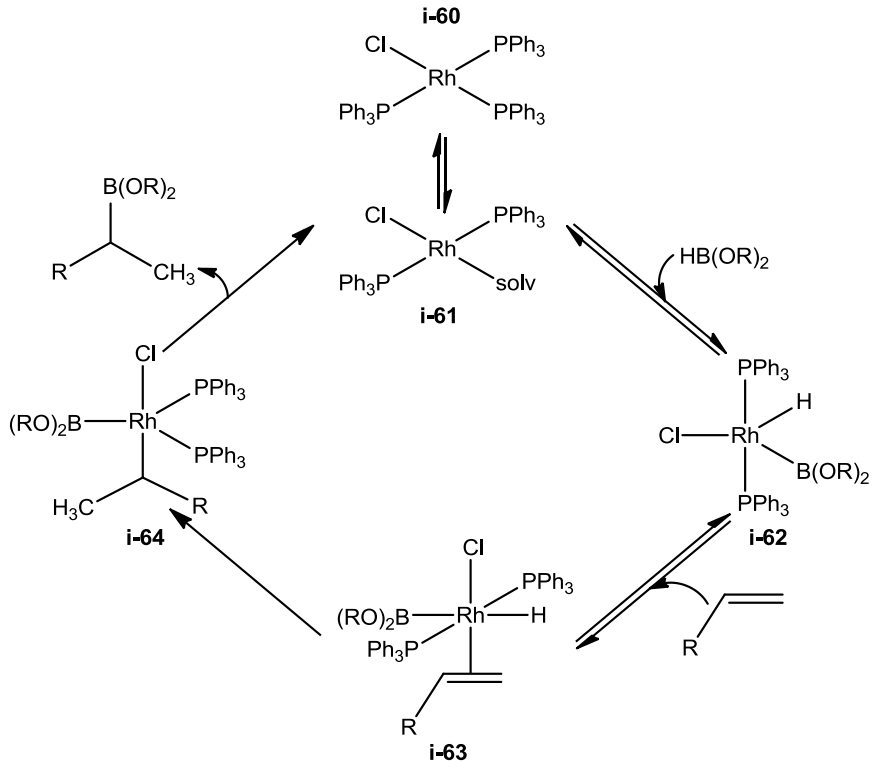
Hydroboration is typically anti-Markovnikov; the hydrogen adds to the more substituted carbon. This regiochemistry reflects the polar nature of the $B^{\delta+}$-$H^{\delta-}$ bond and is the reverse of a typical H-X addition. Non-metal catalysed hydroboration proceeds *via* a four-membered transition state with both atoms added on to the same face of the double bond (Scheme 1.18). The nature of the transition state explains the observed regiochemistry; the carbon atom bares a partial positive charge which is better supported by the more substituted carbon.[110]



Scheme 1.18 Non-metal catalysed hydroboration.

Although the borane carriers BH_3·THF and BH_3·SMe_2 are highly active hydroboration reagents both have their disadvantages;[111] BH_3·THF is only available in low concentrations in THF (~1 M) and suffers from instability over prolonged periods of time while boranedimethylsulfide releases stoichiometric amounts of SMe_2 as a by-product and is also highly flammable, volatile and malodorous. The use of more stable borane sources such as amine-boranes[68] or catecholborane[106] are favoured due to their increased stability, although this has the concomitant requirement for a metal catalyst or higher reaction temperatures.

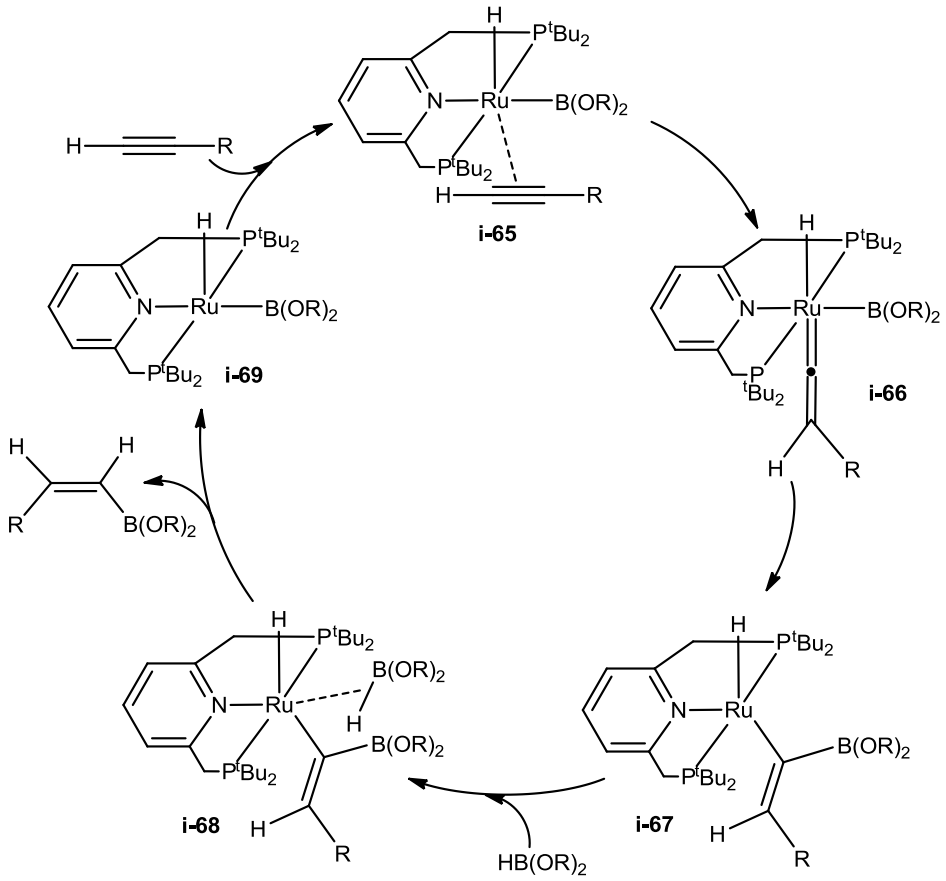
The ability of late transition metals to catalyse the hydroboration of unsaturated C-C bonds was discovered by Wilczynski and Sneddon thirty years ago using cobalt.[112] However, rhodium has since become the transition metal of choice for hydroboration catalysis. The use of other metals such as Pd[113] and Ru[114] has been reported along with lanthanide-catalysed hydroboration reactions.[115, 116] Extensive mechanistic investigations have been carried out using Wilkinson's catalyst leading to the basic mechanism seen in Scheme 1.19.[109]



Scheme 1.19 Hydroboration of olefins using Wilkinson's catalyst.

Initial dissociation of a phosphine is followed by oxidative addition of the borane forming **i-62**. The solid state structure of **i-62** has been determined by X-ray crystallography for the P^iPr_3 analogue where $HB(OR)_2$ = catecholborane.[117] Coordination of the olefin generates **i-63**, followed by insertion of the olefin into the metal-hydride bond to generate **i-64**. The organoborane is then reductively eliminated to regenerate the catalyst **i-61**.

Interestingly, a recent paper by Gunanathan *et al.* reported the ruthenium catalyzed hydroboration of terminal alkynes to generate *Z*-vinylboronates rather than the expected *E*-vinylboronates *via* anti-Markovnikov and *syn*-addition.[118] They proposed that the apparent *trans*-addition of the borane results from a 1,2-hydrogen shift at the alkyne, producing **i-66**, and addition of the boron and hydrogen centres of a second pinacolborane reagent to produce **i-68** (Scheme 1.20).



Scheme 1.20 Proposed mechanism for *Z*-selective *trans*-hydroboration of terminal alkynes. $HB(OR)_2$ = pinacol borane.

1.3.2.2 Hydrido-boryl compounds

As mentioned previously, B-H activation of boranes at transition metal centres has been studied extensively due to its importance with respect to transition metal catalysed hydroboration of olefins and recently, the dehydrocoupling of amine-boranes. There are many examples of rhodium and iridium boryl compounds resulting from the oxidative addition of three coordinate borane species, with a particular focus on those relevant to hydroboration (Figure 1.10).[117, 119, 120]

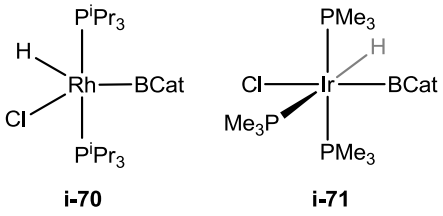
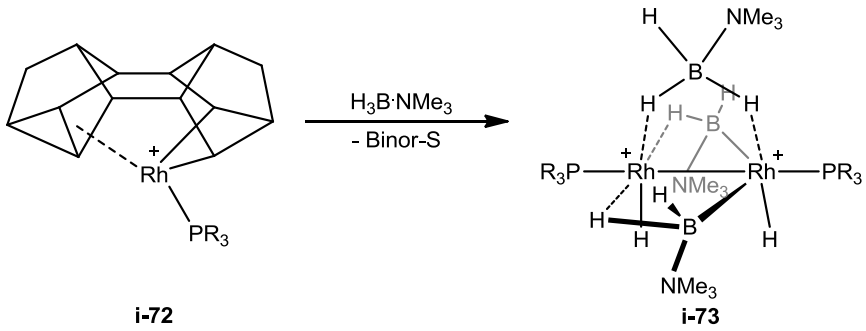


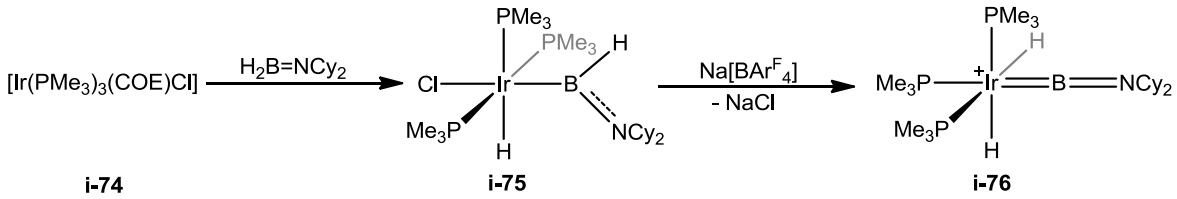
Figure 1.10 Transition metal hydrido-boryl compound. Cat = catecholato.

Despite the abundance of examples resulting from B-H activation of a tri-coordinate borane, examples of base-stabilised boryl compounds resulting from oxidative addition of four-coordinate boranes such as amine-boranes are less common. In 2010, Chaplin *et al.* reported the synthesis of a dinuclear metal-metal bonded complex (**i-73**) featuring base-stabilised boryl and hydride ligands resulting from B-H activation of an amine-borane at a rhodium(I) centre (Scheme 1.21).[121] Analysis by X-ray crystallography (R = Cy) revealed two rhodium centres bridged by three $H_3B{\cdot}NMe_3$ ligands, two of which have undergone B-H activation. The solid-state structure is retained in solution.



Scheme 1.21 Formation of a dinuclear metal-metal bonded complex featuring base-stabilised boryl and hydride ligands. R = Cy, ^{i}Pr. $[BAr^F_4]^-$ anions not shown.

Recently Aldridge and co-workers have used an electron rich iridium(I) precursor (**i-74**) to activate an amino-borane to afford a hydrido-boryl complex $[Ir(H)(PMe_3)_3\{B(H)NCy_2\}]$ (**i-75**) (Scheme 1.22).[122] In the presence of $Na[BAr^F_4]$, **i-75** undergoes chloride extraction which triggers a B-to-Ir α-hydride migration to generate the borylene dihydride complex $[Ir(H)_2(PMe_3)_3(BNCy_2)][BAr^F_4]$ (**i-76**).

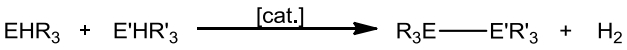


Scheme 1.22 Synthesis of the aminoboryl (**i-75**) and its subsequent reactivity to generate the borylene (**i-76**). $[BAr^F_4]^-$ anion not shown.

1.4 Dehydrogenation and dehydrocoupling of amine-boranes

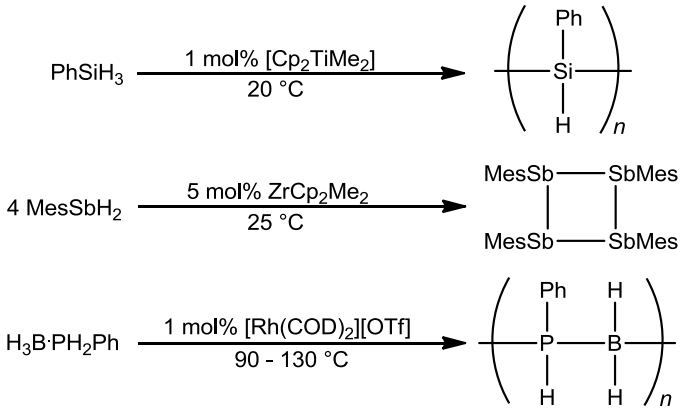
1.4.1 Introduction

The dehydrocoupling of main group elements is an important way to create a new element-element bond alongside concomitant release of a molecule of dihydrogen (Scheme 1.23).[123]



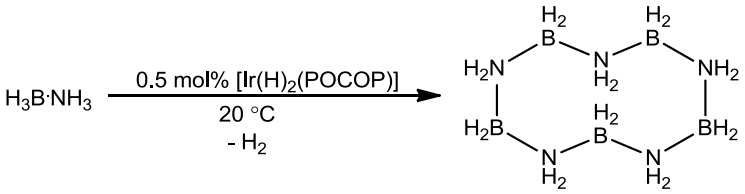
Scheme 1.23 Dehydrocoupling and the concomittant release of dihydrogen. E = main group element. R, R' = alkyl, H.

Examples have been reported for a variety of Group 13-15 elements, but it is beyond the scope of this introduction to discuss them all (Scheme 1.24).



Scheme 1.24 Examples of the dehydrocoupling of Groups 13-15.

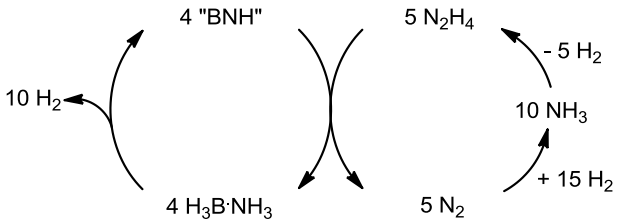
The dehydrocoupling of amine-boranes has attracted particular interest in the past decade due to the high gravimetric hydrogen content (19.6%) of the parent amine-borane, ammonia borane (AB, $H_3B{\cdot}NH_3$), and the possibilities that this creates for hydrogen storage.[124] Although heating AB to temperatures greater than 120 °C leads to the elimination of 2 equivalents of dihydrogen,[69] the addition of a catalyst allows dehydrocoupling to occur at room temperature. For example, the use of Brookhart's iridium pincer complex $[Ir(H)_2(POCOP)]$ (POCOP = κ^3-1,3-$(OP^tBu_2)_2C_6H_3$)[125] (**i-77**) dehydrocouples AB to yield the cyclic pentamer $(H_2B\text{-}NH_2)_5$ after 14 minutes at 20 °C (Scheme 1.25).[126] However the pentamer is not the only possible product of dehydrocoupling with other products including borazine ($[HBNH]_3$), polyborazylene (formed upon the removal of more than 2 equivalents of H_2 per molecule of AB) and oligomeric polyamino-boranes ($[H_2BNH_2]_n$) that arise from dehydropolymerisation, each observed depending on the catalyst and conditions employed.[127-130] Indeed, Manners and co-workers subsequently used **i-77** to dehydrocouple AB, under slightly different conditions to Goldberg, Heinekey and co-workers earlier report, and characterised the insoluble white product to be short chain oligomers with *ca*. 20 repeat units.[127]



Scheme 1.25 Dehydrocoupling of AB using Brookhart's iridium pincer catalyst (**i-77**).

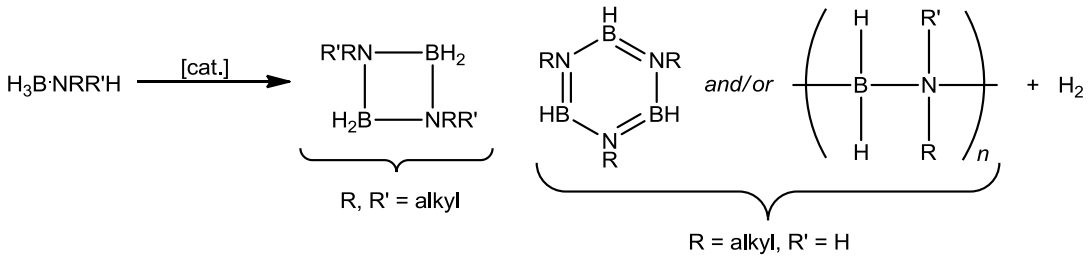
For AB to be a viable material for hydrogen storage the B-N polymeric products need to be easily rehydrogenated. In 2011, Sutton *et al.* reported the regeneration of the polyborazylene by direct reaction with hydrazine and liquid ammonia (Scheme

1.26).[131] Although this report is encouraging, ideally regeneration would occur using H_2 directly; this has been achieved by Dixon and Liu and co-workers using cyclic amine-boranes.[132]



Scheme 1.26 Cycle showing regeneration of AB. "BNH" = polyborazylene.

Recent interest on amine-boranes has also been focused on the inorganic polymers that are produced on the dehydrocoupling of primary and secondary amine-boranes such as $H_3B{\cdot}NMeH_2$ (MMAB) and $H_3B{\cdot}NMe_2H$ (DMAB) (Scheme 1.27).[127, 133] The isoelectronic relationship between B-N and C-C bonds has fuelled interest in the area with the possibility for production of new materials with interesting properties due to the polar nature of the B-N bond.

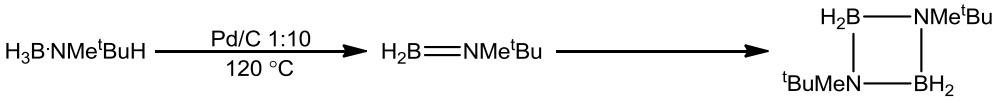


Scheme 1.27 Dehydrocoupling of primary and secondary amine-boranes.

$[Ir(H)_2(POCOP)]$ (**i-77**) and $[Rh(PPh_2(CH_2)_nPPh_2)(\eta^6\text{-}C_6H_5F)][BAr^F{}_4]$ (n = 3 – 5) (**i-78**) have been found to be some of the most efficient catalysts for the dehydrocoupling of MMAB producing polyamino-boranes of high molecular weight and reasonable polydispersities.[127, 133]

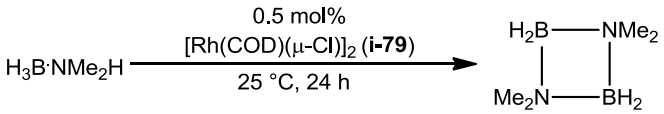
1.4.2 Early examples of dehydrocoupling

Roberts and co-workers reported the first example of transition metal catalysed dehydrocoupling of an amine-borane in 1989. 10% palladium on charcoal was used to catalytically dehydrogenate $H_3B{\cdot}NMe^tBuH$ to the corresponding amino-borane $H_2B{=}NMe^tBu$ at 120 °C (Scheme 1.28).[134] The amino-borane rapidly dimerised at room temperature to yield the cyclic amino-borane dimer $[H_2BNMe^tBu]_2$.



Scheme 1.28 Dehydrogenation of $H_3B{\cdot}NMe^tBuH$ to yield $H_2B{=}NMe^tBu$.

It was not until 2001 that the next example of transition metal catalysed dehydrocoupling of amine-boranes was reported. Manners and co-workers observed the dehydrocoupling of DMAB at 25 °C in the presence of 0.5 mol% $[Rh(COD)(\mu\text{-}Cl)]_2$ (**i-79**) to give $[H_2BNMe_2]_2$ as the sole product (Scheme 1.29).[128] Further research showed dehydrocoupling was not limited to DMAB and investigation of the mechanism indicated that the catalyst was heterogeneous, which shall be discussed in Section 1.4.3.1.[135]

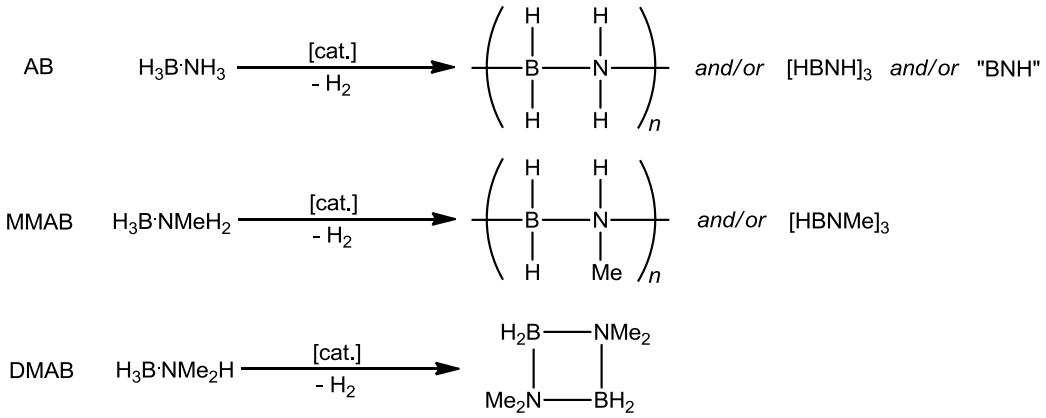


Scheme 1.29 Rh(I) catalysed dehydrocoupling of dimethylamine-borane

Since this publication by Manners, there have been many reports of catalytic systems capable of dehydrocoupling a range of amine-boranes. Key examples will be discussed in subsequent sections.

1.4.3 Mechanistic studies

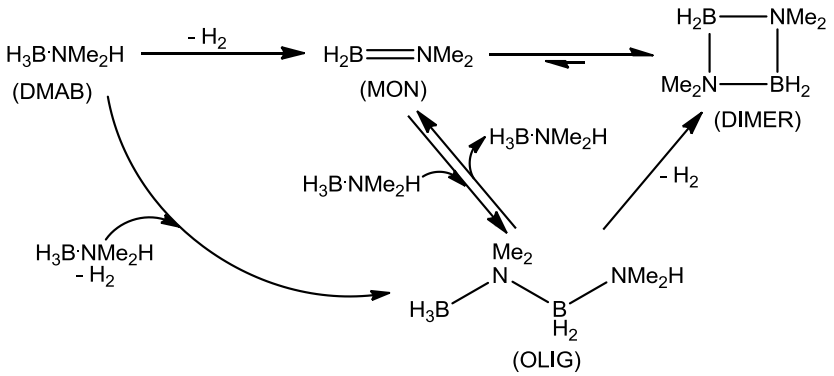
Although AB and MMAB are the more interesting amine-boranes with regard to hydrogen storage and dehydropolymerisation, the oligomeric and polymeric materials that they form on dehydrocoupling are often ill-defined and insoluble (Scheme 1.30) which complicates mechanistic studies. The next amine-borane in the series, DMAB, produces just one major product on dehydrocoupling, $[H_2BNMe_2]_2$, which along with intermediates along the pathway, is soluble in a wide range of solvents aiding mechanistic investigations. Because of this, a considerable number of main group and transition metal systems have been reported to dehydrogenate DMAB.[51, 123, 128, 129, 136-143]



Scheme 1.30 The possible B-N containing products resulting from the dehydrocoupling of AB, MMAB and DMAB. "BNH" = polyborazylene.

From the B-N containing species detected during dehydrocoupling, sometimes in combination with stoichiometric and kinetic studies, a number of mechanisms have been suggested.[129, 138, 141, 144-147] These are summarised in Scheme 1.31. Initial dehydrogenation of DMAB occurs to yield the amino-borane $H_2B{=}NMe_2$ (MON); coupling of 2 DMAB (with loss of H_2) or of DMAB and MON yields the intermediate linear diborazane $H_3B{\cdot}NMe_2BH_2{\cdot}NMe_2H$ (OLIG); and formation of the final product

$[H_2BNMe_2]_2$ (DIMER) can occur *via* off-metal dimerisation of 2 MON or dehydrocyclisation of OLIG mediated by a metal. Not all pathways necessarily operate for each catalyst system.[139-141, 146]



Scheme 1.31 Suggested intermediates and pathways for the dehydrocoupling of DMAB using transition metal catalysts.

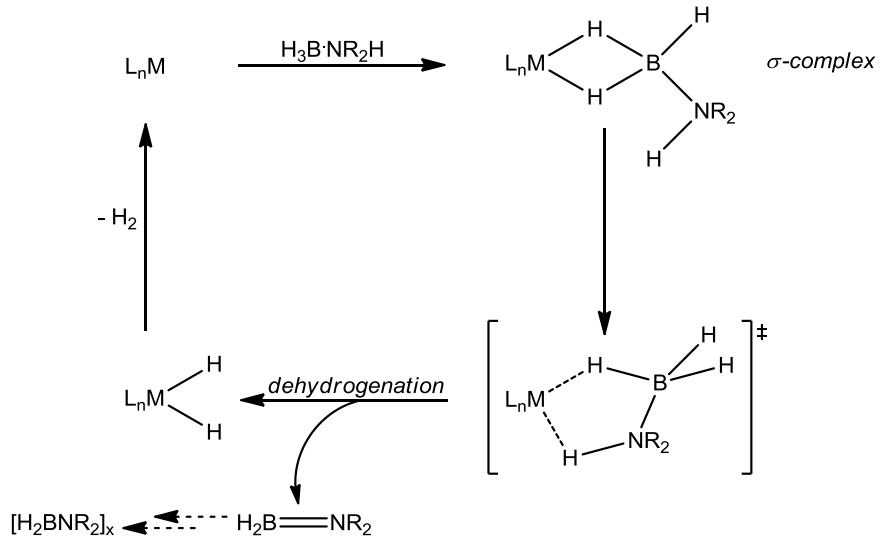
1.4.3.1 Heterogeneous *vs.* homogeneous dehydrocoupling

In 2003, Finke and co-workers developed a series of tests to distinguish between true homogeneous catalysis and soluble or insoluble metal-particle heterogeneous catalysts.[148] The rhodium catalyst system reported by Manners and co-workers in 2001 which utilised $[Rh(COD)(\mu\text{-}Cl)]_2$ (**i-79**) as a precatalyst (Scheme 1.29) was later investigated using the tests developed by Finke and found to operate *via* a predominantly heterogeneous process.[135] Analysis of the catalytically active solution by transmission electron microscopy (TEM) indicated the presence of Rh particles, which was reinforced by a broad plasmon absorption (characteristic of Rh colloids) observed by UV-visible spectroscopy. To confirm that these rhodium colloids were catalytically active, analysis of the kinetic curves and poisoning experiments were conducted. Monitoring of catalysis by ^{11}B NMR spectroscopy revealed the presence of an induction period (during which a black precipitate and "rhodium mirror" were observed to form) followed by significant dehydrocoupling, resulting in a sigmoidal-

shaped kinetic curve, characteristic for metal-particle formation reactions.[149-151] Addition of further DMAB at the end of catalysis resulted in immediate dehydrocoupling with no induction period while addition of mercury, which poisons colloids *via* the formation of an amalgam, dramatically reduced catalytic activity. Finally filtration of a catalytically active solution was found to almost completely suppress catalytic activity. The results of these tests are all indicative of the presence of heterogeneous catalysis. Chen *et al.* later disputed aspects of this work, claiming that a homogeneous Rh_6 cluster was responsible for dehydrocoupling, rather than colloidal Rh based upon *in situ* EXAFS studies.[152]

Although the first examples of dehydrocoupling of DMAB reported were using heterogeneous systems, homogeneous catalysts now dominate. Homogeneous catalysts operate *via* two possible pathways; outer sphere and inner sphere. Bifunctional ruthenium catalysts have been shown to catalyse the dehydrogenation of amine-boranes *via* an outer sphere mechanism that allows dehydrogenation without direct coordination of the amine-borane to the metal centre.[153-155] This is a similar mechanism to that invoked for the transfer dehydrogenation of alcohols.

Inner sphere dehydrogenation involves the coordination of the amine-borane to the metal centre, with a generic simplified scheme shown in Scheme 1.32. A number of mechanistic scenarios for the dehydrogenation step have been implicated; B-H oxidative addition followed by N-H β-elimination[130], intermolecular stepwise transfer of N-H then B-H[156], concerted N-H/B-H activation[157] or N-H transfer to a co-ligand.[158]



Scheme 1.32 Pathway for inner-sphere dehydrogenation.

Suggested mechanisms for homogeneous catalysts (both inner sphere and outer sphere) will be examined in Section 1.4.3.3.

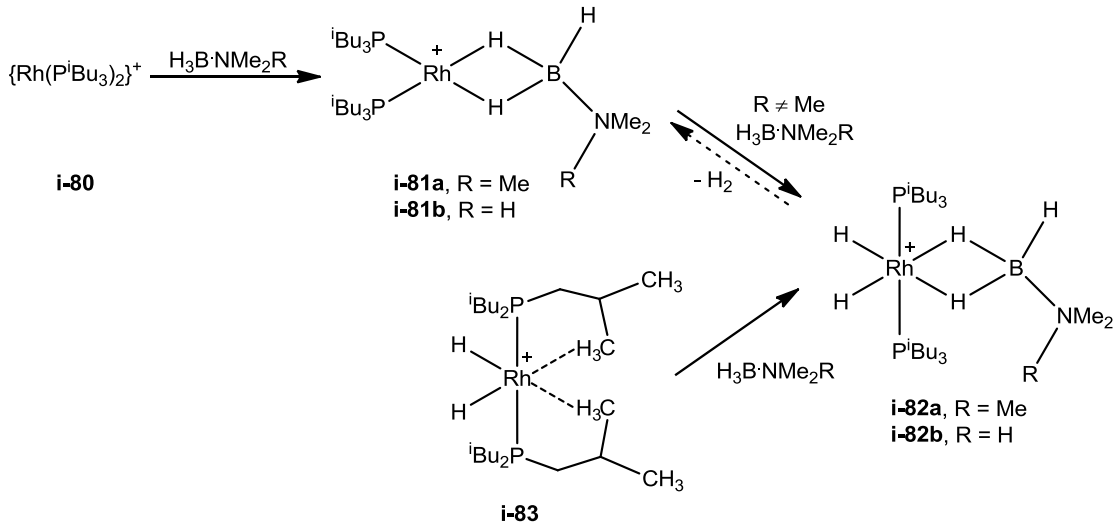
1.4.3.2 Amine- and amino-borane σ-complexes

σ-complexes of amine- and amino-boranes are likely to play a key role in the dehydrocoupling process for homogeneous catalysts proceeding *via* an inner-sphere mechanism. As mentioned earlier (Scheme 1.6) Shimoi and co-workers reported the first example of an amine-borane coordinated to a transition metal (**i-27**, **i-28** and **i-29**).[62] Shimoi utilised the tertiary amine-borane $H_3B{\cdot}NMe_3$ (TMAB) which cannot undergo dehydrogenation due to the lack of N-H functionality. Since then, there have been a number of reported examples where TMAB has been used as a model compound for studying the interaction of amine-boranes at metal centres.[146, 159-161]

On moving to secondary amine-boranes such as DMAB, the isolation of σ-complexes is complicated by the presence of hydridic B-H and protic N-H bonds which can undergo H_2 loss. In 2008 Douglas *et al.* reported the first examples of rhodium σ-

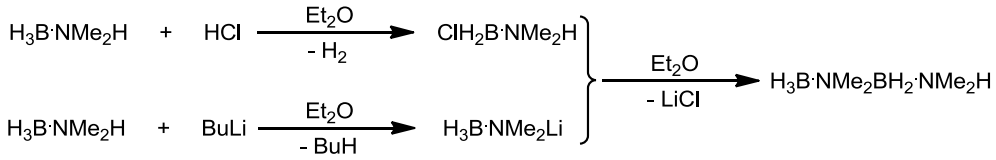
complexes of tertiary and secondary amine-boranes and their involvement in catalytic dehydrogenation (Scheme 1.33).[159]

Addition of 2 equivalents of DMAB or TMAB to $[Rh(P^iBu_3)_2(\eta^6\text{-}C_6H_5F)][BAr^F{}_4]$ (**i-57**), a source of the $\{Rh(P^iBu_3)_2\}^+$ fragment (**i-80**), formed the corresponding rhodium(I) σ-complex $[Rh(P^iBu_3)_2(\eta^2\text{-}H_3B{\cdot}NMe_2R)][BAr^F{}_4]$ (**i-81a** R = Me; **i-81b** R = H). ^{1}H NMR spectra show the coordinated borane group as a broad integral 3H signal at δ -2.12 ppm (**i-81a**) and δ -2.13 ppm (**i-81b**) indicating rapid exchange between the terminal and bound B-H's as seen for Shimoi's complexes.[62] Due to the presence of an N-H group allowing dehydrogenation, **i-81b** rapidly reacted on ($t_{1/2}$ ~ 1 min) to yield the rhodium(III) σ-complex $[Rh(H)_2(P^iBu_3)_2(\eta^2\text{-}H_3B{\cdot}NMe_2H)][BAr^F{}_4]$ (**i-82b**) and DIMER as a product of dehydrocoupling. The use of TMAB prevented this onward reactivity, with **i-81a** indefinitely stable under air-sensitive conditions. The Rh(III) TMAB σ-complex (**i-82a**) could be prepared by the addition of dihydrogen to **i-81a**, or the addition of TMAB to the Rh(III) fragment $\{Rh(H)_2(P^iBu_3)_2\}^+$ (**i-83**). Interestingly, **i-82a** lost dihydrogen to return to the Rh(I) complex much more easily than **i-82b**, with Weller and co-workers attributing this to the added steric bulk from the additional N-methyl group interacting with the phosphine alkyl groups forcing the rhodium centre to adopt a less crowded Rh(I) square-planar configuration. **i-80**, **i-82b** and **i-83** were found to be active catalysts for the dehydrocoupling of DMAB. The organometallic product at the end of catalysis was identified by NMR spectroscopy and ESI-MS as the Rh(III) amino-borane σ-complex $[Rh(H)_2(P^iBu_3)_2(\eta^2\text{-}H_2B{=}NMe_2)][BAr^F{}_4]$ (**i-84**).



Scheme 1.33 Formation of Rh(I) and Rh(III) σ-amine-borane complexes. $[BAr^F{}_4]^-$ anions not shown.

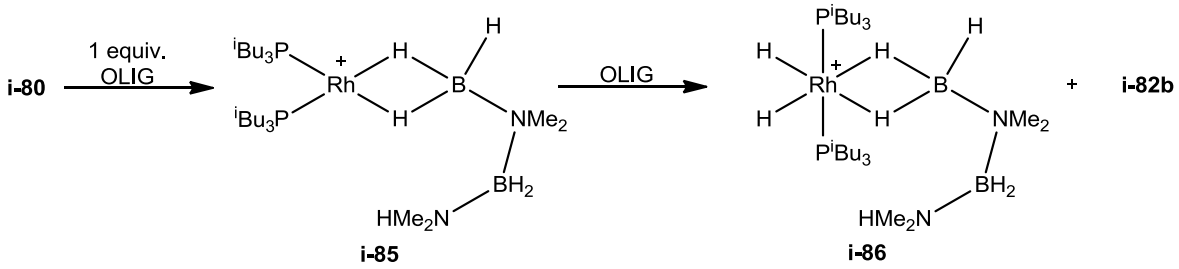
An extension of this work examined the coordination chemistry of the intermediate linear diborazane (OLIG) and the final product (DIMER) with **i-80** and **i-83**.[147] OLIG can be synthesised independently by a route published by Jaska *et al.* (Scheme 1.34).[129]



Scheme 1.34 Manners' synthesis of the intermediate linear diborazane (OLIG).

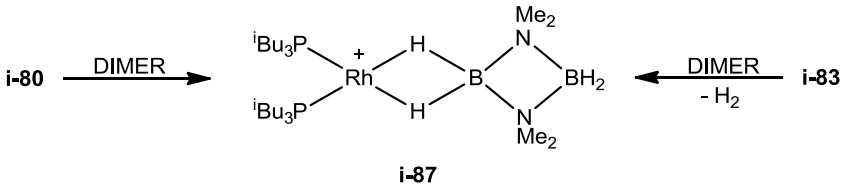
Addition of 1 equivalent of OLIG to **i-80** gave immediate and quantitative formation of $[Rh(P^iBu_3)_2(\eta^2\text{-}H_3B{\cdot}NMe_2BH_2{\cdot}NMe_2H)][BAr^F{}_4]$ (**i-85**) (Scheme 1.35). **i-85** did not undergo further dehydrocoupling to form DIMER indicating that **i-85** does not dehydrocouple to give DIMER *via* a simple intramolecular route. Addition of an extra equivalent of OLIG to **i-85** resulted in an immediate reaction in support of a more complex process, possibly involving outersphere $B\text{-}H^{\delta-}\cdots^{\delta+}H\text{-}N$ interactions.[162] After several hours, two organometallic products are present; **i-82b** and a complex

identified as $[Rh(H)_2(P^iBu_3)_2(\eta^2\text{-}H_3B{\cdot}NMe_2BH_2{\cdot}NMe_2H)][BAr^F{}_4]$ (**i-86**). Exchanging the phosphine for P^iPr_3 allowed the determination of the solid-state structure of the P^iPr_3 analogue of **i-86**, **i-86-^{i}Pr**.[163]



Scheme 1.35 Addition of OLIG to the Rh(I) fragment **i-80**. $[BAr^F{}_4]^-$ anions not shown.

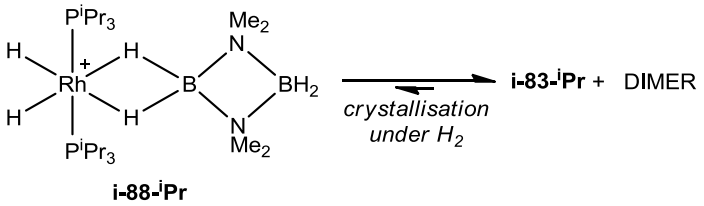
Addition of DIMER to either **i-80** or **i-83** resulted in the formation of the rhodium(I) σ-complex $[Rh(P^iBu_3)_2\{\eta^2\text{-}(H_2BNMe_2)_2\}][BAr^F{}_4]$ (**i-87**) (and H_2 for **i-83**) (Scheme 1.36). The H_2 loss is likely a result of the steric pressure between the *trans* phosphines and the cyclic amino-borane. The Rh(III) σ-complex $[Rh(H)_2(P^iBu_3)_2\{\eta^2\text{-}(H_2BNMe_2)_2\}][BAr^F{}_4]$ (**i-88**) was not observed for this complex. In solution DIMER is static on the metal centre with two BH_2 environments observed in the ^{1}H NMR spectrum with the signal for the coordinated BH_2 shifted upfield (δ -5.07 ppm *vs.* 2.90 ppm).



Scheme 1.36 Addition of DIMER to **i-80** and **i-83**. $[BAr^F{}_4]^-$ anions not shown.

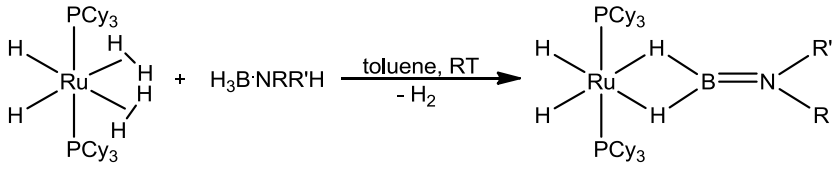
Utilising $\{Rh(H)_2(P^iPr_3)_2\}^+$ (**i-83-^{i}Pr**) allowed the determination of the solid-state structure of $[Rh(H)_2(P^iPr_3)_2\{\eta^2\text{-}(H_2BNMe_2)_2\}][BAr^F{}_4]$ (**i-88-^{i}Pr**).[160] An equilibrium exists between **i-88-P^{i}r** and **i-83-^{i}Pr** which prevented the observation of **i-88-^{i}Pr** in

solution, but slow crystallisation of a mixture of **i-83-^{i}Pr** and DIMER under a H_2 atmosphere gave colourless crystals of **i-88-^{i}Pr** (Scheme 1.37). The relatively long Rh···B distance (2.386(15) Å) and small P-Rh-P angle (151.10(14) °) point to a relatively crowded molecule, consistent with the fact that it can only be observed in the solid state. Complete dissociation of DIMER was observed on dissolution of **i-88-^{i}Pr**.



Scheme 1.37 Equilibrium between **i-83-^{i}Pr**, DIMER and **i-88-^{i}Pr**. $[BAr^{F}_{4}]^{-}$ anions not shown.

In 2010, Alcaraz *et al.* reported the dehydrogenation of amine-boranes at a ruthenium centre to give an early example of a *bis* (σ-B-H) amino-borane ruthenium complex.[164] The reaction between the amine-borane and **i-19** in toluene proceeded with gas evolution. Analysis of the isolated solids by NMR spectroscopy and X-ray crystallography revealed them to have the general formula $[Ru(H)_2(PCy_3)_2(\eta^2\text{-}H_2B{=}NRR')]$ (**i-89**) (R, R' = H, Me) (Scheme 1.38). For **i-89a** (R = R' = H) a broad signal was observed in the ^{11}B NMR spectrum at δ 46 ppm, which is highly shifted from that of the starting AB (δ -21.6 ppm).[165] It is also slightly downfield from the free monomeric amino-borane $H_2B{=}NR_2$ (δ 35 – 36 ppm).[166] In the solid-state a lengthening of the B-H bonds was observed (1.25(2) Å and 1.22(3) Å *vs*. 1.15(3) Å and 1.18(3) Å in AB) along with a shortening of the B-N bond (1.396(3) Å *vs*. 1.58(2) Å in AB). The metal hydrides, and the amino-borane are all located in the equatorial plane resulting in the observation of a sharp singlet in the $^{31}P\{^{1}H\}$ NMR spectrum.



i-19

i-89a, R = R' = H
i-89b, R = Me, R' = H
i-89c, R = R' = Me

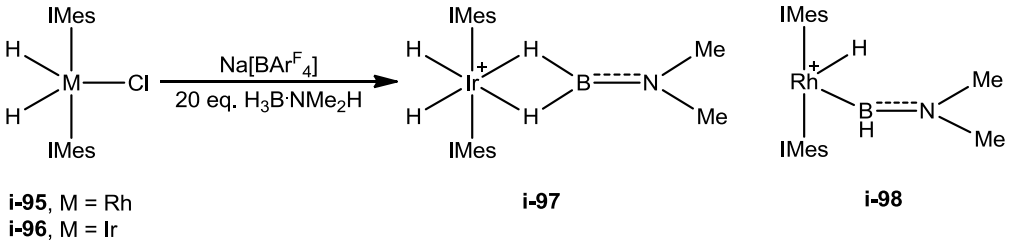
Scheme 1.38 Synthesis of **i-89** by the dehydrogenation of amine-boranes.

It should be noted at this point that amino-boranes can be represented as $H_2B{=}NR_2$ which recognises the significant dative B-N π-interaction, or $H_2B{-}NR_2$ indicating the availability of the empty boron p orbital and the lone pair on the nitrogen.[146, 167, 168] For the purpose of this introduction, B=N and B···N are used interchangeably.

The Sabo-Etienne and Weller groups have reported a comparison of the amino-borane binding strength in Ru, Rh and Ir complexes.[169] $[Ru(H)_2(PCy_3)_2(\eta^2\text{-}H_2B{=}N^iPr_2)]$ (**i-90**) and $[M(H)_2(PCy_3)_2(\eta^2\text{-}H_2B{=}N^iPr_2)][BAr^F{}_4]$ (**i-91**, M = Rh; **i-92**, M = Ir) were synthesised by the addition of a slight excess of the amino-borane ($H_2B{=}N^iPr_2$) to the corresponding *bis*-dihydrogen metal complex (**i-19**, **i-20** and **i-21**, Figure 1.6). In the solid-state stronger interactions were seen in the Ru and Ir congeners compared with the Rh complex with a significantly shorter M···B distance observed for Ru and Ir (1.980(3) Å and 2.022(14) Å *vs.* 2.140(13) Å for Rh). This is mirrored in solution; the M-H-B resonance in the ^{1}H NMR spectrum was more shielded for Ru and Ir (δ -6.91 ppm and -6.58 ppm) compared with rhodium (δ -2.30 ppm). The differences are explained by considering the interaction of the orbitals between the metal and amino-borane fragment; the orbitals of the cationic Rh complex will be more contracted than the neutral Ru complex resulting in a less effective overlap with the B-H orbitals reducing the σ-donation and also the back-donation into the amino-borane π* orbital, while a third row transition metal such as

iridium will have more diffuse orbitals allowing better overlap. Equivalent rhodium and iridium complexes featuring an N-heterocyclic carbene have also been reported by Aldridge and co-workers.[170] $[M(H)_2(IMes)_2(H_2B{\cdots}NR_2)][BAr^F{}_4]$ (IMes = *N,N*=*bis*(2,4,6-trimethylphenyl)imidazol-2-ylidene) (**i-93a**, M = Rh, R= ^{i}Pr; **i-93b**, M = Rh, R = Cy) (**i-94a**, M = Ir, R= ^{i}Pr; **i-94b**, M = Ir, R = Cy) was formed by the catalytic dehydrogenation of the corresponding amine-borane.

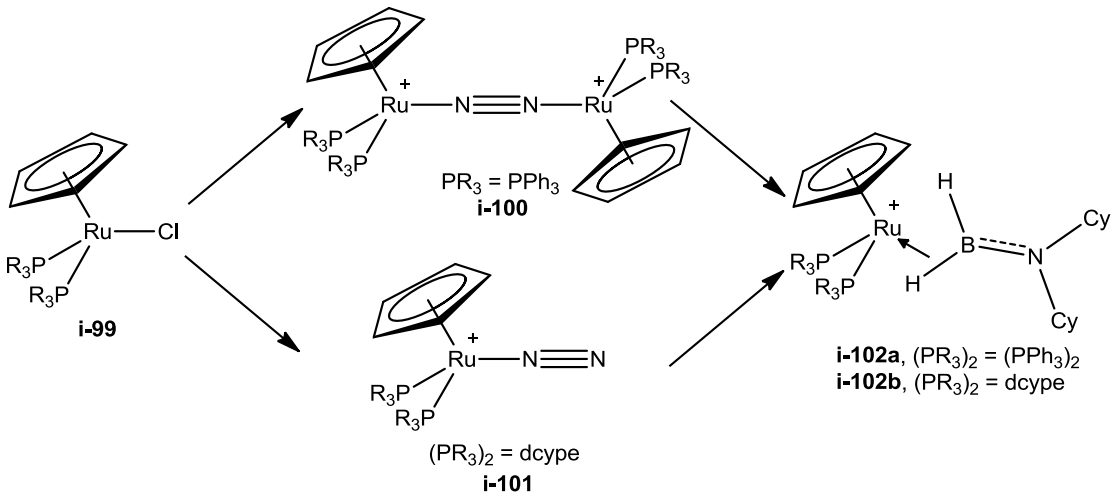
In 2012, Aldridge and co-workers reported the reactivity of $\{M(H)_2(IMes)_2\}^+$ (M = Rh, Ir) with DMAB.[171] Addition of 20 equivalents of DMAB to a mixture of $M(H)_2(IMes)_2Cl$ (**i-95**, M = Rh; **i-96**, M = Ir) and $Na[BAr^F{}_4]$ (a source of the 14 electron fragment $\{M(H)_2(IMes)_2\}^+$) led to the formation of an 18-electron iridium amino-borane adduct $[Ir(H)_2(IMes)_2(\eta^2\text{-}H_2BNMe_2)][BAr^F{}_4]$ (**i-97**) and a 14-electron rhodium amino-boryl complex $[Rh(H)(IMes)_2\{B(H)NMe_2\}][BAr^F{}_4]$ (**i-98**) (Scheme 1.39). The formation of **i-98** went against previously reported examples of the reactivity of $\{Rh(H)_2(IMes)_2\}^+$ with amine-boranes such as **i-93** where just dehydrogenation is observed. Aldridge and co-workers postulated that the observed difference in reactivity between rhodium and iridium could be due to the different tendencies of $[M(H)_2(IMes)_2(H_2BNMe_2)][BAr^F{}_4]$ (M = Rh, Ir) to reductively eliminate dihydrogen.



Scheme 1.39 Synthesis of an iridium amino-borane complex (**i-97**) and a rhodium amino-boryl complex (**i-98**). $[BAr^F{}_4]^-$ anions not shown.

In 2011, Vidovic *et al.* reported the first example of an amino-borane coordinated to a 16-electron metal centre, $\{CpRu(PR_3)_2\}^+$.[172] They rationalised that the use of a 16-

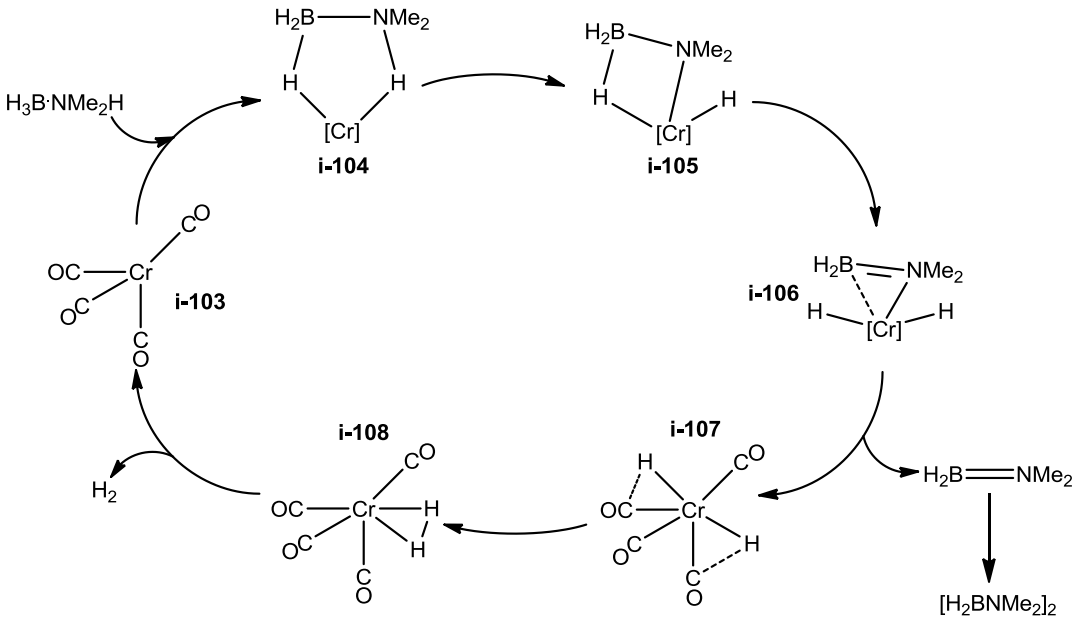
electron fragment, rather than the 14-electron fragments such as $\{M(H)_2(IMes)_2\}^+$ used previously would allow investigation of the 2-electron donor properties of an amino-borane. Examination of the coordination mode of the amino-borane H_2BNCy_2 revealed a novel mono (σ-B-H) binding mode in $[CpRu(PR_3)_2(\kappa^1\text{-}H_2BNCy_2)][BAr^F{}_4]$ (**i-102a**, $(PR_3)_2$ = $(PPh_3)_2$; **i-102b**, $(PR_3)_2$ = dcype (dcype = dicyclohexylphosphinoethane] (Scheme 1.40). Characterisation by X-ray crystallography revealed a bent Ru···B-N framework (**i-102a**, 130.2(3) °; **i-102b**, 133.1(4) °). This contrasts with the linear M···B-N framework seen for the η^2 bound H_2BNCy_2 in **i-93b** (178.4(3) °). ^{1}H NMR spectroscopy revealed the presence of distinct Ru-H-B and B-H signals [δ -14.56 ppm (br, 1H, Ru-H-B) and 5.80 ppm (br, 1H, BH) for **i-102b**] further supporting the κ^1 binding mode. A single resonance in the $^{31}P\{^1H\}$ NMR spectrum is a result of rapid rotation of the amino-borane ligand about the Ru-(BH centroid) axis.



Scheme 1.40 Novel mono (σ-B-H) binding mode of an amino-borane at a 16-electron Ru fragment. $[BAr^F{}_4]^-$ anions not shown.

1.4.3.3 Proposed mechanisms of dehydrocoupling (homogeneous systems)

Shimoi and co-workers reported an extension of their initial work using tertiary amine-boranes (Scheme 1.6) to include secondary and primary amine-boranes.[138] Photolysis of a THF solution of DMAB and a catalytic amount of $[Cr(CO)_6]$ (**i-24**) (0.6 mol%) resulted in dehydrocoupling and the production of DIMER. Shimoi investigated the reaction mechanism by DFT calculations which revealed a stepwise intramolecular pathway (Scheme 1.41). Initially the active catalyst $[Cr(CO)_4]$ (**i-103**) is generated by photodissociation, followed by coordination of the amine-borane to the metal centre forming the σ-complex **i-104**. N-H activation (**i-105**) precedes B-H activation (**i-106**) generating the amino-borane which dissociates from the metal. The resulting dihydride (**i-107**) isomerises to place the hydrides *cis* (**i-108**) allowing reductive elimination of dihydrogen to regenerate the active catalyst.

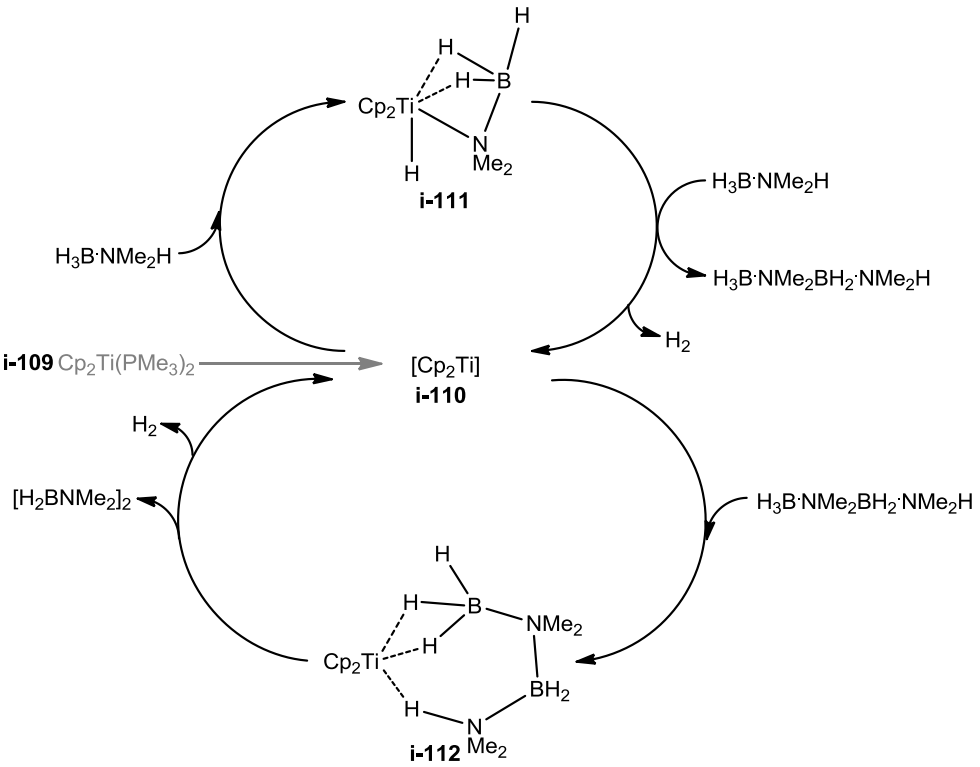


Scheme 1.41 Catalytic cycle for the dehydrocoupling of DMAB by a $[Cr(CO)_6]$ (**i-24**) precatalyst. [Cr] = $[Cr(CO)_4]$.

In 2006 Manners and co-workers reported the efficient catalytic dehydrocoupling of DMAB by $[Cp_2Ti]$ (**i-110**).[123] Computational studies by Ohno and Luo in 2007

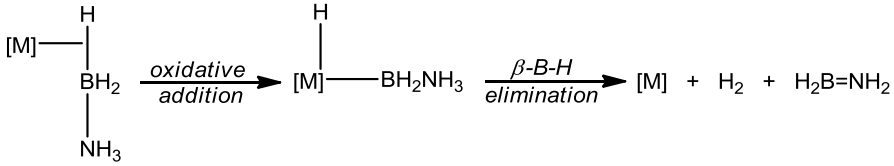
suggested a mechanism involving an intramolecular stepwise process with N-H activation followed by B-H activation to generate MON, which undergoes off-metal dimerisation to generate DIMER.[156] However the later observation by the Manners group of OLIG during catalysis called the Ohno and Luo mechanism into question. Through a combination of mechanistic studies and kinetic modelling the Manners group proposed a two-cycle, four-step mechanism (Scheme 1.42).[139]

Experiments investigating the dehydrocoupling of OLIG did not result in the observation of DMAB or significant quantities of MON (<1%) indicating that OLIG was the sole precursor to DIMER. The proposed Manners mechanism involves the coordination of DMAB to **i-110**, which then undergoes N-H activation to yield the (unobserved) β-B-agostic amido-borane complex [$Cp_2Ti(H)NMe_2BH_3$] (**i-111**). N-H activation resulting in β-B-agostic amido-borane complexes has also been observed for the dehydrocoupling of amine-boranes by zirconium[173] and main group[136] catalysts. The approach of a second molecule of DMAB leads to the formation of a new B-N bond at the metal centre followed by the dissociation of OLIG and loss of dihydrogen from the Ti centre to regenerate **i-110**. The second cycle proceeds *via* coordination of OLIG to the metal centre (**i-112**) which then undergoes a catalytic ring closing process with loss of dihydrogen to release DIMER.



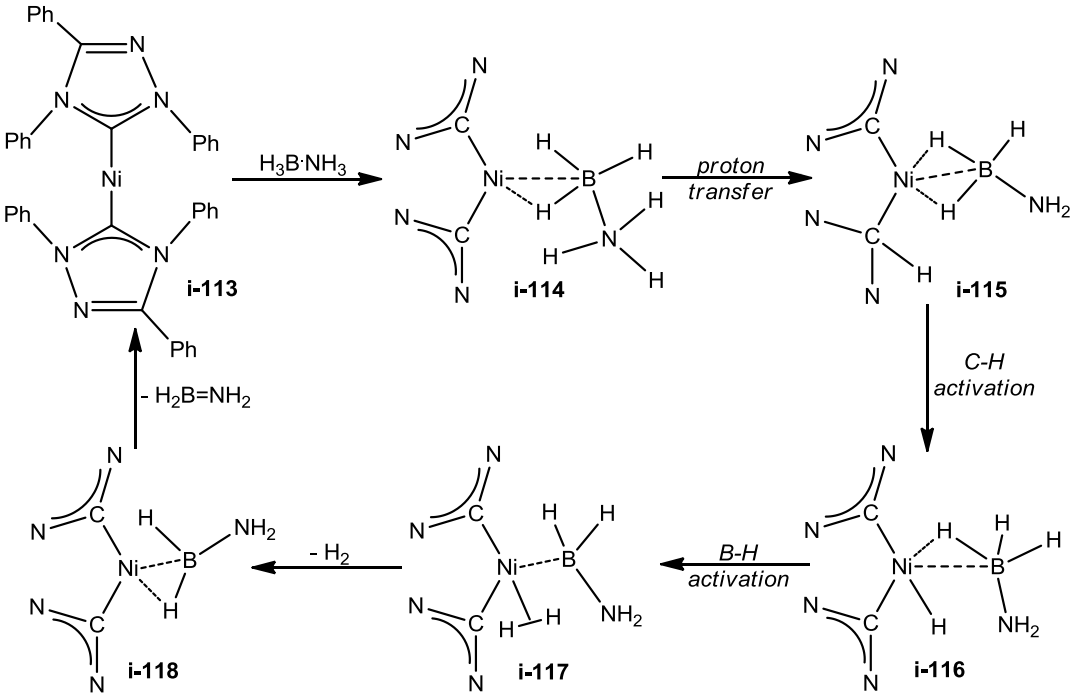
Scheme 1.42 Catalytic cycle for the dehydrocoupling of DMAB by [Cp_2Ti] with proposed intermediates.

Chirik and co-workers have also investigated the reactivity of Group 4 metallocenes with DMAB.[144] In contrast to the mechanism proposed by Manners, they suggest initial B-H oxidative addition to generate a Ti-boryl complex, which on the basis of deuterium experiments was found to be reversible. B-H activation is followed by β-hydride elimination to generate MON, which then dimerises in a mechanism similar to that proposed by Baker for the dehydrocoupling of AB by $Ni(NHC)_2$ (NHC = 2,2'-*bis*-(1,3,4-triphenyl-4,5-dihydro-1H-1,2,4-triazol-5-ylidene) (**i-110**) (Scheme 1.43).[130] The formation of OLIG was not noted.



Scheme 1.43 Proposed initial steps for AB dehydrogenation by a Ni catalyst. [M] = $Ni(NHC)_2$.

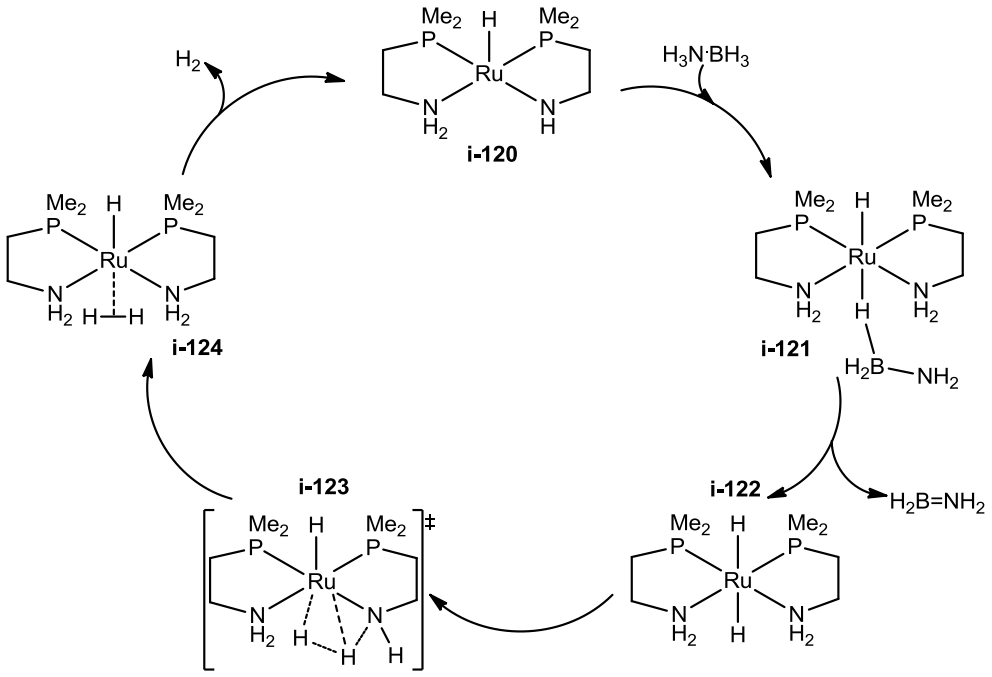
Yang and Hall later computationally investigated the dehydrogenation of AB by Baker's Ni catalyst (**i-113**) (Scheme 1.44).[158] After initial coordination of the AB (**i-114**), they proposed proton transfer from the nitrogen to the carbene to generate **i-115**, in a process related to the outer sphere mechanisms.[153-155] This is followed by transfer to the metal *via* C-H activation (**i-116**). Finally the hydrogen on the boron is transferred to generate H_2 and the amino-borane coordinated to the metal (**i-117**). Loss of H_2 formed **i-118**, followed by loss of the amino-borane to regenerate **i-113**. The calculated kinetic isotope effects were consistent with those observed experimentally by Baker.



Scheme 1.44 Yang and Hall's proposed reaction mechanism for the dehydrogenation of AB by Baker's $Ni(NHC)_2$ catalyst.

Fagnou and co-workers reported the efficient dehydrogenation of AB and MMAB by a ruthenium catalyst, $[Ru(Cl)_2(^iPr_2PCH_2CH_2NH_2)_2]$ (**i-119**) and KO^tBu at low catalyst loadings (0.03 mol%).[154] DFT calculations probed a reaction pathway similar to that involved in alcohol oxidation/reduction; outer sphere hydrogen transfer from the

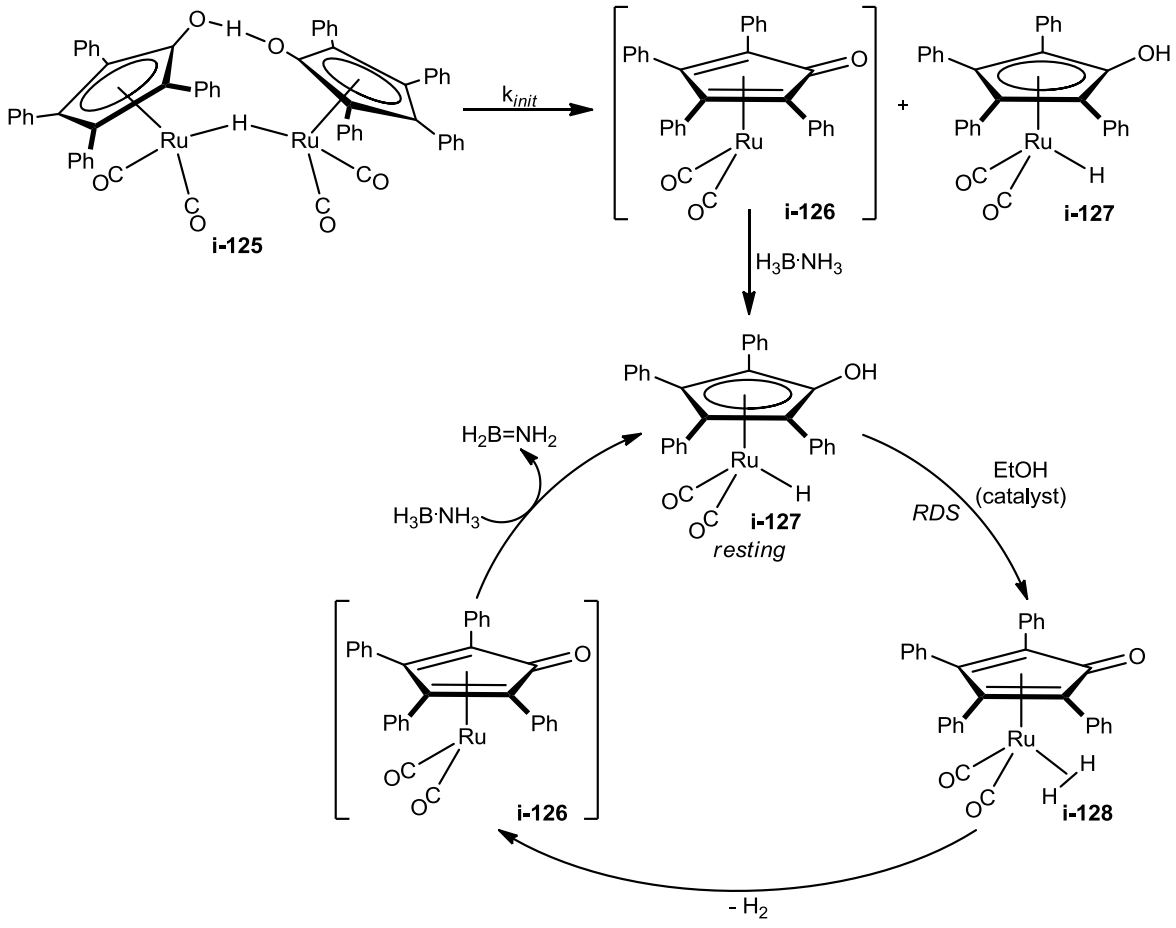
amine-borane to an amide ligand on the Ru metal in the ruthenium hydride species (**i-120**) was found to be energetically favoured (Scheme 1.45). The rate limiting step was found to be the formation of the dihydrogen complex (**i-124**) *via* transition state **i-123**.



Scheme 1.45 Catalytic cycle for the dehydrogenation of AB with Fagnou's Ru catalyst.

Similarly, H-H bond formation was found by Williams and co-workers to be the turnover limiting step during their investigations into the dehydrogenation of AB using Shvo's catalyst, $[(\eta^5\text{-}C_5Ph_4O)_2HRu_2H(CO)_4]$ (**i-125**) (Scheme 1.46).[155, 174] Analysis of the kinetic profile of AB dehydrogenation by **i-125** revealed three different periods of catalysis: catalyst initiation, fast catalysis and finally slow catalysis. The dissociation of **i-125** to generate its reduced monomer **i-127** and its (presumably) oxidised monomer **i-126** is responsible for the initiation period, after which a period of fast catalysis occurs. Williams and co-workers propose that fast catalysis ends due to the hydroboration of **i-126** by $[HBNH]_3$, to give a hydroborated species, which they propose can then dimerise to form a O-B-O and Ru-H-Ru bridged

dimer. The formation of the dimer, and its necessary dissociation prior to further dehydrocoupling, accounts for the observed half-order kinetic dependence on [Ru]. They suggest that the dimer is cleaved by AB, explaining its first-order kinetic dependence. The mechanism by which this occurs was not commented on. Further work by the Williams group has reported on the use of the air-stable catalyst trisacetonitrile μ-hydroxide ruthenium triflate (**i-129**) for the efficient dehydrogenation of AB with the release of up to 4.6 wt% H_2.[175, 176]

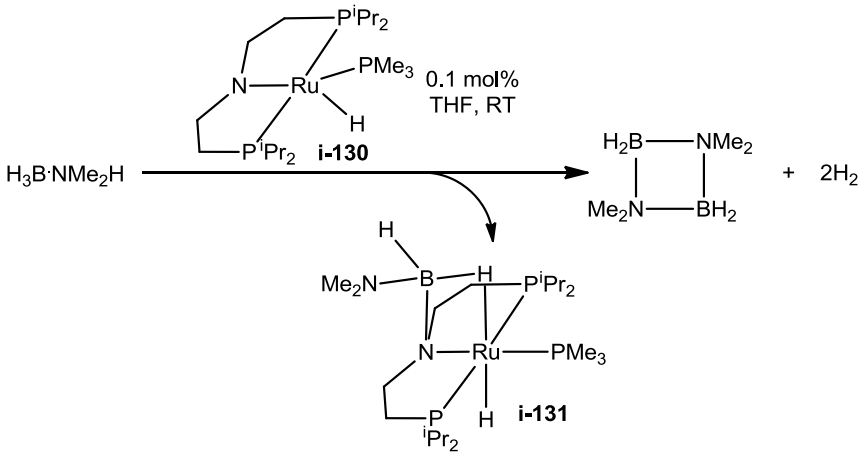


Scheme 1.46 Proposed mechanism for the dehydrogenation of AB by Shvo's catalyst (**i-125**).

At a similar time to the report by Fagnou, Schneider and co-workers reported the dehydrogenation of AB by a ruthenium pincer complex, [Ru(H)(PMe_3)(PNP)] (PNP =

$N(CH_2CH_2P^iPr_2)_2$) (**i-130**), which exhibits comparable activities to Fagnou's catalyst.[153] Mechanistic studies suggested a bifunctional Noyori-Morris mechanism, similar to that suggested by Fagnou.

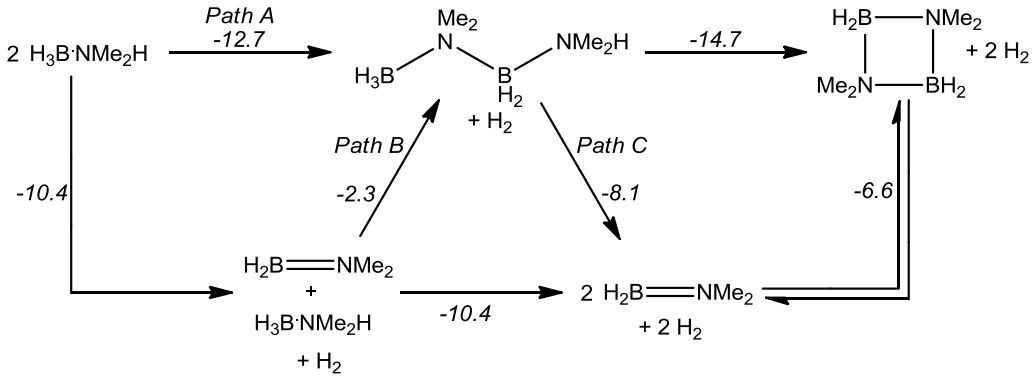
Schneider and co-workers later utilised the Ru-amido pincer complex **i-130** to investigate the dehydrocoupling of DMAB.[141] During dehydrocoupling, the only ruthenium species detected initially was **i-130**. However, a new ruthenium species was soon observed by $^{31}P\{^1H\}$ and ^{11}B NMR spectroscopy (**i-131**) (Scheme 1.47). **i-131**, which can be isolated in 70% yield by the reaction of 2.3 equivalents of DMAB with **i-130**, features a rare M-N-B-H four-membered borametallacycle. **i-131** was found to catalytically dehydrocouple both AB and DMAB; no H_2BNMe_2/H_2BNH_2 metallacycle exchange was seen during the dehydrocoupling of AB, which indicated the inertness of the B-N bond in this ligand.



Scheme 1.47 Dehydrocoupling of DMAB with Schneider's Ru catalyst (**i-130**) and formation of the borametallacycle (**i-131**).

OLIG was also observed to be formed using this catalyst. Thermodynamic calculations and experimental evidence probed the role of the metal in OLIG formation with two possible pathways investigated: Path A, metal-centred dehydrocoupling of 2

molecules of DMAB; and Path B, metal catalysed dehydrogenation of DMAB followed by the uncatalysed rearrangement of MON with DMAB (Scheme 1.48).[141]

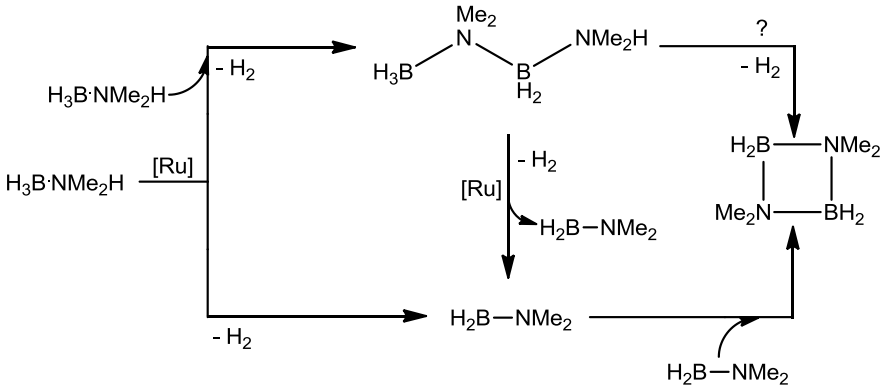


Scheme 1.48 Thermochemistry of the dehydrocoupling of $H_3B{\cdot}NMe_2H$. Free enthalpies in kcal mol^{-1}.

The equilibrium between MON and DIMER is known to be rapid,[177] although the equilibrium lies well on the side of the dimer,[146] and, coupled with the thermodynamic calculations which predicted that a high kinetic barrier prevents Path B occurring, Schneider concluded that OLIG formation occurred *via* metal-centred dehydrocoupling (Path A). This conclusion contrasted that reported by Musgrave *et al.* which suggested on the basis of a computational study that free AB can react with $H_2B{=}NH_2$ to form $H_3B{\cdot}NH_2BH_2{\cdot}NH_3$.[178]

The results of the calculations were supported by experimental evidence; varying the initial concentration of DMAB affected the proportion of MON/OLIG with a greater MON/OLIG at lower substrate concentrations ($[DMAB]_0$ = 0.54 M, [MON]/[OLIG] = 0.44; $[DMAB]_0$ = 0.1 M, [MON]/[OLIG] = 4.03). This demonstrated that not only are MON and OLIG likely to be formed by parallel pathways, but also supported the participation of the metal in the formation of OLIG. MON was also observed as an intermediate in the dehydrocoupling of an independently synthesised sample of OLIG, an observation that has also been noted by the Weller group, suggesting the

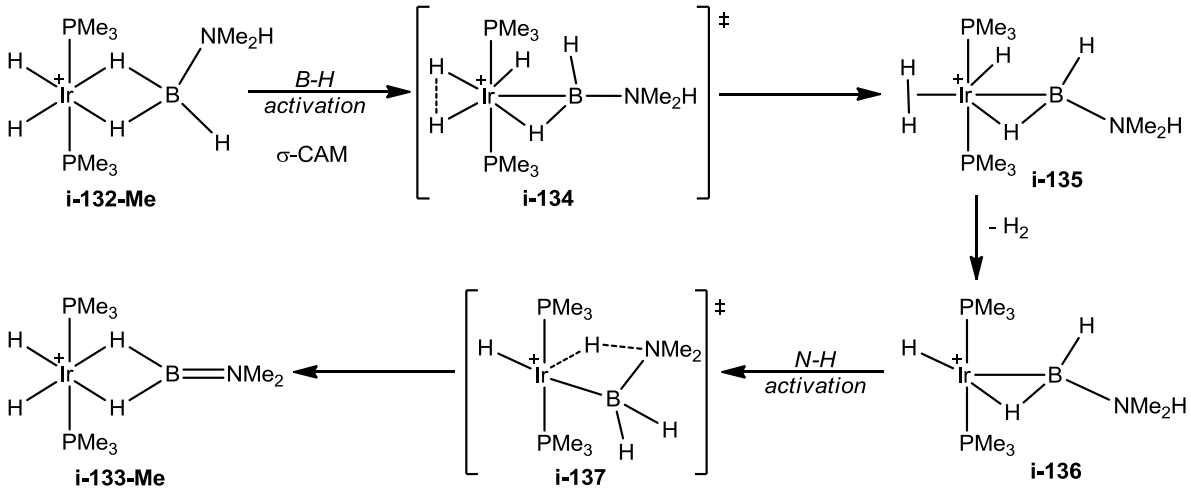
formation of OLIG is reversible.[147, 160] The reversible formation is supported by the thermodynamic calculations, which suggested the B-N bond scission of OLIG to generate DMAB and MON is close to thermoneutral (ΔG = -2.3 kcal mol^{-1}) and therefore the position of the equilibrium is likely to be dependent on their relative concentrations. From these observations and calculations the mechanism in Scheme 1.49 was proposed. Dehydrocyclisation of OLIG mediated by the metal was not probed.



Scheme 1.49 Mechanistic model for the dehydrocoupling of DMAB by Schneider's Ru pincer catalysts. [Ru] = **i-130**.

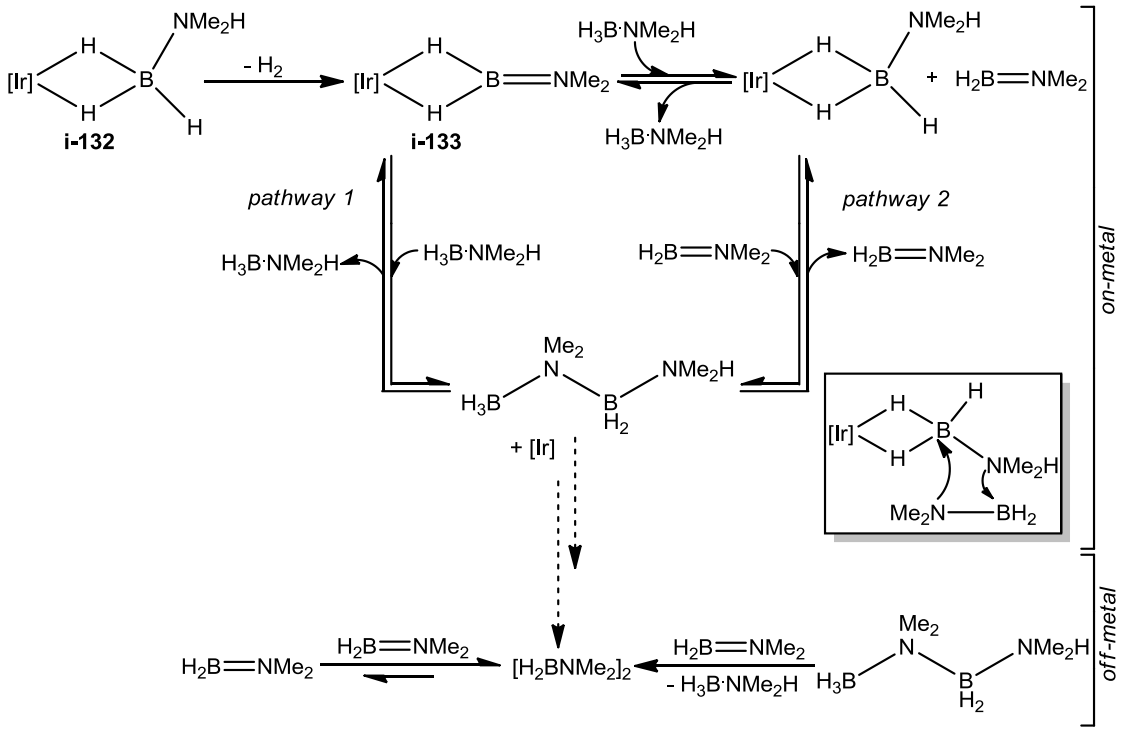
Stevens *et al.* utilised the $\{Ir(H)_2(PCy_3)_2\}^+$ fragment to probe the role of the metal in formation of OLIG.[146] For this iridium system, the formation of OLIG could occur *via* two scenarios; an on-metal process where the metal is involved in both the dehydrogenation of DMAB to give MON and also the oligomerisation; or an off-metal process where the metal is only involved in the dehydrogenation and OLIG is subsequently formed without the involvement of the metal. The combination of 2 molecules of DMAB at iridium to form OLIG, as suggested for the $[Cp_2Ti]$ system (Scheme 1.42),[139] was deemed unlikely as addition of five equivalents of DMAB to $\{Ir(H)_2(PCy_3)_2\}^+$ did not result in the formation of OLIG.

Addition of DMAB to **i-21**, which can lose two molecules of dihydrogen to act as a source of $\{Ir(H)_2(PCy_3)_2\}^+$, led to the formation of $[Ir(H)_2(PCy_3)_2(\eta^2\text{-}H_3B{\cdot}NMe_2H)][BAr^F{}_4]$ (**i-132**). **i-132** is unstable with respect to slow dehydrogenation of the amine-borane yielding the amino-borane complex $[Ir(H)_2(PCy_3)_2(\eta^2\text{-}H_2B{=}NMe_2)][BAr^F{}_4]$ (**i-133**) ($t_{1/2}$ = 24 h, 298 K) (Scheme 1.51), which shares similar characteristics to the $H_2B{=}N^iPr_2$ version **i-92**. DFT calculations investigated the mechanism of dehydrogenation in the related complex $[Ir(H)_2(PMe_3)_2(\eta^2\text{-}H_3B{\cdot}NMe_2H)][BAr^F{}_4]$ (**i-132-Me**) and revealed a σ-CAM (*i.e.* constant oxidation state mechanism) is likely to operate. Initial B-H activation occurs to yield **i-135**, followed by loss of dihydrogen to yield **i-136**. This is followed by β-H N-H transfer to generate $[Ir(H)_2(PMe_3)_2(\eta^2\text{-}H_2B{=}NMe_2)][BAr^F{}_4]$ (**i-133-Me**) (Scheme 1.50). DFT calculations for the related $\{Rh(P^iBu_3)_2\}^+$ system revealed the lowest energy pathways to be initial B-H oxidative addition/N-H transfer or N-H activation followed by B-H transfer to give the coordinated amino-borane complex $[Rh(H)_2(P^iBu_3)_2(\eta^2\text{-}H_2B{=}NMe_2)][BAr^F{}_4]$ (**i-84**).[147] For both systems, the barrier to N-H activation/transfer was higher than B-H activation/transfer.



Scheme 1.50 Mechanism for the dehydrogenation of **i-132-Me** to form **i-133-Me** determined by DFT calculations.

i-133 was used as a latent source of MON allowing the formation of OLIG by an off-metal process to be probed; addition of MeCN formed the known $[Ir(H)_2(PCy_3)_2(NCMe)_2][BAr^F{}_4]$ (**i-138**)[179] releasing free MON, which was followed by immediate addition of DMAB. Monitoring the mixture by ^{11}B, ^{1}H and $^{31}P\{^{1}H\}$ NMR spectroscopy revealed **i-138** to be the only organometallic species present, and importantly no OLIG was detected under these conditions. To interrogate the on-metal route, DMAB was added to a solution of **i-133**; significant quantities of OLIG were detected, suggesting that the formation of OLIG arises from a metal-promoted combination of DMAB and MON, which supports Schneider's suggestion (Scheme 1.49).



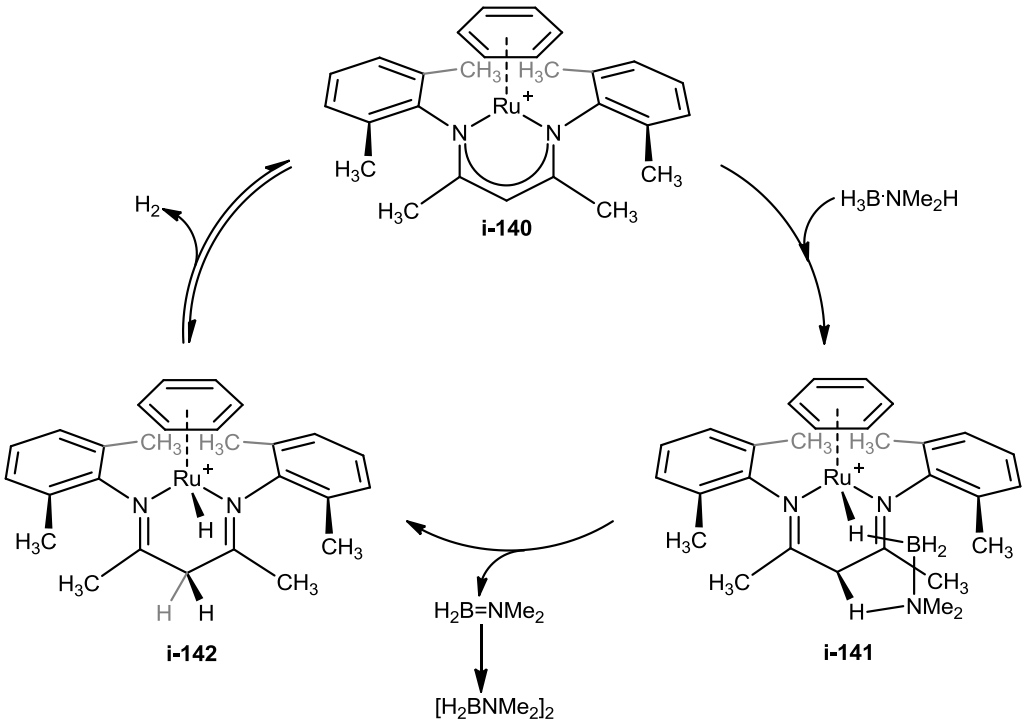
Scheme 1.51 Suggested dehydrogenation/oligomerisation pathway for on- and off-metal processes. Inset shows one possible intermediate for pathway 2. [Ir] = $\{Ir(H)_2(PCy_3)_2\}^+$.

The Weller group also exploited **i-133** as a latent source of MON to measure the rate of off-metal dimerisation of MON to give DIMER. Monitoring the dimerisation by ^{11}B NMR spectroscopy indicated a pseudo-irreversible second-order process where the

equilibrium lies vastly in favour of DIMER. At 298 K and 0.011 M, 50% conversion is observed after 19 minutes (k = 0.080(4) M^{-1} s^{-1}), consistent with the observation of MON during catalysis.

The formation of OLIG is not observed for all catalytic systems.[133, 138, 140, 180] Separate experiments performed by Manners and co-workers tested the dehydrocoupling ability of [{$CpFe(CO)_2$}$_2$] (**i-139**) towards OLIG and a mixture of OLIG and DMAB; no conversion of OLIG to DIMER was observed in either case indicating that OLIG was not an intermediate for the system.[140]

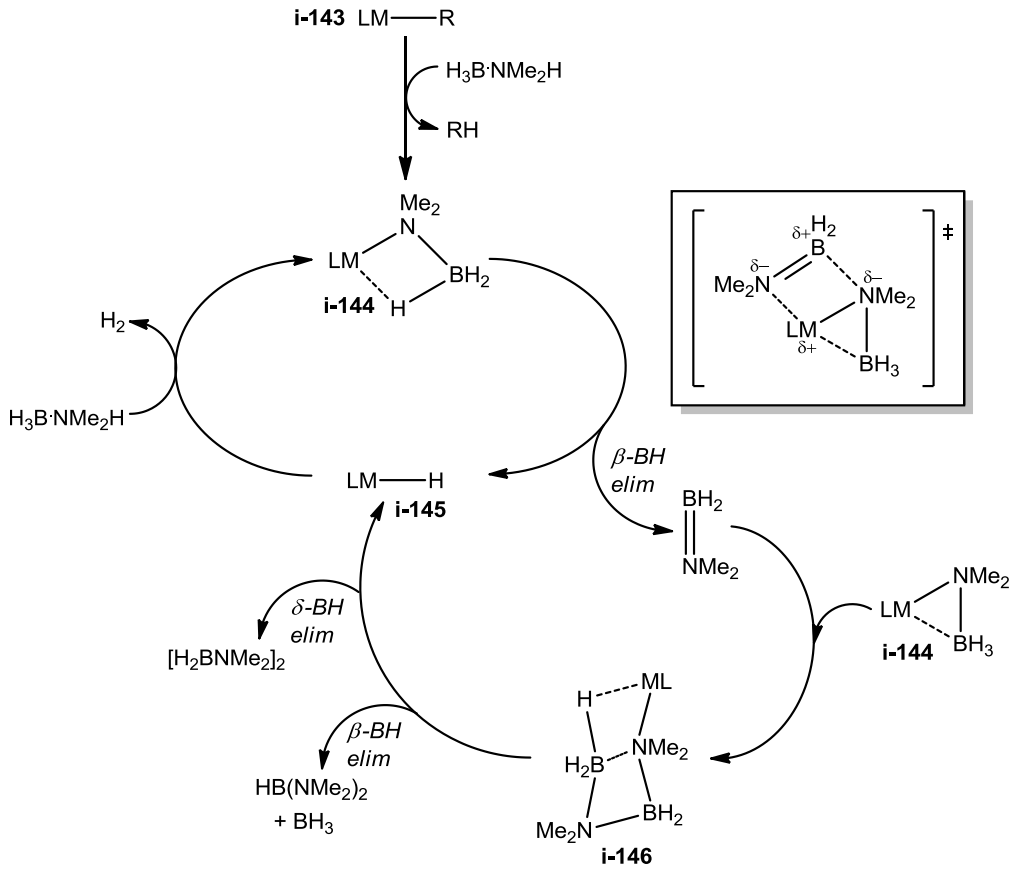
A recent paper by Phillips and co-workers reported the use of a β-diketiminatoarene-substituted Ru(II) complex (**i-140**) for the efficient dehydrocoupling of AB and DMAB (TOF ~360 h^{-1} for DMAB).[181] They proposed the mechanism shown in Scheme 1.52; initial abstraction of the hydridic B-H is followed by protonation of the β-carbon position of the β-diketiminato ligand by the acidic proton of the NMe_2H to form the saturated β-diimine complex **i-142**. **i-142** is speculated to be the true catalyst on the basis of nitrogen/hydrogen experiments: DMAB dehydrocoupling performed in nitrogen-flushed THF which does not allow the rapid formation of **i-142**, showed a reduced rate of dehydrocoupling and shorter induction period compared with the same experiment performed in hydrogen-saturated THF. These findings suggest that the activity of **i-140** is strongly reliant on the rate of formation of the H_2 adduct **i-142**.



Scheme 1.52 Catalytic dehydrocoupling of DMAB by **i-140**. Anions not shown.

Dehydrocoupling of amine-boranes is not limited to transition metal catalysts with a number of main-group species reported to mediate the transformation.[136, 137, 182, 183] Recent work by Hill and co-workers has utilised alkyl and amine Mg and Ca complexes for the dehydrocoupling of DMAB.[136] The observation of MON and coordinated deprotonated OLIG, $[H_3B{\cdot}NMe_2BH_2{\cdot}NMe_2]^-$, during catalysis led to the proposal of the mechanism in Scheme 1.53. Initial N-H activation occurs at **i-143** to yield the amido-borane complex **i-144**. β-B-H elimination from **i-144** leads to the formation of the hydride containing species **i-145** and the release of MON. MON inserts into the amido-borane species **i-144** to form the key catalytic intermediate **i-146** containing the $[H_3B{\cdot}NMe_2BH_2{\cdot}NMe_2]^-$ ion. Hill and co-workers have recently reported indirect evidence for the insertion of MON into additional polarised M-X bonds.[184] From this stage two products are possible; DIMER *via* δ-B-H elimination or the diaminoborane, $HB(NMe_2)_2$, *via* β-B-H elimination. An Al complex which

coordinates $HB(NMe_2)_2$ has recently been reported by Wright and co-workers as a by-product of the dehydrocoupling of DMAB by $Al(NMe_2)_3$.[182]



Scheme 1.53 Catalytic cycle and proposed transition state (inset) for the dehydrocoupling of DMAB by Hill's Group 2 catalysts.

Magnesium-based complexes were found to be more effective at promoting dehydrocoupling than the corresponding calcium complexes. Hill postulates that this order is dependent on the charge density of the Group 2 element centre with a reduction in charge or increase in radius increasing the stability of the resulting amido-borane species (**i-144**) to β-B-H elimination.[185] Investigations have been extended to include other d^0 elements giving the following order of dehydrocoupling activity: Sc > Y > Mg > Ca > Sr, which adds weight to the charge density theory.[137, 185]

As with Manners' [Cp_2Ti] system (Scheme 1.42), d^0 Group 2 elements are found to preferentially N-H activate, forming amido-borane complexes. This contrasts to the reactivity seen for more electron-rich catalytic systems such as rhodium, which proceed *via* B-H oxidative addition (through B-H σ-borane complexes). Sample amido-borane complexes are shown in Figure 1.11.[136] The addition of 1 equivalent of DMAB to [HC{(Me)CN(Dipp)}$_2$Ca{N(SiMe$_3$)$_2$}(THF)] (Dipp = 2,6-di-*iso*propylphenyl) (**i-147**) cleanly produces the amido-borane complex [HC{(Me)CN(Dipp)}$_2$Ca(NMe$_2$BH$_3$)(THF)] (**i-148**). [Mg(NMe$_2$BH$_2$NMe$_2$BH$_3$)$_2$(THF)] (**i-149**), featuring two deprotonated OLIG ligands in the coordination sphere of the magnesium, is formed by the addition of 4 equivalents of DMAB to [Mg{CH(SiMe$_3$)$_2$}(THF)$_2$] (**i-150**).

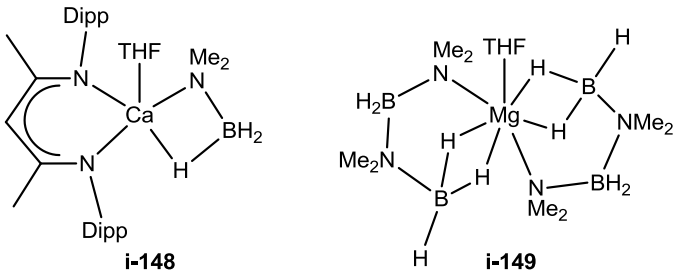
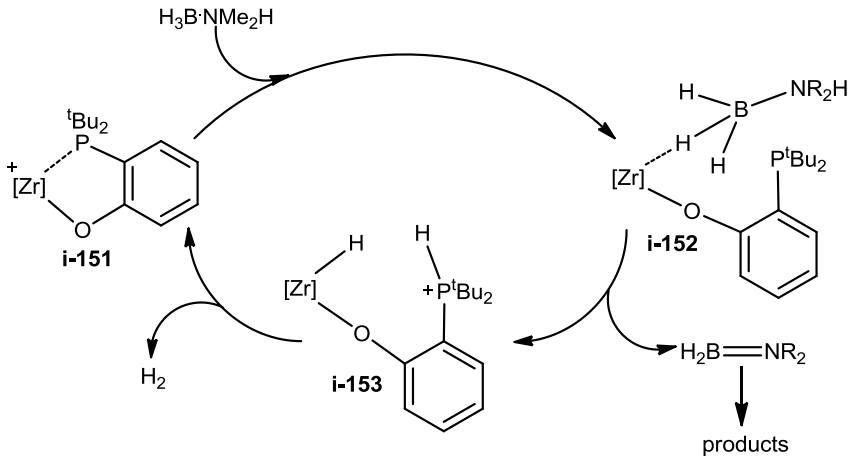


Figure 1.11 Sample Group 2 amido-borane complexes.

Work by Harder and co-workers using Mg, Ca, Zn and Al has focused on their reactivity with AB and primary amine-boranes such as MMAB, with the formation of similar amido-borane complexes observed.[186-191]

In 2010, Bercaw and Miller reported the non-catalytic dehydrogenation of amine-boranes using the frustrated Lewis pair (FLP) $P^tBu_3/B(C_6F_5)_3$.[192] Replacement of the polyfluorinated aryl borane component with an electrophilic transition metal centre such as Zr(IV) by Wass and co-workers led to the catalytic dehydrocoupling of amine-boranes including DMAB.[143] For the dehydrocoupling of DMAB, no OLIG was

observed. Subsequent deuterium experiments utilising deuterated analogues of DMAB lead to the proposal of the mechanism seen in Scheme 1.54. All species in the cycle have been isolated for where [Zr] = Cp_2Zr or Cp^*_2Zr. The mechanism is similar to that proposed by Bercaw and Miller, but for Wass' transition metal containing FLP, dihydrogen loss is more facile allowing catalytic turnover.

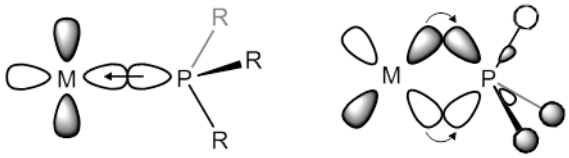


Scheme 1.54 Proposed catalytic cycle for transition metal containing FLPs. [Zr] = Cp_2Zr or Cp^*_2Zr.

1.5 Phosphine ligands

1.5.1 Structure and bonding

Tertiary phosphines, PR_3, are of great importance in organometallic chemistry as they are one of the few series of ligands whose steric and electronic properties can be systematically changed by altering R.[2] Phosphines primarily bind to metals as σ-donor ligands by donation of the lone pair on the phosphorus atom into an empty metal d orbital forming a σ-bond (Figure 1.12). They can also act as π-acceptors, to an extent that depends upon the nature of the R groups present on the PR_3 ligand. π-backdonation occurs from the metal into the σ* orbital of the P-R bond and the phosphorus dπ component.



σ - dσ dπ - σ*/P dπ

Figure 1.12 Interaction of a phosphine ligand with a metal centre.

As the R group becomes more electronegative, the energy of the σ* is lowered, making it more accessible for backbonding; PMe_3 is a weak π-acceptor, while PF_3 is a π-acceptor of similar strength to CO (Figure 1.13).

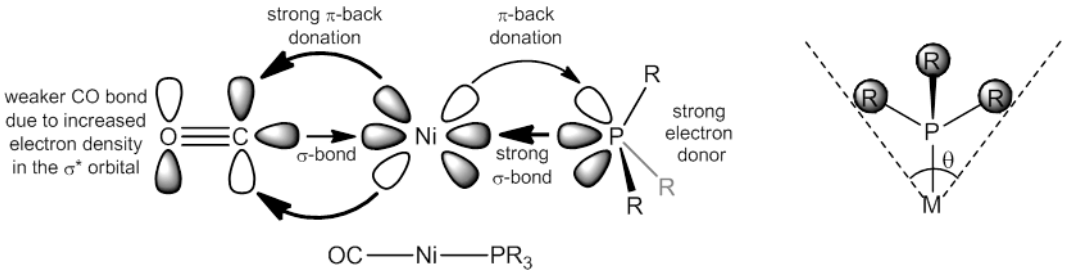
$$PMe_3 \sim P(NR_2)_3 < PAr_3 < P(OMe)_3 < P(OAr)_3 < PCl_3 < PF_3 \sim CO$$

Figure 1.13 Relative π-acidity of various phosphines.

1.5.2 Electronic and steric properties

The electronic properties of phosphines were quantified by Tolman, who compared the *ν*(CO) frequencies of a series of complexes of the type $LNi(CO)_3$ in which L is a phosphine or phosphite (Table 1.1).[193] Measurement of the *ν*(CO) frequency indicates the donor strength of the phosphine; strong donor phosphines increase the electron density on Ni, which transfers some of this increased electron density into the COs by backdonation into the σ* orbital resulting in a weaker CO bond and a lower *ν*(CO). Tolman also quantified the steric effects of phosphines with his cone angle (Table 1.1). The cone angle is obtained by taking a space-filling model of the $M(PR_3)$ group and folding back the R substituents as far as possible; the angle of the cone that will just contain all of the ligand if the metal is at the apex is the cone angle. The steric properties of phosphine ligands have since been refined by Clavier and Nolan.[194]

Table 1.1 *ν*(CO) stretching frequencies for $Ni(CO)_3L$ and cone angles for PR_3. L = PR_3.



PR_3	*ν*(CO) / cm^{-1}	cone angle (θ°)
P^tBu_3	2056	182
PCy_3	2056	170
P^iPr_3	2059	160
PMe_3	2064	118
PPh_3	2069	145
$P(OPh)_3$	2085	128
PF_3	2110	104

1.6 Summary

This thesis builds upon previous results, obtained within the Weller group, into the dehydrocoupling of the secondary amine-borane DMAB, catalysed by rhodium *bis*-phosphine fragments, with a particular focus on the characterisation of intermediate species, the elucidation of catalytic cycles by stoichiometric and kinetic studies, and the use of this knowledge to probe new catalyst types and reactions.

Chapter 2 focuses on the role of the phosphine ligand with regard to the corresponding low-coordinate organometallic species isolated, and investigates their coordination and reactivity with amine-boranes. As part of this an alkene hydroboration catalyst that uses TMAB is developed and studied. Additionally, several fluxional processes pertinent to rhodium and iridium complexes of the model

amine-borane TMAB are examined. Chapter 3 utilises the $\{Rh(PCy_3)_2L_n\}^+$ fragment to develop a generic mechanism for the dehydrocoupling of DMAB by transition metal and main group catalyst systems. Chapter 4 explores the mechanism by which neutral rhodium species catalyse the dehydrocoupling of DMAB, and whether it differs to the cationic rhodium systems researched in Chapter 3.

Overall this thesis provides detailed insight into the dehydrocoupling of DMAB, catalysed by rhodium systems.

1.7 References

1. J. F. Hartwig, *Organotransition Metal Chemistry: From Bonding to Catalysis*, 2010.
2. R. H. Crabtree, *The Organometallic Chemistry of the Transition Metals, Fourth Edition*, John Wiley & Sons: Hoboken, NJ, 2005.
3. J. P. Collman, L. S. Hegedus, J. R. Norton and R. G. Finke, *Principles and Application of Organotransition Metal Chemistry CA*, 1987.
4. N. M. Scott, R. Dorta, E. D. Stevens, A. Correa, L. Cavallo and S. P. Nolan, *J. Am. Chem. Soc.*, 2005, **127**, 3516-3526.
5. M. Ingleson, H. J. Fan, M. Pink, J. Tomaszewski and K. G. Caulton, *J. Am. Chem. Soc.*, 2006, **128**, 1804-1805.
6. P. L. Holland, T. R. Cundari, L. L. Perez, N. A. Eckert and R. J. Lachicotte, *J. Am. Chem. Soc.*, 2002, **124**, 14416-14424.
7. P. J. Zhao, C. Krug and J. F. Hartwig, *J. Am. Chem. Soc.*, 2005, **127**, 12066-12073.
8. P. H. M. Budzelaar, N. N. P. Moonen, R. de Gelder, J. M. M. Smits and A. W. Gall, *Eur. J. Inorg. Chem.*, 2000, 753-769.
9. X. L. Dai, P. Kapoor and T. H. Warren, *J. Am. Chem. Soc.*, 2004, **126**, 4798-4799.
10. J. I. van der Vlugt, E. A. Pidko, D. Vogt, M. Lutz, A. L. Spek and A. Meetsma, *Inorg. Chem.*, 2008, **47**, 4442-4444.
11. H. Braunschweig, K. Radacki, D. Rais and D. Scheschkewitz, *Angew. Chem. Int. Ed.*, 2005, **44**, 5651-5654.
12. N. Arnold, H. Braunschweig, P. Brenner, J. O. C. Jimenez-Halla, T. Kupfer and K. Radacki, *Organometallics*, 2012, **31**, 1897-1907.
13. G. J. Kubas, *Metal Dihydrogen and Sigma Bond Complexes*, Kleuwer Academic/Plenum Publishers, NY, 2001.
14. M. D. Butts, B. L. Scott and G. J. Kubas, *J. Am. Chem. Soc.*, 1996, **118**, 11831-11843.
15. C. Y. Tang, J. Lednik, D. Vidovic, A. L. Thompson and S. Aldridge, *Chem. Commun.*, 2011, **47**, 2523-2525.
16. T. M. Douglas, A. B. Chaplin and A. S. Weller, *Organometallics*, 2008, **27**, 2918-2921.
17. T. M. Douglas, E. Molinos, S. K. Brayshaw and A. S. Weller, *Organometallics*, 2007, **26**, 463-465.
18. S. T. H. Willems, P. H. M. Budzelaar, N. N. P. Moonen, R. de Gelder, J. M. M. Smits and A. W. Gal, *Chem. Eur. J.*, 2002, **8**, 1310-1320.
19. I. Krossing and I. Raabe, *Angew. Chem. Int. Ed.*, 2004, **43**, 2066-2090.
20. M. Bochmann, *Angew. Chem. Int. Ed.*, 1992, **31**, 1181-1182.

21. K. Seppelt, *Angew. Chem. Int. Ed.*, 1993, **32**, 1025-1027.
22. A. G. Massey and A. J. Park, *J. Organomet. Chem.*, 1964, **2**, 245-250.
23. E. Y. X. Chen and T. J. Marks, *Chem. Rev.*, 2000, **100**, 1391-1434.
24. A. B. Chaplin and A. S. Weller, *Eur. J. Inorg. Chem.*, 2010, 5124-5128.
25. I. Krossing and A. Reisinger, *Coord. Chem. Rev.*, 2006, **250**, 2721-2744.
26. C. A. Reed, *Acc. Chem. Res.*, 2010, **43**, 121-128.
27. S. Korbe, P. J. Schreiber and J. Michl, *Chem. Rev.*, 2006, **106**, 5208-5249.
28. E. Molinos, S. K. Brayshaw, G. Kociok-Kohn and A. S. Weller, *Organometallics*, 2007, **26**, 2370-2382.
29. J. Powell, A. Lough and T. Saeed, *J. Chem. Soc. Dalton. Trans.*, 1997, 4137-4138.
30. S. D. Pike, A. L. Thompson, A. s. G. Algarra, D. C. Apperley, S. A. Macgregor and A. S. Weller, *Science*, 2012, **337**, 1648-1651.
31. W. V. Konze, B. L. Scott and G. J. Kubas, *Chem. Commun.*, 1999, 1807-1808.
32. H. Salem, L. J. W. Shimon, G. Leitus, L. Weiner and D. Milstein, *Organometallics*, 2008, **27**, 2293-2299.
33. S. G. Weber, D. Zahner, F. Rominger and B. F. Straub, *Chem. Commun.*, 2012, **48**, 11325-11327.
34. G. J. Kubas, R. R. Ryan, B. I. Swanson, P. J. Vergamini and H. J. Wasserman, *J. Am. Chem. Soc.*, 1984, **106**, 451-452.
35. S. Schlecht and J. F. Hartwig, *J. Am. Chem. Soc.*, 2000, **122**, 9435-9443.
36. W. Jetz and W. A. G. Graham, *Inorg. Chem.*, 1971, **10**, 4-9.
37. P. Gualco, A. Amgoune, K. Miqueu, S. Ladeira and D. Bourissou, *J. Am. Chem. Soc.*, 2011, **133**, 4257-4259.
38. A. B. Chaplin, J. C. Green and A. S. Weller, *J. Am. Chem. Soc.*, 2011, **133**, 13162-13168.
39. W. H. Bernskoetter, C. K. Schauer, K. I. Goldberg and M. Brookhart, *Science*, 2009, **326**, 553-556.
40. D. L. Lichtenberger and A. Rai-Chaudhuri, *J. Chem. Soc. Dalton. Trans.*, 1990, 2161-2166.
41. C. N. Muhoro, X. He and J. F. Hartwig, *J. Am. Chem. Soc.*, 1999, **121**, 5033-5046.
42. S. L. Matthews, V. Pons and D. M. Heinekey, *J. Am. Chem. Soc.*, 2004, **127**, 850-851.
43. R. H. Crabtree, *Angew. Chem. Int. Ed.*, 1993, **32**, 789-805.
44. G. J. Kubas, *Chem. Rev.*, 2007, **107**, 4152-4205.
45. J. Li, R. M. Dickson and T. Ziegler, *J. Am. Chem. Soc.*, 1995, **117**, 11482-11487.
46. R. H. Crabtree and D. G. Hamilton, *J. Am. Chem. Soc.*, 1986, **108**, 3124-3125.
47. D. W. Hart, R. Bau and T. F. Koetzle, *J. Am. Chem. Soc.*, 1977, **99**, 7557-7564.
48. F. L. Taw, H. Mellows, P. S. White, F. J. Hollander, R. G. Bergman, M. Brookhart and D. M. Heinekey, *J. Am. Chem. Soc.*, 2002, **124**, 5100-5108.
49. T. M. Gilbert and R. G. Bergman, *J. Am. Chem. Soc.*, 1985, **107**, 3502-3507.
50. Z. Lin and M. B. Hall, *Coord. Chem. Rev.*, 1994, **135-136**, 845-879.
51. G. Alcaraz, M. Grellier and S. Sabo-Etienne, *Acc. Chem. Res.*, 2009, **42**, 1640-1649.
52. A. F. Borowski, B. Donnadieu, J.-C. Daran, S. Sabo-Etienne and B. Chaudret, *Chem. Commun.*, 2000, 543-544.
53. R. H. Crabtree and M. Lavin, *J. Chem. Soc. Chem. Commun.*, 1985, 1661-1662.
54. M. J. Ingleson, S. K. Brayshaw, M. F. Mahon, G. D. Ruggiero and A. S. Weller, *Inorg. Chem.*, 2005, **44**, 3162-3171.
55. J. A. Iggo, *NMR Spectroscopy in Inorganic Chemistry*, Oxford University Press, Oxford, 1999, Vol. 1983.
56. G. J. Kubas, *Catal. Lett.*, 2005, **104**, 79-101.
57. R. N. Perutz and S. Sabo-Etienne, *Angew. Chem. Int. Ed.*, 2007, **46**, 2578-2592.
58. J. F. Hartwig, C. N. Muhoro, X. He, O. Eisenstein, R. Bosque and F. Maseras, *J. Am. Chem. Soc.*, 1996, **118**, 10936-10937.
59. G. Alcaraz and S. Sabo-Etienne, *Angew. Chem. Int. Ed.*, 2010, **49**, 7170-7179.
60. K. K. Pandey, *Coord. Chem. Rev.*, 2009, **253**, 37-55.

61. G. Alcaraz, E. Clot, U. Helmstedt, L. Vendier and S. Sabo-Etienne, *J. Am. Chem. Soc.*, 2007, **129**, 8704-8706.
62. M. Shimoi, S.-i. Nagai, M. Ichikawa, Y. Kawano, K. Katoh, M. Uruichi and H. Ogino, *J. Am. Chem. Soc.*, 1999, **121**, 11704-11712.
63. A. J. Cowan and M. W. George, *Coord. Chem. Rev.*, 2008, **252**, 2504-2511.
64. T. Kakizawa, Y. Kawano and M. Shimoi, *Organometallics*, 2001, **20**, 3211-3213.
65. Y. Kawano, M. Hashiva and M. Shimoi, *Organometallics*, 2006, **25**, 4420-4426.
66. T. B. Marder, *Angew. Chem. Int. Ed.*, 2007, **46**, 8116-8118.
67. C. W. Hamilton, R. T. Baker, A. Staubitz and I. Manners, *Chem. Soc. Rev.*, 2009, **38**, 279-293.
68. A. Staubitz, A. P. M. Robertson, M. E. Sloan and I. Manners, *Chem. Rev.*, 2010, **110**, 4023-4078.
69. A. Staubitz, A. P. M. Robertson and I. Manners, *Chem. Rev.*, 2010, **110**, 4079-4124.
70. R. H. Crabtree, *Chem. Rev.*, 1985, **85**, 245-269.
71. C. Hall and R. N. Perutz, *Chem. Rev.*, 1996, **96**, 3125-3146.
72. J. A. Labinger and J. E. Bercaw, *Nature*, 2002, **417**, 507-514.
73. W. D. Jones, *Inorg. Chem.*, 2005, **44**, 4475-4484.
74. R. G. Bergman, *Science*, 1984, **223**, 902-908.
75. R. N. Perutz and J. J. Turner, *J. Am. Chem. Soc.*, 1975, **97**, 4791-4800.
76. R. D. Young, A. F. Hill, W. Hillier and G. E. Ball, *J. Am. Chem. Soc.*, 2012, **133**, 13806-13809.
77. J. A. Calladine, S. B. Duckett, M. W. George, S. L. Matthews, R. N. Perutz, O. Torres and K. Q. Vuong, *J. Am. Chem. Soc.*, 2011, **133**, 2303-2310.
78. B. K. McNamara, J. S. Yeston, R. G. Bergman and C. B. Moore, *J. Am. Chem. Soc.*, 1999, **121**, 6437-6443.
79. D. R. Evans, T. Drovetskaya, R. Bau, C. A. Reed and P. D. W. Boyd, *J. Am. Chem. Soc.*, 1997, **119**, 3633-3634.
80. I. Castro-Rodriguez, H. Nakai, P. Gantzel, L. N. Zakharov, A. L. Rheingold and K. Meyer, *J. Am. Chem. Soc.*, 2003, **125**, 15734-15735.
81. M. Brookhart and M. L. H. Green, *J. Organomet. Chem.*, 1983, **250**, 395-408.
82. M. Brookhart, M. L. H. Green and G. Parkin, *Proc. Natl. Acad. Sci. USA*, 2007, **104**, 6908-6914.
83. S. Trofimenko, *J. Am. Chem. Soc.*, 1968, **90**, 4754-4755.
84. A. C. Cooper, W. E. Streib, O. Eisenstein and K. G. Caulton, *J. Am. Chem. Soc.*, 1997, **119**, 9069-9070.
85. A. C. Cooper, E. Clot, J. C. Huffman, W. E. Streib, F. Maseras, O. Eisenstein and K. G. Caulton, *J. Am. Chem. Soc.*, 1999, **121**, 97-106.
86. A. B. Chaplin, R. Tonner and A. S. Weller, *Organometallics*, 2010, **29**, 2710-2714.
87. A. Albinati, P. S. Pregosin and F. Wombacher, *Inorg. Chem.*, 1990, **29**, 1812-1817.
88. M. Lein, *Coord. Chem. Rev.*, 2009, **253**, 625-634.
89. A. C. Albeniz, G. Schulte and R. H. Crabtree, *Organometallics*, 1992, **11**, 242-249.
90. B. Rybtchinski, L. Konstantinovsky, L. J. W. Shimon, A. Vigalok and D. Milstein, *Chem. Eur. J.*, 2000, **6**, 3287-3292.
91. D. Buccella and G. Parkin, *J. Am. Chem. Soc.*, 2006, **128**, 16358-16364.
92. A. Toner, J. Matthes, S. Grundemann, H. H. Limbach, B. Chaudret, E. Clot and S. Sabo-Etienne, *Proc. Natl. Acad. Sci. USA*, 2007, **104**, 6945-6950.
93. L. Mole, J. L. Spencer, N. Carr and A. G. Orpen, *Organometallics*, 1991, **10**, 49-52.
94. J. F. Hartwig, *Organotransition Metal Chemistry*, University Science Books, 2010.
95. R. G. Bergman, *Nature*, 2007, **446**, 506-506.
96. R. H. Crabtree, E. M. Holt, M. Lavin and S. M. Morehouse, *Inorg. Chem.*, 1985, **24**, 1986-1992.
97. M. Albrecht, *Chem. Rev.*, 2010, **110**, 576-623.
98. J. L. Mcbee, J. Escalada and T. D. Tilley, *J. Am. Chem. Soc.*, 2009, **131**, 12703-12713.
99. B. A. Vastine and M. B. Hall, *Coord. Chem. Rev.*, 2009, **253**, 1202-1218.

100. D. Balcells, E. Clot and O. Eisenstein, *Chem. Rev.*, 2010, **110**, 749-823.
101. A. E. Shilov and G. B. Shul'pin, *Chem. Rev.*, 1997, **97**, 2879-2932.
102. R. Dorta, E. D. Stevens and S. P. Nolan, *J. Am. Chem. Soc.*, 2004, **126**, 5054-5055.
103. A. Y. Verat, M. Pink, H. Fan, J. Tomaszewski and K. G. Caulton, *Organometallics*, 2008, **27**, 166-168.
104. N. S. Townsend, A. B. Chaplin, M. Abu Naser, A. L. Thompson, N. H. Rees, S. A. Macgregor and A. S. Weller, *Chem. Eur. J.*, 2010, **16**, 8376-8389.
105. K. Burgess, W. A. Vanderdonk, S. A. Westcott, T. B. Marder, R. T. Baker and J. C. Calabrese, *J. Am. Chem. Soc.*, 1992, **114**, 9350-9359.
106. D. Mannig and H. Noth, *Angew. Chem. Int. Ed.*, 1985, **24**, 878-879.
107. D. A. Evans, G. C. Fu and B. A. Anderson, *J. Am. Chem. Soc.*, 1992, **114**, 6679-6685.
108. I. A. I. Mkhalid, J. H. Barnard, T. B. Marder, J. M. Murphy and J. F. Hartwig, *Chem. Rev.*, 2010, **110**, 890-931.
109. C. M. Crudden and D. Edwards, *Eur. J. Org. Chem.*, 2003, 4695-4712.
110. J. McMurry, *Organic Chemistry*, Brooks/Cole Publishing Company, 1995.
111. B. Carboni and L. Monnier, *Tetrahedron*, 1999, **55**, 1197-1248.
112. R. Wilczynski and L. G. Sneddon, *J. Am. Chem. Soc.*, 1980, **102**, 2857-2858.
113. I. D. Gridnev, N. Miyaura and A. Suzuki, *J. Org. Chem.*, 1993, **58**, 5351-5354.
114. K. Burgess and M. Jaspars, *Organometallics*, 1993, **12**, 4197-4200.
115. G. A. Molander and D. Pfeiffer, *Org. Lett.*, 2001, **3**, 361-363.
116. D. A. Evans, A. R. Muci and R. Stuermer, *J. Org. Chem.*, 1993, **58**, 5307-5309.
117. S. A. Westcott, N. J. Taylor, T. B. Marder, R. T. Baker, N. J. Jones and J. C. Calabrese, *J. Chem. Soc. Chem. Commun.*, 1991, 304-305.
118. C. Gunanathan, M. Holscher, F. Pan and W. Leitner, *J. Am. Chem. Soc.*, 2012, **134**, 14349-14352.
119. J. R. Knorr and J. S. Merola, *Organometallics*, 1990, **9**, 3008-3010.
120. S. Aldridge and D. L. Coombs, *Coord. Chem. Rev.*, 2004, **248**, 535-559.
121. A. B. Chaplin and A. S. Weller, *Angew. Chem. Int. Ed.*, 2010, **49**, 581-584.
122. M. O'Neill, D. A. Addy, I. Riddlestone, M. Kelly, N. Phillips and S. Aldridge, *J. Am. Chem. Soc.*, 2011, **133**, 11500-11503.
123. T. J. Clark, K. Lee and I. Manners, *Chem. Eur. J.*, 2006, **12**, 8634-8648.
124. A. Gutowska, L. Li, Y. Shin, C. M. Wang, X. S. Li, J. C. Linehan, R. S. Smith, B. D. Kay, B. Schmid, W. Shaw, M. Gutowski and T. Autrey, *Angew. Chem. Int. Ed.*, 2005, **44**, 3578-3582.
125. I. Gottker-Schnetmann, P. S. White and M. Brookhart, *Organometallics*, 2004, **23**, 1766-1776.
126. M. C. Denney, V. Pons, T. J. Hebden, D. M. Heinekey and K. I. Goldberg, *J. Am. Chem. Soc.*, 2006, **128**, 12048-12049.
127. A. Staubitz, M. E. Sloan, A. P. M. Robertson, A. Friedrich, S. Schneider, P. J. Gates, J. Gunne and I. Manners, *J. Am. Chem. Soc.*, 2010, **132**, 13332-13345.
128. C. A. Jaska, K. Temple, A. J. Lough and I. Manners, *Chem. Commun.*, 2001, 962-963.
129. C. A. Jaska, K. Temple, A. J. Lough and I. Manners, *J. Am. Chem. Soc.*, 2003, **125**, 9424-9434.
130. R. J. Keaton, J. M. Blacquiere and R. T. Baker, *J. Am. Chem. Soc.*, 2007, **129**, 1844-1845.
131. A. D. Sutton, A. K. Burrell, D. A. Dixon, E. B. Garner, J. C. Gordon, T. Nakagawa, K. C. Ott, P. Robinson and M. Vasiliu, *Science*, 2011, **331**, 1426-1429.
132. P. G. Campbell, L. N. Zakharov, D. J. Grant, D. A. Dixon and S.-Y. Liu, *J. Am. Chem. Soc.*, 2010, **132**, 3289-3291.
133. R. Dallanegra, A. P. M. Robertson, A. B. Chaplin, I. Manners and A. S. Weller, *Chem. Commun.*, 2011, **47**, 3763-3765.
134. I. G. Green, K. M. Johnson and B. P. Roberts, *J. Chem. Soc. Perkin Trans. 2*, 1989, 1963-1972.
135. C. A. Jaska and I. Manners, *J. Am. Chem. Soc.*, 2004, **126**, 9776-9785.

136. D. J. Liptrot, M. S. Hill, M. F. Mahon and D. J. MacDougall, *Chem. Eur. J.*, 2010, **16**, 8508-8515.
137. M. S. Hill, M. Hodgson, D. J. Liptrot and M. F. Mahon, *Dalton Trans.*, 2011, **40**, 7783-7790.
138. Y. Kawano, M. Uruichi, M. Shimoi, S. Taki, T. Kawaguchi, T. Kakizawa and H. Ogino, *J. Am. Chem. Soc.*, 2009, **131**, 14946-14957.
139. M. E. Sloan, A. Staubitz, T. J. Clark, C. A. Russell, G. C. Lloyd-Jones and I. Manners, *J. Am. Chem. Soc.*, 2010, **132**, 3831-3841.
140. J. R. Vance, A. P. M. Robertson, K. Lee and I. Manners, *Chem. Eur. J.*, 2011, **17**, 4099-4103.
141. A. Friedrich, M. Drees and S. Schneider, *Chem. Eur. J.*, 2009, **15**, 10339-10342.
142. C. Y. Tang, A. L. Thompson and S. Aldridge, *J. Am. Chem. Soc.*, 2010, **132**, 10578-10591.
143. A. M. Chapman, M. F. Haddow and D. F. Wass, *J. Am. Chem. Soc.*, 2011, **133**, 8826-8829.
144. D. Pun, E. Lobkovsky and P. J. Chirik, *Chem. Commun.*, 2007, 3297-3299.
145. M. Vogt, B. de Bruin, H. Berke, M. Trincado and H. Grutzmacher, *Chem. Sci.*, 2011, **2**, 723-727.
146. C. J. Stevens, R. Dallanegra, A. B. Chaplin, A. S. Weller, S. A. Macgregor, B. Ward, D. McKay, G. Alcaraz and S. Sabo-Etienne, *Chem. Eur. J.*, 2011, **17**, 3011-3020.
147. T. M. Douglas, A. B. Chaplin, A. S. Weller, X. Z. Yang and M. B. Hall, *J. Am. Chem. Soc.*, 2009, **131**, 15440-15456.
148. J. A. Widegren and R. G. Finke, *J. Mol. Catal. A: Chem.*, 2003, **198**, 317-341.
149. J. A. Widegren, M. A. Bennett and R. G. Finke, *J. Am. Chem. Soc.*, 2003, **125**, 10301-10310.
150. K. S. Weddle, J. D. Aiken and R. G. Finke, *J. Am. Chem. Soc.*, 1998, **120**, 5653-5666.
151. M. A. Watzky and R. G. Finke, *J. Am. Chem. Soc.*, 1997, **119**, 10382-10400.
152. Y. S. Chen, J. L. Fulton, J. C. Linehan and T. Autrey, *J. Am. Chem. Soc.*, 2005, **127**, 3254-3255.
153. M. Kass, A. Friedrich, M. Drees and S. Schneider, *Angew. Chem. Int. Ed.*, 2009, **48**, 905-907.
154. N. Blaquiere, S. Diallo-Garcia, S. I. Gorelsky, D. A. Black and K. Fagnou, *J. Am. Chem. Soc.*, 2008, **130**, 14034-14035.
155. Z. Lu, B. L. Conley and T. J. Williams, *Organometallics*, 2012, **31**, 6705-6714.
156. Y. Luo and K. Ohno, *Organometallics*, 2007, **26**, 3597-3600.
157. A. Paul and C. B. Musgrave, *Angew. Chem. Int. Ed.*, 2007, **46**, 8153-8156.
158. X. Z. Yang and M. B. Hall, *J. Am. Chem. Soc.*, 2008, **130**, 1798-1799.
159. T. M. Douglas, A. B. Chaplin and A. S. Weller, *J. Am. Chem. Soc.*, 2008, **130**, 14432-14433.
160. A. B. Chaplin and A. S. Weller, *Inorg. Chem.*, 2010, **49**, 1111-1121.
161. R. Dallanegra, A. B. Chaplin and A. S. Weller, *Angew. Chem. Int. Ed.*, 2009, **48**, 6875-6878.
162. S. Aldridge, A. J. Downs, C. Y. Tang, S. Parsons, M. C. Clarke, R. D. L. Johnstone, H. E. Robertson, D. W. H. Rankin and D. A. Wann, *J. Am. Chem. Soc.*, 2009, **131**, 2231-2243.
163. A. B. Chaplin and A. S. Weller, *Acta Crystallogr., Sect. C: Cryst. Struct. Commun.*, 2011, **67**, M355-M358.
164. G. Alcaraz, L. Vendier, E. Clot and S. Sabo-Etienne, *Angew. Chem. Int. Ed.*, 2010, **49**, 918-920.
165. W. J. Shaw, J. C. Linehan, N. K. Szymczak, D. J. Heldebrant, C. Yonker, D. M. Camaioni, R. T. Baker and T. Autrey, *Angew. Chem. Int. Ed.*, 2008, **47**, 7493-7496.
166. L. Euzenat, D. Horhant, Y. Ribourdouille, C. Duriez, G. Alcaraz and M. Vaultier, *Chem. Commun.*, 2003, 2280-2281.
167. D. J. Grant and D. A. Dixon, *J. Phys. Chem. A*, 2006, **110**, 12955-12962.
168. B. L. Kormos and C. J. Cramer, *Inorg. Chem.*, 2003, **42**, 6691-6700.
169. G. Alcaraz, A. B. Chaplin, C. J. Stevens, E. Clot, L. Vendier, A. S. Weller and S. Sabo-Etienne, *Organometallics*, 2010, **29**, 5591-5595.

170. C. Y. Tang, A. L. Thompson and S. Aldridge, *Angew. Chem. Int. Ed.*, 2010, **49**, 921-925.
171. C. Y. Tang, N. Phillips, J. I. Bates, A. L. Thompson, M. J. Gutmann and S. Aldridge, *Chem. Commun.*, 2012, **48**, 8096-8098.
172. D. Vidovic, D. A. Addy, T. Kramer, J. McGrady and S. Aldridge, *J. Am. Chem. Soc.*, 2011, **133**, 8494-8497.
173. T. D. Forster, H. M. Tuononen, M. Parvez and R. Roesler, *J. Am. Chem. Soc.*, 2009, **131**, 6689-6691.
174. B. L. Conley and T. J. Williams, *Chem. Commun.*, 2010, **46**, 4815-4817.
175. B. L. Conley and T. J. Williams, *J. Am. Chem. Soc.*, 2010, **132**, 1764-1765.
176. B. L. Conley, D. Guess and T. J. Williams, *J. Am. Chem. Soc.*, 2011, **133**, 14212-14215.
177. H. Noth and Vahrenka.H, *Chem. Ber. Recl.*, 1967, **100**, 3353-3354.
178. P. M. Zimmerman, A. Paul, Z. Y. Zhang and C. B. Musgrave, *Inorg. Chem.*, 2009, **48**, 1069-1081.
179. O. W. Howarth, C. H. Mcateer, P. Moore and G. E. Morris, *J. Chem. Soc. Dalton. Trans.*, 1981, 1481-1485.
180. T. Miyazaki, Y. Tanabe, M. Yuki, Y. Miyake and Y. Nishibayashi, *Organometallics*, 2011, **30**, 2394-2404.
181. D. F. Schreiber, C. O'Connor, C. Grave, Y. Ortin, H. Müller-Bunz and A. D. Phillips, *ACS Catal.*, 2012, 2505-2511.
182. H. J. Cowley, M. S. Holt, R. L. Melen, J. M. Rawson and D. S. Wright, *Chem. Commun.*, 2011, **47**, 2682-2684.
183. M. M. Hansmann, R. L. Melen and D. S. Wright, *Chem. Sci.*, 2011, **2**, 1554-1559.
184. P. Bellham, M. S. Hill, G. Kociok-Kohn and D. J. Liptrot, *Dalton Trans.*, 2013.
185. P. Bellham, M. S. Hill, D. J. Liptrot, D. J. MacDougall and M. F. Mahon, *Chem. Commun.*, 2011, **47**, 9060-9062.
186. S. Harder and J. Spielmann, *Chem. Commun.*, 2011, **47**, 11945-11947.
187. J. Spielmann, M. Bolte and S. Harder, *Chem. Commun.*, 2009, 6934-6936.
188. J. Spielmann and S. Harder, *J. Am. Chem. Soc.*, 2009, **131**, 5064-5065.
189. J. Spielmann and S. Harder, *Dalton Trans.*, 2011, **40**, 8314-8319.
190. J. Spielmann, G. Jansen, H. Bandmann and S. Harder, *Angew. Chem. Int. Ed.*, 2008, **47**, 6290-6295.
191. J. Spielmann, D. F. J. Piesik and S. Harder, *Chem. Eur. J.*, 2010, **16**, 8307-8318.
192. A. J. M. Miller and J. E. Bercaw, *Chem. Commun.*, 2010, **46**, 1709-1711.
193. C. A. Tolman, *Chem. Rev.*, 1977, **77**, 313-348.
194. H. Clavier and S. P. Nolan, *Chem. Commun.*, 2010, **46**, 841-861.

2 B-H and C-H Activation Processes

2.1 Introduction

The importance of low-coordinate, and often low-valent, metal centres to C-H and B-H activation processes has been discussed in depth in Chapter 1. This chapter details the synthesis of a low-coordinate metal complex of empirical formula $[Rh(P^tBu^iBu_2)_2][BAr^F_4]$, followed by an investigation into its reactivity with the tertiary amine-borane, TMAB, a model substrate of relevance to the dehydrocoupling of amine-boranes. This is followed by a detailed mechanistic investigation into the role of $[Rh(P^tBu^iBu_2)_2][BAr^F_4]$ as a catalyst in the hydroboration of alkenes by amine-boranes.

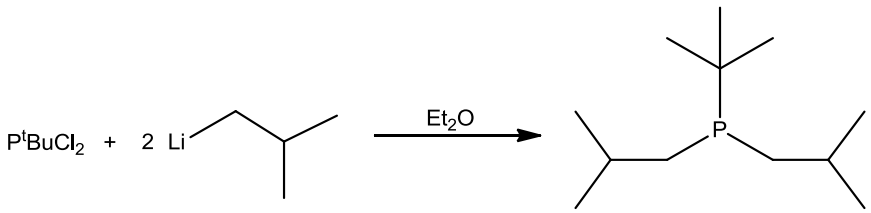
The latter section of this chapter investigates several of the fluxional processes that σ-complexes of TMAB can undergo. These are correlated with preliminary computational investigations performed on one of the fluxional processes by Prof. Stuart A. Macgregor (Heriot-Watt University).

2.2 Synthesis of a low-coordinate rhodium complex

The Weller group has previously reported on the synthesis of the formally 12 electron rhodium(I) complex $[Rh(P^iBu_3)_2][BAr^F_4]$ (**i-80**) *via* the loss (or removal by a sacrificial acceptor) of dihydrogen from $[Rh(H)_2(P^iBu_3)_2][BAr^F_4]$ (**i-83**).[1] Complex **i-80** is particularly interesting as it is formally 12-electron and thus is related to the catalytically important $Pd(PR_3)_2$.[2, 3] **i-80** undergoes oxidative addition reactions with dihydrogen or aryl halides[4] and catalyses the dehydrocoupling of the secondary

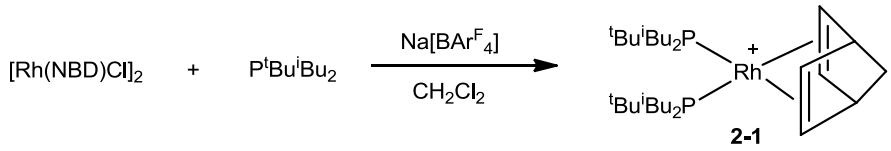
amine-borane, $H_3B{\cdot}NMe_2H$ (DMAB).[5, 6] Although trapping experiments using ligands such as C_6H_5F and $ClCH_2CH_2Cl$ indicated a Rh(I) formulation for **i-80**, a definitive solid-state structure could not be obtained due to extensive disorder in the solid-state.

We reasoned that a subtle change in the phosphine might well enforce a different packing regime in the solid-state and allow the determination of the solid-state structure of $[Rh(PR_3)_2][BAr^F{}_4]$. As such, we targeted the synthesis of the new mixed phosphine $P^tBu^iBu_2$. The phosphine was synthesised by Joseph A. B. Abdalla (summer student in the Weller group). Addition of an ethereal solution of P^tBuCl_2 to *iso*-butyllithium in Et_2O at 0 °C, followed by a 3 hour reflux and subsequent workup produced $P^tBu^iBu_2$ in a good yield (69%) (Scheme 2.1). ^1H and $^{31}P\{^1H\}$ NMR data were as expected and are reported in full in the experimental section (Chapter 5).



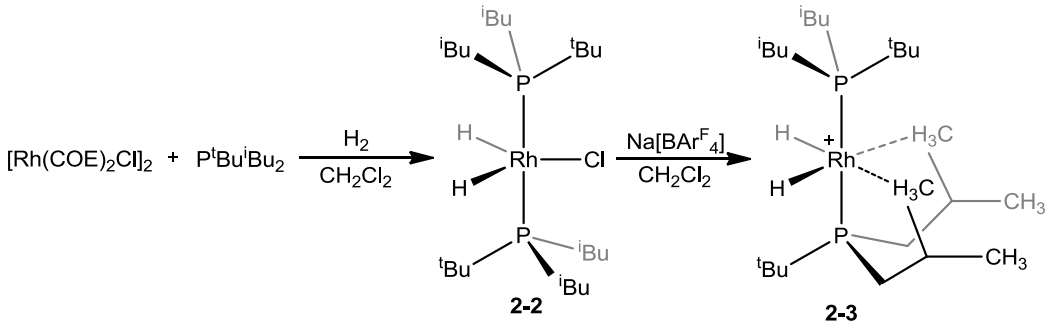
Scheme 2.1 Synthesis of the new phosphine, $P^tBu^iBu_2$.

The Rh(I) *bis*-phosphine NBD complex, $[Rh(P^tBu^iBu_2)_2(NBD)][BAr^F{}_4]$ (**2-1**), was targeted as a suitable precursor to $[Rh(P^tBu^iBu_2)][BAr^F{}_4]$, and was synthesised by an analogous route to the synthesis of $[Rh(P^iBu_3)_2(NBD)][BAr^F{}_4]$ (Scheme 2.2).[1] NMR data for **2-1** were analogous to other known NBD complexes,[1, 7] but a low yield of only 30% was obtained as compared with the P^iBu_3 analogue (83%).[1] Presumably this was due to the added steric bulk of $P^tBu^iBu_2$ compared with P^iBu_3 forcing alternative, deleterious pathways. In line with this, the related NBD complex containing P^tBu_3 cannot be prepared.[8]



Scheme 2.2 Synthesis of $[Rh(P^tBu^iBu_2)_2(NBD)][BAr^F_4]$ (**2-1**). $[BAr^F_4]^-$ anions not shown.

Due to the low yield obtained for **2-1**, an alternative complex, $Rh(H)_2(P^tBu^iBu_2)_2Cl$ (**2-2**) was synthesised from the addition of $P^tBu^iBu_2$ to $[Rh(COE)_2Cl]_2$ in CH_2Cl_2 under a hydrogen atmosphere (Scheme 2.3). Recrystallisation from pentane at -80 °C gave complex **2-2** as yellow crystals in good yield (70%). The ^1H NMR spectrum of **2-2** revealed equivalent hydrides [δ -22.84 ppm (dt, 2H, $^1J_{RhH}$ = 27.7 Hz, $^2J_{PH}$ = 15.5 Hz)], which appear as a doublet in the $^1H\{^{31}P\}$ NMR spectrum. One phosphorus environment showing coupling to a rhodium(III) metal centre [δ 44.9 (d, $^1J_{RhP}$ = 115 Hz)] was observed in the $^{31}P\{^1H\}$ NMR spectrum.[9] Complex **2-2** was additionally characterised by elemental microanalysis (CHN).



Scheme 2.3 Synthesis of $Rh(H)_2(P^tBu^iBu_2)_2Cl$ (**2-2**) and $[Rh(H)_2(P^tBu^iBu_2)_2][BAr^F_4]$ (**2-3**). $[BAr^F_4]^-$ anions not shown.

Addition of 1 equivalent of $Na[BAr^F_4]$ to **2-2** in CH_2Cl_2 or C_6H_5F abstracts the chloride ($NaCl_{(s)}$), generating $[Rh(H)_2(P^tBu^iBu_2)_2][BAr^F_4]$ (**2-3**) in good isolated yield after recrystallisation (71%) (Scheme 2.3). Slow diffusion of pentane into a CH_2Cl_2 solution of **2-3** afforded crystals suitable for single crystal X-ray diffraction. In the solid-state, **2-3** crystallises with two independent cations in the unit cell, both of which are

disordered equally over crystallographically imposed inversion centres, and have similar structural metrics. The cations adopt a *trans* phosphine / *cis* dihydride arrangement of ligands, which is completed by two agostic[10] C-H interactions from *iso*-butyl groups on the same phosphine, which makes the cation approximately C_s symmetric (Figure 2.1). This contrasts the C_2 symmetric arrangement of the agostic ligands in the P^iBu_3 analogue, although the Rh1···C bond distances of 2.940(9) Å (C7) and 2.820(8) Å (C3) are broadly similar [*viz.* 2.90(3) Å and 2.891(5) Å in the P^iBu_3 analogue].[1] The rather weak nature of these interactions reflects their position relative to the high *trans* influence hydride ligands.[11] The interactions are, however, strong enough to cause more compressed Rh–P–C angles for the *iso*-butyl groups involved in agostic bonding, *cf.* P1–C1–C2, 108.6(10)° *versus* P2–C17–C18, 125.4(11)°.

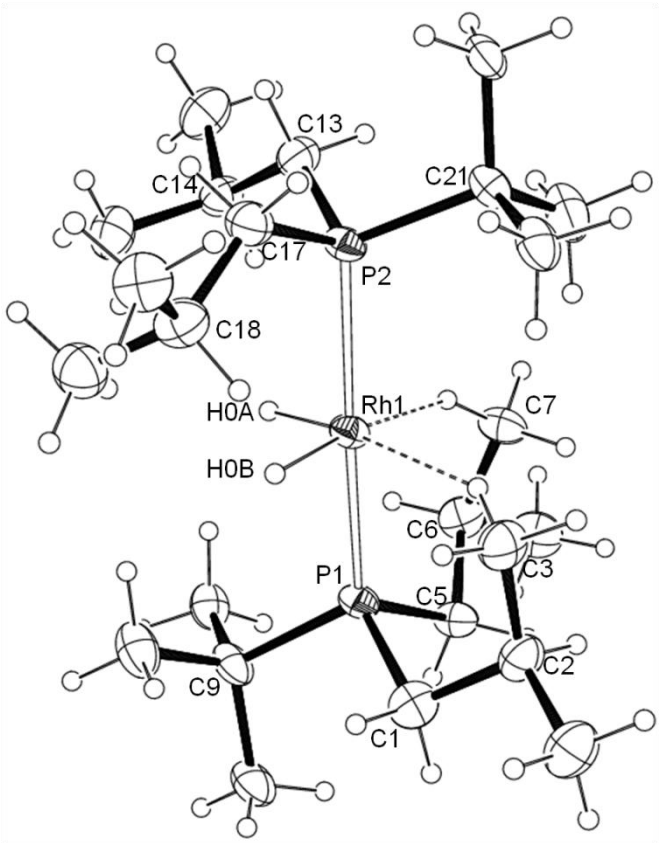
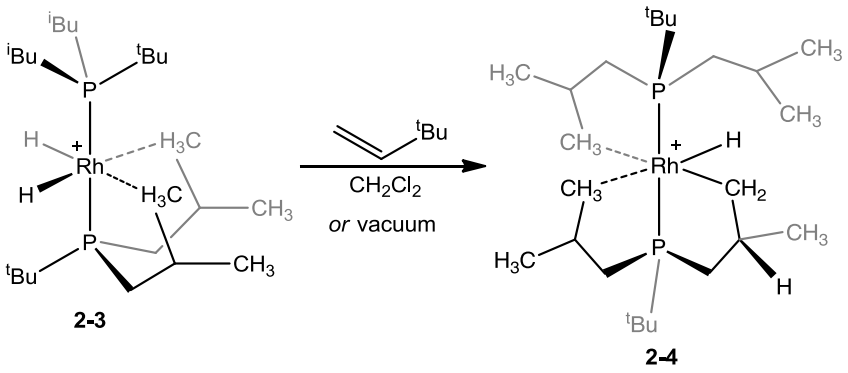


Figure 2.1 Solid-state structure of one of the independent cations in the unit cell for **2-3**. Disordered components and $[BAr^F{}_4]^-$ anion are not shown. Displacement ellipsoids are given at the 30% probability level. Selected bond lengths and angles: Rh1···C7, 2.940(9) Å; Rh1···C3, 2.820(8) Å; Rh1-P1 2.24(2) Å; Rh1-H0A, 1.457(11) Å; Rh1-H0B, 1.448(11) Å; P1-C5-C6, 108.8(9)°; P1-C1-C2, 108.6(20)°; P2-C17-C18, 125.4(11)°; P2-C13-C14, 124.2(12)°.

Analysis of **2-3** by ^1H and $^{31}P\{^1H\}$ NMR spectroscopy revealed the presence of one phosphine environment [δ 56.9 ppm (d, $^1J_{RhP}$ = 109 Hz)], two diastereotopic ^{i}Bu groups [δ 0.89 ppm (d, 12H, $^3J_{HH}$ = 6.5 Hz, ^{i}Bu{Me}), 0.81 ppm (d, 12H, $^3J_{HH}$ = 6.5 Hz, ^{i}Bu{Me})], and one hydride environment [δ -22.03 ppm (dt, $^1J_{RhH}$ = 47.1 Hz, $^2J_{PH}$ = 13.3 Hz)] indicating that in solution at room temperature (298 K) the cation of **2-3** is fluxional and adopts a time-averaged symmetry that renders the phosphine ligands equivalent on the ^1H and ^{31}P NMR timescales, in contrast to the solid-state structure. The relatively large $^1J_{RhH}$ value for the metal hydrides in **2-3** (47.1 Hz) is consistent with the weak *trans* influence of the agostic interactions. Cooling a sample of **2-3** in

CD_2Cl_2 to 190 K revealed no high-field signals corresponding to the agostic CH_3 groups observed in the solid-state, suggesting that rapid exchange on the ^1H NMR timescale is occurring between the free and agostic CH_3 groups. Similar behaviour was observed for the P^iBu_3 analogue.[1] Analysis by ESI-MS revealed a molecular ion at *m/z* 509.29 [M^+] (calc. 509.29) with the correct isotopic pattern. An IR spectrum of **2-3** displays a broad absorbance at 2671 cm^{-1} and is assigned as a C-H stretching frequency of the agostic CH_3 groups.[12] Caulton[12] and Nolan[13] have reported Rh(III) and Ir(III) *bis*-phosphine and *bis*-*N*-heterocyclic carbene complexes (*e.g.* **i-44**), which feature *bis*-agostic interactions similar to those observed with **2-3**.

Addition of the sacrificial hydrogen acceptor *tert*-butylethylene, TBE, to a solution of **2-3** in CH_2Cl_2 rapidly generates the new complex **2-4** of empirical formula $[Rh(P^tBu^iBu_2)_2][BAr^F_4]$ (Scheme 2.4) in 70% isolated yield. Loss of hydrogen can also be promoted by placing a solid sample under a dynamic vacuum, however this is much slower with an approximate half life, $t_{1/2}$ of ~15 hours (6 x 10^{-2} mbar). ESI-MS [m/z, 507.28 [M^+] (calc. 507.28), with the correct isotopic pattern] and elemental microanalysis (CHN) results were in agreement with the proposed empirical formula for complex **2-4**.



Scheme 2.4 Reaction of **2-3** with TBE to yield $[Rh(P^tBu^iBu_2)_2][BAr^F_4]$ (**2-4**). $[BAr^F_4]^-$ anions not shown.

Crystals of **2-4** suitable for single crystal X-ray diffraction were grown by slow diffusion of pentane into a CH_2Cl_2 solution of **2-4** at 2 °C. Complex **2-4** crystallises with two independent cations in the unit cell, both of which are disordered equally over crystallographically imposed inversion centres. The solid-state structure demonstrates ε-C-H activation of an *iso*-butyl group forming a Rh(III) metallacycle, Rh1-C3 2.151(15) Å (Figure 2.2). Two relatively close Rh···C interactions [Rh1···C7 2.811(13) Å and Rh1···C15 2.981(13) Å)] indicate that as in **2-3**, **2-4** is a *bis*-agostic complex, which is supported by an observed broad absorbance at 2684 cm^{-1} in the IR spectrum and upfield signals in the ^1H NMR spectrum characteristic of agostic C-H resonances (*vide infra*). The coordination environment of the rhodium(III) centre is completed by a hydride, which was not located crystallographically, but its presence was confirmed by ^1H NMR spectroscopy. The hydride is presumed, on the basis of NMR spectroscopy and the structural analysis, to be located in the vacant coordination site of the crystallographic model for **2-4**, *trans* to the agostic C-H interaction from C7.

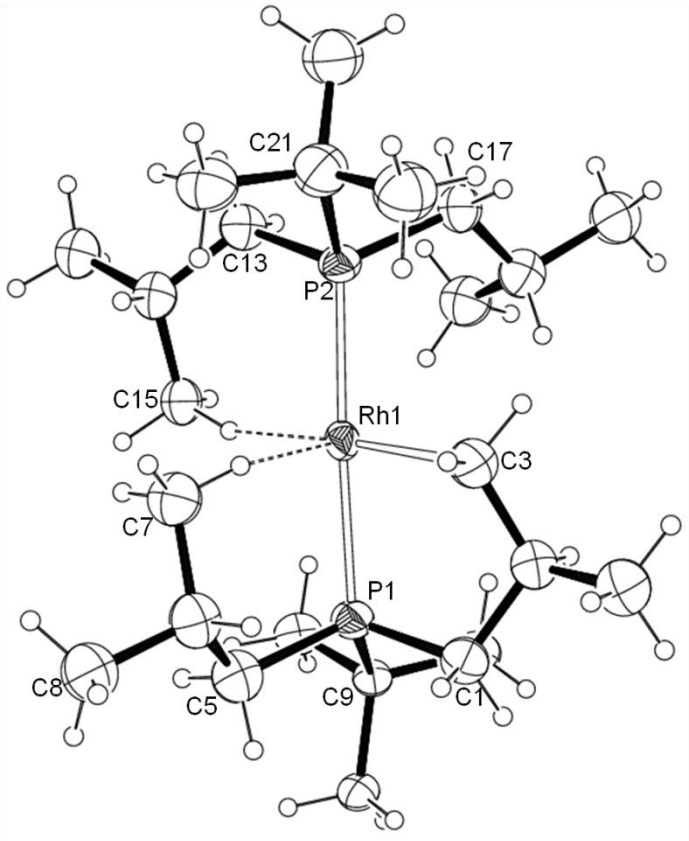


Figure 2.2 Solid-state structure of one of the independent cations in the unit cell for **2-4**. Disordered components and $[BAr^F_4]^-$ anion are not shown. Displacement ellipsoids are given at the 30% probability level. The hydride ligand on Rh1 was not located, but is proposed to sit *cis* to C3. Selected bond lengths and angles: Rh1-C3, 2.152(15) Å; Rh1···C7, 2.811(13) Å; Rh1···C15, 2.981(13) Å; Rh1-P1, 2.312(15) Å; Rh1-P2, 2.312(15) Å; P1-C1-C2, 106.9(12)°; P2-C13-C14, 116.3(11)°; P2-C17-C18, 117.3(10)°; P1-C5-C6, 116.1(11)°.

In solution at room temperature, resonances in the $^{31}P\{^1H\}$ and ^1H NMR spectra are broad, indicating a fluxional process is occurring. Cooling to 173 K in CD_2Cl_2 halts the fluxionality, revealing four closely related species. In the ^1H NMR spectrum four hydride resonances (total integral 1H) are observed as broad doublets with unresolved additional coupling around δ -22 ppm, all of which show coupling to ^{103}Rh ($^1J_{RhH}$ ~ 24 Hz) (Figure 2.3, lower inset). In the $^1H\{^{31}P\}$ NMR spectrum these signals are observed to sharpen to doublets. Between δ 0.25 and -0.34 ppm (total relative integral of 6H) several broad peaks are observed, assigned to the agostic interactions from the ^{i}Bu CH_3 groups seen in the solid-state (Figure 2.3, upper inset).

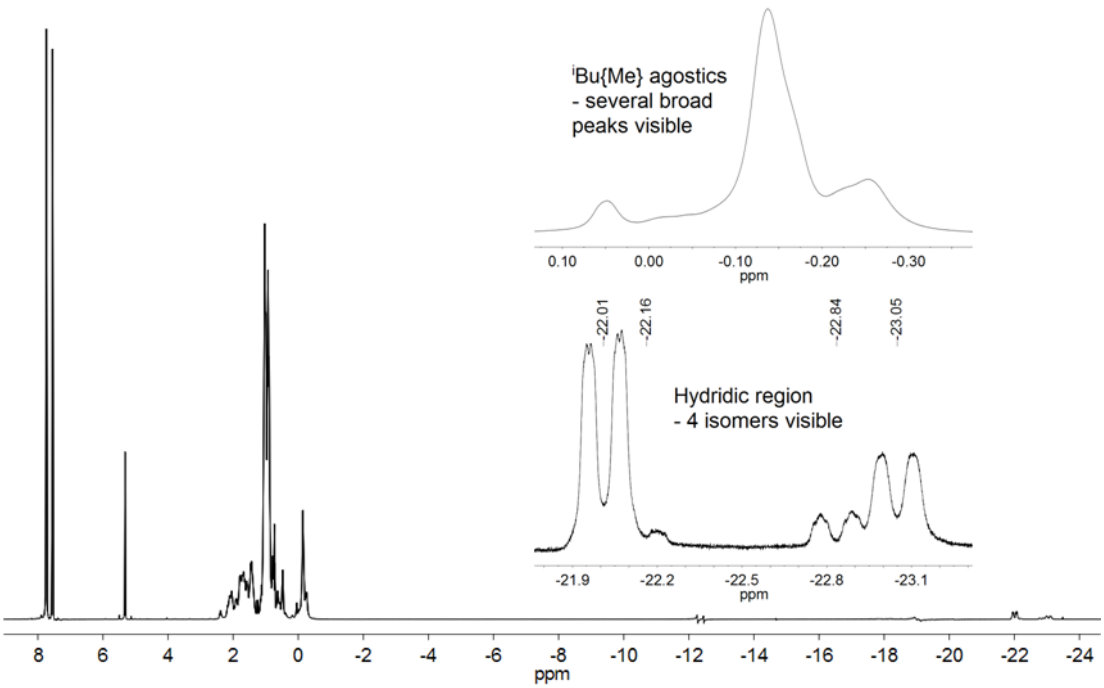


Figure 2.3 ^{1}H NMR spectrum (CD_2Cl_2) of **2-4** at 173 K. Insets show the agostic (upper) and hydridic (lower) regions.

Four pairs of phosphine environments are observed in the $^{31}P\{^{1}H\}$ NMR spectrum that show mutual *trans* ^{31}P-^{31}P coupling ($^{2}J_{PP}$ ~300 Hz) on a rhodium(III) centre ($^{1}J_{RhP}$ ~ 115 Hz) (Figure 2.4).[9]

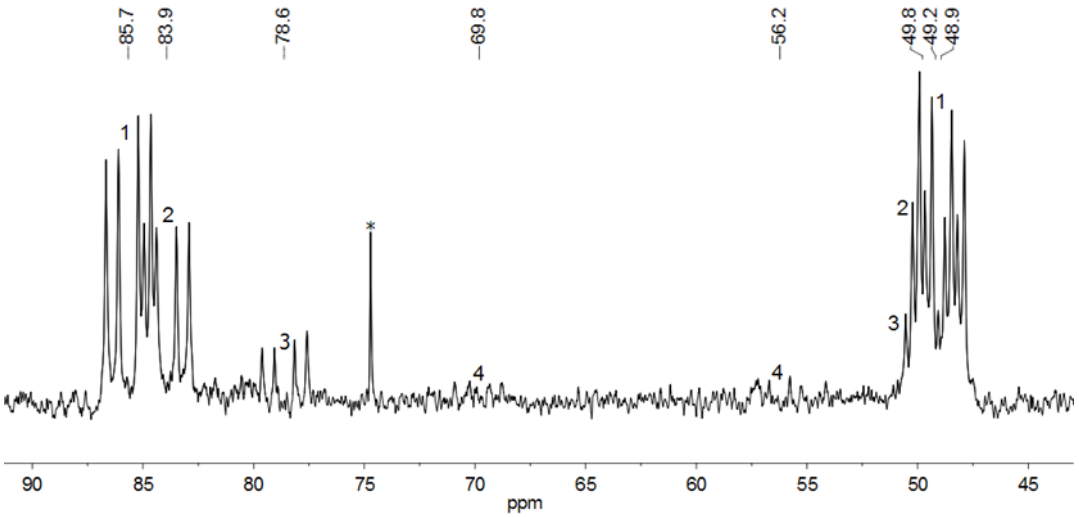


Figure 2.4 $^{31}P\{^{1}H\}$ NMR spectrum (CD_2Cl_2) of **2-4** at 173 K. * = $HP^{t}Bu^{i}Bu_2^{+}$.

This low temperature data is fully consistent with the observed solid-state structure. We suggest that the observation of four isomers results from a difference in the

position of C-H activation from the diastereotopic ^{i}Bu phosphine groups (*e.g.* C3, C4, Figure 2.5). The relatively narrow chemical shift range for the hydride environments argues for a similar structure for the four species observed.

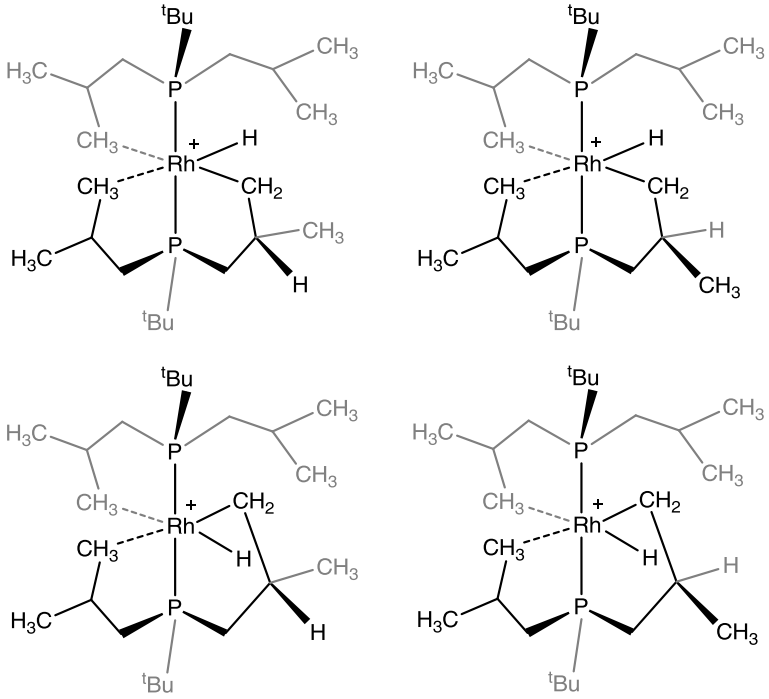


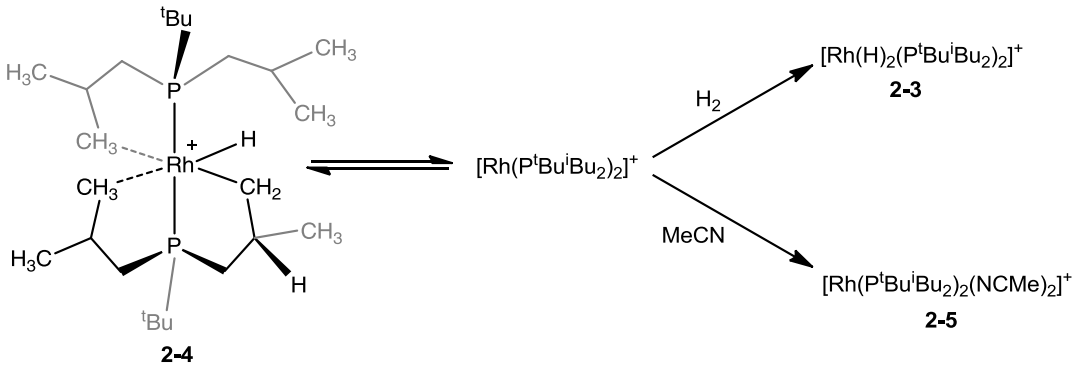
Figure 2.5 Representations of four possible isomers of **2-4** observed in solution at low temperature that arise from C-H activation of the diastereotopic ^{i}Bu CH_3 groups. $[BAr^F_4]^-$ anions not shown.

The structure of complex **2-4** is in contrast to that for $[Rh(P^iBu_3)_2][BAr^F_4]$ for which no cyclometalation was observed at low temperature by NMR spectroscopy.[1] The facile cyclometalation on incorporation of a *tert*-butyl group is directly connected to Shaw's "*gem-tert-butyl*" effect[14] as well as the more general influence of a phosphine's steric bulk on the ability of its C-H bonds to interact with metal centres.[12]

2.2.1 Reactivity of 2-4

While the solid-state structure and low temperature NMR data indicate a Rh(III) species, the room temperature NMR data for **2-4** indicates a fluxional process is occurring. As **2-4** reacts with dihydrogen and acetonitrile presumably *via* a

rhodium(I) species, we suggest that the fluxional process is one that rapidly equilibrates the Rh(I) with the Rh(III) cyclometalated species *via* reversible H-C(sp^3) bond cleavage (Scheme 2.5). Such behaviour has previously been noted by Caulton and co-workers who observed that the Rh(I) complex [(^{t}Bu$_2$PCh$_2$SiMe$_2$)$_2$N]Rh (**i-56**) is in rapid equilibrium with a cyclometalated Rh(III) hydride species (**i-55**) where a *tert*-butyl group has undergone C-H activation.[15] Others have also noted reversible cyclometalation.[16-22]



Scheme 2.5 Reactivity of **2-4** with dihydrogen and acetonitrile *via* the unobserved Rh(I) intermediate. [BAr$^F{}_4$]$^-$ anions not shown.

Addition of dihydrogen to **2-4** rapidly reforms the Rh(III) dihydride species **2-3**, while addition of acetonitrile immediately forms the *trans bis*-acetonitrile adduct [Rh(P^{t}Bu^{i}Bu$_2$)$_2$(NCMe)$_2$][BAr$^F{}_4$] (**2-5**). The quick formation of the *trans* isomer is in contrast to the reactivity observed for the P^{i}Bu$_3$ analogue, which slowly converts from the *cis* isomer to the *trans* isomer (24 hours).[8] Presumably the observed difference is due to the added steric bulk of P^{t}Bu^{i}Bu$_2$ increasing the amount of steric repulsion between the phosphines, forcing them to adopt the *trans* configuration. The assignment of the phosphines in complex **2-5** as *trans* is based upon the observed Rh-P coupling constant ($^1J_{RhP}$ = 128 Hz) in the $^{31}P\{^1H\}$ NMR spectrum and a comparison to those reported for [Rh(P^{i}Bu$_3$)$_2$(NCMe)$_2$][BAr$^F{}_4$] (*cis,* $^1J_{RhP}$ = 176 Hz; *trans*, $^1J_{RhP}$ =

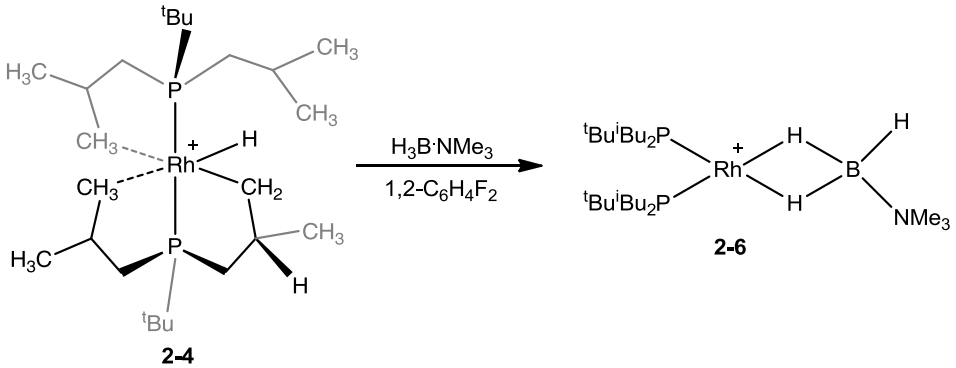
125 Hz). The smaller coupling constant for the *trans* isomer is a result of the relatively high *trans* influence of the phosphine ligand,[11] resulting in a weaker M-X bond and hence a reduced coupling constant. The high *trans* influence of a phosphine ligand has been noted by Meek and co-workers in $[Rh(ttp)L]^+$ [ttp = $PhP(CH_2CH_2CH_2PPh_2)_2$, L = ligand].[23] When L = PEt_3 the *trans* Rh-P coupling constant was 113 Hz, a significant reduction in comparison to when L = NCMe ($^1J_{RhP}$ = 152 Hz). Unlike the P^iBu_3 analogue which was only characterised *in situ* by $^{31}P\{^1H\}$ NMR spectroscopy, **2-5** was more thoroughly characterised by ^1H and $^{31}P\{^1H\}$ NMR spectroscopy, elemental microanalysis (CHN) and ESI-MS. The Rh-P coupling constant of the related *trans*-$[Rh(P^iPr_3)_2(NCMe)_2][BAr^F_4]$ has recently been reported; the observed value of 128 Hz is the same as for **2-5**.[24] The solid-state structure of *trans*-$[Rh(PCy_3)_2(NCMe)_2][BF_4]$ has also been reported, but no NMR data were given.[25]

The addition of fluorobenzene to **2-4** might be expected to lead to the formation of the 18 electron complex $[Rh(P^tBu^iBu_2)_2(\eta^6\text{-}C_6H_5F)][BAr^F_4]$ where coordination of a molecule of fluorobenzene acts to stabilise the 12 electron $\{Rh(P^tBu^iBu_2)_2\}^+$ fragment. Such behaviour has previously been observed for the P^iBu_3 analogue amongst others.[26-28] However, no evidence for coordination is seen by ^1H and $^{31}P\{^1H\}$ NMR spectroscopy, with data identical to those for **2-4** and no upfield shifted aromatic signals for coordinated fluorobenzene observed. The added steric bulk of the *tert*-butyl group is likely preventing coordination of the fluorobenzene. Likewise, **2-4** does not form a benzene adduct. Consistent with these observations, **2-4** does not promote C-X activation with alkyl halides, likely due to its inability to form a Rh(I) η-complex with the arene prior to oxidative cleavage. This is in contrast to $\{Rh(P^iBu_3)_2\}^+$ which

oxidatively cleaves a range of aryl halides to form dimeric dications such as $[Rh(P^iBu_3)_2(C_6H_5)(\mu\text{-}Cl)]_2[BAr^F{}_4]_2$.[1, 4]

2.2.1.1 Reactivity of 2-4 with TMAB

Further indication that complex **2-4** is in rapid equilibrium with a Rh(I) $\{Rh(P^tBu^iBu_2)_2\}^+$ species is that it also reacts with $H_3B{\cdot}NMe_3$ (TMAB), forming the highly air-sensitive purple Rh(I) σ-complex $[Rh(P^tBu^iBu_2)_2(\eta^2\text{-}H_3B{\cdot}NMe_3)][BAr^F{}_4]$ (**2-6**) (Scheme 2.6). The P^iPr_3 and P^iBu_3 analogues have previously been reported.[6, 24] The reactivity with TMAB is of relevance to the dehydrocoupling of amine-boranes catalysed by transition metal catalysts due to their propensity to react *via* σ-complexes. As mentioned in Chapter 1, the lack of N-H functionality on TMAB allows it to act as a model for the binding of primary and secondary amine-boranes, which would rapidly react further by B-H then N-H transfer and lose dihydrogen. Complex **2-6** has been characterised by a combination of ^1H, $^{31}P\{^1H\}$ and ^{11}B NMR spectroscopy, ESI-MS, elemental microanalysis (CHN) and X-ray crystallography.



Scheme 2.6 Formation of $[Rh(P^tBu^iBu_2)_2(\eta^2\text{-}H_3B{\cdot}NMe_3)][BAr^F{}_4]$ (**2-6**). $[BAr^F{}_4]^-$ anions not shown.

Notable in the ^1H NMR spectrum of **2-6** is the presence of a quadrupolar-broadened relative 3H integral signal at δ -2.80 ppm. In the ^{11}B NMR spectrum, a 34.1 ppm downfield shifted signal is observed for coordinated TMAB (δ 26.8 ppm), compared

with the free amine-borane ligand (δ -7.3 ppm). Both these spectroscopic markers are indicative of 3-centre 2-electron Rh-H-B interactions that are undergoing fast exchange on the NMR timescale between terminal B-H and bridging B-H-Rh sites.[6, 24, 29, 30] The ^{11}B shift lies in between those observed for the P^iBu_3 (δ 23.1 ppm)[6] and P^iPr_3 (δ 28.8 ppm)[24] analogues indicating that the Rh···H_3B interaction in **2-6** lies between the two, with a greater downfield shift in the ^{11}B NMR spectrum indicative of a tighter interaction (*i.e.* P^iPr_3 analogue).[26] In the ^{1}H NMR spectrum, a more hydridic resonance for the B-H atoms is also suggestive of a greater Rh···H_3B interaction, and correlating with the ^{11}B NMR data, the resonance for **2-6** (δ -2.80 ppm) is in between those observed for the P^iBu_3 (δ -2.12 ppm)[6] and P^iPr_3 (δ -3.09 ppm)[24] analogues. The solid-state structure reveals an approximate Rh···B distance of 2.18 Å which is the same as that reported for $[Rh(P^iBu_3)_2(\eta^2\text{-}H_3B{\cdot}NMe_3)][BAr^F{}_4]$ (**i-81a**) (2.180(4) Å). However, the X-ray data is of poor quality and as such cannot be used to do draw too many conclusions. The structure presented in Figure 2.6 is only to confirm bond connectivity.

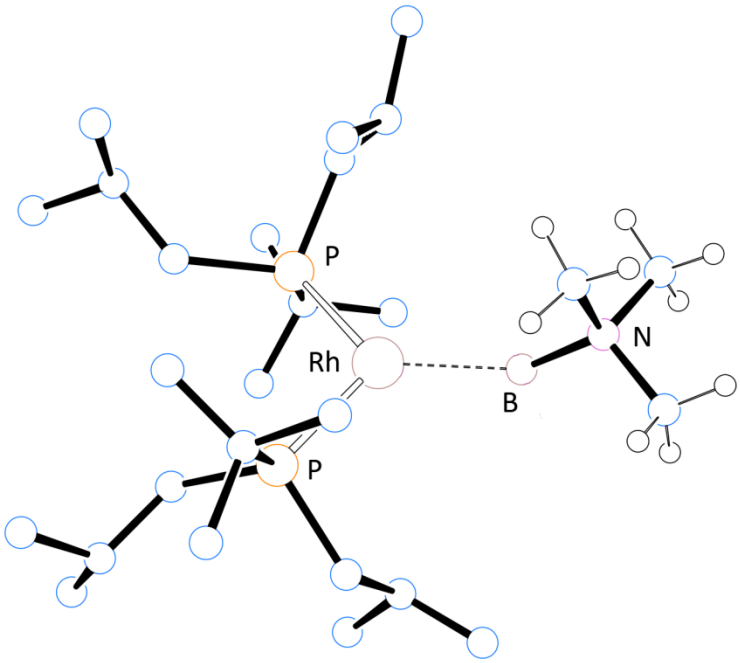
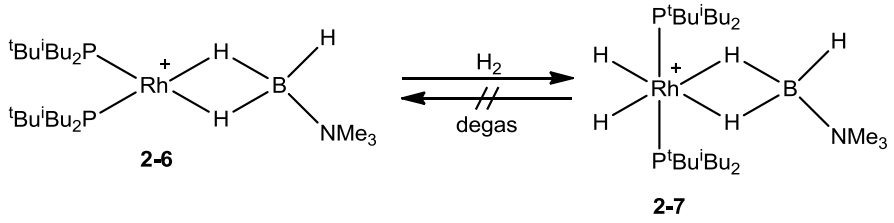


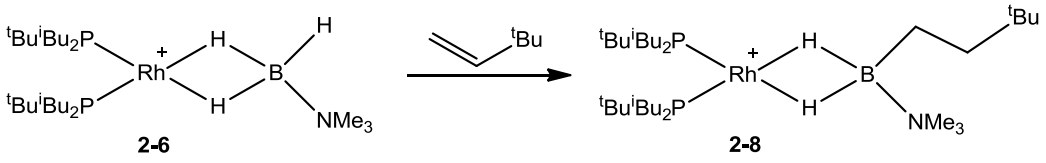
Figure 2.6 Ball and stick representation of a partially refined structure of **2-6**. Hydrogen atoms placed in calculated positions. Anions and most hydrogen atoms omitted for clarity. The X-ray data is of poor quality and the structure presented here is only to confirm bond connectivity. Selected crystallographic data: Tetragonal, $P4_2/n$, a = 29.6685(8) Å, c = 19.7362(4) Å.

Addition of hydrogen (1 atm or 4 atm) generates the colourless Rh(III) σ-complex $[Rh(H)_2(P^tBu^iBu_2)_2(\eta^2\text{-}H_3B{\cdot}NMe_3)][BAr^F{}_4]$ (**2-7**) (Scheme 2.7) on time of mixing, which was characterised *in situ* by NMR spectroscopy in comparison with the P^iBu_3 and P^iPr_3 analogues.[6, 24] The formation of a Rh(III) compound is confirmed by a rhodium-phosphorus coupling of 110 Hz in the $^{31}P\{^1H\}$ NMR spectrum[9] and the presence of a hydridic signal [δ -19.92 ppm (br, 2H, RhH_2)] in the ^1H NMR spectrum. Analysis of **2-7** by ESI-MS revealed a molecular ion at *m/z* 509.28 [M^+], consistent with loss of TMAB from **2-7** *i.e.* formation of **2-3** (calc. 509.29).



Scheme 2.7 Addition of H_2 to **2-6** to form $[Rh(H)_2(P^tBu^iBu_2)(\eta^2\text{-}H_3B{\cdot}NMe_3)][BAr^F{}_4]$ (**2-7**). $[BAr^F{}_4]^-$ anions not shown.

Degassing (freeze-pump-thaw cycles) a solution of **2-7** in 1,2-$C_6H_4F_2$ does not result in the loss of dihydrogen and the return of **2-6**, in contrast to $[Rh(H)_2(P^iBu_3)_2(\eta^2\text{-}H_3B{\cdot}NMe_3)][BAr^F{}_4]$ (**i-82a**).[6] This lack of loss of H_2 might be traced to the increased steric demands of the $P^tBu^iBu_2$ ligand, however, as we show in Chapter 3, H_2 loss from a Rh(III) dihydride species like **2-7** can be promoted by addition of a bulky exogenous ligand. Similar behaviour was observed for the P^iPr_3[24] and PCy_3 analogues (Chapter 3), where addition of the hydrogen acceptor TBE was necessary to regenerate the respective Rh(I) σ-complex. However, addition of TBE to a 1,2-$C_6H_4F_2$ solution of **2-7** leads to unexpected reactivity; TBE facilitates the reduction of rhodium to Rh(I) but is also hydroborated by TMAB. The product of this hydroboration, $Me_3N{\cdot}\mathit{H_2B}CH_2CH_2CMe_3$, coordinates to a Rh(I) metal centre forming the rhodium(I) σ-complex $[Rh(P^iBu_2{}^tBu)_2(\eta^2\text{-}Me_3N{\cdot}\mathit{H_2B}CH_2CH_2CMe_3)][BAr^F{}_4]$ (**2-8**). Complex **2-8** can alternatively, and more simply, be formed by the addition of TBE to the Rh(I) σ-complex **2-6** (Scheme 2.8). This unexpected behaviour was investigated further and shall be discussed in the next section.



Scheme 2.8 Addition of TBE to **2-6** results in the hydroboration of TBE, the product of which binds to $\{Rh(P^tBu^iBu_2)_2\}^+$ to generate **2-8**. $[BAr^F{}_4]^-$ anions not shown.

2.3 Hydroboration

2.3.1 Hydroboration by TMAB

Addition of TBE to **2-6** results in its hydroboration by TMAB and the formation of **2-8**, which features the hydroboration product bound in an η^2 fashion to the Rh metal centre. No intermediates were observed apart from **2-6** and **2-8**. Although it was possible to obtain crystalline samples of **2-8**, they were found to diffract poorly and so a different anion, $[BAr^{Cl}{}_4]^-$, was used to obtain the solid-state structure (Figure 2.7). The solid-state structure was still poorly resolved, suffering from extensive disorder, but was sufficient to confirm connectivity and show that the anti-Markovnikov product had been formed.

As the X-ray data are of poor quality, it is unclear how the organic fragment coordinates to the rhodium centre *i.e.* through CH_2 or BH_2 as BH_2NMe_3 is isoelectronic with CH_2CMe_3. However, analysis by NMR spectroscopy clearly indicates coordination through BH_2: the ^1H NMR spectrum shows a quadrupolar broadened, relative 2H integral at δ -7.07 ppm for the Rh-H-B 3-centre 2-electron interactions that collapses to an apparent triplet ($^2J_{HP}$ = 32 Hz and $^1J_{RhH}$ = 32 Hz) in the $^1H\{^{11}B\}$ NMR spectrum.[24] Signals due to NMe_3, CMe_3 and the two methylene groups are all observed. ^{11}B NMR spectroscopy shows the coordinated borane as a broad signal at δ 37.9 ppm, shifted to higher frequency compared with the free borane (*vide infra*), as expected.[30, 31] The $^{31}P\{^1H\}$ NMR spectrum shows one environment (δ 53.8 ppm) with Rh-P coupling (182 Hz) indicative of a Rh(I) metal centre.[9] Complex **2-8** was additionally characterised by ESI-MS [*m/z* 664.48 $[M^+]$ (calc. 664.48), with the correct isotopic pattern] and elemental microanalysis (CHN).

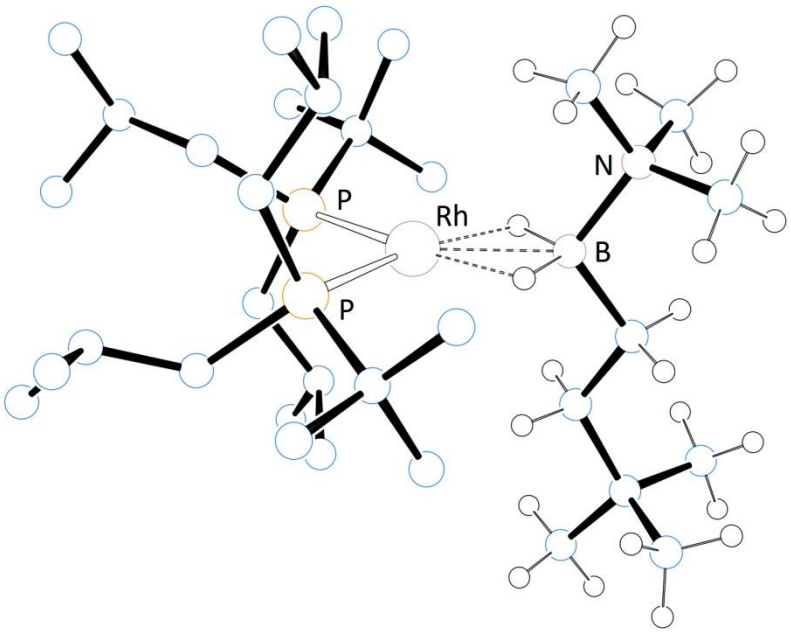
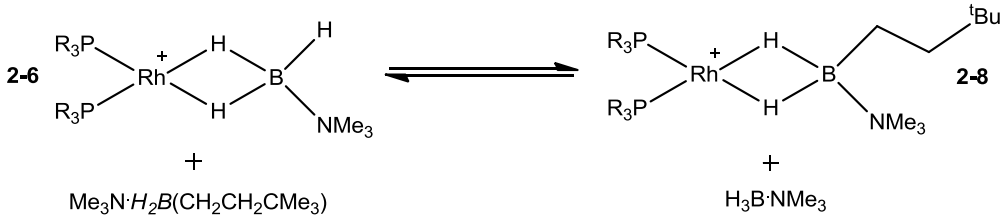


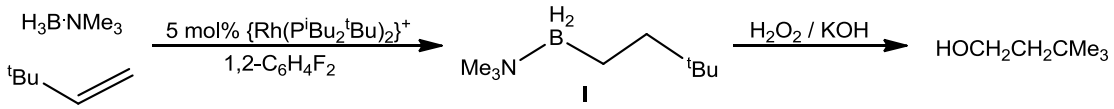
Figure 2.7 Ball and stick representation of a partially refined structure of **2-8**. One of the four independent cations in the asymmetric unit only (each with different phosphine substituent conformations). Hydrogen atoms placed in calculated positions. Anions and most hydrogen atoms omitted for clarity. The X-ray data is of poor quality and the structure presented here is only to confirm bond connectivity. Selected crystallographic data: Triclinic, *P*-1 (Z'=4), a = 23.7290(2) Å, b = 25.4785(2) Å, c = 25.6623(3) Å, α = 72.4864(4)°, β = 67.6371(4)°, γ = 67.4747(4)°.

Addition of TMAB to **2-8** (1:1 ratio) established an equilibrium between **2-6** and **2-8**, which favours the hydroborated product [K(298 K) = 1.62, ΔG = -1.1 kJ mol^{-1}] (Scheme 2.9). Shimoi and co-workers have previously reported similar behaviour from the reaction of *B*-substituted boranes with metal fragments *e.g.* [$CpMn(CO)_2(\eta^1$-$BH_2Me{\cdot}NMe_3)$].[32] It is suggested that the alkyl borane complexes are favoured over the TMAB adducts due to the presence of electron-donating alkyl groups, which increase the energy of the B-H σ orbital, favouring overlap with the metal LUMO. Complex **2-8** also models alkane complexes of Rh(I) that are only stable in solution at low temperature (*e.g.* Brookhart's Rh(I) methane complex, **i-37**)[33] or in the solid state (*e.g.* Weller's Rh norbornane complex, **i-41**)[34] which bind through a Rh-H-C σ-interaction



Scheme 2.9 Equilibrium between **2-6** and **2-8**. $[BAr^F_4]^-$ anions not shown.

Under catalytic conditions (5 mol%, 1.475 mM of TMAB, 1,2-$C_6H_4F_2$, 94 h) $\{Rh(P^tBu^iBu_2)_2\}^+$ promotes the hydroboration of TBE by TMAB to form free $Me_3N{\cdot}H_2BCH_2CH_2CMe_3$ (**I**) [^{11}B δ -0.83 ppm (t, $^1J_{BH}$ = 96 Hz)] (Scheme 2.10). **I** could not be isolated cleanly due to its volatile nature combined with the relatively high boiling point of 1,2-$C_6H_4F_2$ (92 °C), but work up of the catalytic mixture with H_2O_2/KOH afforded $HOCH_2CH_2CMe_3$ as the only product (analysis by ^1H NMR spectroscopy and comparison with literature data),[35] confirming both the chemical composition and the regiochemistry of hydroboration. There was no evidence by ^1H NMR spectroscopy for the branched product, as has been previously seen for the Rh(III) catalysed, and the uncatalysed, hydroboration of TBE using $BH_3{\cdot}THF$.[36]



Scheme 2.10 Catalytic hydroboration of TBE by TMAB generating $Me_3N{\cdot}H_2BCH_2CH_2CMe_3$ (**I**) and subsequent work up to yield $HOCH_2CH_2CMe_3$.

During catalysis, a maximum conversion of only ~70% is ever reached, with ~30% unreacted TMAB and TBE remaining (Figure 2.8). This is suggested to be due to product inhibition of the catalyst, with **I** competing effectively with TMAB for coordination to the metal (Scheme 2.9). It is possible that more coordinating solvents than 1,2-$C_6H_4F_2$ may promote 100% conversion, but this has not been investigated.[36] Addition of a further 20 equivalents each of TMAB and TBE after the reaction had

halted, restarted catalysis but at a slightly slower initial rate [(3.9 ± 0.4) x 10^{-6} M s^{-1} *vs.* (2.2 ± 0.3) x 10^{-6} M s^{-1}], consistent with inhibition by the product. Again, only ~70% conversion is achieved (Figure 2.8).

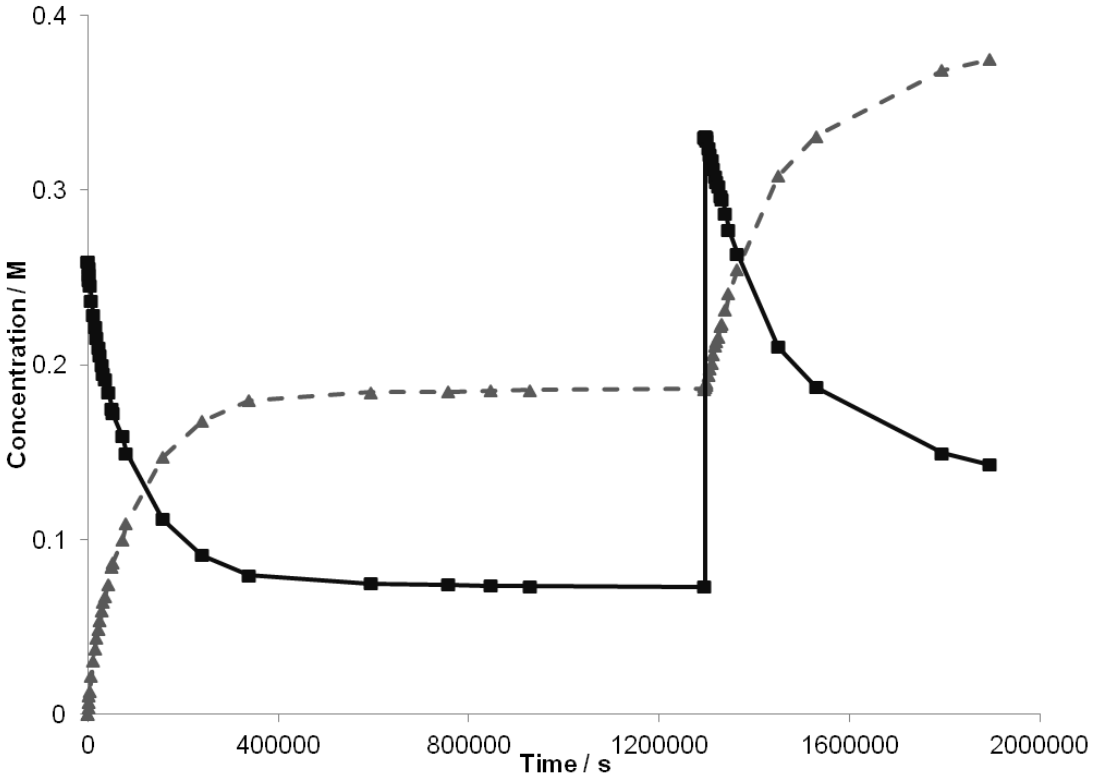


Figure 2.8 Plot of concentration *versus* time for the hydroboration of TBE by TMAB catalysed by $\{Rh(P^tBu^iBu_2)_2\}^+$ (5 mol%). A further 20 equivalents of TMAB and TBE were added at t = 1296300 s. ■, TMAB; ▲, **I**.

In line with these observations, the main species observed at the start of catalysis is **2-6** (^{1}H and ^{31}P{^{1}H} NMR spectroscopy, Figure 2.9). As the reaction proceeds, **2-8** becomes the dominant organometallic species present (time = 2 days). Exo-nido $[Rh(PR_3)_2(\eta^2\text{-carborane})]$ complexes have been reported as the resting states during the insertion of an alkene into the B-H bond of a carborane, a related transformation to that reported here.[37, 38]

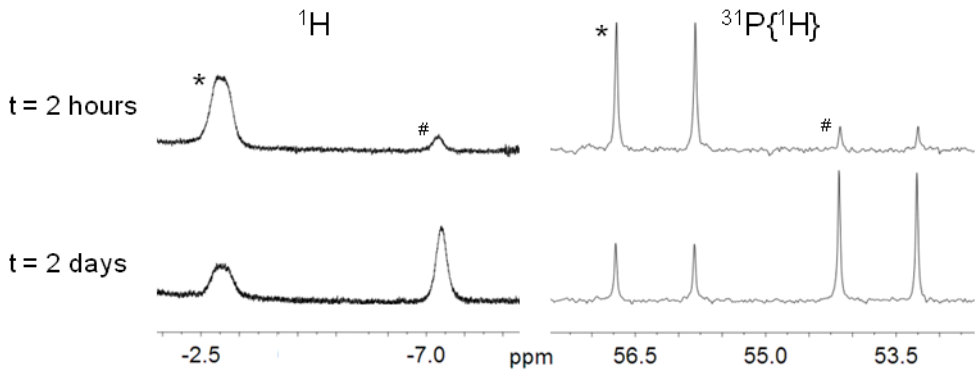


Figure 2.9 ^{1}H (left) and ^{31}P{^{1}H} (right) NMR spectra (selected regions) showing the organometallic species present after 2 hours (upper) and 2 days (lower) for the hydroboration of TBE by TMAB catalysed by $\{Rh(P^tBu^iBu_2)_2\}^+$ (5 mol%). * = **2-6**; # = **2-8**.

The mechanism of hydroboration was investigated using initial rates as product inhibition prevented the data being fitted to a first order plot. A time/concentration plot for the hydroboration of TBE (298 K, ^{11}B NMR spectroscopy, 5 mol%, 0.259 M TMAB, 0.259 M TBE) gave an initial rate of (3.9 ± 0.4) x 10^{-6} M s^{-1} over the first 1900 seconds of reaction (Figure 2.10). Errors were calculated assuming a 10% error in ^{11}B NMR integration. Catalysis with a 2-fold excess of TBE to TMAB (40:20 relative to $\{Rh(P^tBu^iBu_2)_2\}^+$) doubled the initial rate [(8.1 ± 1.0) x 10^{-6} M s^{-1}], while addition of a 10-fold excess of TMAB resulted in no change [(4.2 ± 0.5) x 10^{-6} M s^{-1}]. Catalysis at 10 mol% effectively doubled the initial rate [(6.5 ± 0.7) x 10^{-6} M s^{-1}].

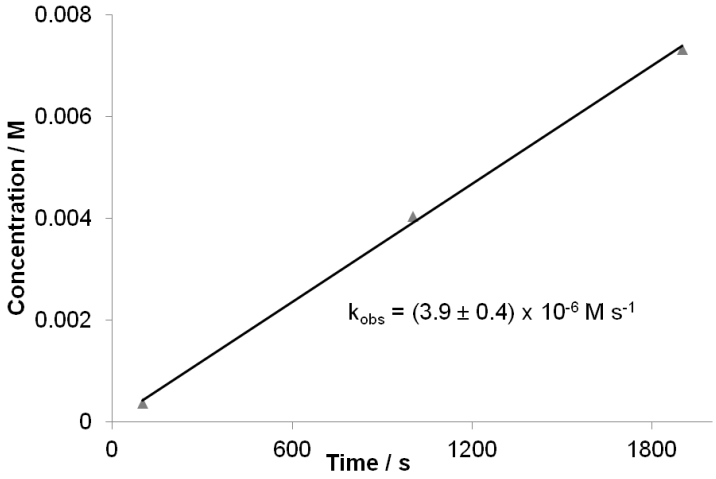
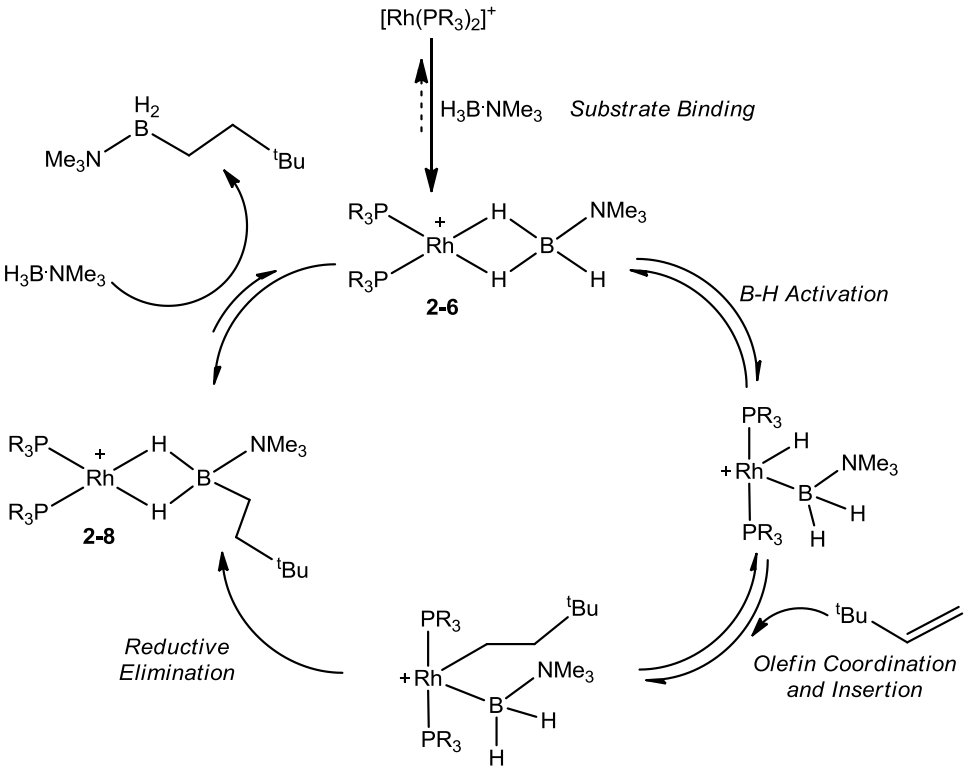


Figure 2.10 Sample kinetic plot showing the initial rate over the first 1900 seconds (5 mol% $\{Rh(P^tBu^iBu_2)_2\}^+$, 0.259 M TMAB, 298K, 1,2-$C_6H_4F_2$, 1:1 TMAB:TBE).

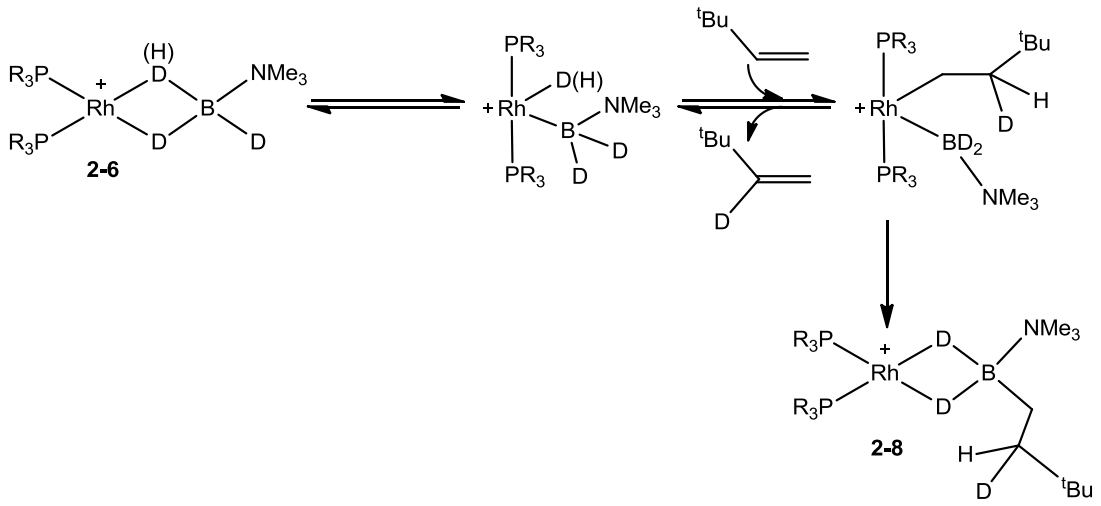
As discussed previously, the addition of 1 equivalent of TMAB to $\{Rh(P^tBu^iBu_2)_2\}^+$ immediately and cleanly forms **2-6**, while addition of an excess of TBE to $\{Rh(P^tBu^iBu_2)_2\}^+$ results in no observable reaction. Combined with the initial rates, these results indicate a first order process in $\{Rh(P^tBu^iBu_2)_2\}^+$ and TBE only, in which fast and essentially irreversible binding of TMAB forms **2-6**, which proceeds *via* B-H activation, olefin coordination and insertion, then reductive B-C bond formation followed by substitution to yield the product of hydroboration, **I**. The proposed mechanism is shown in Scheme 2.11. These results are in line with those suggested for rhodium-catalysed hydroboration of olefins using substrates such as catecholborane, although in these cases there can be multiple pathways operating.[39-41] The control reaction of TBE with TMAB in 1,2-$C_6H_4F_2$ resulted in no reaction after 2 days.



Scheme 2.11 Suggested catalytic cycle for the hydroboration of TBE by TMAB, catalysed by $\{Rh(P^tBu^iBu_2)_2\}^+$. R = $^tBu^iBu_2$. $[BAr^F{}_4]^-$ anions not shown.

To probe the potential reversibility of the olefin coordination and insertion step in the catalytic cycle, catalysis (5 mol% $\{Rh(P^tBu^iBu_2)\}^+$, 298 K) was repeated with $D_3B{\cdot}NMe_3$ (d_3-TMAB) in place of TMAB.[i] Monitoring the reaction by ^2H NMR spectroscopy revealed the incorporation of deuterium into TBE in one position only, as evidenced by the growth of a peak at δ 5.89 ppm in the ^2H NMR spectrum and the reduction of the equivalent peak at δ 5.89 ppm in the ^1H NMR spectrum (Scheme 2.12). This demonstrated the reversible nature of the coordination and insertion step. Over time deuterium was observed to be present in one of the methylene groups of the hydroboration product, evidenced by a signal at δ 1.40 ppm in the ^2H NMR spectrum, which corresponds to $Me_3N{\cdot}(D/H)_2BCH_2C(\underline{D/H})_2CMe_3$.

[i] An initial rate was not determined for this reaction as due to the H/D exchange a meaningful result would not be obtained.



Scheme 2.12 Use of d_3-TMAB to test the reversibility of the olefin coordination and insertion step. R = $^{t}Bu^{i}Bu_2$. $[BAr^{F}_4]^-$ anions not shown.

Interestingly, after 2 days *i.e.* when both **2-6** and **2-8** are present (Figure 2.9), seven different species were observed in the $^{31}P\{^{1}H\}$ NMR spectrum (Figure 2.11). We suggest that these are isotopologues of **2-6** and **2-8** with different levels of hydrogen incorporation into the BD_3 (**2-6**: BH_2D, BHD_2 and BH_3) and BD_2 (**2-8**: BHD and BH_2) positions. No evidence for these different products was seen in the ^{1}H and ^{2}H NMR spectra as the broad nature of the M-H-B peaks likely prevents the observation of separate peaks.

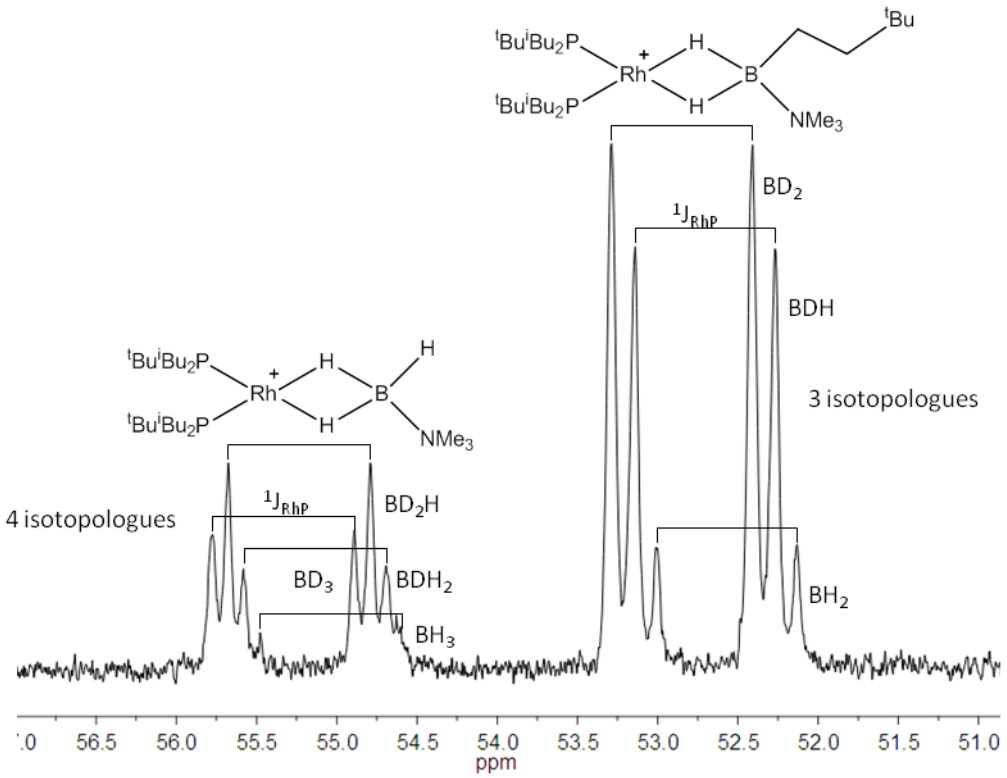


Figure 2.11 $^{31}P\{^{1}H\}$ NMR spectrum of $\{Rh(P^tBu^iBu_2)_2\}^+$ (5 mol%), d_3-TMAB and TBE in 1,2-$C_6H_4F_2$ after 2 days. $[BAr^F_4]^-$ anions not shown.

Analysis of the reaction mixture by ESI-MS revealed **2-6** and **2-8** to be present, with varying levels of deuterium present in the coordinated TMAB or **I** (Figure 2.12). For **2-6**, four isotope patterns were seen corresponding to **2-6** with either BD_3 [*m/z* 583.40 (calc. 583.40)], BHD_2 [*m/z* 582.40 (calc. 582.39)], BH_2D [*m/z* 581.39 (calc. 581.39)] or BH_3 [*m/z* 580.39 (calc. 580.38)]. In the ESI-MS spectrum of **2-8**, four signals were observed for the presence of one [*m/z* 665.49 (calc. 665.48)], two [*m/z* 666.49 (calc. 666.49)], three [*m/z* 667.49 (calc. 667.49)] or four [*m/z* 668.80 (calc. 668.50)] deuterium atoms. These signals cannot be specifically assigned to BH_2, BHD or BD_2 as deuterium can additionally be present in the methylene position as a result of the reversible insertion of TBE (Scheme 2.12) and as such several isotopomers are possible for each level of deuterium incorporation. For example there are three possible isotopomers for **2-8** incorporating two deuterium atoms:

$Me_3N{\cdot}D_2BCH_2CH_2CMe_3$, $Me_3N{\cdot}HDBCH_2CHDCMe_3$ or $Me_3N{\cdot}H_2BCH_2CD_2CMe_3$. The naturally abundant isotopic pattern for **2-8** was not observed.

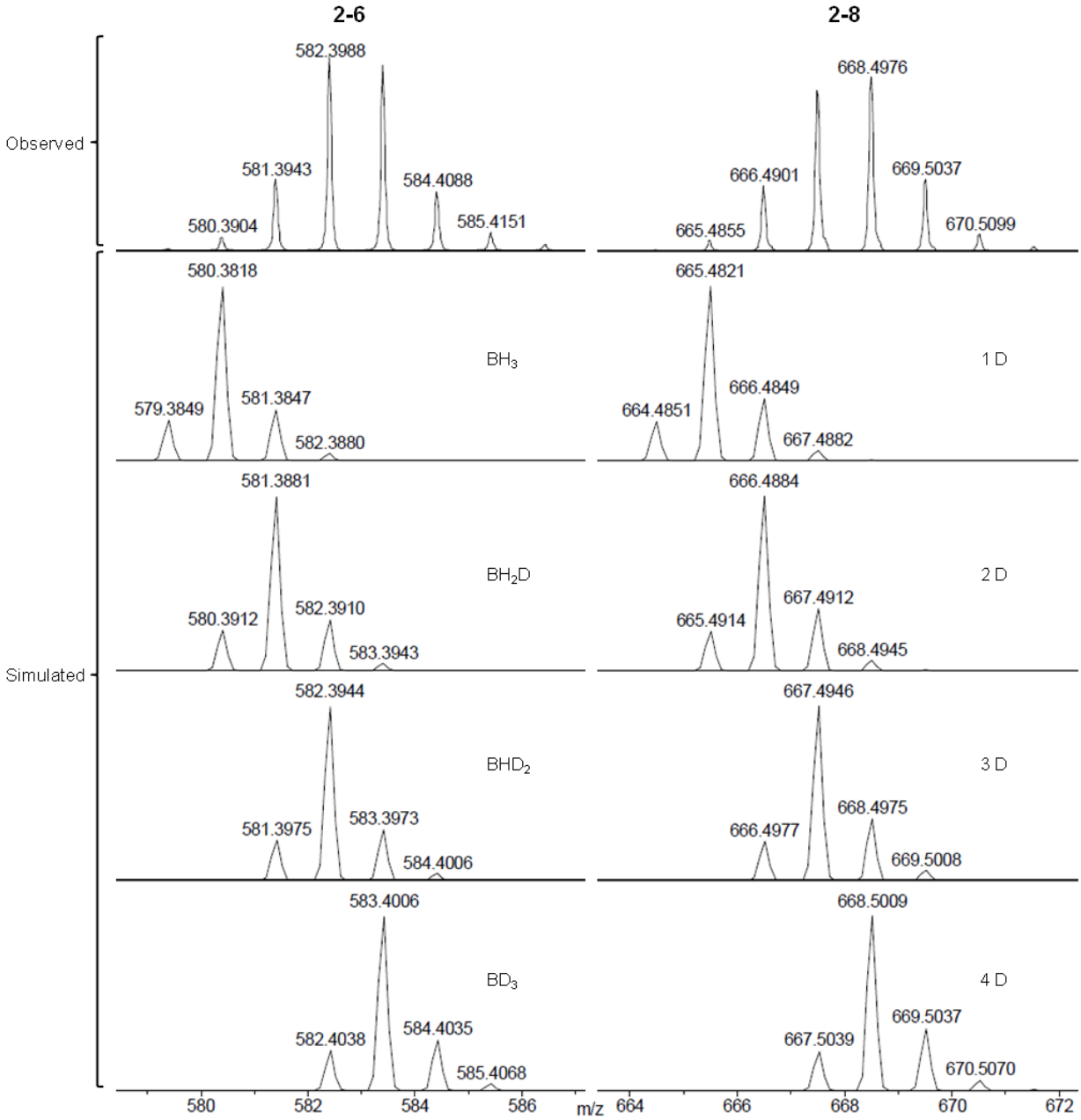


Figure 2.12 ESI-MS of the reaction between $\{Rh(P^tBu^iBu_2)_2\}^+$, d_3-TMAB and TBE in 1,2-$C_6H_4F_2$ after 2 days showing the incorporation of deuterium into **2-6** (left) and **2-8** (right).

Addition of excess acetonitrile to the reaction mixture containing these isotopologues/isotopomers resulted in the formation of only one rhodium complex, the *bis*-acetonitrile adduct **2-5**, confirmed by ^1H and $^{31}P\{^1H\}$ NMR spectroscopy,

further confirmation that the multiple signals seen in the preliminary mixture arise from the coordinated borane and not H/D exchange in $\{Rh(P^tBu^iBu_2)_2\}^+$. Free TMAB and **I** were observed in the ^{11}B NMR spectrum, where B-H coupling was also evident indicating the incorporation of H into the B-D positions.

The observation of separate signals for the different levels of deuterium incorporation in **2-6** is a result of secondary isotopic perturbation of equilibrium. Such a primary effect is observed due to a preference for the heavier deuterium atom to be in the terminal rather than bridging position, thus the H-bridged forms will be slightly more abundant than the D-bridged forms when an equilibrium can be established. As the bridging H atom resonates at a lower frequency than the terminal H atom, this change in distribution results in a net upfield shift of the BHD_2 signal relative to the BH_2D signal in the ^1H NMR spectrum.[42] Secondary deuterium isotope effects result in such changes in the chemical shift being observed in the phosphorus NMR data.[43] The position of $P^tBu^iBu_2$ *trans* to a B-H/D likely increases the effect. For **2-8**, which has only bridging B-H's, the observation of separate signals is a result of isotopic perturbation of resonance, such as seen in the ^1H NMR data for CH_2Cl_2 and $CHDCl_2$. Deuterium-induced secondary isotope effects again result in the changes in the chemical shift being observed in the $^{31}P\{^1H\}$ NMR spectrum. For **2-6**, the difference in chemical shifts in the $^{31}P\{^1H\}$ NMR spectrum between the isotopologues is 0.10 ppm, while a slightly larger chemical shift separation of 0.14 ppm is observed between the variations of **2-8**. This reflects the static nature **2-8**, while **2-6** is fluxional on the NMR timescale and hence the signals observed are frequency averaged. The shifts of ~0.1 ppm are in line with previously observed secondary isotope effects for phosphorus and other nuclei such as carbon.[43-45]

Intrigued as to whether this hydroboration of TBE was specific to the $P^tBu^iBu_2$ system, TBE was added to $[Rh(P^iBu_3)_2(\eta^2\text{-}H_3B{\cdot}NMe_3)][BAr^F{}_4]$ (**i-81a**). The P^iPr_3[24] and PCy_3 (Chapter 3) systems are known to not facilitate the hydroboration. $\{Rh(P^iBu_3)_2\}^+$ was observed to catalyse the hydroboration of TBE by TMAB but at a slower rate compared with $\{Rh(P^tBu^iBu_2)_2\}^+$. A time/concentration plot (298 K, ^{11}B NMR spectroscopy, 5 mol%, 0.259 M TMAB, 0.259 M TBE) gave an initial rate over the first 1900 seconds of reaction of (3.0 ± 0.8) x 10^{-7} M s^{-1}, an order of magnitude slower than for the $P^tBu^iBu_2$ system [(3.9 ± 0.4) x 10^{-6} M s^{-1}]. The observed difference in initial rates between $P^tBu^iBu_2$ and P^iBu_3 is perhaps attributable to the added steric bulk the *tert*-butyl group confers, which could be expected to aid both the insertion and overall reductive steps of the catalytic cycle, as both of these steps will reduce the steric congestion around the metal.

As a new phosphine, the cone angle of $P^tBu^iBu_2$ is unknown, but is likely to be intermediate between P^tBu_3 (182°) and P^iBu_3 (143°), which would make it approximately similar to those reported for P^iPr_3 (160°) and PCy_3 (170°).[46] As mentioned earlier, neither $\{Rh(PCy_3)_2\}^+$ or $Rh(P^iPr_3)_2\}^+$ catalyse the hydroboration of TBE by TMAB, indicating that steric bulk of the phosphine is not the only factor in determining the ability of a $\{Rh(PR_3)_2\}^+$ fragment to catalyse the hydroboration reaction. We propose that it is the flexibility the methylene spacer in the *iso*-butyl group confers, which is responsible for the observed differences in reactivity. The bulk of TBE combined with the size of P^iPr_3 and PCy_3 is likely to prevent the coordination and insertion step of TBE at the B-H activated intermediate. While $P^tBu^iBu_2$ is likely to be of a similar size the methylene group will allow the *iso*-butyl group to fold out of the way to allow the incoming TBE to coordinate and insert.

2.3.2 Tandem hydroboration and dehydrogenation

Having successfully delivered a catalysed hydroboration using a tertiary amine-borane we reasoned that use of secondary amine-boranes would allow for a tandem dehydrogenation reaction to give *B*-substituted amino-boranes; R(H)B=NR'$_2$. {Rh(PR$_3$)$_2$}$^+$ fragments are well established to catalyse amine-borane dehydrogenation[5, 6, 24] and a sealed system (sealed high pressure NMR tube) test of {Rh(P^{t}Bu^{i}Bu$_2$)$_2$}$^+$ indicated that it is also proficient at catalysing the dehydrocoupling. Related tandem (or transfer) dehydrogenation/alkene hydrogenation catalysis has previously been reported.[47, 48]

Dropwise addition of a dilute solution of H$_3$B·NMe$_2$H (DMAB) in 1,2-C$_6$H$_4$F$_2$ to a solution of {Rh(P^{t}Bu^{i}Bu$_2$)$_2$}$^+$ (5 mol%) and TBE (DMAB : TBE, 1:1) in 1,2-C$_6$H$_4$F$_2$ resulted in complete consumption of the starting materials and a mixture of 3 major products. The ^{11}B NMR spectrum (Figure 2.13) showed: a doublet [δ 43.2 ppm ($^1J_{HB}$ = 118 Hz)] which is tentatively assigned to the hindered amino-borane Me$_2$N=BH(CH$_2$CH$_2$^{t}Bu) (**II**); a singlet [δ 45.8 ppm], which is suggested to be Me$_2$N=B(CH$_2$CH$_2$^{t}Bu)$_2$ (**III**); and a triplet [δ 5.4 ppm ($^1J_{HB}$ = 113 Hz)], assigned to the cyclic amino-borane [H$_2$BNMe$_2$]$_2$ (DIMER), a well–established product from the dehydrogenation of H$_3$B·NMe$_2$H.[49] The ^{11}B chemical shifts and coupling patterns of **II** and **III** are consistent with their formulation as primary and secondary amino–boranes respectively.[50-52]

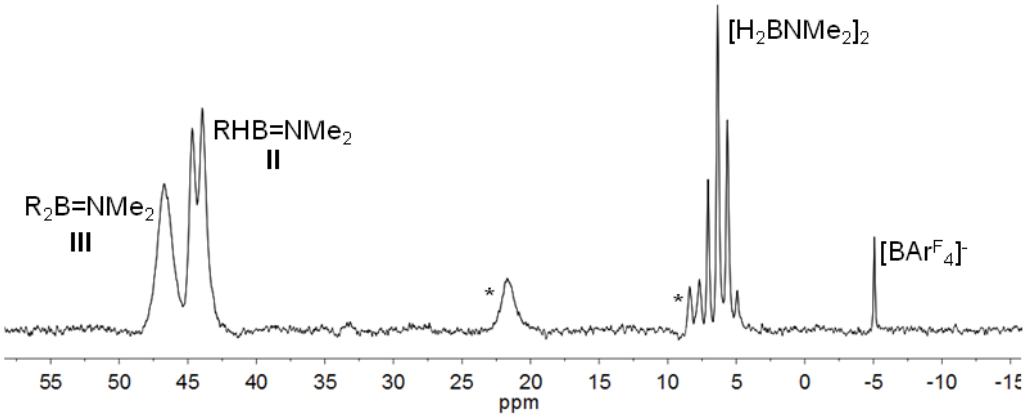
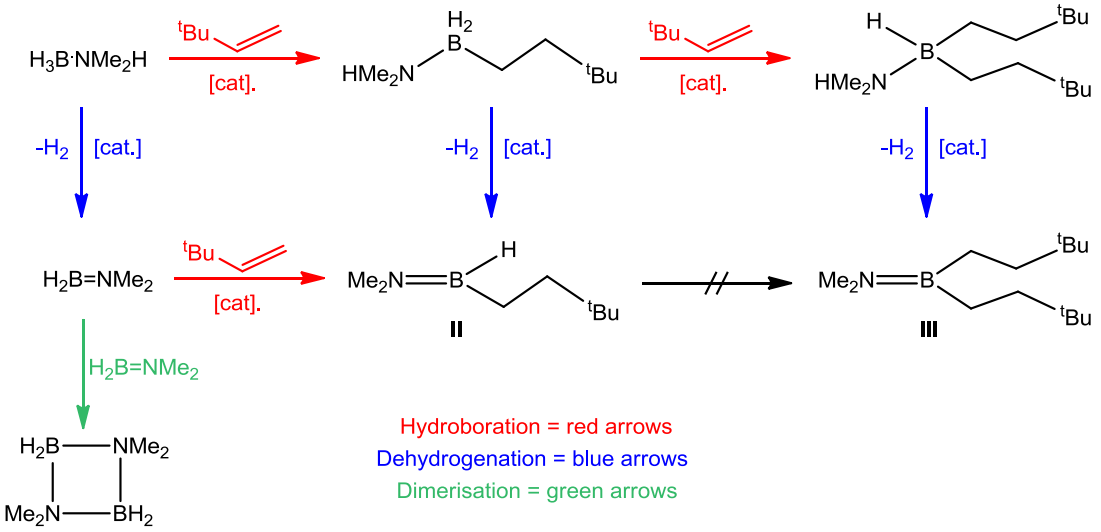


Figure 2.13 ^{11}B NMR spectrum from the reaction of TBE with DMAB catalysed by $\{Rh(P^tBu^iBu_2)_2\}^+$ (5 mol%) in 1,2-$C_6H_4F_2$ showing tandem hydroboration /dehydrogenation products. R = $CH_2CH_2CMe_3$. * = unknown.

Addition of further TBE and catalyst did not convert **II** to **III** indicating that they were produced by parallel routes, and that **III** does not arise from the hydroboration of TBE using **II**. On the basis of these results we suggest a mechanism in which DMAB partakes in successive hydroborations with TBE to finally afford $HMe_2N{\cdot}BH(CH_2CH_2{}^tBu)_2$, which then undergoes dehydrogenation to yield **III** (Scheme 2.13). Dehydrogenation (and dimerisation of $H_2B{=}NMe_2$) is competitive at each step, thus accounting for the product distributions. TBE can also be hydroborated using the stable amino-borane, $H_2B{=}N^iPr_2$, yielding $^iPr_2N{=}BH(CH_2CH_2{}^tBu)$ (**II-^{i}Pr**) as the sole product, indicating that **II** could also be formed by dehydrogenated DMAB, *i.e.* $H_2B{=}NMe_2$, hydroborating TBE. $H_2B{=}N^iPr_2$ can hydroborate TBE in the absence of $\{Rh(P^tBu^iBu_2)_2\}^+$ but the rate is accelerated by the presence of $\{Rh(P^tBu^iBu_2)_2\}^+$. Using a 200-fold excess of TBE relative to $\{Rh(P^tBu^iBu_2)_2\}^+$ increased the relative ratio of **III** at the expense of **II** and $[H_2BNMe_2]_2$ (final relative ratios 1.5 : 1.5 : 1 respectively). Pure material of the hindered amine-boranes could not be isolated, due to both their volatile nature and the relatively high boiling point of 1,2-$C_6H_4F_2$ (92 °C). The multiple hydroboration of TMAB was not observed, presumably for steric reasons.



Scheme 2.13 Possible routes for the tandem hydroboration/dehydrogenation catalysed by $\{Rh(P^tBu^iBu_2)_2\}^+$. [cat] = $\{Rh(P^tBu^iBu_2)_2\}^+$.

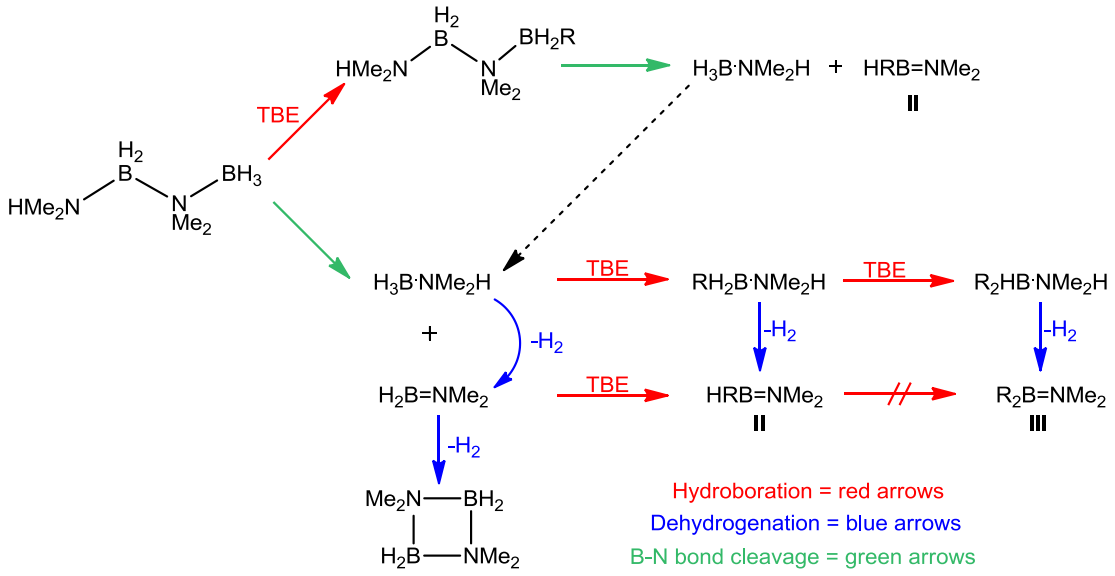
2.3.3 Post functionalisation of linear diborazane, OLIG

Intrigued by the reaction of DMAB with TBE catalysed by $\{Rh(P^tBu^iBu_2)_2\}^+$, we next investigated the possibility of post functionalising the linear diborazane $H_3B{\cdot}NMe_2BH_2{\cdot}NMe_2H$ (OLIG), an intermediate in the dehydrocoupling of DMAB with some catalyst systems.[5, 24, 53] The introduction of new functional groups to the backbone of polymers is of interest as a useful methodology for altering the properties of the polymer to allow their use for a wider range of applications.[54] To be able to control the level and type of functional group incorporation would greatly increase the versatility of these materials.

Dropwise addition of a dilute solution of OLIG in 1,2-$C_6H_4F_2$ to a solution of $\{Rh(P^tBu^iBu_2)_2\}^+$ and TBE in 1,2-$C_6H_4F_2$ (5 mol%) resulted in complete consumption of the starting materials and the observation of one main product, **II** (~80%), with smaller amounts of **III** (~20%) and negligible amounts of $[H_2BNMe_2]_2$ (<5%). No functionalised OLIG was observed, presumably due to the ability of $\{Rh(P^tBu^iBu_2)_2\}^+$ to also mediate the B-N bond cleavage of OLIG. Addition of 1 equivalent of OLIG (no

TBE) to $\{Rh(P^tBu^iBu_2)_2\}^+$ results in the formation of the Rh(I) σ-complex $[Rh(P^tBu^iBu_2)_2(\eta^2\text{-}H_3B{\cdot}NMe_2BH_2{\cdot}NMe_2H)][BAr^F{}_4]$ (**2-9**). Complex **2-9** rapidly reacts further to yield the Rh(III) σ-complexes: $[Rh(H)_2(P^tBu^iBu_2)_2(\eta^2\text{-}H_3B{\cdot}NMe_2H)][BAr^F{}_4]$ (**2-10**), $[Rh(H)_2(P^tBu^iBu_2)_2(\eta^2\text{-}H_2B{=}NMe_2)][BAr^F{}_4]$ (**2-11**) and $[Rh(H)_2(P^tBu^iBu_2)_2(\eta^2\text{-}H_3B{\cdot}NMe_2BH_2{\cdot}NMe_2H)][BAr^F{}_4]$ (**2-12**). All σ-complexes were identified by comparison with *in situ* ^1H, ^{11}B and $^{31}P\{^1H\}$ NMR spectroscopic data of the equivalent P^iBu_3[5] and PCy_3 (Chapter 3) complexes.[5] Free $H_2B{=}NMe_2$ (MON) is also observed in the ^{11}B NMR spectrum, which along with the formation of **2-10** and **2-11** indicates the B-N bond cleavage of OLIG. B-N bond cleavage of OLIG by $\{Rh(PR_3)_2\}^+$ fragments has been observed previously.[5, 28]

Two possible reaction routes could be operating to give the observed products (Scheme 2.14): OLIG could first be split and then undergo hydroboration or OLIG may first be hydroborated and then undergo B-N bond cleavage. As no free MON, which would arise from the splitting of OLIG, was seen and only minimal amounts of the dimeric amino-borane, this suggests that OLIG hydroborates TBE prior to B-N bond cleavage. However, as results with $H_2B{=}NiPr_2$ indicate that MON can hydroborate TBE (*vide supra*), and the relative rates of hydroboration of TBE by MON *versus* the dimerisation of MON are unknown, it cannot be said definitively by which mechanism the reaction occurs.



Scheme 2.14 Possible routes for the attempted post-functionalisation of linear diborazane. $\{Rh(P^tBu^iBu_2)_2\}^+$ is assumed to be involved as a catalyst in all steps except the dimerisation of $H_2B{=}NMe_2$. R = $CH_2CH_2CMe_3$.

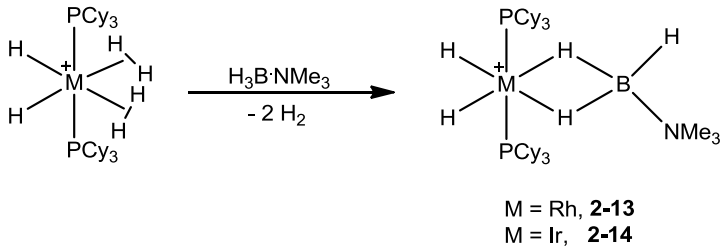
Although it was not possible to post-functionalise OLIG, it does allow the cleaner production of **II** in comparison with starting from DMAB (80% *vs.* ~35%). The effect of varying the concentration of OLIG or TBE on the product ratios to further improve the ratios has not been investigated.

2.4 Investigation of fluxional processes in amine-borane σ-complexes

Sigma complexes of amine-boranes such as **2-6** are of importance in the transition metal catalysed dehydrocoupling of amine-boranes, particularly for those that proceed *via* an inner-sphere mechanism (Section 1.4.3).[55-58] Despite their significance in dehydrocoupling, a detailed investigation, utilising both computational and experimental methods, into the fluxional/exchange processes of such compounds has not been performed for Group 9. A combined computational and experimental investigation into fluxional behaviour in Group 6 and Group 7 amine-borane

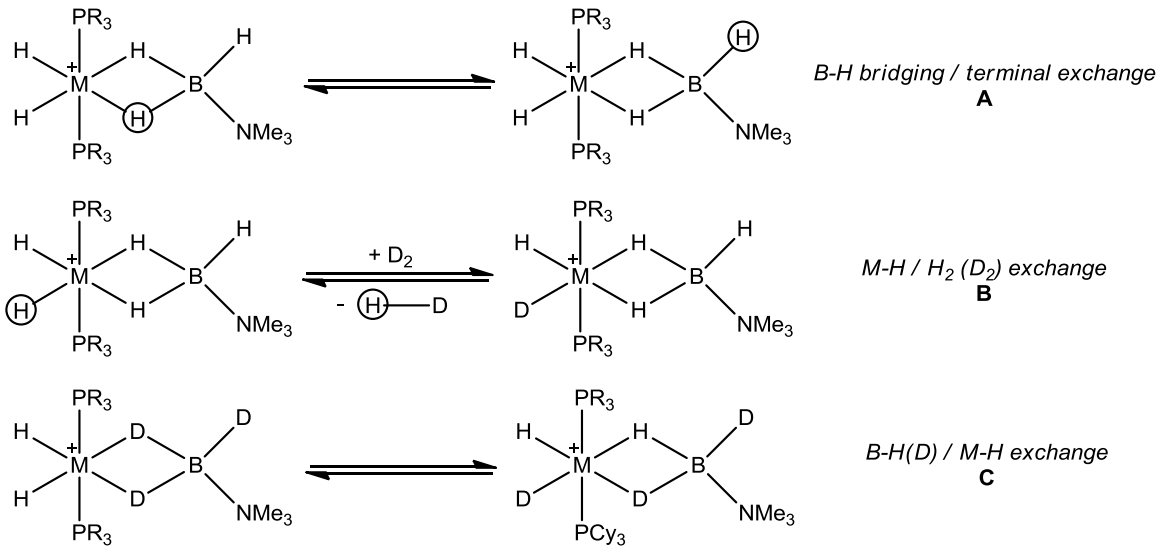
complexes has been performed by Shimoi and co-workers.[32, 59] Knowledge of such processes may provide key information to aid understanding of their reactivity. The aim of this section is to provide experimental data so that the ongoing computational investigations (Prof. Stuart A. Macgregor, Heriot-Watt University) can be benchmarked.

The system chosen for our investigations were the known M(III) complexes $[M(H)_2(PCy_3)_2(\eta^2\text{-}H_3B{\cdot}NMe_3)][BAr^F{}_4]$ [M = Rh, **2-13** (Chapter 3); M = Ir, **2-14**].[53] Both are readily prepared by the addition of TMAB to the corresponding *bis*-dihydrogen dihydride complex $[M(H)_2(PCy_3)_2(\eta^2\text{-}H_2)_2][BAr^F{}_4]$ (M = Rh, **i-20**; M = Ir, **i-21**) (Scheme 2.15). The chosen system was selected as both the Rh and Ir congeners are known, allowing for comparison of the fluxional/exchange processes down a group in the periodic table. Additionally, as **2-13** does not lose H_2 easily to return to the Rh(I) oxidation state (Chapter 3), only the fluxional and exchange processes pertinent to Rh(III) will be probed. This is useful as it allows for comparison with the iridium system, which has previously been shown to operate in a constant oxidation state Ir(III) manifold, with Ir(I) not implicated in the mechanism.[53] The use of the tertiary amine-borane TMAB prevents undesired onward reactivity *i.e.* dehydrocoupling.



Scheme 2.15 Formation of $[M(H)_2(PCy_3)_2(\eta^2\text{-}H_3B{\cdot}NMe_3)][BAr^F{}_4]$ (**2-13**, M = Rh; **2-14**, M = Ir). $[BAr^F{}_4]^-$ anions not shown.

Three fundamental exchange processes that can occur at the borane in sigma complexes such as **2-13** and **2-14** have been investigated (Scheme 2.16): B-H bridging/terminal exchange (**A**); exchange of the metal hydrides with exogenous H_2 (**B**) and B-H/M-H exchange (**C**). The processes were probed using variable temperature NMR experiments and H/D exchange experiments.

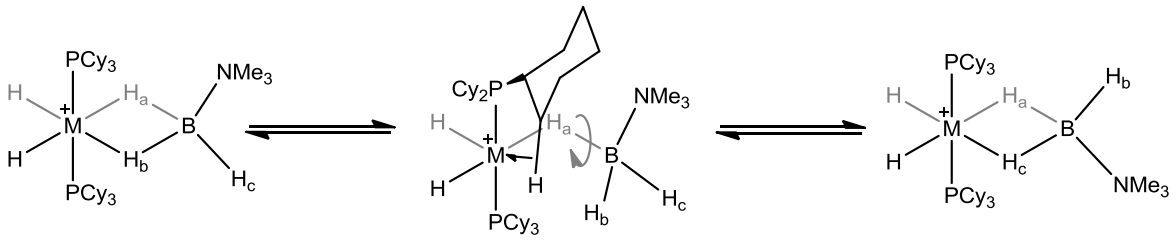


Scheme 2.16 Three possible exchange processes at the borane in σ-amine-borane complexes. M = Rh, **2-13**; M = Ir, **2-14**. $[BAr^F_4]^-$ anions not shown.

2.4.1 B-H bridging/terminal exchange

The first process probed was B-H bridging/terminal exchange, which is responsible for the equivalence of the phosphines in **2-13** and **2-14** at room temperature by NMR spectroscopy. Computational results on the iridium system indicate that the process involves initial B-H dissociation from the metal (η^2 to η^1), which is followed by rotation about the remaining M-H-B interaction, and finally coordination of the other B-H bond (Scheme 2.17). Rotation around the M-H-B bond causes the NMe_3 group to change position (*i.e.* up *versus* down), resulting in equivalent phosphines. An additional feature of the η^1 intermediate is the presence of an agostic interaction resulting from the approach of one cyclohexyl group towards the iridium centre

(Figure 2.14). Key calculated bond distances are: Ir···C, 3.00 Å; Ir···H, 2.20 Å; C-H, 1.13 Å. This intermediate is closely connected to the transition state to rotation in which the cyclohexyl group was also calculated to be approaching the iridium in the transition state (Ir···C, 3.33 Å; Ir···H, 2.55 Å; C-H, 1.11 Å). Calculations on the rhodium system, **2-13**, have yet to identify a transition state or intermediate equivalent to that identified for the iridium system. Current tactics to pursue the identification of this transition state/intermediate include the use of a smaller model, PMe_3.



Scheme 2.17 Overall process that makes the phosphine ligands equivalent as calculated. $[BAr^F_4]^-$ anions not shown.

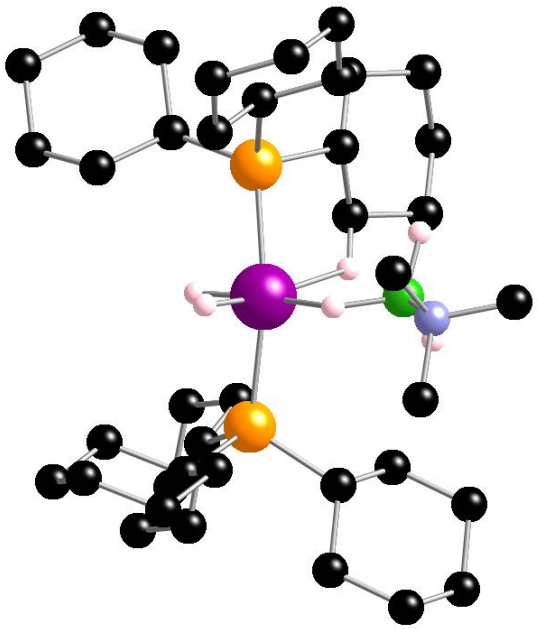
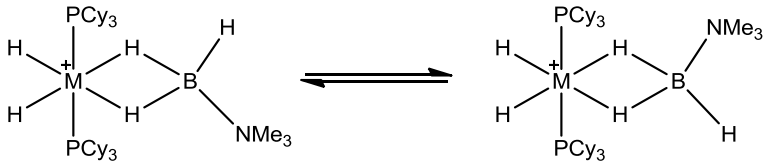


Figure 2.14 Calculated structure of agostic intermediate for B-H bridging/terminal exchange in $[Ir(H)_2(PCy_3)_2(\eta^2\text{-}H_3B{\cdot}NMe_3)][BAr^F_4]$. $[BAr^F_4]^-$ anion not shown. Key bond lengths: Ir···C, 3.00 Å; Ir···H, 2.20 Å; C-H, 1.13 Å.

The room temperature ^{1}H NMR spectra of both complexes, **2-13** and **2-14**, show a relative 3H integral, quadrupolar broadened, signal at δ -0.28 ppm (Rh) and δ -1.76 ppm (Ir), assigned to the BH_3 group which is undergoing rapid exchange between the terminal and bridging sites on the ^{1}H NMR timescale.[6, 24, 29, 30] The $^{31}P\{^{1}H\}$ NMR spectra show single environments indicating equivalent phosphorus atoms due to the fluxional processes.

Gradual cooling of a CD_2Cl_2 solution of **2-13** and **2-14** to 180 K results in an increased broadening of the BH_3 signals, but as these signals are already significantly quadrupolar broadened, modelling of this change and subsequent extraction of a rate constant for exchange at each temperature is problematic. Instead the $^{31}P\{^{1}H\}$ NMR data were utilised, and in particular the non equivalence of the phosphines at the low temperature limit. For **2-13** the low temperature limit was not reached (180 K) although significant broadening was observed (Figure 2.15, upper), but for **2-14** two environments in a tightly coupled AB doublet ($^{2}J_{PP}$ = 260 Hz] are observed at 210 K (Figure 2.16, upper), consistent with a static structure (Scheme 2.18). These observations are consistent with those previously reported for **2-14** but not studied in detail.[53]



Scheme 2.18 Rotation about the M-H-B interaction resulting in inequivalent phosphines. $[BAr^{F}_{4}]^{-}$ anions not shown.

The $^{31}P\{^{1}H\}$ NMR spectra of **2-13** and **2-14** at each temperature were modelled using gNMR (Figure 2.15 and Figure 2.16)

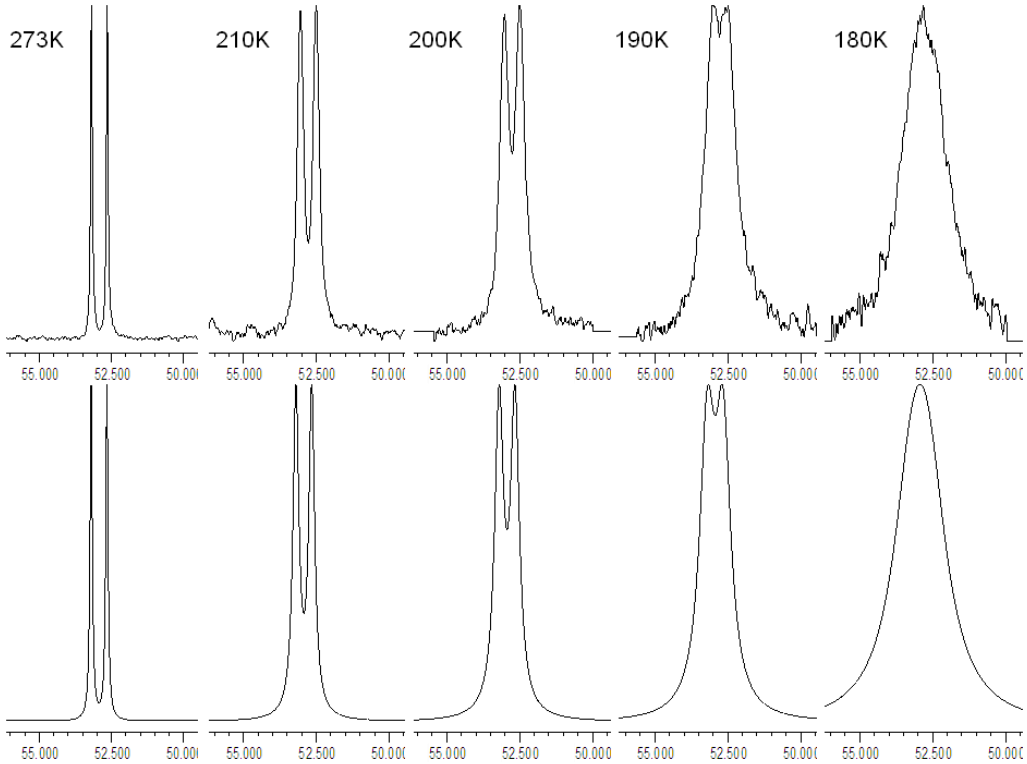


Figure 2.15 $^{31}P\{^{1}H\}$ NMR spectra of $[Rh(H)_2(PCy_3)_2(\eta^2\text{-}H_3B{\cdot}NMe_3)][BAr^F{}_4]$ (**2-13**) in CD_2Cl_2 at a range of temperatures (upper) and gNMR simulations (lower).

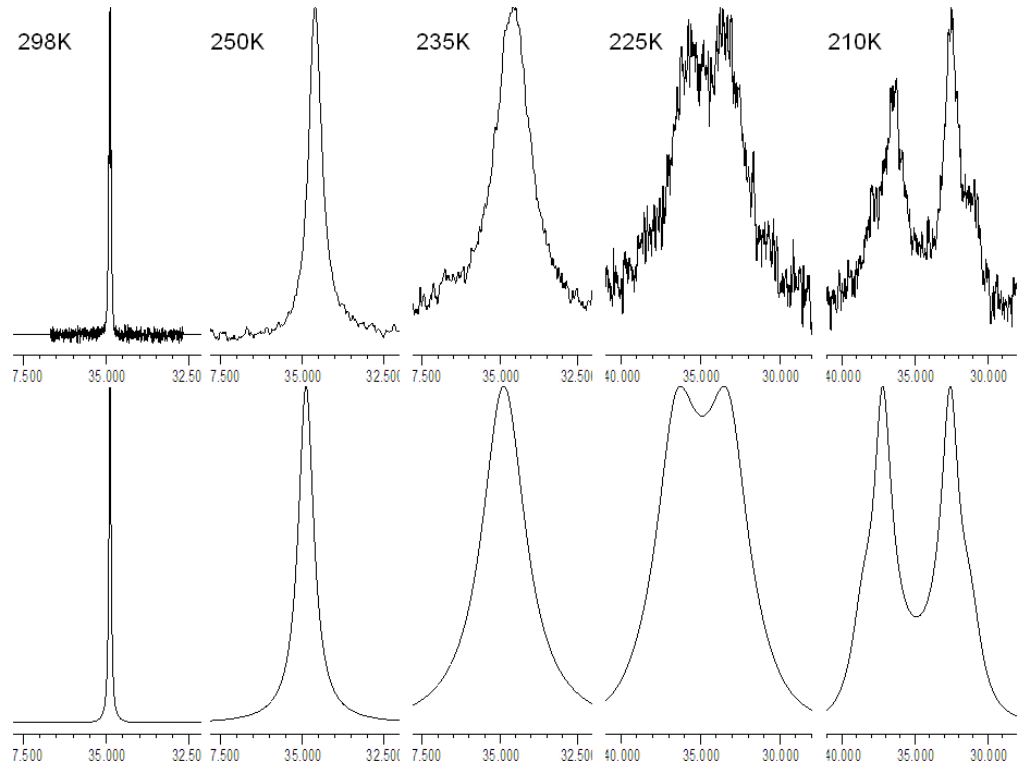


Figure 2.16 $^{31}P\{^{1}H\}$ NMR spectra of $[Ir(H)_2(PCy_3)_2(\eta^2\text{-}H_3B{\cdot}NMe_3)][BAr^F{}_4]$ (**2-14**) in CD_2Cl_2 at a range of temperatures (upper) and gNMR simulations (lower).

Table 2.1 Rate constants for the exchange of bridging M–H–B and terminal B–H protons at different temperatures for **2-13** (Rh) and **2-14** (Ir).

Rh		**Ir**	
Temperature / K	**Rate, k** / s^{-1}	**Temperature** / K	**Rate, k** / s^{-1}
273	1.0×10^{6}	298	1.0×10^{6}
210	7.0×10^{4}	250	2.5×10^{4}
200	4.0×10^{4}	235	8.0×10^{3}
190	2.1×10^{4}	225	3.0×10^{3}
180	8.0×10^{3}	210	1.1×10^{3}

The corresponding rates of exchange (Table 2.1) were used to perform an Eyring analysis (see Figure 2.17 for a sample plot for **2-13**) allowing the determination of the activation parameters for the exchange process (Table 2.2).

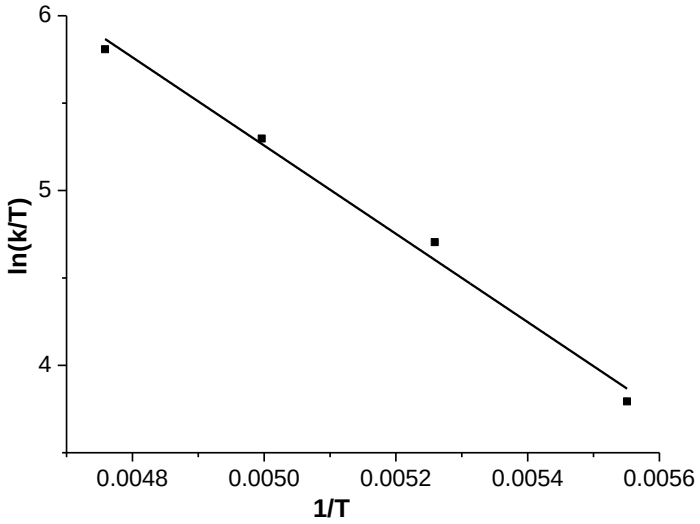


Figure 2.17 Eyring Plot for the fluxional process that exchanges Rh–H–B and B–H protons in $[Rh(H)_2(PCy_3)_2(\eta^2\text{-}H_3B{\cdot}NMe_3)][BAr^F{}_4]$ (**2-13**).

Table 2.2 Activation parameters derived from the variable temperature NMR data for the B-H exchange process in $[M(H)_2(PCy_3)_2(\eta^2\text{-}H_3B{\cdot}NMe_3)][BAr^F{}_4]$ (M = Rh, Ir).

	Rh	**Ir**
$\Delta H^{\ddagger}$ / kJ mol^{-1}	21.0 ± 1.4	32.6 ± 2.5
$\Delta S^{\ddagger}$ / J mol^{-1} K^{-1}	-48.9 ± 7.2	-29.7 ± 11.1
$\Delta G^{\ddagger}$ / kJ mol^{-1}	35.6 ± 3.6	41.4 ± 5.8

For both complexes, exchange of terminal and bridging B-H's is a low energy process (**2-13**, 35.6 ± 3.6 kJ mol^{-1} and **2-14**, 41.4 ± 5.8 kJ mol^{-1}) as has been noted for related systems.[5, 29, 31, 32, 59-61] The larger barrier for **2-14** reflects the breaking of stronger Ir···H_3B interactions, as evidenced by the greater upfield shift in the ^{1}H NMR spectrum for Ir-H-B from the free amine-borane for **2-14** (**2-13**, δ -0.28 ppm; **2-14**, δ -1.76 ppm). The smaller barrier for **2-13** is also in line with the failure to reach the low temperature limit and freeze out the fluxional process (Figure 2.15). Interestingly both processes have a negative activation entropy associated with them (**2-13**, -48.9 ± 7.2 J mol^{-1} K^{-1} and **2-14**, -29.7 ± 11.1 J mol^{-1} K^{-1}), indicative of a more ordered transition state. This negative entropy could be accounted for by a transition state featuring an agostic[10] C-H interaction from a cyclohexyl phosphine as calculated (Figure 2.14). The errors of the experimentally determined entropies of activation are significant and as such the values for **2-13** and **2-14** are best considered to be similar, although both clearly negative.

A comparison of the computed and experimentally determined values for the enthalpy of activation for **2-14** reveals a good agreement; 34.1 kJ mol^{-1} and 32.6 ± 2.5 kJ mol^{-1} respectively (Table 2.3). However the calculated free energy of activation, 32.9 kJ mol^{-1}, is lower than the experimentally determined value, 41.4 ± 5.8 kJ mol^{-1}.

This suggests that the computational investigation is not capturing the negative entropy of activation, which in turn suggests it is minimal. A possible source of error in the calculations is the neglect of solvent rearrangement in the model used. As discussed earlier, calculations on **2-14** are still ongoing.

Table 2.3 Calculated and experimentally determined enthalpy of activation and free energy of activation for $[Ir(H)_2(PCy_3)_2(\eta^2\text{-}H_3B{\cdot}NMe_3)][BAr^F{}_4]$ (**2-14**).

	ΔH‡ / kJ mol^{-1}	**ΔG‡** / kJ mol^{-1}
Calculated	34.1	32.9
Experimental	32.6 ± 2.5	41.4 ± 5.8

Hemilabile η^2 to η^1 changes in coordination mode have been reported for borohydride ligands[62] and chelating phosphine-boranes[31, 63] on addition of two electron ligands such as MeCN or CO. Such ligands obviously bind more strongly than the postulated agostic intermediates of **2-13** and **2-14**, and as such the η^1 intermediate can be isolated or observed in solution. For example, the addition of the nucleophile PMe_2Ph to $[Ru(PMe_2Ph)_2(H)(CO)(\eta^2\text{-}BH_4)]$ affords the η^1 complex $[Ru(PMe_2Ph)_3(H)(CO)(\eta^1\text{-}BH_4)]$.[62] In a reverse of our system, Shimoi and co-workers have calculated that their η^1 TMAB complexes, such as $[Cr(CO)_5(\eta^1\text{-}H_3B{\cdot}NMe_3)]$ (**i-27**), undergo B-H exchange *via* an η^2 transition state.[32, 59]

We cannot comment on whether this associative mechanism involving a phosphine is a general one as to the best of our knowledge no other entropies of activation for σ-bound amine-borane fluxionality have been reported.

2.4.2 M-H and B-H exchange

The next processes to be investigated were the relative rates of M-H and B-H exchange, which were investigated through H/D exchange experiments. Initially, a sample of **2-13** or **2-14** in 1,2-$C_6H_4F_2$ was placed under an atmosphere of D_2 (4 atm). On warming to 298 K, the samples were monitored using ^1H NMR spectroscopy. Resulting integration of the BH_3 and metal hydride (M-H_2) signals generated the plots seen in Figure 2.18. These showed incorporation of deuterium into both sites by a reduction of the appropriate integral value.

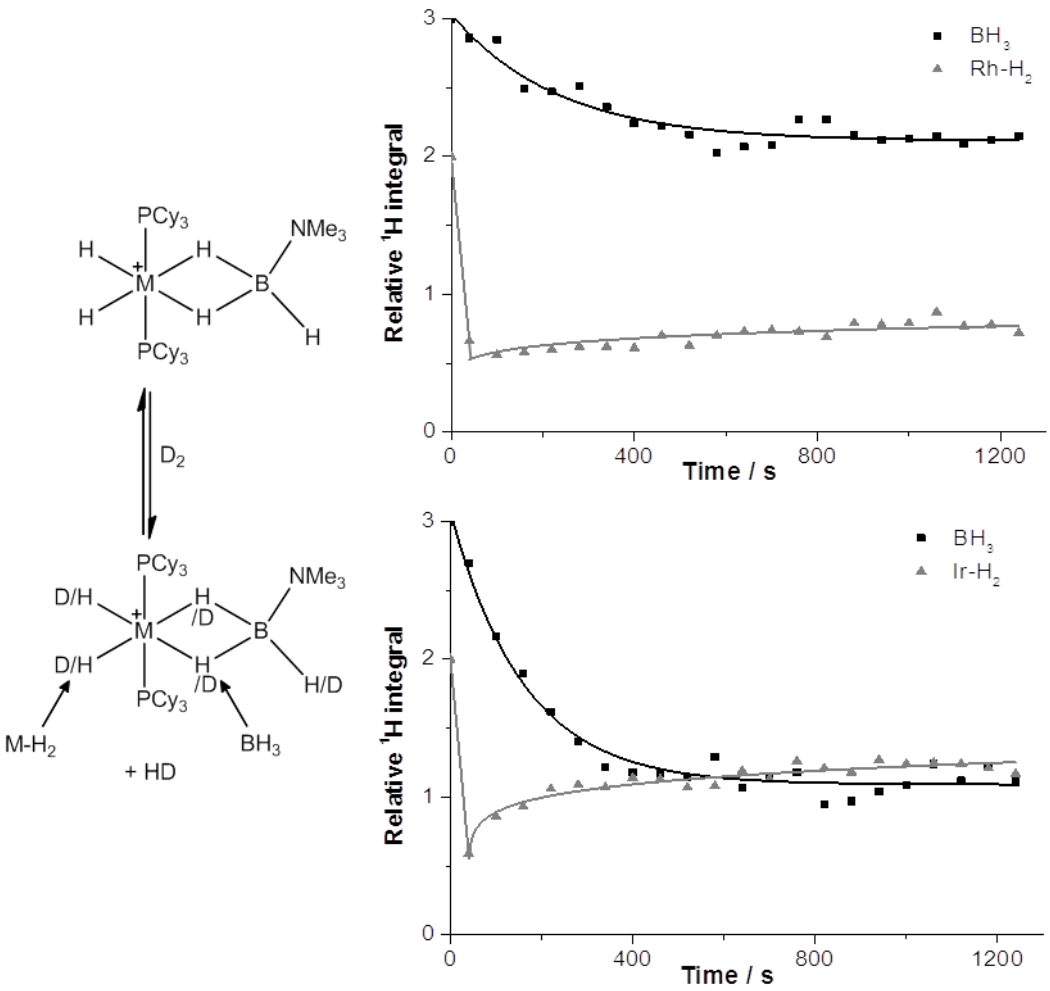
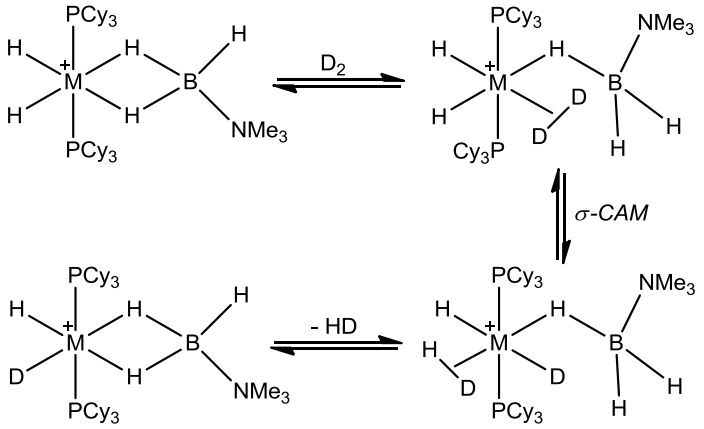


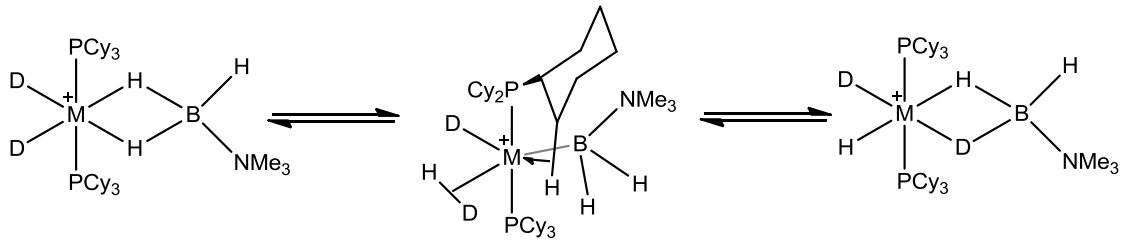
Figure 2.18 Relative ^1H integrals of M-H-B and M-H_2 of $[M(H)_2(PCy_3)_2(\eta^2\text{-}H_3B{\cdot}NMe_3)][BAr^F{}_4]$ over time, under a pressure of D_2. Upper = **2-13** (Rh); Lower = **2-14** (Ir). $[BAr^F{}_4]^-$ anions not shown.

Deuterium was observed to be incorporated into the rhodium and iridium hydrides at about the same rates; similar incorporation (~ 75%) was seen at the first measured point (t = 40 seconds). The formation of HD was observed in the ^{1}H NMR spectra [δ 4.56 ppm, (t, $^1J_{HD}$ = 43 Hz)]. The mechanism by which the exchange is postulated to occur is shown in Scheme 2.19: one B-H bond dissociates (η^2 to η^1) to give an intermediate similar to that for BH_3 exchange but the vacant site at the metal is now occupied by D_2 rather than the weak agostic interaction in Scheme 2.17. D_2 then exchanges with the metal hydrides *via* a σ-complex assisted metathesis (σ-CAM).[64] Finally loss of HD occurs followed by re-coordination of the B-H bond (η^1 to η^2).



Scheme 2.19 Mechanism of M-H/D_2 H/D exchange in **2-13** (Rh) and **2-14** (Ir). $[BAr^F{}_4]^-$ anions not shown.

Following rapid M-H/H_2 H/D exchange, slower B-H/M-H exchange occurs *via* reversible B-H activation, which we propose to occur *via* an agostic intermediate (Scheme 2.20). As a consequence of this exchange the M-H_2 integral is observed to increase slightly after the initial drop as H from the BH_3 is incorporated into the M-D (Figure 2.18). It should also be noted here that the presence of excess D_2 means that it is not just the rate of intrinsic H/D exchange that is being measured, as additional D_2 is incorporated until the system reaches equilibrium.



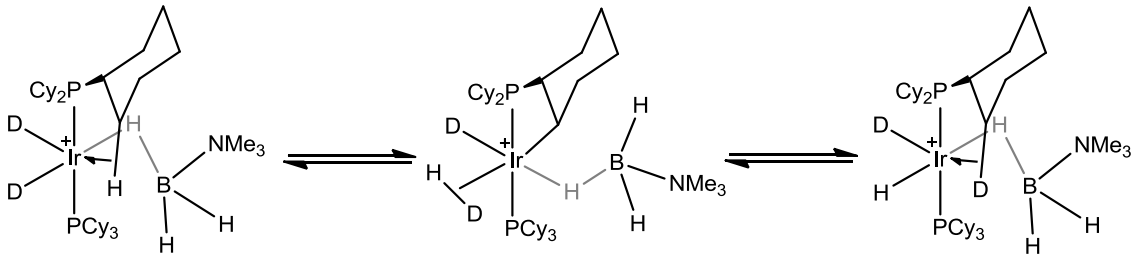
Scheme 2.20 Postulated mechanism of M-H/B-H H/D exchange. $[BAr^F_4]^-$ anions not shown.

M-H/B-H exchange (Scheme 2.20) could also account for the B-H terminal/bridging fluxionality and the resulting equivalence of the phosphines at 298 K, but the timescale for this is much slower than the NMR timescale. If this process was very fast, then only one frequency averaged M-H/B-H environment could be expected, as observed for $[Rh(H)_2(PCy_3)_2(\eta^2\text{-}H_2)_2][BAr^F_4]$ (**i-20**) at 298 K.[65] However, as separate environments are observed for M-H_2 and BH_3 this suggests that this process is not responsible for the equivalence of the phosphines at room temperature.

The incorporation of deuterium into the BH_3 group *via* reversible B-H activation is observed to be much slower for **2-13** than its iridium counterpart **2-14**. This is speculated to be due to the presence of the agostic intermediate/transition state on the pathway of reversible B-H activation (Scheme 2.20), which, by nature of iridium's 5d orbitals *versus* rhodium's 4d orbitals, might be stronger for **2-14**. Such an intermediate/transition state is suggested to lower the barrier to B-H exchange. The isolation of $[Ir(H)\{PCy_2(\eta^2\text{-}C_6H_9)\}\{PCy_2(\eta^3\text{-}C_6H_8)\}][BAr^F_4]$, which features dehydrogenated phosphines, provides evidence for the relative ease at which the iridium compound can C-H activate the cyclohexyl group, presumably *via* an agostic intermediate.[53, 66] Addition of 4 atm of H_2 rehydrogenates the cyclohexyl groups, reforming the *bis*-dihydrogen dihydride complex $[Ir(H)_2(PCy_3)_2(\eta^2\text{-}H_2)_2][BAr^F_4]$ **i-21** (Scheme 2.15), demonstrating the reversibility of the C-H activation and subsequent

dehydrogenation. The equivalent rhodium complex is not known, although related complexes featuring dehydrogenated tricyclopentylphosphine ligands are.[67]

Monitoring the same reaction by ^{2}H NMR spectroscopy, reveals that incorporation of deuterium into the cyclohexyl phosphines (δ 2.5 – 0.8 ppm) for **2-14** also occurs. No deuterium incorporation into phosphines was observed for **2-13**, supporting the presence of a stronger agostic interaction for the iridium complex, which can undergo reversible C-H activation (Scheme 2.21).



Scheme 2.21 Reversible C-H activation of cyclohexyl phosphine resulting in incorporation of deuterium into the cyclohexyl. $[BAr^F_4]^-$ anions not shown.

Interestingly, evidence for the isotopic perturbation of equilibrium was observed in the ^{2}H NMR spectra of **2-14** when under an atmosphere of D_2 (Figure 2.19). Three separate signals were observed for the different levels of deuterium incorporation into the BH_3; BH_2D, BHD_2 and BD_3 of Ir···$H_3B{\cdot}NMe_3$. As mentioned previously for **2-6**, such an effect is observed due to a preference for the heavier deuterium atom to be in the terminal rather than bridging position, resulting in a net upfield shift of the BHD_2 signal (δ -1.1 ppm) relative to the BH_2D signal (δ -0.6 ppm) when in equilibrium exchange. The observed difference in shifts of 0.4 and 0.5 ppm are in line with others observed for related borane and alkane systems.[68-71] De Gala and Hartwig observed isotopic perturbation of equilibrium for the niobium compound, $[Cp_2Nb(H_2BCat)]$.[69] In contrast to our system, different chemical shifts were observed for the fully protio

and fully deuterio complexes (~ 1 ppm difference), which they suggest is due to a rapid equilibrium between the hydridoborate and boryl complexes *i.e.* [$Cp_2Nb(H_2BCat)$] and [$Cp_2Nb(H)_2(BCat)$]. More recently Calladine *et al.* have reported a difference in chemical shift of 0.75 ppm for the coordination of partially deuterated propane to the [$CpMn(CO)_2$] fragment.[71] The chemical shift difference is much greater than observed for **2-6** (Figure 2.11), which was a result of secondary deuterium isotope effects and hence smaller. Attempts to perturb this equilibrium by cooling the sample resulted in the broadening of the BH_3 signal and the subsequent splitting into the separate terminal and bridging hydrogen signals as reported previously.[53] Slight asymmetry in the BH_3 peak was observed for **2-13** (Rh), evidence for the isotopic perturbation of equilibrium, but the effect was more pronounced for **2-14**, likely due to the stronger Ir···H_3B interaction.

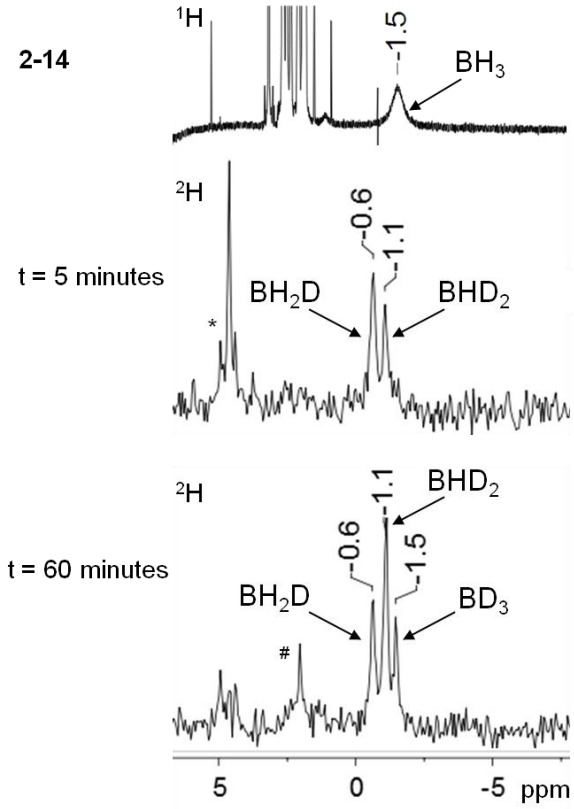


Figure 2.19 Isotopic perturbation of equilibrium of the $BH(D)_3$ signals in the ^{2}H NMR spectrum of [$Ir(H)_2(PCy_3)_2(\eta^2$-$H_3B{\cdot}NMe_3)$][$BAr^F{}_4$] (**2-14**) under an atmosphere of D_2 (middle and lower). * = HD/D_2. # = PCy_3. ^{1}H NMR spectrum of **2-14** (upper).

For both complexes, no deuterium secondary isotope effects were observed in the $^{31}P\{^{1}H\}$ NMR spectrum in contrast to **2-6**. This is likely due to the bound B-H being located *cis* to the phosphines rather than *trans* as for **2-6**. Slight asymmetry of the BH_3 peak was observed in the ^{1}H NMR spectrum indicative of isotopic perturbation of resonance (Figure 2.20), but the effect was less pronounced due to the broad nature of the BH_3 resonance.

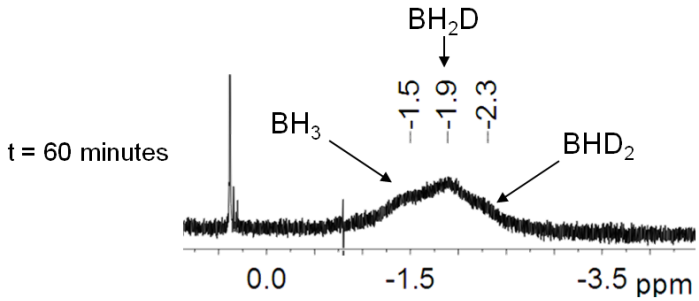
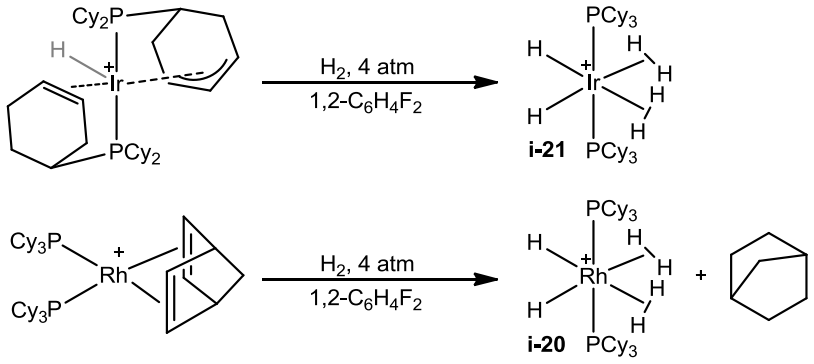


Figure 2.20 Isotopic perturbation of equilibrium of the $BH(D)_3$ signals in the ^{1}H NMR spectrum of $[Ir(H)_2(PCy_3)_2(\eta^2\text{-}H_3B{\cdot}NMe_3)][BAr^F{}_4]$ (**2-14**) under an atmosphere of D_2.

The above experiments contained exogenous D_2, which can be incorporated into the BH_3 and M-H_2 until equilibrium is established, and so it is not just the intrinsic H/D exchange that is measured, but a combination of B-H/M-H and M-H/H_2. To eliminate the excess D_2 and probe just the relative rates of B-H/M-H exchange ideally $[M(D)_2(PCy_3)_2(\eta^2\text{-}H_3B{\cdot}NMe_3)][BAr^F{}_4]$ would be prepared and the relative integrals of M-H_2 and BH_3 would be monitored over time by ^{1}H NMR spectroscopy. However for iridium, the fragment $\{M(D)_2(PCy_3)_2\}^+$ cannot be synthesised without incorporation of deuterium into the cyclohexyl groups of the phosphine as the precursor features dehydrogenated phosphines (Scheme 2.22). As we have shown that the phosphines are not spectator ligands (Scheme 2.21) the presence of deuterium in the phosphine could affect the rate of M-H/B-H exchange.



Scheme 2.22 Formation of the *bis*-dihydrogen dihydride complexes **i-20** (Rh) and **i-21** (Ir). $[BAr^F{}_4]^-$ anions not shown.

Instead $[M(H)_2(PCy_3)_2(\eta^2\text{-}D_3B{\cdot}NMe_3)][BAr^F{}_4]$ (M = Rh, **2-15**; M = Ir, **2-16**) was synthesised by the addition of a solution of $D_3B{\cdot}NMe_3$ in 1,2-$C_6H_4F_2$ to $[M(H)_2(PCy_3)_2(\eta^2\text{-}H_2)_2][BAr^F{}_4]$ in the absence of H_2 (solution was degassed prior to addition of $D_3B{\cdot}NMe_3$). The relative ^1H integrals of the metal hydride and BH_3 signals of **2-15** and **2-16** in 1,2-$C_6H_4F_2$ were monitored over time by ^1H NMR spectroscopy (Figure 2.21). Consistent with the results under a D_2 atmosphere, it was apparent that the rate of B-H/D exchange was much faster for the iridium analogue, which reached the equilibrium between M-H/B-H exchange by the first measured point (t = 40 seconds), while **2-15** had not reached equilibrium after ~30 minutes. Upon reaching the equilibrium, it could be expected that hydrogen would be distributed in a ratio of 2:3, M-H_2:BH_3. However, a ratio of closer to 1:1 is observed, indicating that hydrogen is equally distributed between the two sites. It is possible that isotopic perturbation of equilibrium results in Ir-D being favoured over Ir-D-B, which skews the equilibrium.

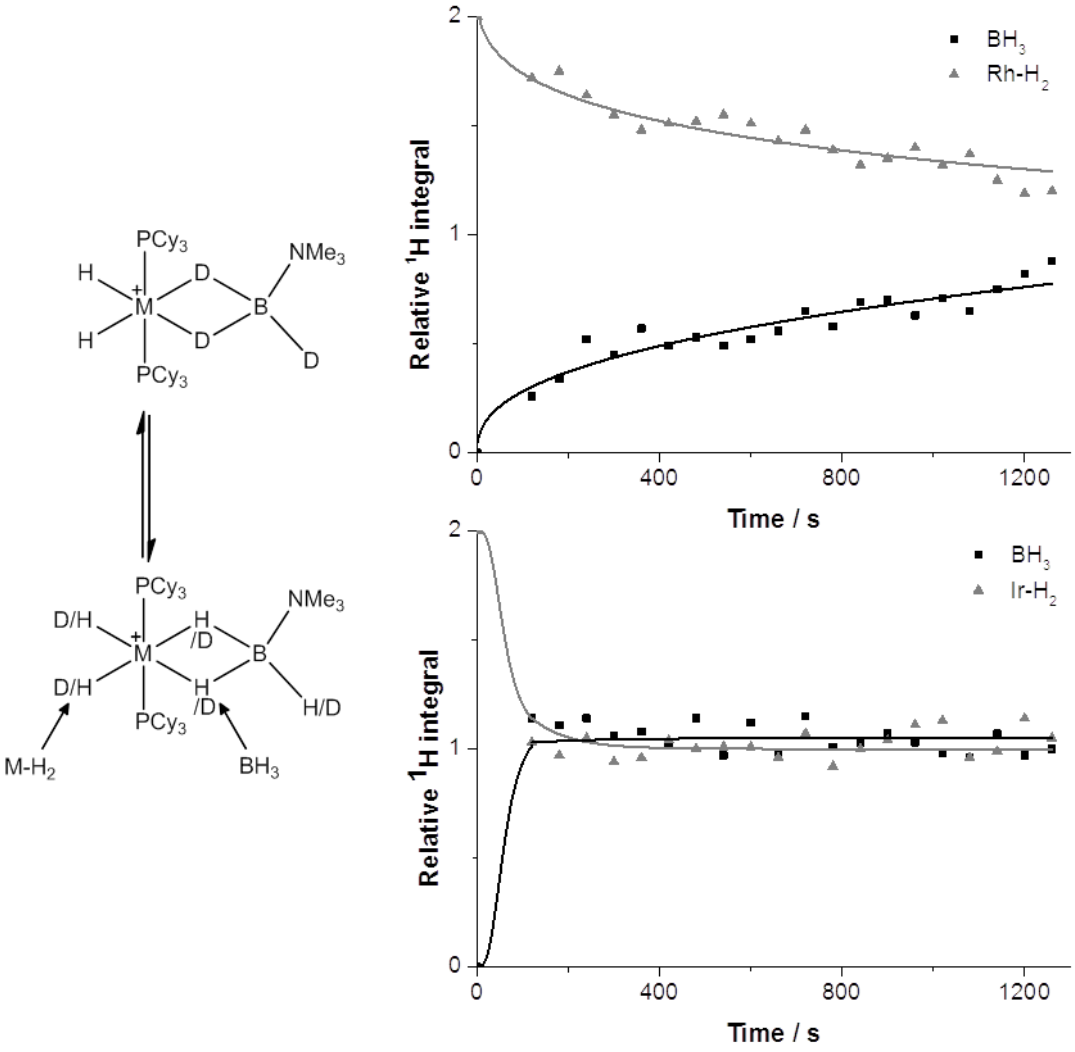


Figure 2.21 Relative ^{1}H integrals of M-H-B and M-H_2 of $[M(H)_2(PCy_3)_2(\eta^2\text{-}D_3B{\cdot}NMe_3)][BAr^F{}_4]$ over time. Upper = **2-15** (Rh); Lower = **2-16** (Ir).

The observation of slower deuterium incorporation into the BH_3 signal for **2-15** (Rh) in comparison to **2-16** (Ir) goes against the overall rate at which their respective dihydrogen complexes catalyse the dehydrocoupling of DMAB; *i.e.* **i-21** (Ir) is a slower catalyst (TOF = 0.07 h^{-1}, 20 mol%, sealed system)[53] than **i-20** (Rh) (TOF ~ 0.4 h^{-1}, 5 mol%, sealed system, Chapter 3). This is unexpected given that B-H activation of DMAB *via* a σ-complex is calculated to be on the pathway to dehydrogenation and these experiments indicate that B-H activation is apparently slower for Rh. However, for both systems N-H activation has been calculated to be the rate determining step

for overall dehydrogenation.[5, 53] Consideration should also be given to the metals' ability to access the +1 oxidation state. Experiments have shown that the rhodium complex can dehydrogenate DMAB *via* a constant oxidation state Rh(III) manifold (Chapter 3). However, it can also access the Rh(I) oxidation state allowing a Rh(I)/Rh(III) cycle, which operates much more rapidly with DMAB. We do not probe such a process here. Rhodium catalysts featuring chelating phosphines, which strongly favour the Rh(I) oxidation state over Rh(III), have been found to be one of the fastest catalysts for the dehydrogenation of DMAB.[26] Iridium has been calculated to dehydrogenate DMAB *via* a constant Ir(III) oxidation state cycle in a σ-CAM fashion (Scheme 1.50).[53] Ir(I) was not implicated in the mechanism. The related $Ir(H)_2(POCOP^{Me})$ ($POCOP^{Me}$ = κ^3-1,3-$(OPMe_2)_2C_6H_3$) system has also been calculated to favour an Ir(III)/Ir(III) mechanism over a Ir(I)/Ir(III) manifold.[72]

It is also possible that the rate of B-H/D exchange could be increased by the presence of excess amine-borane, as for DMAB this could allow intermolecular $BH^{\delta-}\cdots^{\delta+}HN$ dihydrogen interactions, which might lower the energy of any transition state.[73-77] However, attempts to investigate the effect of excess TMAB on the rate of incorporation of deuterium into BH_3 were unsuccessful. Exchange between the free and bound TMAB resulted in significant broadening of the BH_3 signal in the ^1H NMR spectrum, causing overlap with other signals and preventing reliable integration.

Detailed computational investigations into the fluxional and exchange processes mentioned above are underway (Prof. Stuart A. Macgregor, Heriot-Watt University). However, at the time of writing this thesis they were not complete.

2.5 Conclusions

The low-coordinate rhodium *bis*-phosphine fragment of empirical formula $\{Rh(P^tBu^iBu_2)_2\}^+$ has been synthesised and found to undergo a reversible cyclometalation of one of the *iso*-butyl groups at room temperature to give a Rh(III) species. However, $\{Rh(P^tBu^iBu_2)_2\}^+$ reacts as if a Rh(I) species indicating that a fluxional process is occurring that rapidly equilibrates the Rh(I) with the Rh(III) cyclometalated species *via* reversible H-C(sp^3) bond cleavage. Complex **2-4** reacts with TMAB to form a σ-complex (**2-6**). Addition of TBE to **2-6** resulted in hydroboration of TBE to generate $Me_3N{\cdot}H_2BCH_2CH_2CMe_3$ (**I**), which coordinates to the rhodium centre. $\{Rh(P^tBu^iBu_2)_2\}^+$ can also promote the hydroboration of TBE under catalytic conditions, but only to ~70% conversion, due to product inhibition. The ability of $\{Rh(P^tBu^iBu_2)_2\}^+$ to catalyse the hydroboration appears to be specific to this phosphine, which we propose is due to the steric bulk of the ^{t}Bu and also the ligand flexibility that the methylene spacer confers. The mechanism of hydroboration was investigated through a combination of stoichiometric reactions, selective deuteration experiments and determination of initial rates, resulting in the mechanism proposed in Scheme 2.11. The use of d_3-TMAB in this study revealed the reversibility of the coordination and insertion steps, but also apparent were interesting secondary deuterium isotope effects in the $^{31}P\{^1H\}$ NMR spectra of **2-6** and **2-8** resulting from the isotopic perturbation of equilibrium and resonance respectively. $\{Rh(P^tBu^iBu_2)_2\}^+$ is also capable of promoting the catalytic hydroboration of TBE by the secondary amine-borane, DMAB, the products of which can also undergo a tandem dehydrogenation producing the *B*-amino-boranes $Me_2N{=}BH(CH_2CH_2CMe_3)$ (**II**) and $Me_2N{=}B(CH_2CH_2CMe_3)_2$ (**III**).

Three fluxional processes were investigated in the amine-borane σ-complexes **2-13** (Rh) and **2-14** (Ir) through a combination of H/D exchange and variable temperature NMR experiments. Preliminary computational calculations were also reported. For both complexes, an unexpected negative entropy was found for the fluxional processes exchanging bridging and terminal B-H atoms, which we suggest can be accounted for by the formation of an agostic interaction from a cyclohexyl group in the transition state. Initial computational results for **2-14** support this theory. Placing **2-13** or **2-14** under an atmosphere of deuterium resulted in rapid incorporation of deuterium into the metal hydrides of each. But, for **2-13**, B-H activation was observed to be a much slower process. This was supported by monitoring the ^{1}H NMR spectra of the partially deuterated isotopomers of **2-13** and **2-14**, **2-15** and **2-16**. The observed difference could be due to the involvement of the cyclohexyl phosphines in the iridium complexes, helping to stabilise intermediates. No such involvement was observed for the rhodium complexes. Computational studies to further probe these fluxional processes are underway.

Isotopic perturbation of the equilibria was observed in ^{2}H NMR spectra of **2-13** and **2-14** under an atmosphere of deuterium, due to a preference for the lighter hydrogen atom to be in the bridging rather than terminal position. The effect was more apparent in **2-14** due to the stronger Ir···H_3B interactions. No secondary deuterium isotope effect was observed in the ^{31}P{^{1}H} NMR spectra due to the location of the phosphines *cis* to the amine-borane, as opposed to the *trans* conformation in **2-6** and **2-8**.

2.6 References

1. T. M. Douglas, A. B. Chaplin and A. S. Weller, *Organometallics*, 2008, **27**, 2918-2921.
2. N. Miyaura and A. Suzuki, *Chem. Rev.*, 1995, **95**, 2457-2483.
3. J. F. Hartwig, *Organotransition Metal Chemistry*, University Science Books, 2010.
4. N. S. Townsend, A. B. Chaplin, M. Abu Naser, A. L. Thompson, N. H. Rees, S. A. Macgregor and A. S. Weller, *Chem. Eur. J.*, 2010, **16**, 8376-8389.
5. T. M. Douglas, A. B. Chaplin, A. S. Weller, X. Z. Yang and M. B. Hall, *J. Am. Chem. Soc.*, 2009, **131**, 15440-15456.
6. T. M. Douglas, A. B. Chaplin and A. S. Weller, *J. Am. Chem. Soc.*, 2008, **130**, 14432-14433.
7. R. J. Pawley, G. L. Moxham, R. Dallanegra, A. B. Chaplin, S. K. Brayshaw, A. S. Weller and M. C. Willis, *Organometallics*, 2010, **29**, 1717-1728.
8. T. M. Douglas, DPhil Thesis, Oxford University, 2009.
9. R. W. Kunz and P. S. Pregosin, *^{31}P and ^{13}C NMR of transition metal phosphine complexes*, Springer-Verlag, Berlin ; New York, 1979.
10. M. Brookhart, M. L. H. Green and G. Parkin, *Proc. Natl. Acad. Sci. USA*, 2007, **104**, 6908-6914.
11. R. H. Crabtree, *The Organometallic Chemistry of the Transition Metals, Fourth Edition*, John Wiley & Sons: Hoboken, NJ, 2005.
12. A. C. Cooper, E. Clot, J. C. Huffman, W. E. Streib, F. Maseras, O. Eisenstein and K. G. Caulton, *J. Am. Chem. Soc.*, 1999, **121**, 97-106.
13. N. M. Scott, R. Dorta, E. D. Stevens, A. Correa, L. Cavallo and S. P. Nolan, *J. Am. Chem. Soc.*, 2005, **127**, 3516-3526.
14. B. L. Shaw, *J. Am. Chem. Soc.*, 1975, **97**, 3856-3857.
15. A. Y. Verat, M. Pink, H. Fan, J. Tomaszewski and K. G. Caulton, *Organometallics*, 2008, **27**, 166-168.
16. M. Albrecht, *Chem. Rev.*, 2010, **110**, 576-623.
17. F. Mohr, S. H. Priver, S. K. Bhargava and M. A. Bennett, *Coord. Chem. Rev.*, 2006, **250**, 1851-1888.
18. J. Chatt and J. M. Davidson, *J. Chem. Soc.*, 1965, 843-846.
19. N. P. Tsvetkov, M. F. Laird, H. J. Fan, M. Pink and K. G. Caulton, *Chem. Commun.*, 2009, 4578-4580.
20. A. C. Albeniz, G. Schulte and R. H. Crabtree, *Organometallics*, 1992, **11**, 242-249.
21. A. Y. Verat, M. Pink, H. J. Fan, B. C. Fullmer, J. Telser and K. G. Caulton, *Eur. J. Inorg. Chem.*, 2008, 4704-4709.
22. M. A. Rankin, D. F. MacLean, R. McDonald, M. J. Ferguson, M. D. Lumsden and M. Stradiotto, *Organometallics*, 2009, **28**, 74-83.
23. G. G. Christoph, P. Blum, W. C. Liu, A. Elia and D. W. Meek, *Inorg. Chem.*, 1979, **18**, 894-897.
24. A. B. Chaplin and A. S. Weller, *Inorg. Chem.*, 2010, **49**, 1111-1121.
25. M. H. Chisholm, J. C. Huffman and S. S. Iyer, *J. Chem. Soc. Dalton. Trans.*, 2000, 1483-1489.
26. R. Dallanegra, A. P. M. Robertson, A. B. Chaplin, I. Manners and A. S. Weller, *Chem. Commun.*, 2011, **47**, 3763-3765.
27. A. B. Chaplin, A. I. Poblador-Bahamonde, H. A. Sparkes, J. A. K. Howard, S. A. Macgregor and A. S. Weller, *Chem. Commun.*, 2009, 244-246.
28. L. J. Sewell, G. C. Lloyd-Jones and A. S. Weller, *J. Am. Chem. Soc.*, 2012, **134**, 3598-3610.
29. M. Shimoi, S.-i. Nagai, M. Ichikawa, Y. Kawano, K. Katoh, M. Uruichi and H. Ogino, *J. Am. Chem. Soc.*, 1999, **121**, 11704-11712.
30. G. Alcaraz and S. Sabo-Etienne, *Coord. Chem. Rev.*, 2008, **252**, 2395-2409.
31. N. Merle, G. Koicok-Kohn, M. F. Mahon, C. G. Frost, G. D. Ruggerio, A. S. Weller and M. C. Willis, *Dalton Trans.*, 2004, 3883-3892.

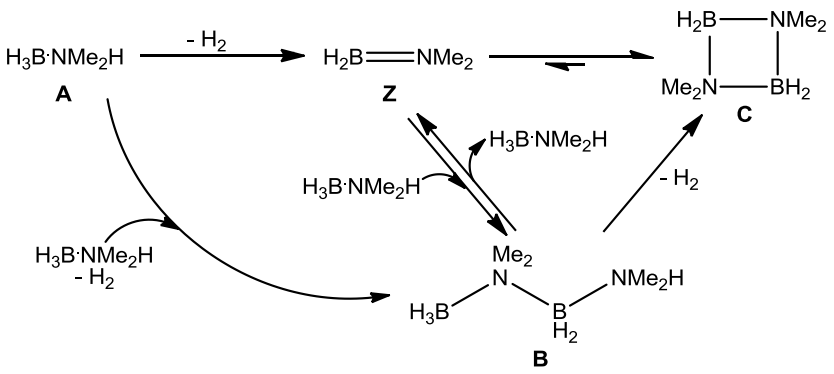
32. Y. Kawano, K. Yamaguchi, S. Y. Miyake, T. Kakizawa and M. Shimoi, *Chem. Eur. J.*, 2007, **13**, 6920-6931.
33. W. H. Bernskoetter, C. K. Schauer, K. I. Goldberg and M. Brookhart, *Science*, 2009, **326**, 553-556.
34. S. D. Pike, A. L. Thompson, A. s. G. Algarra, D. C. Apperley, S. A. Macgregor and A. S. Weller, *Science*, 2012, **337**, 1648-1651.
35. Sigma-Aldrich, 15/01/2013.
36. T. C. Morrill, C. A. D'Souza, L. Yang and A. J. Sampognaro, *J. Org. Chem.*, 2002, **67**, 2481-2484.
37. E. Molinos, S. K. Brayshaw, G. Kociok-Kohn and A. S. Weller, *Organometallics*, 2007, **26**, 2370-2382.
38. J. D. Hewes, C. W. Kreimendahl, T. B. Marder and M. F. Hawthorne, *J. Am. Chem. Soc.*, 1984, **106**, 5757-5759.
39. K. Burgess, W. A. Vanderdonk, S. A. Westcott, T. B. Marder, R. T. Baker and J. C. Calabrese, *J. Am. Chem. Soc.*, 1992, **114**, 9350-9359.
40. D. A. Evans, G. C. Fu and B. A. Anderson, *J. Am. Chem. Soc.*, 1992, **114**, 6679-6685.
41. J. M. Brown and G. C. Lloyd-Jones, *J. Am. Chem. Soc.*, 1994, **116**, 866-878.
42. R. B. Calvert and J. R. Shapley, *J. Am. Chem. Soc.*, 1978, **100**, 7726-7727.
43. A. K. Jameson and C. J. Jameson, *J. Magn. Reson.*, 1978, **32**, 455-457.
44. J. C. Christofides and D. B. Davies, *J. Am. Chem. Soc.*, 1983, **105**, 5099-5105.
45. P. Vujanić, E. Gacs-Baitz, Z. Meić, T. Šuste and V. Smrečki, *Magn. Reson. Chem.*, 1995, **33**, 426-430.
46. C. A. Tolman, *Chem. Rev.*, 1977, **77**, 313-348.
47. M. E. Sloan, A. Staubitz, K. Lee and I. Manners, *Eur. J. Org. Chem.*, 2011, 672-675.
48. Y. Jiang, J. Hess, T. Fox and H. Berke, *J. Am. Chem. Soc.*, 2010, **132**, 18233-18247.
49. A. Staubitz, A. P. M. Robertson, M. E. Sloan and I. Manners, *Chem. Rev.*, 2010, **110**, 4023-4078.
50. H. Feulner, N. Metzler and H. Noth, *J. Organomet. Chem.*, 1995, **489**, 51-62.
51. L. Euzenat, D. Horhant, Y. Ribourdouille, C. Duriez, G. Alcaraz and M. Vaultier, *Chem. Commun.*, 2003, 2280-2281.
52. T. Miyazaki, Y. Tanabe, M. Yuki, Y. Miyake and Y. Nishibayashi, *Organometallics*, 2011, **30**, 2394-2404.
53. C. J. Stevens, R. Dallanegra, A. B. Chaplin, A. S. Weller, S. A. Macgregor, B. Ward, D. McKay, G. Alcaraz and S. Sabo-Etienne, *Chem. Eur. J.*, 2011, **17**, 3011-3020.
54. N. K. Boaen and M. A. Hillmyer, *Chem. Soc. Rev.*, 2005, **34**, 267-275.
55. R. J. Keaton, J. M. Blacquiere and R. T. Baker, *J. Am. Chem. Soc.*, 2007, **129**, 1844-1845.
56. Y. Luo and K. Ohno, *Organometallics*, 2007, **26**, 3597-3600.
57. A. Paul and C. B. Musgrave, *Angew. Chem. Int. Ed.*, 2007, **46**, 8153-8156.
58. X. Z. Yang and M. B. Hall, *J. Am. Chem. Soc.*, 2008, **130**, 1798-1799.
59. Y. Kawano, T. Kakizawa, K. Yamaguchi and M. Shimoi, *Chem. Lett.*, 2006, **35**, 568-569.
60. T. Kakizawa, Y. Kawano and M. Shimoi, *Organometallics*, 2001, **20**, 3211-3213.
61. R. Macias, N. P. Rath and L. Barton, *Angew. Chem. Int. Ed.*, 1999, **38**, 162-164.
62. B. Chamberlain, S. B. Duckett, J. P. Lowe, R. J. Mawby and J. C. Stott, *Dalton Trans.*, 2003, 2603-2614.
63. N. Merle, C. G. Frost, G. Kociok-Kohn, M. C. Willis and A. S. Weller, *Eur. J. Inorg. Chem.*, 2006, 4068-4073.
64. R. N. Perutz and S. Sabo-Etienne, *Angew. Chem. Int. Ed.*, 2007, **46**, 2578-2592.
65. M. J. Ingleson, S. K. Brayshaw, M. F. Mahon, G. D. Ruggiero and A. S. Weller, *Inorg. Chem.*, 2005, **44**, 3162-3171.
66. G. Alcaraz, A. B. Chaplin, C. J. Stevens, E. Clot, L. Vendier, A. S. Weller and S. Sabo-Etienne, *Organometallics*, 2010, **29**, 5591-5595.
67. T. M. Douglas, S. K. Brayshaw, R. Dallanegra, G. Kociok-Köhn, S. A. Macgregor, G. L. Moxham, A. S. Weller, T. Wondimagegn and P. Vadivelu, *Chem. Eur. J.*, 2008, **14**, 1004-1022.

68. O. W. Howarth, C. H. Mcateer, P. Moore and G. E. Morris, *J. Chem. Soc. Chem. Commun.*, 1981, 506-507.
69. J. F. Hartwig and S. R. De Gala, *J. Am. Chem. Soc.*, 1994, **116**, 3661-3662.
70. D. R. Lantero, S. L. Miller, J. Y. Cho, D. L. Ward and M. R. Smith, *Organometallics*, 1999, **18**, 235-247.
71. J. A. Calladine, S. B. Duckett, M. W. George, S. L. Matthews, R. N. Perutz, O. Torres and K. Q. Vuong, *J. Am. Chem. Soc.*, 2011, **133**, 2303-2310.
72. A. Paul and C. B. Musgrave, *Angew. Chem. Int. Ed.*, 2007, **46**, 8153-8156.
73. H. C. Johnson, A. P. M. Robertson, A. B. Chaplin, L. J. Sewell, A. L. Thompson, M. F. Haddow, I. Manners and A. S. Weller, *J. Am. Chem. Soc.*, 2011, **133**, 11076-11079.
74. R. Dallanegra, A. B. Chaplin and A. S. Weller, *Angew. Chem. Int. Ed.*, 2009, **48**, 6875-6878.
75. P. M. Zimmerman, A. Paul, Z. Y. Zhang and C. B. Musgrave, *Inorg. Chem.*, 2009, **48**, 1069-1081.
76. S. Aldridge, A. J. Downs, C. Y. Tang, S. Parsons, M. C. Clarke, R. D. L. Johnstone, H. E. Robertson, D. W. H. Rankin and D. A. Wann, *J. Am. Chem. Soc.*, 2009, **131**, 2231-2243.
77. J. Li, S. M. Kathmann, H. S. Hu, G. K. Schenter, T. Autrey and M. Gutowski, *Inorg. Chem.*, 2010, **49**, 7710-7720.

3 Mechanistic Insights into the Dehydrocoupling of DMAB using Cationic Rhodium Complexes

3.1 Introduction

As discussed in Chapter 1, the transition-metal catalysed dehydrocoupling[1] of amine-boranes has received significant interest in the past decade due to the possibility for the controlled and rapid release of dihydrogen (hydrogen storage) or dehydropolymerisation (the production of new B-N polymeric materials).[2-9] Although the parent ammonia-borane, $H_3B{\cdot}NH_3$, and the primary amine-borane, $H_3B{\cdot}NMeH_2$, are the most interesting with regards to hydrogen storage and dehydropolymerisation respectively, the products of their dehydrocoupling are often ill-defined and insoluble, which complicates mechanistic studies. As a result, much attention has been focussed on the secondary amine-borane, $H_3B{\cdot}NMe_2H$ (DMAB), which produces just one main product on dehydrocoupling, $[H_2BNMe_2]_2$, which is soluble in a wide range of solvents.



Scheme 3.1 Suggested B-N containing intermediates and pathways for the dehydrocoupling of DMAB using transition metal catalysts.

Based on the B-N products identified during initial kinetic studies (Scheme 3.1), several mechanisms have been suggested,[10-17] which were discussed in Chapter 1 (Section 1.4.3.3). Despite much attention on the area, a generic mechanism for the dehydrocoupling of DMAB has not been developed, aspects of which could then be applied to other reported transition metal and main group catalyst systems, or act as a framework to base future mechanistic studies on. This chapter features a detailed study on the dehydrocoupling of DMAB with the $\{Rh(PCy_3)_2L_n\}^+$ (L = solvent or agostic interaction) catalyst system using a combined approach of catalysis, stoichiometric reactions, isolated intermediates and kinetic simulations with the aim of producing a unified model for the dehydrocoupling of DMAB.

For the purpose of this chapter and Chapter 4, DMAB and the intermediates and final products of its dehydrocoupling shall be represented by the following letters: $H_3B{\cdot}NMe_2H$ (**A**), $H_3B{\cdot}NMe_2BH_2{\cdot}NMe_2H$ (**B**), $[H_2BNMe_2]_2$ (**C**) and $H_2B{=}NMe_2$ (**Z**) (Scheme 3.1).

3.2 Choice of catalyst system

The ability of cationic $\{Rh(PR_3)_2L_n\}^+$ (R = ^{i}Bu, ^{i}Pr) fragments to catalyse the dehydrocoupling of **A** has recently been reported by the Weller group.[16-18] Such fragments are ideal candidates for mechanistic studies due to their ability to form σ-complexes with amine-boranes allowing the isolation of intermediate and model complexes. They are competent but slow catalysts compared with some of the systems reported to catalyse the dehydrocoupling of **A** such as Schneider's Ru catalyst, [Ru(H)(PMe_3)(PNP)] [PNP = $N(CH_2CH_2P^iPr_2)_2$], for which a TOF of ~ 3600 h^{-1} (2 mol%, 70% conversion) was reported. However, this reduced TOF (Table 3.1)

allows monitoring of the evolution of B-N products by ^{11}B NMR spectroscopy and the production of time/concentration plots to interrogate the kinetics. Computational studies on $\{Rh(P^iBu_3)_2L_n\}^+$ indicate that it can operate in a constant oxidation state Rh(III) cycle where B-H activation occurs in a σ-CAM fashion, or in a lower energy Rh(I)/Rh(III) manifold, where B-H oxidative addition is followed by N-H transfer.[17] The calculations revealed dehydrogenation in the Rh(I)/Rh(III) manifold to be a lower energy process (106 kJ mol^{-1}) compared with the Rh(III)/Rh(III) cycle (133 kJ mol^{-1}). The closely related $\{Ir(H)_2(PCy_3)_2L_n\}^+$ system also operates in a constant oxidation state [Ir(III)] cycle, with calculations on $\{Ir(H)_2(PMe_3)_2L_n\}^+$ suggesting an overall barrier (126 kJ mol^{-1}) to dehydrogenation, approximately the same as for the Rh(III)/Rh(III) cycle (133 kJ mol^{-1}) given the difference in basis set and phosphine (P^iBu_3 *versus* PMe_3).[15] The observed significantly slower catalysis for the iridium system (days *versus* hours for Rh), despite the similar barriers to dehydrogenation, is thus likely a result of the ability to access the Rh(I)/Rh(III) part of the cycle and concomitantly lower barriers. Calculations suggested that an Ir(I) species was not involved in the dehydrogenation.[15] For both the Rh and Ir systems, N-H activation was calculated to be a higher energy process than B-H activation, which was backed up by experimental deuterium incorporation experiments.[19] The Weller group has also reported other related Rh fragments capable of catalysing the dehydrocoupling of DMAB.[20-22]

$\{Rh(P^iPr_3)_2L_n\}^+$ has previously been reported to catalyse the dehydrocoupling of **A** at a slightly slower overall TOF than $\{Rh(P^iBu_3)_2L_n\}^+$.[16] As part of this thesis, an additional number of $\{Rh(PR_3)_2L_n\}^+$ fragments have now been screened for their activity towards the dehydrocoupling of **A**, which further demonstrates a dependence

of the overall TOF on the R groups of the phosphine. There appears to be a loose relationship between the size of the phosphine[23] and the TOF (Table 3.1), with smaller phosphines operating slightly faster. This suggests that perhaps the electronic and steric properties of the phosphine are both influential in determining the rate. The cone angle of P^cPr_3 (^{c}Pr = cyclopropyl) is unknown but is assumed to be smaller than P^iPr_3 (160 °).

Table 3.1 Effect of R on the ability of $\{Rh(PR_3)_2L_n\}^+$ fragments to catalyse the dehydrocoupling of **A**. 5 mol% catalyst, 0.072 M **A**, open to a low flow of argon. * Approximate cone angle.

R	TOF / h^{-1}	Cone Angle / °
^{i}Bu	12.0	143
Cy	7.5	170
^{c}Pr	5.0	< 160 *
^{i}Pr	3.3	160

Catalysis was monitored by taking regular aliquots, quenching them with an excess of acetonitrile and subsequent analysis by ^{11}B NMR spectroscopy, as has been used for previous studies[16] (Figure 3.1). The acetonitrile can coordinate strongly to rhodium, effectively saturating possible coordination sites for the amine-boranes and quenching the reaction. For all four $\{Rh(PR_3)_2L_n\}^+$ fragments a similar reaction profile was observed: **A** [δ -12.6 ppm (q, $^1J_{BH}$ = 98 Hz)] was consumed, **B** [δ -13.0 ppm (BH_3, q, $^1J_{BH}$ = 94 Hz) and 2.5 ppm (BH_2, t, $^1J_{BH}$ = 108 Hz)] was formed as an intermediate and **C** [δ -5.4 ppm (t, $^1J_{BH}$ = 111 Hz)] accumulated as the final product. However, no **Z** [δ 37.8 ppm (t, $^1J_{BH}$ = 126 Hz)] was observed. The screening revealed $\{Rh(PCy_3)_2L_n\}^+$ to have an appropriate rate for studying the reaction kinetics, with a rate in between that of $\{Rh(P^iPr_3)_2L_n\}^+$ and $\{Rh(P^iBu_3)_2L_n\}^+$.

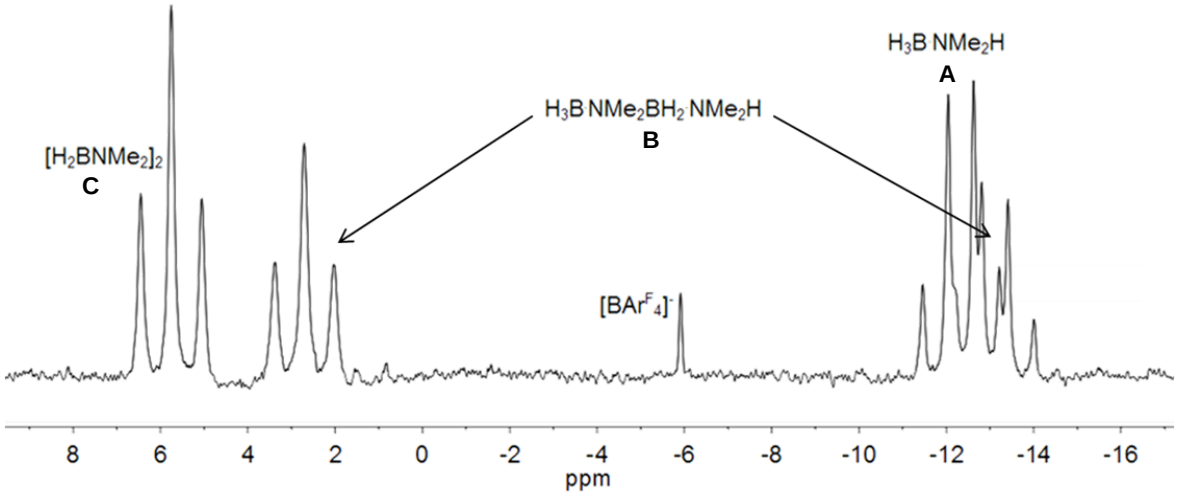
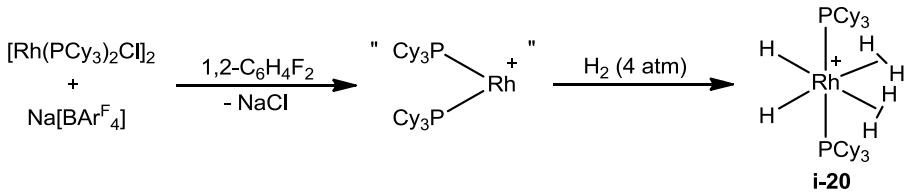


Figure 3.1 Representative ^{11}B NMR spectrum of the dehydrocoupling of **A** (0.072 M) catalysed by $\{Rh(PCy_3)_2L_n\}^+$ (5 mol%) in 1,2-$C_6H_4F_2$ after 60 minutes in an open system. 0.1 mL aliquot quenched with excess acetonitrile (0.25 mL).

A suitable starting point for previous studies of dehydrocoupling using the $\{Rh(PR_3)_2L_n\}^+$ fragment has been η^6 coordinated fluorobenzene complexes of the general formula $[Rh(PR_3)_2(\eta^6\text{-}C_6H_5F)][BAr^F_4]$ (*e.g.* **i-57**).[16-18, 24, 25] In the presence of amine-boranes, the labile fluorobenzene ligand is readily substituted. Attempts to synthesise the equivalent complex using the PCy_3 ligand were unsuccessful, presumably due to the added steric bulk of the phosphine coupled with the lability of the fluorobenzene. Instead the $[Rh(PCy_3)_2L_n][BAr^F_4]$ precatalyst was generated *in situ* by the addition of $Na[BAr^F]_4$ to a 1,2-$C_6H_4F_2$ solution of $[Rh(PCy_3)_2Cl]_2$[26] (Scheme 3.2). Analysis of the resulting orange solution by $^{31}P\{^1H\}$ spectroscopy revealed a broad resonance at δ 60 ppm. The use of 1,2-$C_6H_4F_2$ as the solvent prevented cooling of the sample to lower temperatures in an attempt to gain further structural information. Addition of H_2 (4 atm) to this solution immediately and cleanly (to the detection limits of $^{31}P\{^1H\}$ NMR spectroscopy) generates the known Rh(III) dihydride *bis*-dihydrogen complex $[Rh(H)_2(PCy_3)_2(\eta^2\text{-}H_2)_2][BAr^F_4]$ (**i-20**) (Scheme 3.2) strongly suggestive of the proposed Rh(I) formulation.[27] Initial screening indicated that the

sodium chloride precipitate played no role in the dehydrocoupling process; the overall rate of reaction and the time/concentration plots were similar for when either $[Rh(P^iPr_3)_2(\eta^6\text{-}C_6H_5F)][BAr^F{}_4]$[16] or $[Rh(P^iPr_3)_2Cl]_2/Na[BAr^F]_4$ were used.



i-20

Scheme 3.2 *In situ* generation of $[Rh(PCy_3)_2L_n][BAr^F{}_4]$ and subsequent addition of H_2 to form the known dihydride *bis*-dihydrogen complex (**i-20**). $[BAr^F{}_4]^-$ anions not shown.

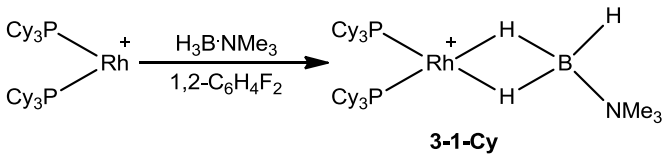
3.3 Synthesis of new complexes and their reactivity

Addition of amine-borane substrates, intermediates and final products to the Rh(I) and Rh(III) cationic fragments ($\{Rh(PCy_3)_2L_n\}^+$ and $\{Rh(H)_2(PCy_3)_2L_n\}^+$) generated new complexes. These were characterised by a combination of *in situ* NMR spectroscopy and, where possible, ESI-MS, and their reactivity in the presence of excess amine-borane investigated. $\{Rh(H)_2(PCy_3)_2L_n\}^+$ was generated by degassing (freeze-pump-thaw) a 1,2-$C_6H_4F_2$ solution of **i-20** as reported previously.[27]

3.3.1 Reactivity with TMAB

Initial studies used the model amine-borane, $H_3B{\cdot}NMe_3$ (TMAB), which cannot undergo dehydrocoupling due to the lack of N-H functional group, as the amine-borane substrate. Addition of TMAB to the rhodium(I) fragment $\{Rh(PCy_3)_2L_n\}^+$ rapidly formed the purple Rh(I) σ-complex $[Rh(PCy_3)_2(\eta^2\text{-}H_3B{\cdot}NMe_3)][BAr^F{}_4]$ (**3-1-Cy**), which has been characterised by NMR spectroscopy and ESI-MS (Scheme 3.3). Complex **3-1-Cy** can be isolated as a lilac solid in a reasonable yield (63%), although by NMR spectroscopy its formation is quantitative. Analysis by NMR spectroscopy revealed several features indicative of time-averaged 3-centre 2-electron Rh-H-B

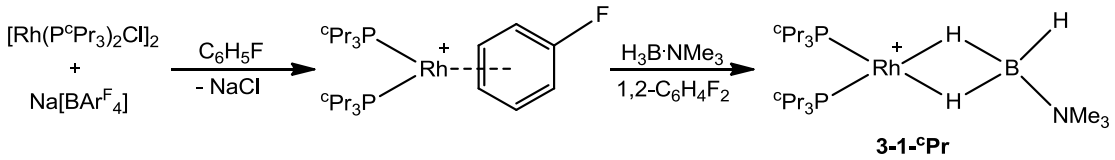
interactions that are undergoing fast exchange on the NMR timescale between terminal B-H and bridging B-H-Rh sites.[16, 18, 28, 29] In the ^{11}B NMR spectrum, a large 34.4 ppm downfield shift, indicative of η^2 Rh-H_2B coordination,[30] was observed for coordinated TMAB (δ 27.1 ppm), compared with free TMAB (δ -7.3 ppm), and a quadrupolar-broadened integral 3H signal was evident in the ^1H NMR spectrum at δ -2.87 ppm. The expected molecular ion was observed by ESI-MS: *m/z* 736.48 [M^+] (calc. 736.48), with the observed isotopic pattern fully consistent with the molecular formula.



3-1-Cy

Scheme 3.3 Formation of the Rh(I) σ-complex **3-1-Cy**. $[BAr^F_4]^-$ anions not shown.

The equivalent P^iBu_3 (**3-1-^{i}Bu**) and P^iPr_3 (**3-1-^{i}Pr**) analogues have previously been reported (Table 3.2). [16, 18] To explore if there was any correlation between the degree of interaction between $\{Rh(PR_3)_2L_n\}^+$ and TMAB, with the overall TOF of dehydrocoupling of **A** to ultimately give **C**, the equivalent P^cPr_3 complex (**3-1-^{c}Pr**), as this would be expected to have a cone angle less than P^iPr_3 and PCy_3, was synthesised. For P^cPr_3 the η^6 fluorobenzene complex could be synthesised readily (Scheme 3.4). $[Rh(P^cPr_3)_2(\eta^6\text{-}C_6H_5F)][BAr^F_4]$ was characterised by a combination of NMR spectroscopy, ESI-MS and elemental microanalysis (CHN), details of which are reported in the experimental section (Chapter 5). All data were as expected, and correspond with previously reported fluorobenzene complexes.[22, 24, 25]



Scheme 3.4 Synthesis of $[Rh(P^cPr_3)_2(\eta^6\text{-}C_6H_5F)][BAr^F_4]$ and the formation of a Rh(I) σ-complex, $[Rh(P^cPr_3)_2(\eta^2\text{-}H_3B{\cdot}NMe_3][BAr^F_4]$ (**3-1-^{c}Pr**), upon addition of TMAB. $[BAr^F_4]^-$ anions not shown.

The addition of TMAB to $[Rh(P^cPr_3)_2(\eta^6\text{-}C_6H_5F)][BAr^F_4]$ formed **3-1-^{c}Pr** (Scheme 3.4), which was analysed by a combination of NMR spectroscopy and ESI-MS [*m/z* 484.19 [M^+] (calc. 484.19)]. Crystals suitable for single crystal X-ray diffraction were grown from 1,2-$C_6H_4F_2$/pentane at 2 °C (Figure 3.2).

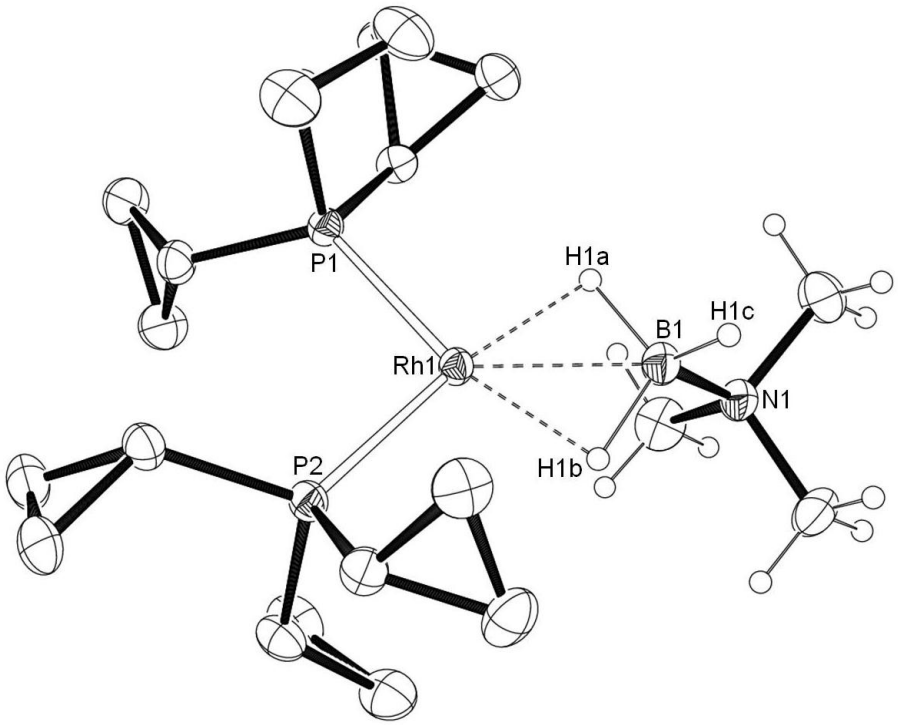


Figure 3.2 Solid state structure of **3-1-^{c}Pr**. Disordered components and $[BAr^F_4]^-$ anion are not shown. Displacement ellipsoids are given at the 30% probability level. H1a, H1b and H1c were located on the Fourier difference map; their isotropic displacement parameters were fixed to ride on the parent atoms. The B1-H1a and B1-H1b bonds were restrained to equal length, the position of H1c was freely refined. Selected bond lengths and angles: Rh1-P1, 2.2131(9) Å; Rh1-P2, 2.2405(9) Å; Rh1-B1, 2.177(5) Å; Rh1-H1a, 1.75(5) Å; Rh1-H1b, 1.81(5) Å; B1-H1a, 1.23(3) Å; B1-H1b, 1.23(3) Å; B1-H1c, 1.17(6) Å; P1-Rh1-P2, 96.77(3)°; B1-Rh1-P1, 129.21(4)°; B1-Rh1-P2, 133.85(14)°; N1-B1-Rh1, 126.3(3)°.

The solid-state structure of **3-1-^{c}Pr** shows a cation with a pseudo-square-planar Rh(I) centre and an η^2-coordinated amine-borane, as previously observed for **3-1-^{i}Bu** and **3-1-^{i}Pr**.[16, 17] It is also consistent with the solution NMR data; a broad integral 3H signal was observed at δ -2.38 ppm in the ^{1}H NMR spectrum consistent with time-averaged 3-centre 2-electron Rh-H-B interactions. The signal is shifted slightly downfield from that of **3-1-Cy** (δ -2.87 ppm) indicative of a weaker Rh···H_3B interaction. Likewise, a broad signal at δ 24.3 ppm in the ^{11}B NMR spectrum was less shifted with respect to free TMAB than for **3-1-Cy** (Δδ^{11}B 31.6 ppm *versus* 34.4 ppm), further evidence for a slightly weaker Rh···H_3B interaction.

The Rh···B distances (Table 3.2) of **3-1-R** indicate a shorter distance in **3-1-^{i}Bu** (2.180(4) Å) and **3-1-^{c}Pr** (2.177(5) Å), and a slightly longer distance in **3-1-^{i}Pr** (2.137(6) Å). Within error, the Rh···B distances in **3-1-^{i}Bu** and **3-1-^{c}Pr** are the same. Correlating with this, they exhibit similar shifts in their ^{1}H and ^{11}B NMR spectra: δ^{1}H -2.12 ppm (**3-1-^{i}Bu**), -2.38 ppm (**3-1-^{c}Pr**); δ^{11}B 23.1 ppm (**3-1-^{i}Bu**), 24.3 ppm (**3-1-^{c}Pr**). However, a comparison of their overall TOF's for the dehydrocoupling of **A**, [12.0 h^{-1} (**3-1-^{i}Bu**) and 5.0 h^{-1} (**3-1-^{c}Pr**)], reveals a difference in their ability to catalyse the dehydrocoupling of **A** to ultimately yield **C**, indicating that there does not appear to be a significant correlation between the strength of the Rh···H_3B interaction and their TOF for the dehydrocoupling of **A**. **3-1-^{i}Pr** and **3-1-Cy** also exhibit similar shifts in their ^{1}H and ^{11}B NMR spectra: δ^{1}H -3.09 ppm (**3-1-^{i}Pr**), -2.83 ppm (**3-1-Cy**); δ^{11}B 28.8 ppm (**3-1-^{i}Pr**), 27.1 ppm (**3-1-Cy**). A comparison of their Rh···B distances is not possible as despite repeated attempts, crystals suitable for an X-ray study could not be grown of **3-1-Cy**. However, based on the NMR data, **3-1-Cy** could be expected to have a Rh···B distance similar to **3-1-^{i}Pr**. A comparison of the TOF's for the

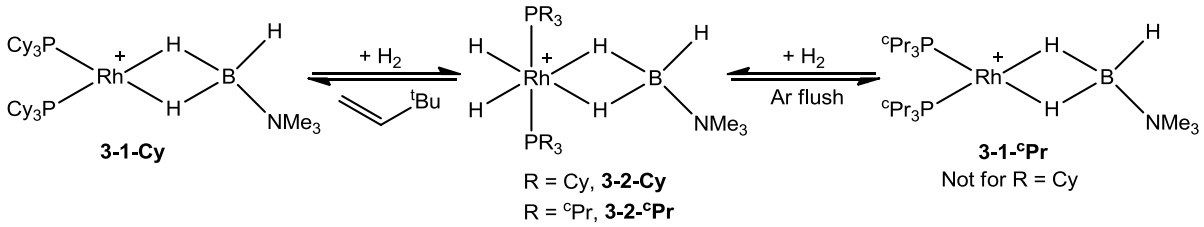
dehydrocoupling of **A** reveals that as for **3-1-^{i}Bu** and **3-1-^{c}Pr** there does not appear to be a significant correlation between the overall TOF and the strength of the Rh···H_3B interaction. These results indicate that although there is a slight correlation between the rate of dehydrocoupling of **A** by $\{Rh(PR_3)_2L_n\}^+$ and the strength of the Rh···H_3B interaction in **3-2-R**, the interaction strength is not the major determining factor. Other contributing factors could include the ease of reductive elimination of dihydrogen from a Rh(III) species to regenerate the Rh(I) species (*vide infra*); as discussed previously, for the dehydrocoupling of **A** catalysed by $\{Rh(P^iBu_3)_2L_n\}^+$ the Rh(I)/Rh(III) cycle is a lower energy process than the alternative Rh(III)/Rh(III) manifold. The calculations also revealed that N-H activation/transfer is the rate determining step,[17] and it is plausible to assume that the rate of N-H activation will not be significantly affected by the strength of the Rh···H_3B interaction, and hence the interaction strength will not have a significant effect on the overall TOF for the dehydrocoupling of **A**. As will be shown later, the overall mechanism is complex, operating under autocatalytic conditions, making a simple correlation difficult. It should also be noted here that TMAB is not a perfect model for **A** due to the added steric bulk caused by the additional N-methyl group.

Table 3.2 Comparison of the strength of the Rh···B interaction by NMR spectroscopy and X-ray crystallography (where possible) of complexes of the general formula $[Rh(PR_3)_2(\eta^2\text{-}H_3B{\cdot}NMe_3)][BAr^F{}_4]$ (**3-1-R**). * no X-ray data.

R	***d*(Rh-B)** / Å	**δ (^{11}B)** / ppm **TMAB**	**δ (^{1}H)** / ppm **Rh-H-B**	**TOF** / h^{-1}
^{i}Bu	2.180(4)	23.1	-2.12	12.0
^{c}Pr	2.177(5)	24.3	-2.38	5.0
Cy	*	27.1	-2.83	7.5
^{i}Pr	2.137(6)	28.8	-3.09	3.3

Addition of H_2 (4 atm) to a 1,2-$C_6H_4F_2$ solution of **3-1-Cy** results in the immediate formation of the Rh(III) complex $[Rh(H)_2(PCy_3)_2(\eta^2\text{-}H_3B{\cdot}NMe_3)][BAr^F{}_4]$ (**3-2-Cy**) (Scheme 3.5). Comparable reactivity was observed for **3-1-^{c}Pr.** Complexes **3-2-Cy** and **3-2-^{c}Pr** were characterised by NMR spectroscopy by comparison with the P^iBu_3 and P^iPr_3 analogues (**3-2-^{i}Bu** and **3-2-^{i}Pr**).[16, 18] In the ^{1}H NMR spectra, the time-averaged quadrupolar broadened BH_3 signal was shifted downfield relative to the respective Rh(I) species: **Cy** δ -0.28 ppm [Rh(III)] *vs.* δ -2.83 ppm [Rh(I)]; **^{c}Pr** δ -0.78 ppm [Rh(III)] *vs.* δ -2.38 ppm [Rh(I)]. The downfield shift relative to **3-1-R** is indicative of a weaker Rh···H_3B interaction, which is as expected as the Rh(III) orbitals will be contracted relative to the Rh(I) species resulting in less effective overlap. Additionally, the position of the phosphines *trans* to each other, as opposed to the *cis* conformation in the Rh(I) species, may prevent the close approach of the bulky TMAB molecule. The ^{11}B NMR data also confirms the weaker interaction with the signals experiencing a smaller downfield shift relative to free TMAB (δ -7.3 ppm): **Cy** $\Delta\delta^{11}$B 12.0 ppm [Rh(III)] *vs.* 34.4 ppm [Rh(I)]; **^{c}Pr** $\Delta\delta^{11}$B 16.8 ppm [Rh(III)] *vs.* δ 31.6 ppm [Rh(I)]. In addition to the quadrupolar broadened BH_3 signal in the ^{1}H NMR spectrum, signals corresponding to the rhodium hydrides were observed in the hydridic region: **3-2-Cy**, δ -19.62 ppm (overlapping dt, 2H, $^1J_{RhH}$ = 22.1 Hz, $^2J_{PH}$ = 15.1 Hz) and **3-2-^{c}Pr**, δ -19.20 ppm (overlapping dt, 2H, $^1J_{RhH}$ = 18.2 Hz, $^2J_{PH}$ = 13.9 Hz). Further evidence for the formation of a Rh(III) species was observed in the $^{31}P\{^1H\}$ NMR spectrum; a $^1J_{RhP}$ coupling of 108 Hz (**3-2-Cy**) and 114 Hz (**3-2-^{c}Pr**) being indicative of coordination to Rh(III).[31] For both **3-2-Cy** and **3-2-^{c}Pr**, analysis by ESI-MS revealed the expected molecular ion minus dihydrogen: **3-2-Cy**, *m/z* 736.48 [M^+ - H_2] (calc. 736.48); **3-2-^{c}Pr**, *m/z* 484.18 [M^+ - H_2] (calc. 484.19). Loss of dihydrogen to reform **3-1-R** under the conditions of mass spectrometry (60 °C, high vacuum) is a plausible theory.

Placing **3-2-Cy** under a moderate vacuum (2 x 10^{-2} mbar) resulted in no change, and only on addition of TBE is the Rh(I) complex **3-1-Cy** reformed (Scheme 3.5). Similar behaviour was observed for **3-2-^{i}Pr**.[16] By contrast **3-2-^{c}Pr**, like **3-2-^{i}Bu**, loses dihydrogen under an Ar flush.[18] However, there appears to be no correlation between the observed TOF's for the catalytic dehydrocoupling of **A** by $\{Rh(PR_3)_2L_n\}^+$ and the ease at which **3-2-R** reductively eliminates dihydrogen under these conditions. There does however appear to be a relationship between the cone angle of the phosphine, and the ease at which the corresponding Rh(III) complex returns to the Rh(I) oxidation state. The effect of L-M-L bite angles on oxidative addition and reductive elimination reactions at metal centres is well established.[32, 33] A report by Dubois and co-workers on the role of phosphine bite angles on determining the position of equilibrium on the addition of H_2 to $\{Rh(L_2)_2\}^+$ cations (L_2 = chelating diphosphine) revealed a small bite angle favoured reductive elimination of H_2.[34] Although our system cannot be directly compared with the Dubois system, consideration of the P-Rh-P angle appears to be important in determining the stability of **3-2-R** with respect to reductive elimination of dihydrogen. Indeed, a comparison of the cone angles of the phosphines (Table 3.1) reveals that $P^{i}Bu_3$ and $P^{c}Pr_3$ have the smallest cone angles (143° and <160° respectively), which will allow a tighter P-Rh-P bite angle in **3-2-R**, which could encourage reductive elimination of H_2. The ability of the phosphine to form agostic interactions, which could stabilise low-coordinate intermediates formed during H_2 loss, lowering the energy of the transition state, could also be influential. Caulton and co-workers have previously commented on the role of agostic interactions in promoting the loss of dihydrogen from Ir(III) dihydride species.[35]



Scheme 3.5 Formation of a Rh(III) σ-complex *via* the addition of dihydrogen to **3-1-R**. $[BAr^F_4]^-$ anions not shown.

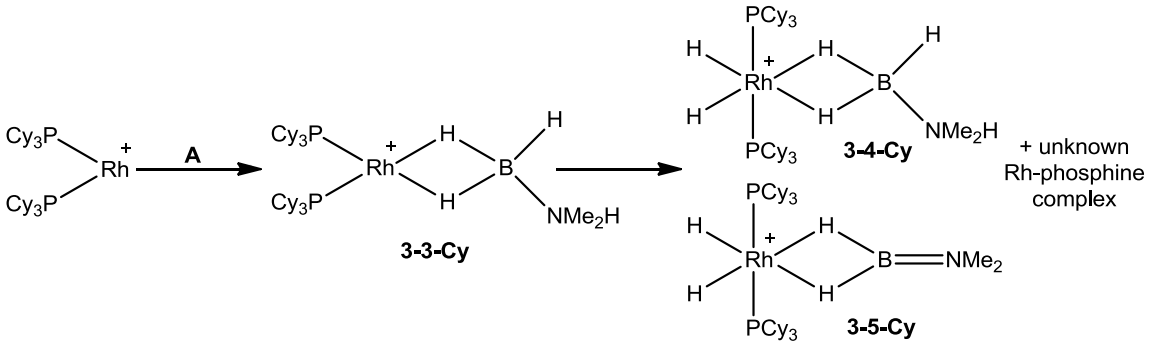
Although **3-2-Cy** and **3-2-^{i}Pr** require the addition of TBE to return to the Rh(I) σ-complex (Scheme 3.5), the TBE is only involved in the reduction of the metal; the TBE does not undergo hydroboration by TMAB as observed in Chapter 2 for **2-7**. As suggested in Chapter 2, this might be due to the increased steric profile of these ligands relative to $P^tBu^iBu_2$, dissuading TBE approach in the hydroboration catalytic cycle, although such effects are likely to be subtle.

3.3.2 Reactivity with DMAB (A)

Having studied the model TMAB complexes, we then explored the interaction of the Rh(I) and Rh(III) fragments with the substrate, **A**. Subsequent studies were only performed on the PCy_3 system, as $\{Rh(PCy_3)_2L_n\}^+$ catalyses the dehydrocoupling at an appropriate rate for studying the reaction kinetics.

As with TMAB, addition of 1 equivalent of **A** to a 1,2-$C_6H_4F_2$ solution of $\{Rh(PCy_3)_2L_n\}^+$ rapidly formed the purple Rh(I) σ-complex $[Rh(PCy_3)_2(\eta^2\text{-}H_3B{\cdot}NMe_2H)][BAr^F_4]$ (**3-3-Cy**) (Scheme 3.6). However unlike **3-1-Cy**, due to the presence of a hydrogen on the nitrogen, **3-3-Cy** is not stable in solution and rapidly reacts further (complete consumption in 5 minutes on warming from 77 K to 298 K) to yield several Rh(III) species: $[Rh(H)_2(PCy_3)_2(\eta^2\text{-}H_3B{\cdot}NMe_2H)][BAr^F_4]$ (**3-4-Cy**) (~50% by $^{31}P\{^1H\}$ NMR spectroscopy) and the amino-borane complex $[Rh(H)_2(PCy_3)_2(\eta^2\text{-}H_2B{=}NMe_2)][BAr^F_4]$

(**3-5-Cy**) (~25%) (Scheme 3.6). An unidentified Rh-phosphine complex is also formed (~25%, $\delta^{31}P\{^1H\}$ 47.8 ppm, J_{RhP} = 118 Hz), which was not observed when additional **A** (2 equivalents) was used suggesting that its formation is a result of insufficient borane present.[i] Complex **3-3-Cy** was characterised by analogy with **3-3-^{i}Bu**[18] *via* rapidly freezing a 1,2-$C_6H_4F_2$ solution of the reactants and warming to 298 K in the NMR probe. As for **3-1-Cy**, the ^1H NMR spectrum of **3-3-Cy** featured an integral 3H quadrupolar broadened signal at δ -2.85 ppm, indicative of 3-centre 2-electron Rh-H-B interactions. A rhodium-phosphorus coupling of 178 Hz observed in the $^{31}P\{^1H\}$ NMR spectrum indicated a Rh(I) oxidation state.[31] A downfield shifted signal (δ 23.3 ppm) relative to free **A** (δ -12.6 ppm) in the ^{11}B NMR spectrum was assigned to the coordinated BH_3. Due to the extremely short-lived nature of **3-3-Cy**, ESI-MS data could not be obtained.



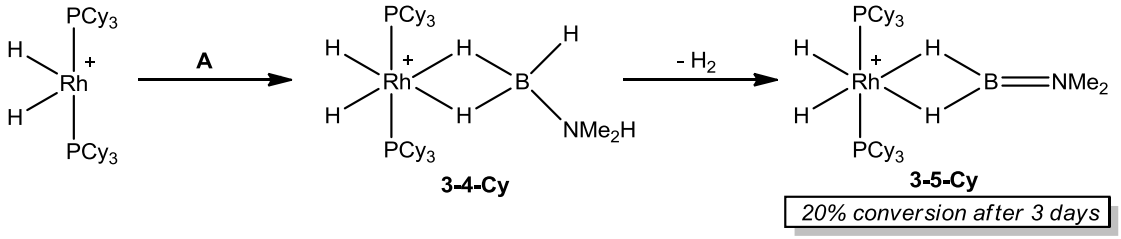
Scheme 3.6 Reactivity of the rhodium(I) fragments with **A** to form **3-3-Cy** and its onward reactivity. $[BAr^F_4]^-$ anions not shown.

Using an excess of **A** (2 equivalents) further shortened the lifetime of **3-3-Cy** with less than 10% observed after 1 minute on warming from 77 K to 298 K. The unidentified Rh-phosphine complex observed upon reaction of $\{Rh(PCy_3)_2L_n\}^+$ with 1 equivalent of **A** (Scheme 3.6) was not seen. Free **Z** was also observed under these conditions, which

[i] The low molecular weight of **A** relative to $\{Rh(PCy_3)_2L_n\}^+$ means addition of exactly one equivalent of **A** is problematic.

dimerised with time to give **C**.[15, 36] Complex **3-4-Cy** was characterised by analogy with **3-4-^{i}Bu,**[18] while **3-5-Cy** has previously been synthesised by the retrodimerisation of **C** trapped by the $\{Rh(H)_2(PCy_3)_2L_n\}^+$ fragment.[15] **3-4-Cy** could alternatively be synthesised *via* the addition of **A** to $\{Rh(H)_2(PCy_3)_2L_n\}^+$ (Scheme 3.7). This reaction is quantitative by NMR spectroscopy.

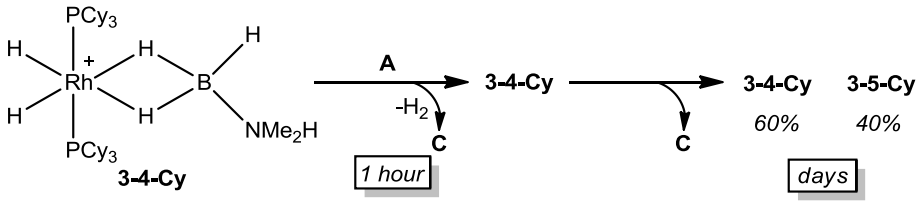
As for **3-1-Cy**, **3-2-Cy** and **3-3-Cy**, NMR data for **3-4-Cy** revealed Rh-H-B 3-centre 2-electron interactions with rapid exchange between the terminal and bound B-H sites on an NMR timescale. The observation of a resonance at δ -18.03 ppm (overlapping dt, 2H, J = 20.8 Hz and 13.8 Hz) in the ^{1}H NMR spectrum which was assigned to the rhodium hydrides, and a rhodium-phosphorus coupling of 110 Hz in the ^{31}P{^{1}H} NMR spectrum are both indicative of a Rh(III) species.[31] As for **3-2-Cy**, the ^{1}H and ^{11}B NMR data are suggestive of a weaker Rh···H_3B interaction relative to the Rh(I) congener, **3-3-Cy**: δ^{1}H -0.80 ppm [Rh(III)] *vs.* -2.85 ppm [Rh(I)]; δ^{11}B 2.7 ppm [Rh(III)] *vs.* 23.3 ppm [Rh(I)].



Scheme 3.7 Formation of **3-4-Cy** and its dehydrogenation to generate the known amino-borane complex **3-5-Cy**. $[BAr^{F}_4]^-$ anions not shown.

In the absence of excess **A**, **3-4-Cy** is relatively stable with only 20% conversion to **3-5-Cy** observed after 3 days (^{1}H NMR spectroscopy) (Scheme 3.7). The enhanced stability of **3-4-Cy** *versus* **3-3-Cy** allowed analysis by ESI-MS: *m/z* 724.47 [M$^+$] (calc. 724.48). The observed isotopic pattern was fully consistent with the molecular formula. Placing **3-4-Cy** under a vacuum did not result in the loss of dihydrogen.

In contrast to the stability in the absence of **A**, addition of an extra equivalent of **A** to a 1,2-$C_6H_4F_2$ solution of **3-4-Cy** resulted in dehydrocoupling with complete conversion of **A** to **C** after 1 hour. **Z** was observed as an intermediate. The only organometallic species observed during dehydrocoupling was **3-4-Cy** (^{1}H and ^{31}P{^{1}H} NMR spectroscopy). After 24 hours, **3-4-Cy** and **3-5-Cy** were observed to be present in approximately equal proportions by NMR spectroscopy (Scheme 3.8).



Scheme 3.8 Reactivity of **3-4-Cy** in the presence of excess **A**. $[BAr^F_4]^-$ anions not shown.

The reactivity of **A** with the Rh(I) and Rh(III) fragments revealed a number of observations key to the overall mechanism of dehydrocoupling. Firstly, the dehydrogenation of bound **A** at a cationic Rh(I) centre to form a Rh(III) dihydride and **Z** is rapid (minutes). By contrast **3-4-Cy** is considerably more stable (days), especially in the absence of excess **A**. In the presence of one equivalent of **A**, slow turnover is observed but at a much reduced rate compared with **3-3-Cy** (minutes *vs*. hours). Under these conditions, H_2 loss from **3-4-Cy** appeared to be negligible, with no Rh(I) species observed. From these results, it would appear that there is a fast Rh(I)/Rh(III) dehydrogenation of **A**, and a slower Rh(III) manifold, which also catalyses the dehydrogenation. Thus the Rh(III) species will form quickly and, as H_2 loss from the Rh(III) species is slow at best, pool during catalysis. This is consistent with the observation of **3-4-Cy** as the resting state during catalysis (*vide infra*) and calculations that show **3-4-^{i}Bu** to sit in a rather deep potential energy well.[17] The rhodium chelating phosphine complexes, $[Rh(Ph_2P(CH_2)_nPPh_2)(\eta^6\text{-}C_6H_5F)][BAr^F_4]$ (n

= 3 – 5) (**i-78**), which strongly favour the Rh(I) oxidation state and hence rapidly reductively eliminate H_2 from the Rh(III)-dihydride, have previously been shown to be extremely efficient catalysts for the dehydrocoupling of DMAB, adding weight to this theory.[22]

Secondly, the requirement of additional **A** for turnover at **3-4-Cy** and the inverse dependence of the lifetime of **3-3-Cy** at higher concentrations of **A**, indicates the involvement of an additional molecule of **A** in the dehydrogenation process. The additional **A** could partake in outer-sphere B-H$^{\delta-}$···$^{\delta+}$H-N intermolecular interactions,[37, 38] which are receiving increasing attention for their involvement in lowering barriers to H_2 loss and oligomerisation processes in amine-boranes.[39-42] Stoichiometric and catalytic studies on the dehydrocoupling of amine-boranes by other metal-based systems have previously suggested the presence of such interactions.[17, 20, 21, 43] The Weller group has recently reported the observation of intramolecular BH···HN bonds between two amine-boranes σ-coordinated to a Rh(I) centre in [Rh{P(C_5H_9)$_2$(η^2-C_5H_7)}(η^2-$H_3B{\cdot}NMe_2H$)(η^1-$H_3B{\cdot}NMe_2H$)][$BAr^F{}_4$].[21]

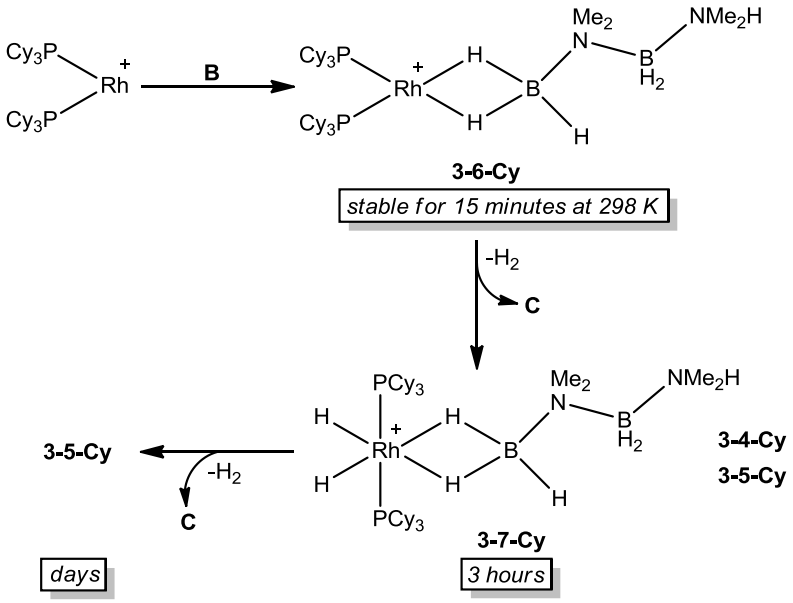
3.3.3 Reactivity with linear diborazane (B)

The intermediate linear diborazane, $H_3B{\cdot}NMe_2BH_2{\cdot}NMe_2H$ (**B**) has previously been observed as an intermediate during catalysis using {Rh(PR_3)$_2$$L_n$}$^+$ fragments (R = ^{i}Bu, ^{i}Pr)[16, 17] among other systems.[12-15, 20, 44] However, **B** is not implicated as an intermediate in all catalytic systems.[22, 45] As mentioned in Chapter 1, **B** is suggested to be formed *via* a metal centred process, which can involve the intermediate **Z** coordinated to the metal,[12, 15] or a simple metal-based intramolecular H_2 elimination, as reported for [$TiCp_2$] systems.[44] The requirement for coordination of an amino-borane related to **Z** at the metal has recently been suggested in the

dehydropolymerisation of the primary amine-borane, MMAB.[43, 46] We report next an investigation into the coordination of **B** to $\{Rh(PCy_3)_2L_n\}^+$ and $\{Rh(H)_2(PCy_3)_2L_n\}^+$, which indicates a more complex mechanism than simple intramolecular dehydrogenation is occurring.[20, 47]

As with **A**, we began our studies into the reactivity of **B** with $\{Rh(PCy_3)_2L_n\}^+$ with a series of stoichiometric reactions. As discussed in Chapter 1, **B** can be synthesised independently (Scheme 1.34),[13] allowing its role as a potential intermediate in the dehydrocoupling of **A** to be probed more readily. The addition of 1 equivalent of **B** to $\{Rh(PCy_3)_2L_n\}^+$ immediately formed the purple Rh(I) σ-complex $[Rh(PCy_3)_2(\eta^2\text{-}H_3B{\cdot}NMe_2BH_2{\cdot}NMe_2H)][BAr^F{}_4]$ (**3-6-Cy**) in a quantitative yield by NMR spectroscopy (Scheme 3.9). Complex **3-6-Cy** was characterised by a comparison of the NMR data with the previously reported data for **3-6-^{i}Bu**, which was additionally characterised by X-ray crystallography.[17] This NMR data suggests that as for **3-6-^{i}Bu**, **B** interacts with $\{Rh(PCy_3)_2L_n\}^+$ through σ-interactions with only the BH_3 group. By contrast, a previous report in the Weller group investigated the binding of **B** to the Rh(I) fragment $[Rh\{PR_2(\eta^2\text{-}C_5H_7)\}]^+$ (R = *cyclo*-C_5H_9, ^{i}Pr) and found **B** to coordinate through both the BH_3 and BH_2 group in an η^2 : η^1 Rh···HB fashion.[20] The difference in coordination mode to **3-6-R** can be attributed to the more open rhodium centre, allowing approach of the BH_2 group to the rhodium. In the ^{1}H NMR spectrum of **3-6-Cy**, a quadrupolar broadened integral 3H signal was observed at δ -3.05 ppm for the coordinated BH_3 undergoing rapid site exchange between terminal and bridging sites. The remaining BH_2 signal could not be assigned, presumably being obscured by aliphatic peaks as noted for **3-6-^{i}Bu**.[16] A broad, downfield shifted signal (δ 28.1 ppm) relative to free **B** (δ -13.0 ppm and 2.5 ppm) observed in the ^{11}B NMR spectrum was

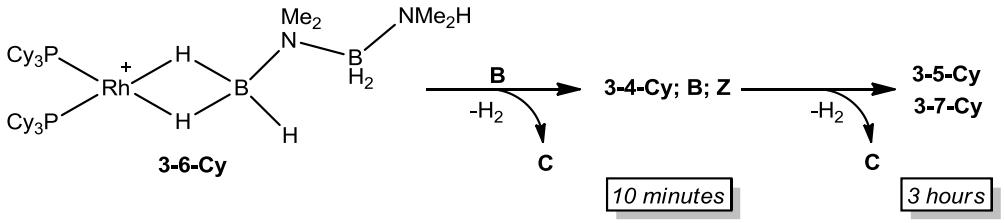
assigned to the coordinated BH_3. The BH_2 group was observed at δ 2.4 ppm, essentially unshifted from free **B**, indicative of its lack of coordination to the metal. A rhodium-phosphorus coupling of 178 Hz in the $^{31}P\{^1H\}$ NMR spectrum is indicative of a Rh(I) species.[31]



Scheme 3.9 Formation of the Rh(I) σ-complex **3-6-Cy** and its onward reactivity. $[BAr^F_4]^-$ anions not shown.

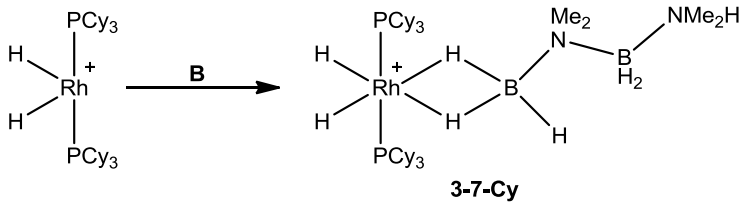
Complex **3-6-Cy** is the only organometallic species observed at 298 K for 15 minutes by NMR spectroscopy, and this significantly enhanced stability compared with that of **3-3-Cy** (Scheme 3.6) allowed additional characterisation by ESI-MS. A positive molecular ion was observed at *m/z* 779.54 [M^+] (calc. 779.54) with an isotopic pattern fully consistent with the molecular formula. After 3 hours in solution at 298 K, **3-6-Cy** is no longer observed (NMR spectroscopy). Instead a mixture of Rh(III) σ-complexes are present: **3-4-Cy**, **3-5-Cy** and the new complex $[Rh(H)_2(PCy_3)_2(\eta^2\text{-}H_3B{\cdot}NMe_2BH_2{\cdot}NMe_2H)][BAr^F_4]$ (**3-7-Cy**). After several days, **3-5-Cy** was the predominant product observed. **C** was also observed, as the only amine-borane product. As noted for **3-3-Cy**, the addition of an extra equivalent of **B** to a 1,2-$C_6H_4F_2$

solution of **3-6-Cy** drastically reduced the lifetime of **3-6-Cy**, and within 10 minutes **3-4-Cy** was the only organometallic species observed along with free **B** and **C** by NMR spectroscopy (Scheme 3.10). Significant quantities of **Z** are also observed under these conditions, which subsequently dimerises off-metal[15] to give **C**.



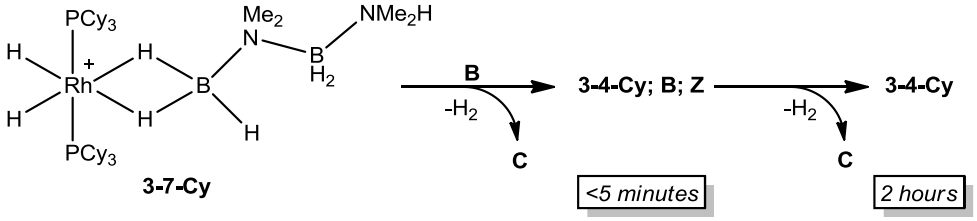
Scheme 3.10 Addition of a second equivalent of **B** to **3-6-Cy**. $[BAr^F_4]^-$ anions not shown.

The Rh(III) σ-complex of **B**, **3-7-Cy**, can also be formed *via* the direct addition of one equivalent of **B** to $\{Rh(H)_2(PCy_3)_2L_n\}^+$ (Scheme 3.11). Complex **3-7-Cy** was characterised by a comparison of the NMR data to that reported in the literature for **3-7-^{i}Bu**[17] and **3-7-^{i}Pr** which has been crystallographically characterised.[48] All data is in full accord with **3-7-Cy** being a Rh(III)-dihydride with an η^2 coordinated **B**. An integral 2H signal at δ -19.45 ppm (overlapping dt, J = 19.4 Hz and 16.0 Hz) in the ^{1}H NMR spectrum is assigned to the rhodium hydrides, while a rhodium-phosphorus coupling of 111 Hz in the $^{31}P\{^1H\}$ NMR data is also indicative of the Rh(III) oxidation state.[31] Analysis by ESI-MS also confirmed the formation of **3-7-Cy**: *m/z* 781.55 [M^+] (calc. 781.55) with the observed isotopic pattern fully consistent with the molecular formula. In the absence of extra **B**, **3-7-Cy** is stable for several days at 298 K; after 4 days **3-7-Cy** accounted for >70% of the organometallic species present (^{1}H and $^{31}P\{^1H\}$ NMR spectroscopy). The solid-state structure of **3-7-iPr**[48] has recently been reported along with an iridium(III) complex of the related linear diborazane $H_3B{\cdot}NMeHBH_2{\cdot}NMeH_2$.[43]



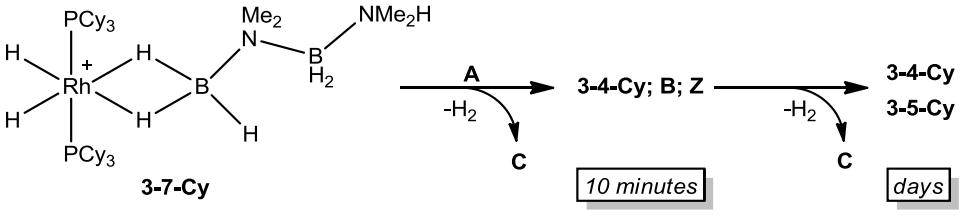
Scheme 3.11 Formation of **3-7-Cy**. $[BAr^F_4]^-$ anions not shown.

However, addition of a further equivalent of **B** to a 1,2-$C_6H_4F_2$ solution of **3-7-Cy** resulted in the rapid (<5 minutes) consumption of **3-7-Cy**, with **3-4-Cy** the only organometallic species present after this time (Scheme 3.12). ^{11}B NMR spectroscopy indicated the formation of **Z** during this process, which along with the formation of **3-4-Cy**, was suggestive of the B-N bond cleavage of **B**. **C** was also observed to be present in solution, which could be formed by the dehydrocyclisation of **B**[44] as well as the dimerisation of 2 molecules of **Z**.



Scheme 3.12 Reaction of **3-7-Cy** with an extra equivalent of **B**. $[BAr^F_4]^-$ anions not shown.

Addition of 1 equivalent of **A** to **3-7-Cy** results in the immediate displacement of **B** and the formation of **3-4-Cy** (Scheme 3.13). Free **B** was observed, along with small amounts of **C** and **Z**. After several days, the mixture had evolved to give **C** and a mixture of the Rh(III) species **3-4-Cy** and **3-5-Cy**.



Scheme 3.13 Reaction of **3-7-Cy** with 1 equivalent of A. $[BAr^F_4]^-$ anions not shown.

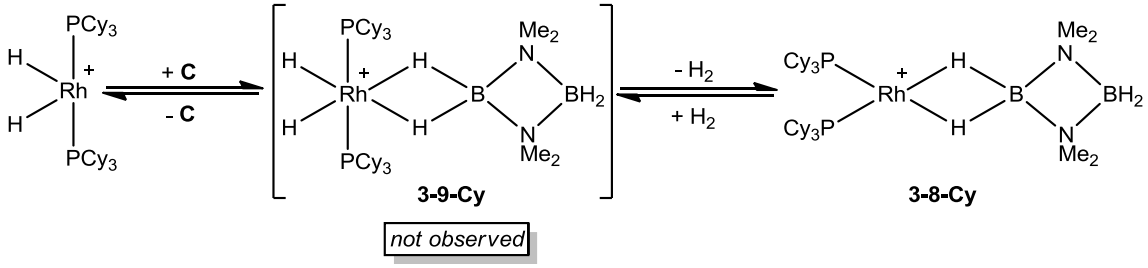
The results emphasise the fast Rh(I)/Rh(III) manifold and the slower constant oxidation state Rh(III) cycle that was evident from the reactivity of $\{Rh(PCy_3)_2L_n\}^+$ and $\{Rh(H)_2(PCy_3)_2L_n\}^+$ with **A**. The consumption of **B** *via* B-N bond cleavage or possibly dehydrocyclisation in the Rh(I) and Rh(III) systems is much slower than the reaction of the Rh(I) complex of **A**, suggesting that **B** will only be consumed at a slow rate during catalysis relative to **A**. The displacement of **B** in **3-7-Cy** by **A** to form **3-4-Cy** indicates that during the early stages of catalysis (high [**A**]), σ-complexes of **A** with rhodium in the +3 oxidation state will be favoured over those of **B**; *i.e.* **3-4-Cy** will dominate. As the concentration of **A** decreases, σ-complexes of **B** will form and B-N bond cleavage of **B** will thus also occur to generate **A** and **Z**,[15, 17] as confirmed by the observation of **3-4-Cy** and free **Z** in reactions of bound **B**. The consumption of **B** appears to be accelerated by the presence of excess **B**. It is also possible that direct dehydrocyclisation of **B** to generate **C** could occur as has been proposed for $[TiCp_2]$ systems.[44] However for our system, dehydrocyclisation would require co-catalysis by **A** or **B** as there is no evidence for **3-6-Cy** or **3-7-Cy** undergoing dehydrocyclisation to generate the Rh(I) and Rh(III) σ-complexes of **C**, $[Rh(PCy_3)_2(\eta^2\text{-}[H_2BNMe_2]_2)][BAr^F{}_4]$ (**3-8-Cy**) and $[Rh(H)_2(PCy_3)_2(\eta^2\text{-}[H_2BNMe_2]_2)][BAr^F{}_4]$ (**3-9-Cy**) respectively. This reactivity is similar to that observed for $[Rh\{P(C_5H_9)_2(\eta^2\text{-}C_5H_7)\}(\eta^2\text{:}\eta^1\text{-}H_3B{\cdot}NMe_2BH_2{\cdot}NMe_2H)][BAr^F{}_4]$, which is stable in the absence of additional **B**.[20] Only in the presence of excess **B** does it react further to yield **C**.

All these observations indicate that during catalysis, **B** will accumulate during the early stages and then, once the [**A**] is lower, **B** will be consumed. This is as observed (Figure 3.4). As for **A** it is clear that the presence of an additional amine-borane accelerates the onward reaction. As previously suggested for **A** this could be through

nonclassical B-H$^{\delta-\cdots\delta+}$H-N interactions.[38] However the slow reaction of **3-7-Cy** with **A** (days, Scheme 3.13) in contrast to the faster reactions observed for **3-4-Cy** with **A** (1 hour, Scheme 3.8) and **3-7-Cy** with **B** (minutes, Scheme 3.12), implies that these accelerating effects are potentially specific to **A** and **B**, potentially through complimentary B-H···H-N interactions.

3.3.4 Reactivity with cyclic dimer (C)

As the concentration of the final product, **C**, builds up during the course of catalysis, its reactivity with the $\{Rh(PCy_3)_2L_n\}^+$ and $\{Rh(H)_2(PCy_3)_2L_n\}^+$ fragments could potentially be of importance. Cr and Rh complexes featuring B-H σ-coordination of **C** have previously been reported.[10, 16, 17] Addition of one equivalent of **C** to a sealed NMR tube containing $\{Rh(H)_2(PCy_3)_2L_n\}^+$ does not result in the Rh(III) σ-complex of **C**, **3-9-Cy**, as might be expected (Scheme 3.14). Instead the purple Rh(I) σ-complex **3-8-Cy** is observed, resulting from the reductive elimination of dihydrogen. The reaction is not quantitative; ~30% **3-8-Cy** results with ~70% $\{Rh(H)_2(PCy_3)_2L_n\}^+$ remaining unreacted alongside **C** (^{1}H and ^{31}P{^{1}H} NMR spectroscopy).

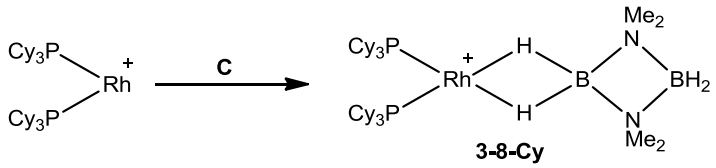


Scheme 3.14 Addition of **C** to $\{Rh(H)_2(PCy_3)_2L_n\}^+$. $[BAr^F{}_4]^-$ anions not shown.

Addition of a further 5 equivalents of **C** changes the ratio to 90:10 in favour of **3-8-Cy** indicating that an equilibrium has been established between the Rh(I) and Rh(III) species (Scheme 3.14). Dissolved H_2 is also observed in the ^{1}H NMR spectrum (δ 4.6 ppm). Presumably the formation of **3-8-Cy** occurs *via* **3-9-Cy** but steric pressure

between the cyclic amino-borane and the *trans* PCy_3 ligands forces the rapid reductive elimination of dihydrogen from the intermediate. Similar behaviour has been observed for **3-8-^{i}Bu**.[17] No evidence is observed (by NMR spectroscopy) for **3-9-Cy**. However, the P^iPr_3 analogue, **3-9-^{i}Pr**, for which H_2 loss is slightly less favourable, has been observed.[16] **3-9-^{i}Pr** can be isolated in the solid state, although only under a H_2 atmosphere. The dissolution of **3-9-^{i}Pr** in solvent results in either the de-coordination of the amino-borane or the loss of H_2.

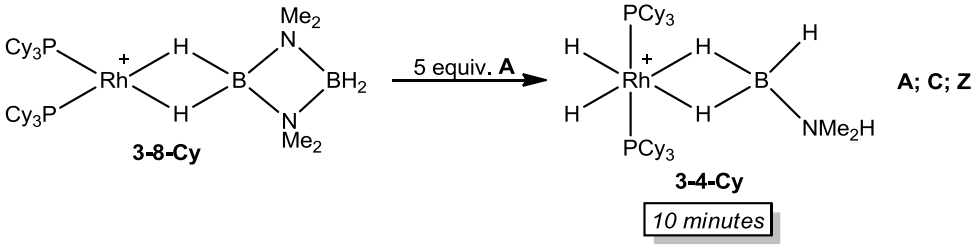
Complex **3-8-Cy** can also be formed *via* the addition of one equivalent of **C** to $\{Rh(PCy_3)_2L_n\}^+$ (Scheme 3.15). The reaction is quantitative by NMR spectroscopy. For **3-8-Cy**, site exchange between the two BH_2 groups does not occur at room temperature: an integral 2H signal is observed at δ -6.33 ppm in the ^1H NMR spectrum for the Rh-H-B hydrogens, while the very broad integral 2H signal observed at δ 2.88 ppm is assigned to the uncoordinated BH_2. The ^{11}B NMR spectrum shows two signals, besides those assigned to $[BAr^F_4]^-$, at δ 33.3 ppm (t, $^1J_{HB}$ = 90 Hz) and 5.4 ppm (v br). The former, which is shifted downfield compared with free **C** [δ 5.4 ppm (q, $^1J_{BH}$ = 111 Hz)] and also shows a reduced B-H coupling constant, is assigned to the boron atom coordinated to the metal, while the latter which is unshifted relative to free **C** is assigned to the uncoordinated boron. Such shifts and reductions in coupling constants are expected on coordination to metal centres.[10, 28, 29, 49] Under the conditions of ESI-MS, $\{Rh(H)_2(PCy_3)_2\}^+$ was observed [*m/z* 665.37 (calc. 665.38)], resulting from loss of **C**.



Scheme 3.15 Formation of **3-8-Cy** *via* the addition of **C** to $\{Rh(PCy_3)_2L_n\}^+$. $[BAr^F{}_4]^-$ anions not shown.

A comparison of the NMR data of **3-8-Cy** with **3-8-^{i}Bu**[17] and **3-8-^{i}Pr**[16] reveals a similar pattern in the strength of the interaction of the amino-borane dimer as for the Rh(I) TMAB complexes, **3-1-R**, as measured by the chemical shift changes. Compared with **3-8-^{i}Bu** (δ^{11}B 31.1 ppm and δ^1H -5.07 ppm) **3-8-Cy** and **3-8-^{i}Pr** have greater downfield shifts (δ -33.3 ppm and 35.3 ppm respectively) in the ^{11}B NMR spectra and larger upfield shifts for the Rh-H-B hydrogen atoms (δ -6.33 ppm and -6.50 ppm respectively) in the ^{1}H NMR spectra, both of which are indicative of a stronger interaction.

Competition reactions revealed that **A** readily displaces bound **C**: addition of 5 equivalents of **A** to **3-8-Cy** resulted in the immediate formation of **3-4-Cy** and the rapid dehydrogenation of bound **A** as expected on a Rh(I) centre (Scheme 3.16). **Z** was observed in the early stages of the reaction.



Scheme 3.16 Reactivity of **3-8-Cy** with **A**. $[BAr^F{}_4]^-$ anions not shown.

These stoichiometric reactions reveal that **C** acts to modify the distribution of Rh(I) and Rh(III) oxidation states. Under catalytic conditions, coordination of **C** at a Rh(III) centre results in the reductive elimination of dihydrogen, potentially providing access

to the Rh(I)/Rh(III) manifold, which is much more reactive towards dehydrogenation of **A** and B-N bond cleavage/dehydrocyclisation of **B**. As **A** binds more strongly to Rh(III) than **C**, this behaviour is only likely to happen towards the end of catalysis when the relative concentration of **C** is greater than that of **A**. The effect of exogenous **C** on catalysis is detailed in a subsequent section (Section 3.4.1.3).

3.4 Catalytic activity

Previous studies on the dehydrocoupling of **A** catalysed by cationic $\{Rh(PR_3)_2\}^+$ fragments have monitored dehydrocoupling in both a sealed high pressure NMR tube and also in systems open to a low flow of argon allowing for the release of H_2.[16, 17] Catalysis in a sealed NMR tube has been observed to be considerably slower than in an open system [$\{Rh(P^iPr_3)_2L_n\}^+$: TOF 4.0 h^{-1} (open, 5 mol%) *versus* TOF 0.3 h^{-1} (closed, 5 mol%, 70% conversion after 48 h)], which has been attributed to inhibition by dihydrogen, which will accumulate during dehydrocoupling. The precise mechanism by which this inhibition occurs is as yet undetermined. Due to the influence of H_2 build up on the overall TOF, we decided to monitor the dehydrocoupling of **A** using $\{Rh(PCy_3)_2L_n\}^+$ (0.072 M **A**, 5 mol%) in an open system.

3.4.1 Open System

3.4.1.1 Dehydrocoupling of DMAB (A)

As discussed in Section 3.2, previous monitoring of catalytic solutions have used a large excess of acetonitrile to quench aliquots of the catalytic solution, which coordinates strongly to rhodium thereby preventing onward reaction *via* σ-complexes.[16]

The dehydrocoupling of **A** catalysed by $\{Rh(PCy_3)_2L_n\}^+$ (5 mol%, 0.072 M **A**, 298 K) was performed in a system open to a low flow of argon. Periodic samples (0.1 mL) were quenched with excess acetonitrile (0.25 mL) and analysed by ^{11}B NMR spectroscopy. It is assumed that the relaxation times for the different species are the same. Subsequent integration of the ^{11}B NMR data gave a time/concentration plot as seen in Figure 3.3.

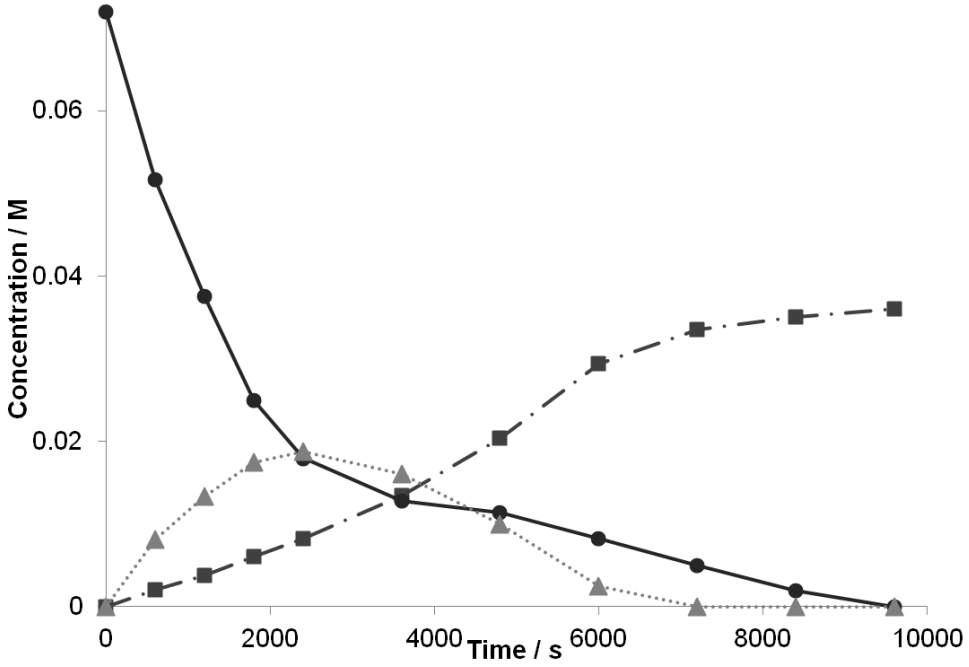


Figure 3.3 MeCN quenched catalysis. Plot of ^{11}B concentration for the dehydrocoupling of $H_3B{\cdot}NMe_2H$ (initial concentration = 0.072 M) using $\{Rh(PCy_3)_2L_n\}^+$ (5 mol%, generated *in situ*). 0.1 mL aliquots quenched with MeCN (0.25 mL). ●, $H_3B{\cdot}NMe_2H$ (**A**); ▲, $H_3B{\cdot}NMe_2BH_2{\cdot}NMe_2H$ (**B**); ■, $[H_2BNMe_2]_2$ (**C**).

The plot shows that **A** decreases with time, **B** is an intermediate and **C** accumulates as the final product, in a profile very similar to that observed for the P^iBu_3[17] and P^iPr_3[16] analogues and during catalyst screening (Figure 3.1). Catalysis was complete after 9600 seconds which gives a turnover frequency of 7.5 h^{-1} which, as mentioned previously, is intermediate between those of the P^iBu_3 (12.0 h^{-1}) and P^iPr_3 (3.3 h^{-1}) systems under the same conditions of concentration and catalyst loading in an open

system (Table 3.1). Interestingly, under these sampling conditions, none of the intermediate amino-borane **Z** was observed. A recent study by the Weller group reported that **Z** dimerises to give the final product **C** in a second order process with 50% conversion after 19 minutes (0.011 M initial concentration, ^{11}B NMR spectroscopy).[15] If **Z** to **C** dimerisation was occurring for this system, then a significant concentration of **Z** would be expected to be observed. It is possible that **A** could be directly dehydrocyclised to give only **B**, as observed for the dehydrocoupling of **A** catalysed by [Cp_2Ti],[44] however the observation of **Z** in closed system catalysis (Figure 3.8) calls this theory into question. An alternate theory that acetonitrile could be influencing the concentration of **Z** proved correct. Repeating the catalysis, but quenching the samples in an alternate manner (dilution with 1,2-$C_6H_4F_2$, rapid freezing in liquid nitrogen and then warming to 298 K in the NMR probe) generated the time/concentration plot in Figure 3.4. In this significant amounts of **Z** are noted, while the overall TOF is the same (7.5 h^{-1}) and the consumption of **A** and profile of **B** are both essentially unchanged. Only the concentration of **Z** and **C** (the product of dimerisation of **Z**) are affected. The observed profile thus is more consistent with the actual catalytic conditions and demonstrates that acetonitrile does perturb the observed relative concentrations of intermediates.

As for acetonitrile quenched catalysis, **A** was observed to decrease with time and **C** accumulated as the final product, with complete conversion after 9600 seconds. **B** is observed as an intermediate with a similar maximum concentration of ~0.02 M and is consumed after 7200 seconds. As predicted by the stoichiometric reactions (Section 3.3.3) **B** is only consumed towards the end of catalysis, once the relative concentration of **A** has dropped sufficiently. **Z** is now observed as an intermediate in

an appreciable concentration (~0.01 M) and there is a slight induction period for the formation of **C**. It thus appears that using a large excess of acetonitrile accelerates the dimerisation of **Z** to **C**, so that no **Z** is observed for acetonitrile quenched catalysis. The related *tert*-butylisonitrile has been noted by Paetzold to act as an effective catalyst, accelerating the cyclisations of iminoboranes.[50]

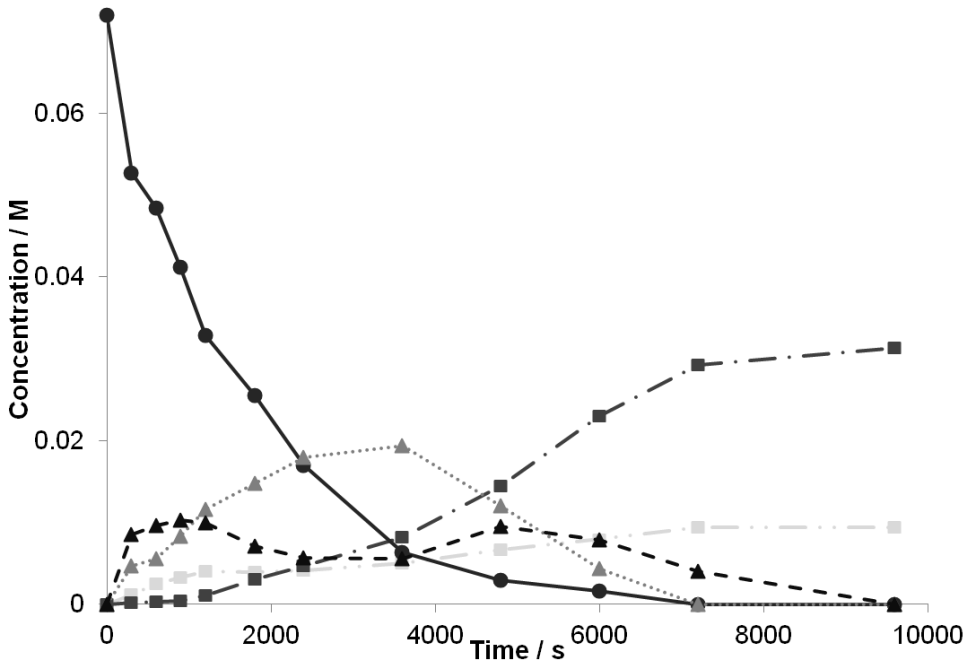


Figure 3.4 1,2-$C_6H_4F_2$ diluted catalysis. Plot of ^{11}B concentration for the dehydrocoupling of $H_3B{\cdot}NMe_2H$ (initial concentration = 0.072 M) using $\{Rh(PCy_3)_2L_n\}^+$ (5 mol%, generated *in situ*). 0.1 mL aliquots diluted with 1,2-$C_6H_4F_2$ (0.25 mL). ●, $H_3B{\cdot}NMe_2H$ (**A**); ▲, $H_3B{\cdot}NMe_2BH_2{\cdot}NMe_2H$ (**B**); ■, $[H_2BNMe_2]_2$ (**C**); ▲, $H_2B{=}NMe_2$ (**Z**); ■, $HB(NMe_2)_2$.

Also observed is the diaminoborane, $HB(NMe_2)_2$,[51] which has been previously observed at a lower concentration in closed system catalysis by the Weller group and others.[10, 17, 21, 22, 44, 52, 53] Addition of NMe_2H to **Z** has been shown to lead to the formation of $HB(NMe_2)_2$.[54] We suggest that since only a very low concentration of $HB(NMe_2)_2$ is observed under sealed tube conditions, and not at all in acetonitrile quenched catalysis, it is likely that the concentration of the diaminoborane is artificially increased due to the decomposition of the highly reactive **Z** during

sampling and analysis. Hence the absolute integrals of **Z** are likely to be unreliable. For this reason, the time/concentration profiles of **Z** shall be considered only in a qualitative rather than quantitative sense.

3.4.1.2 Dehydrocoupling of linear diborazane (B)

Under the same conditions of concentration (0.036 M **B**, 0.072 M B-N units) and sampling (1,2-$C_6H_4F_2$ dilution and rapid freezing) $\{Rh(PCy_3)_2L_n\}^+$ (5 mol% with respect to B-N units) catalysed the dehydrocoupling of **B** to ultimately yield **C** (Figure 3.5).

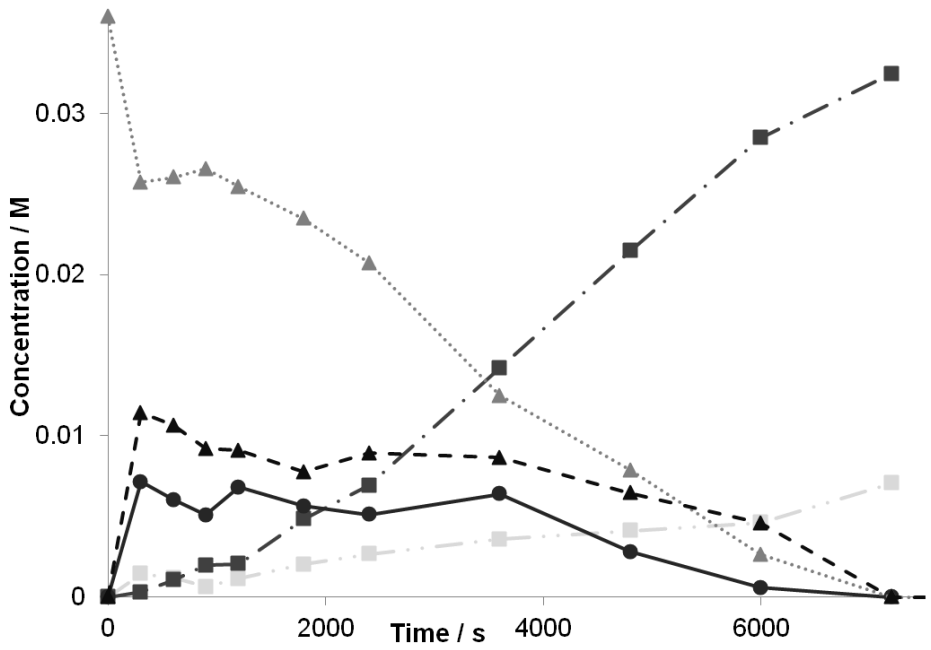


Figure 3.5 Plot of ^{11}B concentration for the dehydrocoupling of $H_3B{\cdot}NMe_2BH_2{\cdot}NMe_2H$ (initial concentration = 0.036 M) using $\{Rh(PCy_3)_2L_n\}^+$ (5 mol% with respect to B-N units, generated *in situ*). 0.1 mL aliquots diluted with 1,2-$C_6H_4F_2$ (0.25 mL). ●, $H_3B{\cdot}NMe_2H$ (**A**); ▲, $H_3B{\cdot}NMe_2BH_2{\cdot}NMe_2H$ (**B**); ■, $[H_2BNMe_2]_2$ (**C**); ▲, $H_2B{=}NMe_2$ (**Z**); ■, $HB(NMe_2)_2$.

Complete conversion of **B** is observed after 7200 seconds. This confirms that **B** is an intermediate in the dehydrocoupling of **A** when using $\{Rh(PCy_3)_2L_n\}^+$ as the catalyst, as has been observed for the P^iBu_3 and P^iPr_3 analogues[16, 17] and other systems.[12-15, 20,

[44] For some systems, **B** is not an intermediate.[22, 45] Interestingly, a significant concentration of both **A** and **Z** is observed during catalysis, and these must arise from the B-N bond cleavage of **B**, which has already been observed in the stoichiometric reactions of **B** with $\{Rh(PCy_3)_2L_n\}^+$ and $\{Rh(H)_2(PCy_3)_2L_n\}^+$ (Section 3.3.3). Relative to **A**, the consumption of **B** is slow; during the dehydrocoupling of **A** (Figure 3.4) the concentration of **A** has halved after ~1200 seconds, while it is ~3000 seconds before the concentration of **B** has decreased by half (Figure 3.5). This is consistent with both the stoichiometric reactions and in the catalytic dehydrocoupling of **A**, where **B** is observed to accumulate.

3.4.1.3 Dehydrocoupling in the presence of excess cyclic dimer (C)

The stoichiometric reactions of **C** with $\{Rh(H)_2(PCy_3)_2L_n\}^+$ revealed that the coordination of **C** to a Rh(III) centre caused the reductive elimination of dihydrogen and the formation of a Rh(I) species (Scheme 3.14), which is more reactive in dehydrocoupling. As the concentration of **C** increases during catalysis, we were interested to see whether adding independently synthesised **C**[13] at the start of catalysis had an influence on the rate of dehydrocoupling, by providing a route back to the more reactive Rh(I) species.

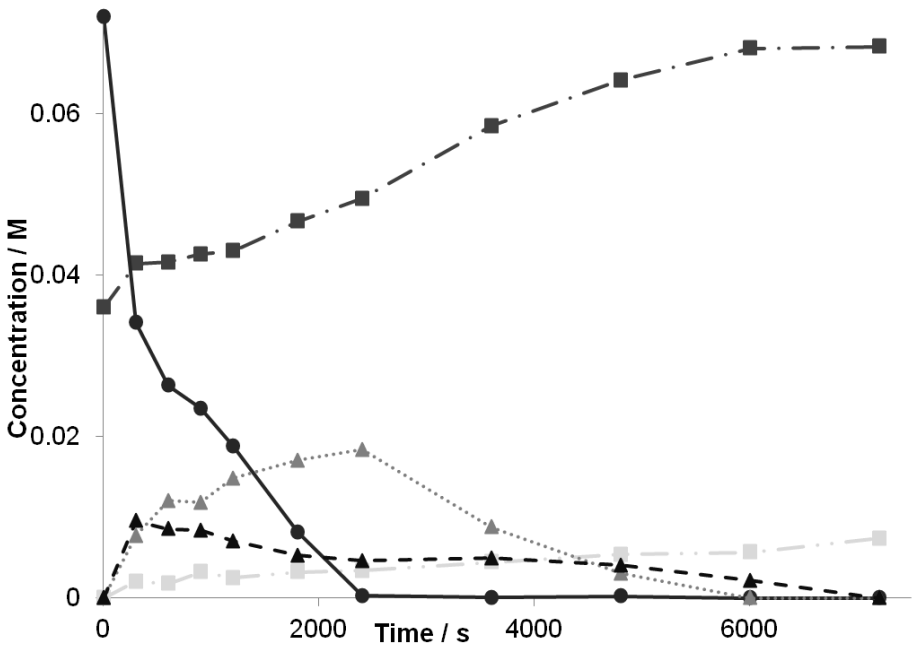


Figure 3.6 Plot of ^{11}B concentration for the dehydrocoupling of **A** (initial concentration = 0.072 M) using $\{Rh(PCy_3)_2L_n\}^+$ (5 mol%, generated *in situ*) with exogenous **C** (initial concentration = 0.036 M). 0.1 mL aliquots diluted with 1,2-$C_6H_4F_2$ (0.25 mL). ●, $H_3B{\cdot}NMe_2H$ (**A**); ▲, $H_3B{\cdot}NMe_2BH_2{\cdot}NMe_2H$ (**B**); ■, $[H_2BNMe_2]_2$ (**C**); ▲, $H_2B{=}NMe_2$ (**Z**); ■, $HB(NMe_2)_2$.

Addition of 10 equivalents of **C** (initial concentration 0.036 M) to a 0.072 M solution of **A** containing $\{Rh(PCy_3)_2L_n\}^+$ (5 mol%) had only a marginal effect on the overall rate of dehydrocoupling to **C**; total conversion occurred after 7200 seconds giving a TOF of 10 h^{-1} (9600 seconds, TOF = 7.5 h^{-1} without exogenous **C**) (Figure 3.6). However the rate of dehydrocoupling of **A** was significantly faster; complete consumption occurred after only 2100 seconds compared with 7200 seconds without added **C** (Figure 3.4).

Addition of 10 equivalents of **C** to a 0.036 M solution of **B** also had an effect on the resulting catalysis by $\{Rh(PCy_3)_2L_n\}^+$ (5 mol% with respect to **B** B-N units) generating the time/concentration plot in Figure 3.7. The concentration of **B** was observed to decrease at a faster rate (full conversion after 3200 seconds *c.f.* 7000 seconds without added **C**), while **C** was also produced faster. **A** and **Z** are also observed as a result of B-N bond cleavage.

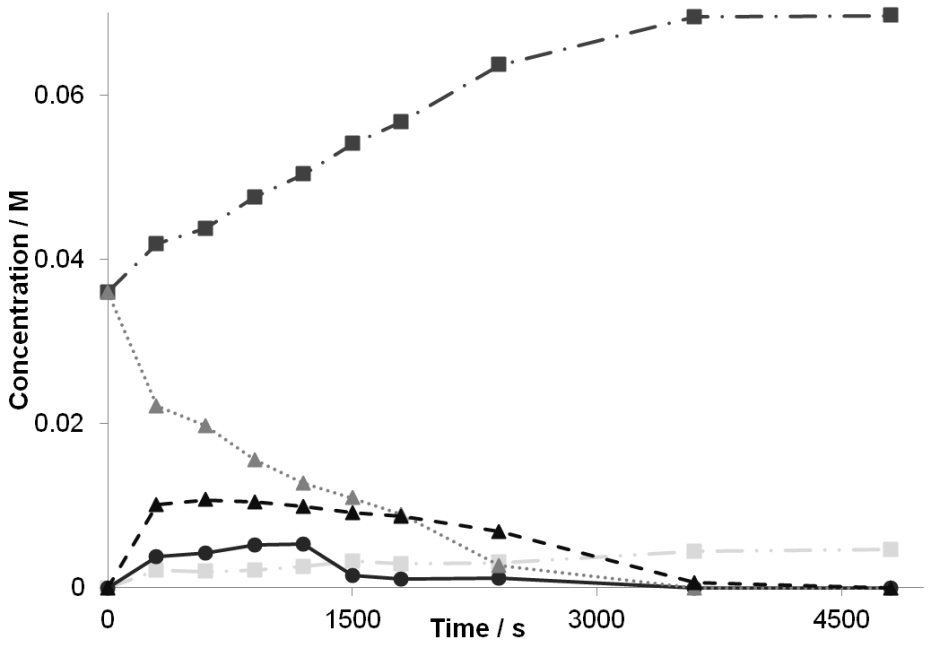
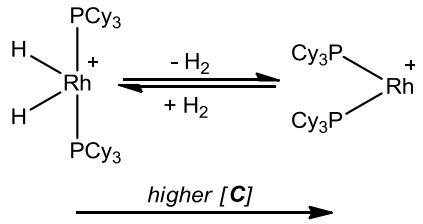


Figure 3.7 Plot of ^{11}B concentration for the dehydrocoupling of **B** (initial concentration = 0.036 M) using $\{Rh(PCy_3)_2L_n\}^+$ (5 mol%, generated *in situ*) with exogenous **C** (initial concentration = 0.036 M). 0.1 mL aliquots diluted with 1,2-$C_6H_4F_2$ (0.25 mL). ●, $H_3B{\cdot}NMe_2H$ (**A**); ▲, $H_3B{\cdot}NMe_2BH_2{\cdot}NMe_2H$ (**B**); ■, $[H_2BNMe_2]_2$ (**C**); ▲, $H_2B{=}NMe_2$ (**Z**); ■, $HB(NMe_2)_2$.

It thus appears that **C** acts as a modifier in catalysis to produce a kinetically significant concentration of Rh(I) species (Scheme 3.17). Since **C** is the product of dehydrocoupling, the effect is autocatalytic. To the best of our knowledge, the autocatalytic effect of **C** has not been reported previously. The increase in the rate of consumption of **A** on addition of extra **C** implies that **A** is rapidly dehydrogenated by a Rh(I) species to generate **Z**, although under the equilibrium conditions with H_2 present it is also possible that **A** is additionally being dehydrogenated more slowly in a constant oxidation state Rh(III) manifold. Likewise the presence of Rh(I) species leads to the significantly faster consumption of **B**. This could occur *via* the direct dehydrocyclisation of **B** to **C** at a Rh(I) centre as has been shown for $[Cp_2Ti]$ systems and suggested for heterogeneous Ni catalysts[55] and Ru-amido pincer complexes.[12] Alternatively, consumption of **B** could occur *via* B-N bond cleavage as mentioned

earlier in the stoichiometric reactions of **B** with $\{Rh(PCy_3)_2L_n\}^+$ and $\{Rh(H)_2(PCy_3)_2L_n\}^+$.



Scheme 3.17 Addition of excess **C** probes Rh(I) by promoting the reductive elimination of H_2. $[BAr^F{}_4]^-$ anions not shown.

3.4.2 Closed system

The stoichiometric reactions discussed in Section 3.3.2 indicated a rapid Rh(I)/Rh(III) dehydrogenation pathway accompanied by a slower constant oxidation state Rh(III) dehydrogenation of **A**. As catalysis in a sealed system will result in a build up of dihydrogen, and it has been shown already that H_2 loss from $\{Rh(H)_2(PCy_3)_2L_n\}^+$ species is slow at best in the absence of **C**, this is likely to force the system to predominantly reside in the +3 oxidation state (Rh(III)-dihydride), allowing the probing of this aspect of the cycle. Dehydrocoupling of **A** under the same conditions as the open system (0.072 M **A**, 5 mol% $\{Rh(PCy_3)_2L_n\}^+$) but in a sealed high pressure NMR tube produced a drastically different time/concentration profile to that of an open system (Figure 3.8).

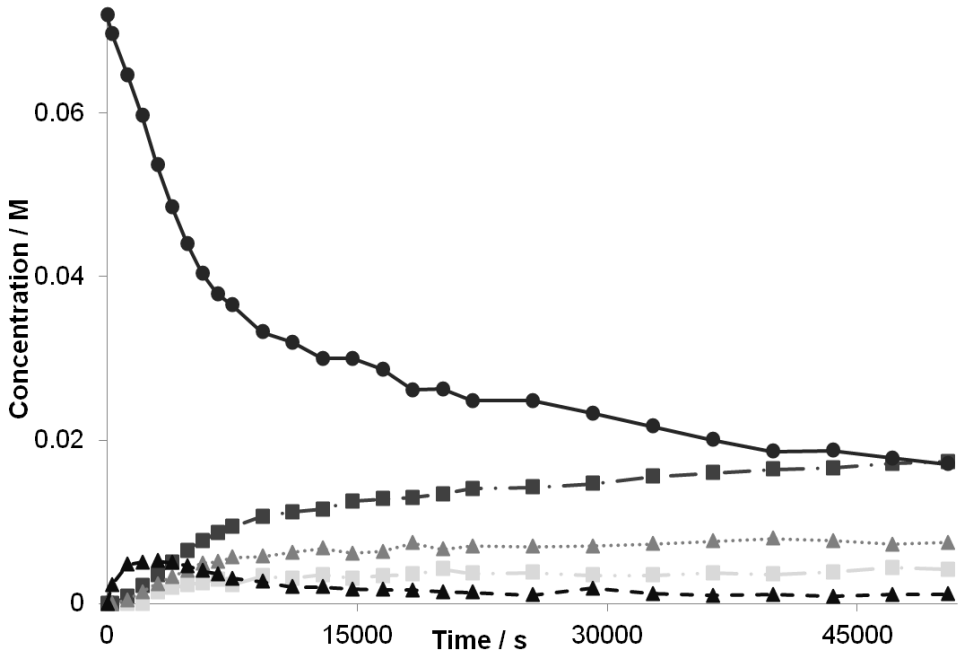
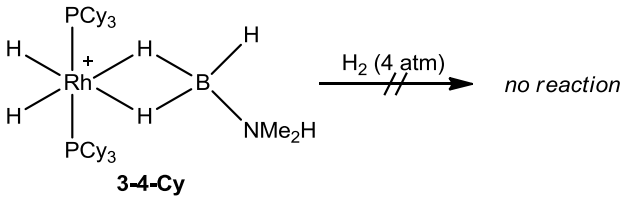


Figure 3.8 Plot of ^{11}B concentration for the dehydrocoupling of **A** (initial concentration = 0.072 M) using $\{Rh(PCy_3)_2L_n\}^+$ (5 mol%, generated *in situ*) in a closed system (sealed high pressure NMR tube). ●, $H_3B{\cdot}NMe_2H$ (**A**); ▲, $H_3B{\cdot}NMe_2BH_2{\cdot}NMe_2H$ (**B**); ■, $[H_2BNMe_2]_2$ (**C**); ▲, $H_2B{=}NMe_2$ (**Z**); ■, $HB(NMe_2)_2$.

Notably, **A** was consumed at a much slower rate; 50% conversion was only achieved after 15000 seconds compared with 1200 seconds in an open system. Smaller quantities, in comparison to the open system, of **B** and **Z** were also observed. During catalysis the only organometallic species observed by ^1H and $^{31}P\{^1H\}$ NMR spectroscopy was **3-4-Cy**, indicating that this is a resting state on the catalytic cycle. This is the same as observed for $\{Rh(P^iPr_3)_2L_n\}^+$, but different to $\{Rh(P^iBu_3)_2L_n\}^+$ where a complex mixture of products were observed, of which **3-4-^{i}Bu** was present as a minor (~20%) component.[16, 17] A comparison to the open system is not possible as the lower Rh concentration in the aliquots as a result of the dilution with 1,2-$C_6H_4F_2$ prevents the analysis of the organometallic products by NMR spectroscopy.

In an attempt to establish the mechanism by which H_2 slows downs the rate of dehydrocoupling, a solution of **3-4-Cy** was placed under 4 atm of hydrogen (Scheme

3.18). We postulated that displacement of **A** to form the known rhodium dihydride *bis*-dihydrogen complex, $[Rh(H)_2(PCy_3)_2(\eta^2\text{-}H_2)_2][BAr^F{}_4]$ (**i-20**),[27] could occur. However no reaction was observed, indicating that catalyst inhibition by hydrogen does not occur *via* the formation of **i-20**. It is speculated that the attenuation in rate is due to the presence of hydrogen, which forces the catalyst to reside predominantly in the Rh(III) oxidation state, which dehydrogenates **A** and facilitates the B-N bond cleavage/dehydrocyclisation of **B** at a slower rate than the Rh(I) species $\{Rh(PCy_3)_2L_n\}^+$.



3-4-Cy

Scheme 3.18 Reaction of 3-4-Cy with hydrogen. $[BAr^F{}_4]^-$ anions not shown.

The dehydrocoupling of **B** in a sealed system (0.036 M **B**, 5 mol% $\{Rh(PCy_3)_2L_n\}^+$ with respect to B-N units) also proceeded at a slower rate (Figure 3.9). Only 35% conversion of **B** was observed at 7200 seconds, at which point complete conversion had occurred in the open system. **A** and **Z** were also observed, arising from B-N bond cleavage.

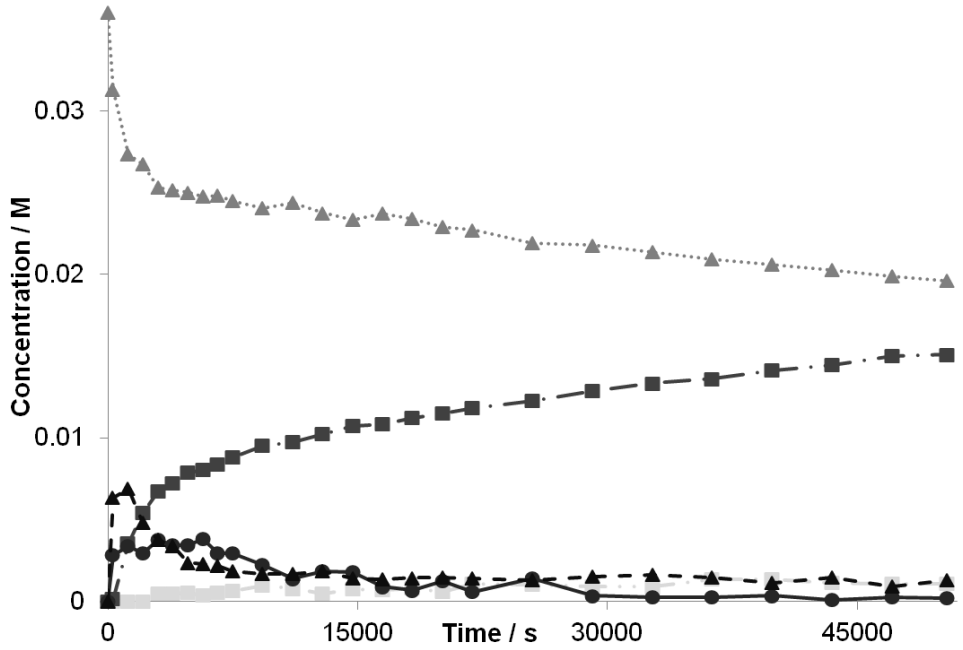


Figure 3.9 Plot of ^{11}B concentration for the dehydrocoupling of **B** (initial concentration = 0.036 M) using $\{Rh(PCy_3)_2L_n\}^+$ (5 mol% with respect to B-N units, generated *in situ*) in a closed system (sealed high pressure NMR tube). ●, $H_3B{\cdot}NMe_2H$ (**A**); ▲, $H_3B{\cdot}NMe_2BH_2{\cdot}NMe_2H$ (**B**); ■, $[H_2BNMe_2]_2$ (**C**); ▲, $H_2B{=}NMe_2$ (**Z**); ■, $HB(NMe_2)_2$.

The slower catalysis in a closed system is consistent with the catalyst system residing predominantly in the constant oxidation state Rh(III) manifold proposed earlier. This suggests that the dehydrocyclisation/B-N bond cleavage of **B** occurs faster at a Rh(I) centre rather than a Rh(III) centre.

The stoichiometric and catalytic investigations have revealed a rather complex mechanistic landscape for the dehydrogenation of **A**. To link these observations together and add weight to our potential mechanism, we turned to kinetic simulations.

3.5 Kinetic simulations

Kinetic simulations on the dehydrocoupling of **A** catalysed by $\{Rh(PCy_3)_2L_n\}^+$ were undertaken by Prof. Guy Lloyd-Jones of Bristol University. His report is reproduced here *verbatim*.

In parallel with the stoichiometric and catalytic exploration of the Rh-catalyzed dehydrocoupling process, we engaged in iterative analyses of the reaction kinetics. These kinetic studies proved valuable not just in the support of the final model for the system, but more pivotally in the interrogation and dismissal of evolving mechanistic hypotheses and thus provision of feedback to the stoichiometric and catalytic investigations. Although full analytical rate equations can be derived for catalytic systems,[56] complex reaction networks, such as the one investigated herein, can be very challenging to simplify for application under limiting conditions. A more pragmatic approach is to test various mechanistic hypotheses *via* model systems that are explored in computationally based kinetics simulations.[57, 58] This technique can be applied in a qualitative manner to evaluate the viability of a model in a general sense, with or without numerical tensioning against experimental data sets, or in a quantitative manner to determine absolute values for the rate constants associated with some or all of the steps in the cycle. A quantitative analysis requires a comprehensive model and is usually limited to simple systems, certainly less complex than those discussed herein. We thus aimed to develop a minimal holistic model that can qualitatively account for the macroscopic temporal evolution of the system when starting from five different initial conditions (Figure 3.10 and Figure 3.11). We emphasize that the rate constants k_1-k_6 in the final model are intended solely to provide a qualitative fit of temporal concentration data in support of the global

mechanistic picture for the dehydrocoupling reaction, including autocatalysis and parallel catalysis. Many of the rate constants are telescoped steps, some to termolecularity with notional irreversibility, and should not be interpreted in isolation or indeed in a quantitative manner.

We began with three data sets experimentally obtained with $[\mathbf{A}]_0$ = 0.072, 0.12, and 0.15 M, all three employing 5 mol% Rh precatalyst. As discussed earlier, data for **Z** were unreliable due to further reactions during sampling, and thus while **Z** was included as a component in our models, we focused on obtaining reliable predictive profiles for the experimental temporal concentration data of **A**, **B**, and **C**. In our initial analysis we examined whether the profiles were consistent with catalysis predominantly proceeding *via* a simple **A->B->C** sequence, as was found for example in the [Cp_2Ti]-catalyzed system,[44] but augmented by partial conversion of **A** to **Z**, and the uncatalysed dimerisation of **Z** to give **C**.[15] The decay in **A** was found to be approximately first order in all three runs, with **B** growing and then decaying as would be expected. However, inconsistent with a simple **A->B->C** sequence was the profile for the decay of **B** and growth of **C** occurring after the peak in concentration of **B**. Instead of a simple decay process, there was the onset of a period of pronounced rate acceleration. Attempts to describe this behaviour by inclusion of H_2 in the model and then controlled inhibition/acceleration of catalysis through solution-phase saturation/outgassing equilibria were not successful, primarily because of a concomitant effect on the decay in **A**. A range of other inhibition/acceleration loops were also tested without success. A second approach lay in Rh-catalyzed equilibration of **A** with **Z** and **B**, and then accelerating the uncatalyzed dimerisation of **Z** to **C**

through a progressive change in reaction medium, *e.g.*, polarity.[50] However, this did not account for the accelerated decay in **B**.

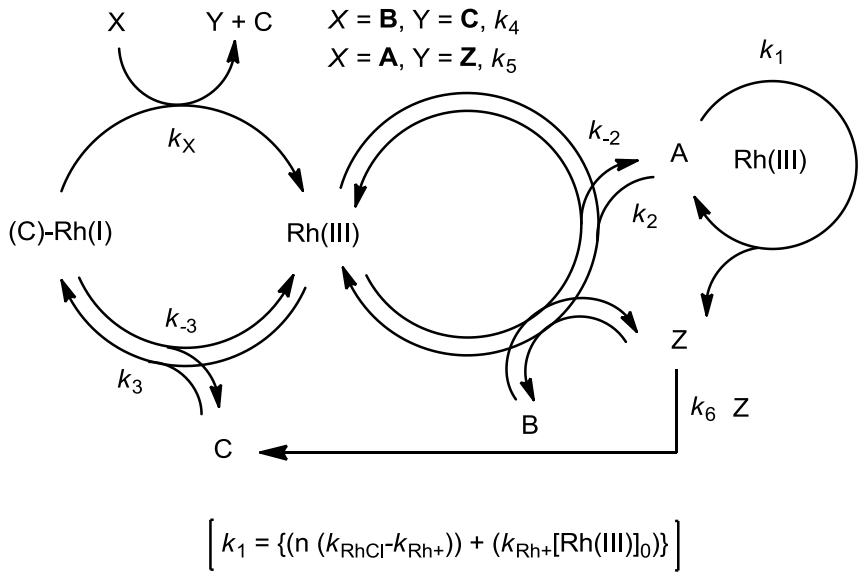


Figure 3.10 Catalytic cycle employed to generate a qualitative predictive model for the kinetics of the catalysed dehydrocoupling of **A** to **C**, *via* **Z** and **B.**

Table 3.3 Rate constants and their standard deviation in models employed to simulate datasets **I**-**V**. SD = standard deviation.

	I	**II**	**III**	**IV**	**V**	**Average**	**SD**
$\boldsymbol{k_1}$ / s^{-1}	5.1×10^{-4}	5.7×10^{-4}	4.2×10^{-4}	6.2×10^{-4}	7.9×10^{-4}	5.8×10^{-4}	1.4×10^{-4}
$\boldsymbol{k_2}$ / $M^{-2}\,s^{-1}$	5.8	5.2	6.1	8.9	7.6	6.7	1.5
$\boldsymbol{k_{-2}}$ / $M^{-1}\,s^{-1}$	7.4×10^{-2}	6.2×10^{-2}	7.4×10^{-2}	8.8×10^{-2}	6.1×10^{-2}	7.2×10^{-2}	1.1×10^{-2}
$\boldsymbol{k_3}$ / $M^{-1}\,s^{-1}$	11.8×10^{-2}	5.5×10^{-2}	3.5×10^{-2}	7.2×10^{-2}	3.5×10^{-2}	6.3×10^{-2}	3.4×10^{-2}
$\boldsymbol{k_{-3}}$ / s^{-1}	2.5×10^{-3}	2.5×10^{-3}	2.5×10^{-3}	2.5×10^{-3}	2.5×10^{-3}	2.5×10^{-3}	0
$\boldsymbol{k_4}$ / $M^{-1}\,s^{-1}$	3.53	1.43	1.93	8.33	1.60	3.36	2.90
$\boldsymbol{k_5}$ / $M^{-1}\,s^{-1}$	10	10	10	10	10	10	0
$\boldsymbol{k_6}$ / $M^{-1}\,s^{-1}$	5.3×10^{-3}	6.8×10^{-3}	6.4×10^{-3}	2.5×10^{-3}	4.8×10^{-3}	0.97×10^{-3}	0.9×10^{-3}

Ultimately, there were two key factors that led to the generation of a successful model (Figure 3.10). The first was the observation that the pseudo-first-order rate constants

(k_1) for decay in **A** were nearly identical for all three data sets: 6.6(±0.3) x 10^{-4} s^{-1} over the first two half-lives. This was inconsistent with the change in $[Rh]_0$, since this is more than doubled across the series, as is reflected in the proportional increases in the rate of generation of **B**. Moreover, additional runs at $[\mathbf{A}]_0 = 0.072$ with $[Rh]_0 = 2.5$ and 7.5 mol% resulted in identical rates of conversion of **A**. Since there is no conversion of **A** in the absence of catalyst, this indicated that there were (at least) two types of catalyst being generated, with the concentration of one of these being independent of $[Rh]_0$ and $[\mathbf{A}]_0$. The latter restriction suggested that the solvent, the only component that is constant between runs, contained a limiting quantity of a high-affinity modifier. Further work, *vide infra*, identified chloride ion as the most likely source of modified catalyst, and the final model thus includes a pseudo-first-order conversion of **A** to **Z** (k_1) arising from parallel catalysis (see inset to Figure 3.10). The unmodified cationic Rh(III) was also employed to turn over **A** + **Z** -> **B** in a reversible telescoped multistage process (k_2). The second key factor was the generation of a mechanism for a mild autocatalytic influence of **C** occurring *via* a Rh(III)-to-Rh(I) switch (K_3). This then allowed rising rates for conversion of **B** to **C** (k_4) and for conversion of **A** to **Z** (k_5) in the later stages of catalysis when **C** begins to accumulate. Finally, the background uncatalysed dimerisation of **Z** (k_6) to **C** provides a pathway for initiation of the autocatalysis. This model, while complex, was then able to qualitatively account not just for catalysis at different initial concentrations of **A** (Figure 3.11, graphs I, II, and III) and the accelerating effect on turnover of **A** (k_5) when **C** is present from the start (graph V), but also for reactions starting with **B**, that generate **A** and **Z** (k_{-2}) and thus **C** (graph IV).

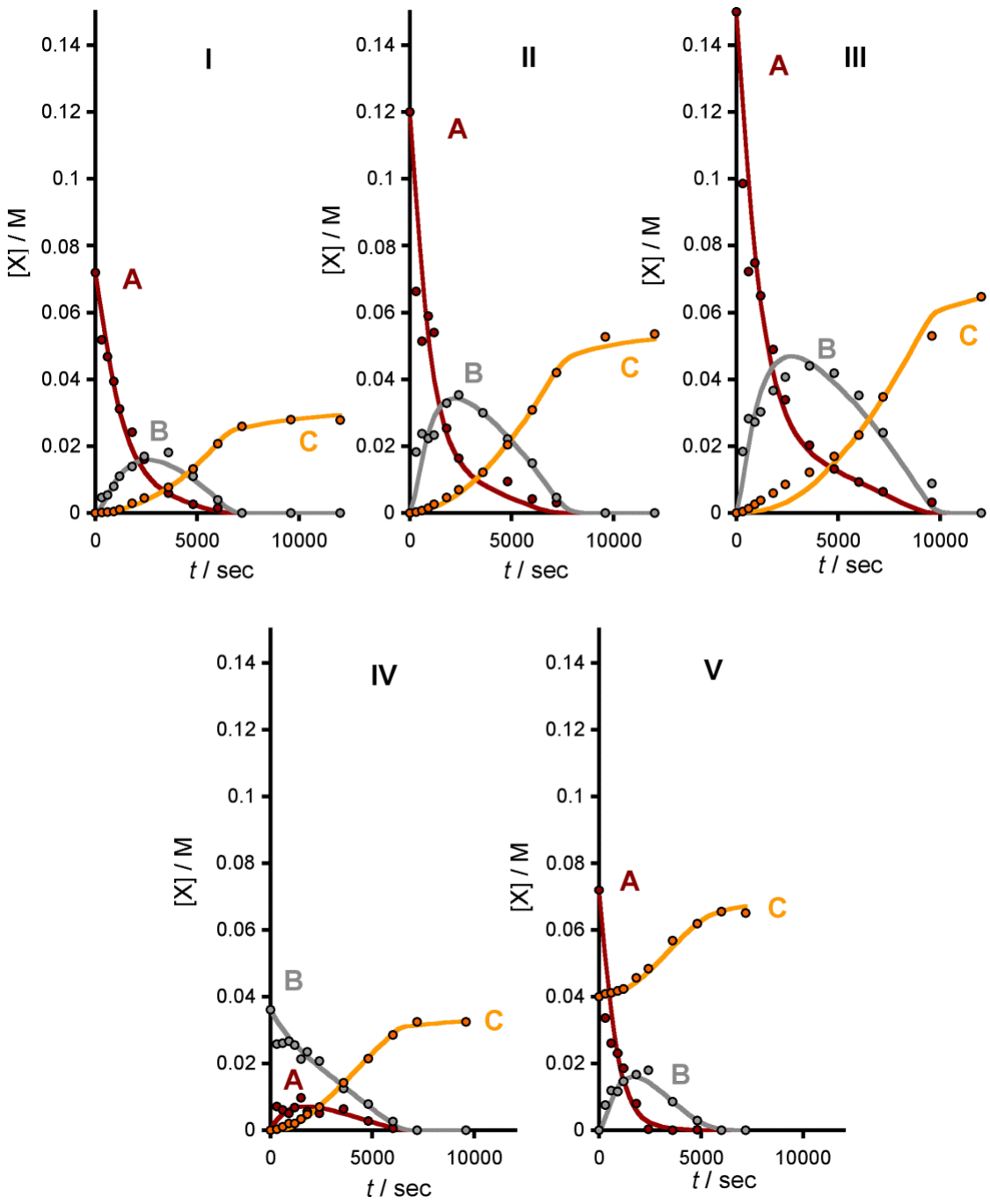
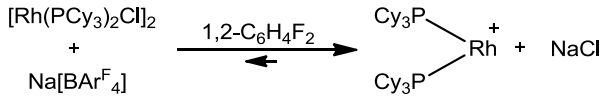


Figure 3.11 Temporal concentration profiles of five different starting conditions in the dehydrocoupling of **A** to **C**, *via* **B** and **Z**. Data points are experimentally determined concentrations. Solid lines are the profiles predicted by the qualitative model outlined in Figure 3.10.

3.6 Second active catalyst

It is apparent from the kinetic simulations that there is a small concentration of a second, more active catalyst present in the catalytic mixture. As mentioned in Section 3.5 the amount of second catalyst is independent of $[Rh]_0$ and $[\mathbf{A}]_0$, with the amount of solvent the only constant between the catalytic runs (Figure 3.11, graphs I, II and III). Potential impurities in the 1,2-$C_6H_4F_2$ could include fluoride and water, however as the solvent is pre-treated by stirring over alumina (to remove fluoride) and then distilled from calcium hydride (to remove water) the level of either present could be expected to be low (and also not reproducible). No evidence for C-F activation of 1,2-$C_6H_4F_2$, a source of a potentially active Rh-F catalyst, is observed.[59] Such reactivity would also be inconsistent with the observed kinetics as this would likely not be reproducible over different times/concentrations.



Scheme 3.19 *In situ* generation of $\{Rh(PCy_3)_2L_n\}^+$ with the concomitant formation of NaCl. $[BAr^F_4]^-$ anions not shown.

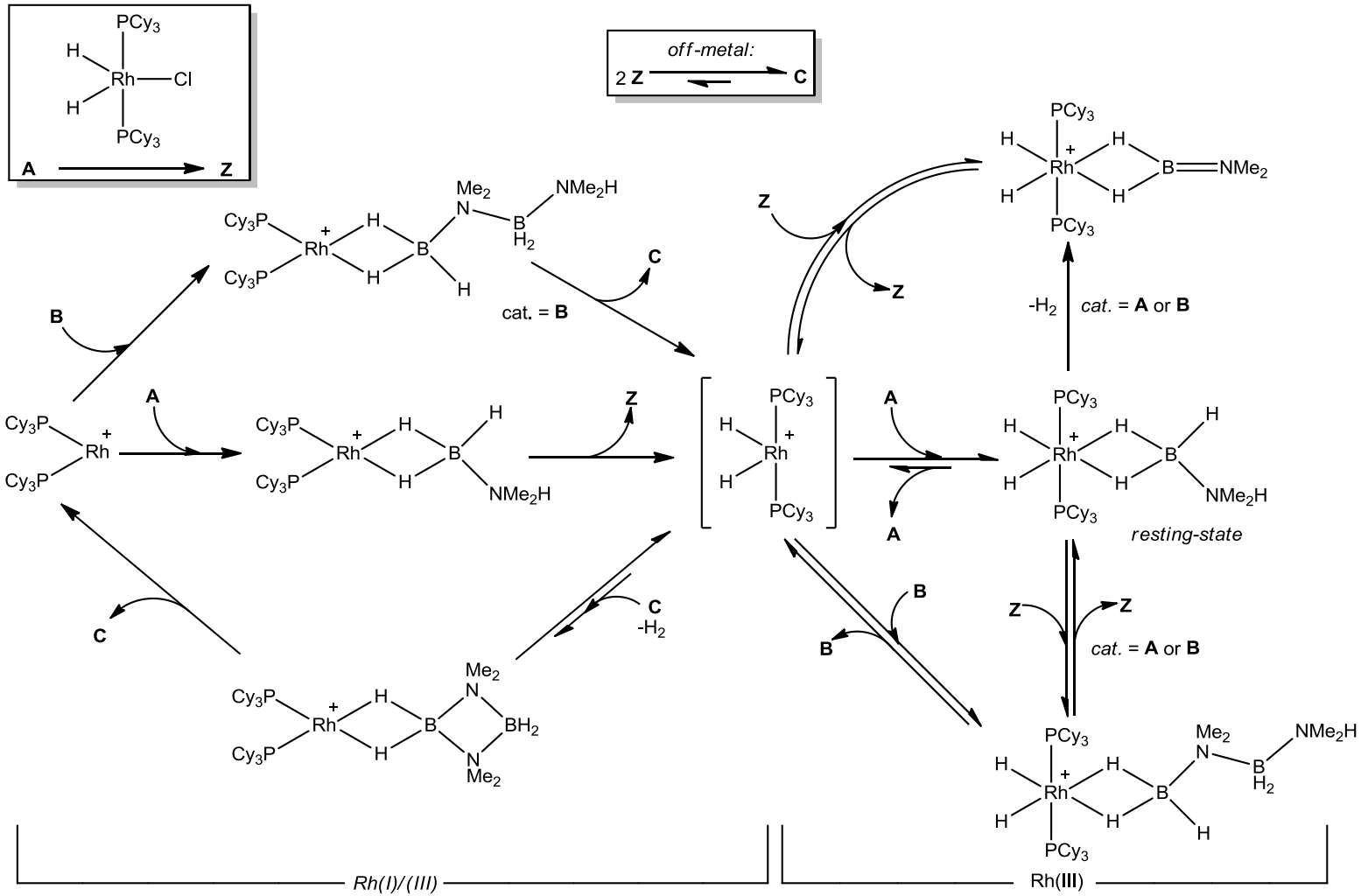
A more plausible candidate is chloride as the exogenous modifier. $\{Rh(PCy_3)_2L_n\}^+$ is generated *in situ* through the abstraction of chloride from $[Rh(PCy_3)_2Cl]_2$ by $Na[BAr^F_4]$ with the concomitant precipitation of sodium chloride (Scheme 3.19). Comparison of the dielectric constant of 1,2-$C_6H_4F_2$ (13.8) with THF (7.4) and CH_2Cl_2 (8.9) shows it to be greater, but lower than that for acetone (21.0) in which NaCl has a measurable solubility (4.2×10^{-3} g kg^{-1}).[60] As such there might be expected to be a low saturated concentration of NaCl in 1,2-$C_6H_4F_2$. This would be constant across all the kinetic runs, consistent with the observed kinetics. Any chloride present in solution could potentially recombine with $\{Rh(PCy_3)_2L_n\}^+$ to reform $[Rh(PCy_3)_2Cl]_2$.

Addition of the more soluble chloride source, $[(Ph_3P)_2N]Cl$, to either $\{Rh(PCy_3)_2L_n\}^+$ or $\{Rh(H)_2(PCy_3)_2L_n\}^+$ lead to the quantitative (by NMR spectroscopy) formation of the known Rh(I) and Rh(III) neutral complexes; $[Rh(PCy_3)_2Cl]_2$[26] and $Rh(H)_2(PCy_3)_2Cl$[61] respectively. Preliminary tests indicated both complexes to be active catalysts for the dehydrocoupling of **A**, and as such they are likely to account for the observed rate of decay of **A**. The process by which these neutral complexes react with amine-boranes is discussed in Chapter 4.

3.7 Mechanistic insights

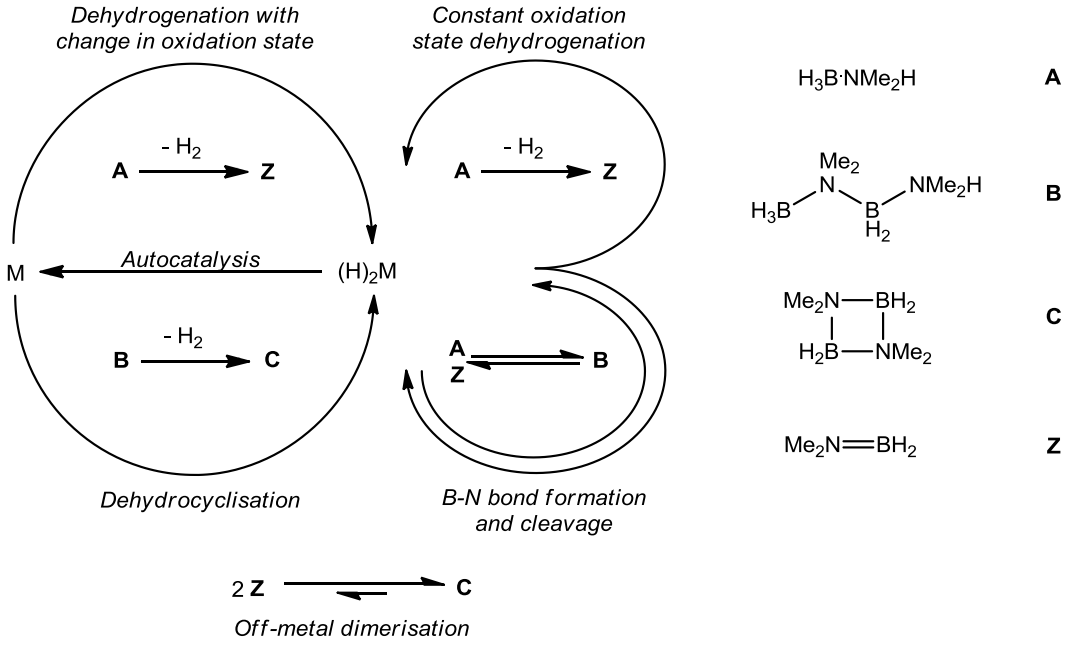
Combining the information acquired from the stoichiometric reactions, catalysis and kinetic simulations allows us to generate the mechanism seem in Scheme 3.20. The mechanistic landscape is undeniably complex, but several key points are apparent. **A** can be dehydrogenated rapidly by a Rh(I) species generating **Z** and a Rh(III) complex. The Rh(III) complex can also dehydrogenate **A** in a constant oxidation state Rh(III) manifold, but at a slower rate than the Rh(I)/Rh(III) cycle. As H_2 loss from the Rh(III) species is slow, the resting state during catalysis will be a Rh(III) complex with either **A** or **B** coordinated (**3-4-Cy** or **3-7-Cy**), dependent on their relative concentrations. The intermediate **B** is likely formed by coupling of **A** and **Z** at a Rh(III) centre, where it can also undergo B-N bond cleavage. Whether **B** is formed or consumed will be dependent on the relative concentrations of **A**, **Z** and **B**; recent calculations have demonstrated the equilibrium between **A**, **Z** and **B** to be close to thermoneutral (ΔG = -2.3 kcal mol^{-1})[12] and as there is no H_2 loss or gain involved, the equilibrium is dependent solely on the relative concentration of **A**, **B** and **Z**. **B** can also potentially be consumed *via* dehydrocyclisation to directly generate the final product **C** (and H_2), which is likely mediated by a Rh(I) species although this is difficult to definitively

show. As the concentration of **C** builds up during catalysis, it influences the rate of dehydrocoupling through provision of a route back from the less reactive Rh(III) centre to generate a Rh(I) species, which reacts more rapidly with both **A** and **B**. Also occurring is the off-metal dimerisation of two molecules of **Z** to give **C** and the parallel catalysis by the neutral Rh species which rapidly dehydrogenates **A**. N-H$^{\delta+\ldots\delta-}$H-B interactions also seem to play a key role with the inverse relationship between the lifetime of **3-3-Cy**, **3-6-Cy** and **3-7-Cy** and increasing concentrations of **A** or **B**, although they have not been studied in detail here.



Scheme 3.20 Relationships between species observed in stoichiometric and catalytic reactions, underpinned by kinetic simulations. $[BAr^F4]^-$ anions not shown.

Although the mechanism in Scheme 3.20 is complex and specific to cationic rhodium *bis*-phosphine catalysts, a simplified scheme has been developed (Scheme 3.21), aspects of which we believe can be applied to previously reported examples of transition metal and main group catalysts. The mechanism has been simplified into five parts: dehydrogenation of **A** with a change in oxidation state of the catalyst, dehydrogenation of **A** with no change in oxidation state, formation and cleavage of **B**, dehydrocyclisation of **B** to give **C** and the off-metal dimerisation of **Z**. Not all parts will necessarily operate for each catalyst system. Also included is the autocatalysis, although we are not aware of this effect being reported for any other systems.



Scheme 3.21 General scheme for the dehydrocoupling of **A** using transition metal and main group catalysts.

There have been several reports of transition metal catalysts where dehydrocoupling of **A** results in a change in the oxidation state of the metal. These include the cationic Rh chelating *bis*-phosphine catalysts, $[Rh(Ph_2P(CH_2)_nPPh_2)(\eta^6\text{-}C_6H_5F)][BAr^F{}_4]$ (n = 3 – 5) (**i-78**), which rapidly dehydrogenate **A** (TOF up to 1250 h^{-1}). For chelates with a small bite angle,[62] the Rh(I) oxidation state is strongly favoured over the +3 oxidation

state,[63] and hence the Rh(III) dihydride intermediate formed upon dehydrogenation of **A** will be short-lived with rapid loss of dihydrogen and a return to a Rh(I) species. This oxidation state preference likely accounts for their markedly faster rate of dehydrogenation than their monodentate phosphine counterparts for which the +3 oxidation state is favoured. Other catalysts systems proposed to undergo a change in oxidation state on dehydrogenation include [$TiCp_2$] and related Group 4 systems[11, 44] and Group 6 carbonyl catalyst systems.[10] Although a recent paper by Manners and co-workers has reported that a paramagnetic Ti(III) species may play a key role in the dehydrogenation of amine-boranes.[64]

Rh(III) and Ir(III) cationic catalyst systems have been reported to catalyse the dehydrogenation of amine-boranes without a change in metal oxidation state in a σ-CAM fashion.[15-17, 65] Schneider and Fagnou's reports of Ru catalysts which efficiently catalyse the dehydrogenation by an outer-sphere Noyori-like mechanism and consequently experience no alteration of the metal's oxidation state could also be included in this section.[12, 66, 67] Mechanisms discussed for main group and d^0 (*e.g.* Ca^{2+}) systems also do not include a change in oxidation state.[52, 68, 69]

Ru, Rh, Ir and Ti based systems have all been observed to catalyse the formation of **B** from the coupling of **A** and **Z**.[10, 12, 13, 15, 44] For [Cp_2Ti] this is proposed to occur *via* an amido-borane intermediate where a molecule of **A** has undergone N-H activation. Main group systems also catalyse the formation of deprotonated **B**, $[H_3B{\cdot}NMe_2BH_2{\cdot}NMe_2]^-$ *via* the insertion of **Z** into an amido-borane intermediate.[53, 68, 69] The formation of **B** is also related to the dehydrogenation/insertion mechanism proposed for the polymerisation of primary amine-boranes.[43, 46, 70] The aforementioned systems also catalyse the consumption of **B** to give **C**. For [Cp_2Ti] this

has been shown to occur *via* dehydrocyclisation.[44] Alternatively B-N bond cleavage can occur to generate **A** and **Z** as seen in Rh, Ir and Ru systems although parallel dehydrocyclisation cannot be ruled out for these systems.[12, 15, 67] Some systems, such as the photogenerated $CpFe(CO)_n$ do not dehydrocouple **A** *via* the intermediate **B**, instead producing **Z** which dimerises off-metal to generate **C**.[45] Off-metal dimerisation of **Z** will occur for all systems where non-metal bound **Z** is produced. The rate of off-metal dimerisation has recently been probed using an iridium system.[15]

The simplified mechanism can also be used to explain the variation in turnover frequencies observed for closely related Group 9 catalysts (Figure 3.12). The differences reflect the oxidation state preference of the catalyst, which in turn influences which area of the simplified mechanism the catalyst operates in. The stronger bonds that iridium can form with amine-boranes *versus* rhodium might be expected to slow catalysis, while the strong preference for the +3 oxidation state over +1 will result in iridium operating solely in the constant oxidation state M(III) manifold. For example, the addition of **C** to $\{Ir(H)_2(PCy_3)_2L_n\}^+$ does not result in the reductive elimination of dihydrogen in contrast to $\{Rh(H)_2(PCy_3)_2L_n\}^+$, demonstrating iridium's reluctance to be in the Ir(I) oxidation state.[15] Additionally, Paul and Musgrave have calculated that the dehydrogenation of AB catalysed by $[Ir(H)_2(POCOP^{Me})]$ ($POCOP^{Me}$ = κ^3-1,3-$(OPMe_2)_2C_6H_3$) occurs at an Ir(III) species, with an Ir(I) species not implicated.[71] As mentioned previously, work by Dubois and co-workers showed that complexes of chelating phosphines such as 1,3-*bis*(diphenylphosphino)propane, which has a relatively small bite angle,[62] strongly favours the Rh(I) oxidation state[63] and will therefore function in the faster M(I)/M(III) manifold. This explains the much greater turnover frequency observed

for $[Rh(Ph_2P(CH_2)_3PPh_2)(\eta^6\text{-}C_6H_5F)][BAr^F{}_4]$ in comparison to catalysts featuring monodentate phosphines.

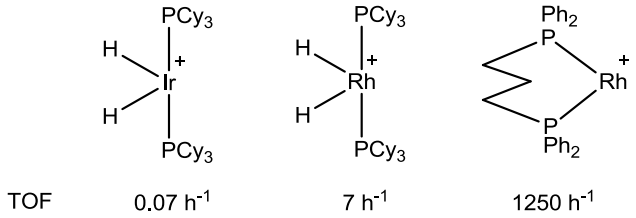


Figure 3.12 Variation in turnover frequency for the dehydrocoupling of **A** in an open system for closely related Group 9 catalysts. $\{Ir\{H)_2(PCy_3)_2L_n\}^+$, 20 mol%; $\{Rh(H)_2(PCy_3)_2L_n\}^+$, 5 mol%; $\{Rh(Ph_2P(CH_2)_3PPh_2)\}^+$, 0.2 mol%. $[BAr^F{}_4]^-$ anions not shown.

3.8 Conclusions and future work

It is clear that the dehydrocoupling of **A** by transition metal catalysts is a complex process, with many nuances, even when just one catalyst system, $\{Rh(PCy_3)_2L_n\}^+$, is focussed on. Through the synthesis and characterisation of σ-complexes of model amine-boranes, substrates and intermediates, monitoring of boron containing species during catalysis and kinetic simulations, we have been able to propose a mechanism by which $\{Rh(PCy_3)_2L_n\}^+$ catalyses the dehydrocoupling of **A**. From this we have generated a generic mechanism, which can be applied wholly or in part to other reported transition metal and main group catalyst systems. The key features of this general scheme include: dehydrogenation of **A** with or without a change in oxidation state at the metal, dehydrocyclisation of **B**, B-N bond cleavage of **B** and autocatalysis.

The kinetic simulations highlighted the presence of second catalyst, which preliminary experiments indicated was likely to be a neutral rhodium catalyst such as $[Rh(PCy_3)_2Cl]_2$ or $Rh(H)_2(PCy_3)_2Cl$. The behaviour of the neutral systems with amine-boranes shall be investigated in more detail in Chapter 4.

3.9 References

1. A. Staubitz, A. P. M. Robertson, M. E. Sloan and I. Manners, *Chem. Rev.*, 2010, **110**, 4023-4078.
2. B. L. Dietrich, K. I. Goldberg, D. M. Heinekey, T. Autrey and J. C. Linehan, *Inorg. Chem.*, 2008, **47**, 8583-8585.
3. T. Hugle, M. Hartl and D. Lentz, *Chem. Eur. J.*, 2011, **17**, 10184-10207.
4. V. Pons and R. T. Baker, *Angew. Chem. Int. Ed.*, 2008, **47**, 9600-9602.
5. V. Pons, R. T. Baker, N. K. Szymczak, D. J. Heldebrant, J. C. Linehan, M. H. Matus, D. J. Grant and D. A. Dixon, *Chem. Commun.*, 2008, 6597-6599.
6. A. Staubitz, A. P. M. Robertson and I. Manners, *Chem. Rev.*, 2010, **110**, 4079-4124.
7. T. B. Marder, *Angew. Chem. Int. Ed.*, 2007, **46**, 8116-8118.
8. G. Alcaraz and S. Sabo-Etienne, *Angew. Chem. Int. Ed.*, 2010, **49**, 7170-7179.
9. F. H. Stephens, V. Pons and R. T. Baker, *Dalton Trans.*, 2007, 2613-2626.
10. Y. Kawano, M. Uruichi, M. Shimoi, S. Taki, T. Kawaguchi, T. Kakizawa and H. Ogino, *J. Am. Chem. Soc.*, 2009, **131**, 14946-14957.
11. D. Pun, E. Lobkovsky and P. J. Chirik, *Chem. Commun.*, 2007, 3297-3299.
12. A. Friedrich, M. Drees and S. Schneider, *Chem. Eur. J.*, 2009, **15**, 10339-10342.
13. C. A. Jaska, K. Temple, A. J. Lough and I. Manners, *J. Am. Chem. Soc.*, 2003, **125**, 9424-9434.
14. M. Vogt, B. de Bruin, H. Berke, M. Trincado and H. Grutzmacher, *Chem. Sci.*, 2011, **2**, 723-727.
15. C. J. Stevens, R. Dallanegra, A. B. Chaplin, A. S. Weller, S. A. Macgregor, B. Ward, D. McKay, G. Alcaraz and S. Sabo-Etienne, *Chem. Eur. J.*, 2011, **17**, 3011-3020.
16. A. B. Chaplin and A. S. Weller, *Inorg. Chem.*, 2010, **49**, 1111-1121.
17. T. M. Douglas, A. B. Chaplin, A. S. Weller, X. Z. Yang and M. B. Hall, *J. Am. Chem. Soc.*, 2009, **131**, 15440-15456.
18. T. M. Douglas, A. B. Chaplin and A. S. Weller, *J. Am. Chem. Soc.*, 2008, **130**, 14432-14433.
19. H. C. Johnson, Part II Thesis, University of Oxford, 2011.
20. R. Dallanegra, A. B. Chaplin, J. Tsim and A. S. Weller, *Chem. Commun.*, 2010, **46**, 3092-3094.
21. R. Dallanegra, A. B. Chaplin and A. S. Weller, *Angew. Chem. Int. Ed.*, 2009, **48**, 6875-6878.
22. R. Dallanegra, A. P. M. Robertson, A. B. Chaplin, I. Manners and A. S. Weller, *Chem. Commun.*, 2011, **47**, 3763-3765.
23. C. A. Tolman, *Chem. Rev.*, 1977, **77**, 313-348.
24. T. M. Douglas, A. B. Chaplin and A. S. Weller, *Organometallics*, 2008, **27**, 2918-2921.
25. A. B. Chaplin, A. I. Poblador-Bahamonde, H. A. Sparkes, J. A. K. Howard, S. A. Macgregor and A. S. Weller, *Chem. Commun.*, 2009, 244-246.
26. P. Binger, J. Haas, G. Glaser, R. Goddard and C. Kruger, *Chem. Ber.*, 1994, **127**, 1927-1929.
27. M. J. Ingleson, S. K. Brayshaw, M. F. Mahon, G. D. Ruggiero and A. S. Weller, *Inorg. Chem.*, 2005, **44**, 3162-3171.
28. M. Shimoi, S.-i. Nagai, M. Ichikawa, Y. Kawano, K. Katoh, M. Uruichi and H. Ogino, *J. Am. Chem. Soc.*, 1999, **121**, 11704-11712.
29. G. Alcaraz and S. Sabo-Etienne, *Coord. Chem. Rev.*, 2008, **252**, 2395-2409.
30. N. Merle, G. Koicok-Kohn, M. F. Mahon, C. G. Frost, G. D. Ruggerio, A. S. Weller and M. C. Willis, *Dalton Trans.*, 2004, 3883-3892.
31. R. W. Kunz and P. S. Pregosin, *^{31}P and ^{13}C NMR of transition metal phosphine complexes*, Springer-Verlag, Berlin ; New York, 1979.
32. Z. Freixa and P. W. N. M. van Leeuwen, *Dalton Trans.*, 2003, 1890-1901.
33. J. M. Brown and P. J. Guiry, *Inorg. Chim. Acta*, 1994, **220**, 249-259.

34. D. L. DuBois, D. M. Blake, A. Miedaner, C. J. Curtis, M. R. DuBois, J. A. Franz and J. C. Linehan, *Organometallics*, 2006, **25**, 4414-4419.
35. A. C. Cooper, J. C. Huffman and K. G. Caulton, *Organometallics*, 1997, **16**, 1974-1978.
36. H. Noth and Vahrenka.H, *Chem. Ber. Recl.*, 1967, **100**, 3353-3354.
37. S. Aldridge, A. J. Downs, C. Y. Tang, S. Parsons, M. C. Clarke, R. D. L. Johnstone, H. E. Robertson, D. W. H. Rankin and D. A. Wann, *J. Am. Chem. Soc.*, 2009, **131**, 2231-2243.
38. W. T. Klooster, T. F. Koetzle, P. E. M. Siegbahn, T. B. Richardson and R. H. Crabtree, *J. Am. Chem. Soc.*, 1999, **121**, 6337-6343.
39. P. M. Zimmerman, A. Paul, Z. Y. Zhang and C. B. Musgrave, *Inorg. Chem.*, 2009, **48**, 1069-1081.
40. J. Li, S. M. Kathmann, H. S. Hu, G. K. Schenter, T. Autrey and M. Gutowski, *Inorg. Chem.*, 2010, **49**, 7710-7720.
41. X. N. Chen, X. G. Bao, J. C. Zhao and S. G. Shore, *J. Am. Chem. Soc.*, 2011, **133**, 14172-14175.
42. W. C. Ewing, A. Marchione, D. W. Himmelberger, P. J. Carroll and L. G. Sneddon, *J. Am. Chem. Soc.*, 2011, **133**, 17093-17099.
43. H. C. Johnson, A. P. M. Robertson, A. B. Chaplin, L. J. Sewell, A. L. Thompson, M. F. Haddow, I. Manners and A. S. Weller, *J. Am. Chem. Soc.*, 2011, **133**, 11076-11079.
44. M. E. Sloan, A. Staubitz, T. J. Clark, C. A. Russell, G. C. Lloyd-Jones and I. Manners, *J. Am. Chem. Soc.*, 2010, **132**, 3831-3841.
45. J. R. Vance, A. P. M. Robertson, K. Lee and I. Manners, *Chem. Eur. J.*, 2011, **17**, 4099-4103.
46. A. P. M. Robertson, E. M. Leitao and I. Manners, *J. Am. Chem. Soc.*, 2011, **133**, 19322-19325.
47. V. Butera, N. Russo and E. Sicilia, *Chem. Eur. J.*, 2011, **17**, 14586-14592.
48. A. B. Chaplin and A. S. Weller, *Acta Crystallogr., Sect. C: Cryst. Struct. Commun.*, 2011, **67**, M355-M358.
49. G. J. Kubas, *Metal Dihydrogen and sigma Bond Complexes; Kluwer: NY*, 2001.
50. P. Paetzold, *Adv. Inorg. Chem.*, 1987, **31**, 123-170.
51. H. Noth and H. Vahrenka, *Chem. Ber. Recl.*, 1966, **99**, 1049-1050.
52. H. J. Cowley, M. S. Holt, R. L. Melen, J. M. Rawson and D. S. Wright, *Chem. Commun.*, 2011, **47**, 2682-2684.
53. M. S. Hill, G. Kociok-Kohn and T. P. Robinson, *Chem. Commun.*, 2010, **46**, 7587-7589.
54. A. B. Burg and C. L. Randolph, *J. Am. Chem. Soc.*, 1951, **73**, 953-957.
55. A. P. M. Robertson, R. Suter, L. Chabanne, G. R. Whittell and I. Manners, *Inorg. Chem.*, 2011, **50**, 12680-12691.
56. E. L. King and C. Altman, *J. Phys. Chem.*, 1956, **60**, 1375-1378.
57. R. N. Stabler and J. P. Chesick, *Int. J. Chem. Kinet.*, 1978, **10**, 461-469.
58. F. J. Weigert, *Comput. Chem.*, 1987, **11**, 273-280.
59. J. A. Panetier, S. A. Macgregor and M. K. Whittlesey, *Angew. Chem. Int. Ed.*, 2011, **50**, 2783-2786.
60. T. R. Otoole, J. N. Younathan, B. P. Sullivan and T. J. Meyer, *Inorg. Chem.*, 1989, **28**, 3923-3926.
61. H. L. M. Vangaal, J. M. J. Verlaak and T. Posno, *Inorg. Chim. Acta*, 1977, **23**, 43-51.
62. P. W. N. M. van Leeuwen, P. C. J. Kamer, J. N. H. Reek and P. Dierkes, *Chem. Rev.*, 2000, **100**, 2741-2769.
63. A. D. Wilson, A. J. M. Miller, D. L. DuBois, J. A. Labinger and J. E. Bercaw, *Inorg. Chem.*, 2010, **49**, 3918-3926.
64. H. Helten, B. Dutta, J. R. Vance, M. E. Sloan, M. F. Haddow, S. Sproules, D. Collison, G. R. Whittell, G. C. Lloyd-Jones and I. Manners, *Angew. Chem. Int. Ed.*, 2013, **52**, 437-440.
65. C. Y. Tang, A. L. Thompson and S. Aldridge, *J. Am. Chem. Soc.*, 2010, **132**, 10578-10591.
66. N. Blaquiere, S. Diallo-Garcia, S. I. Gorelsky, D. A. Black and K. Fagnou, *J. Am. Chem. Soc.*, 2008, **130**, 14034-14035.

67. M. Kass, A. Friedrich, M. Drees and S. Schneider, *Angew. Chem. Int. Ed.*, 2009, **48**, 905-907.
68. M. S. Hill, M. Hodgson, D. J. Liptrot and M. F. Mahon, *Dalton Trans.*, 2011, **40**, 7783-7790.
69. D. J. Liptrot, M. S. Hill, M. F. Mahon and D. J. MacDougall, *Chem. Eur. J.*, 2010, **16**, 8508-8515.
70. A. Staubitz, M. E. Sloan, A. P. M. Robertson, A. Friedrich, S. Schneider, P. J. Gates, J. Gunne and I. Manners, *J. Am. Chem. Soc.*, 2010, **132**, 13332-13345.
71. A. Paul and C. B. Musgrave, *Angew. Chem. Int. Ed.*, 2007, **46**, 8153-8156.

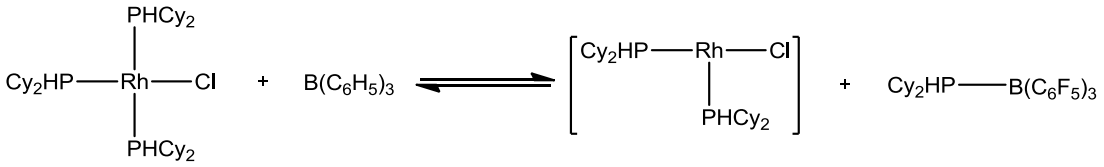
4 Investigating the Reactivity of Neutral Rhodium Complexes with Amine-Boranes

4.1 Introduction

In Chapter 3, kinetic simulations indicated the presence of a second catalyst acting in parallel to cationic $\{Rh(PCy_3)_2L_n\}^+$ that promoted the pseudo first order dehydrogenation of **A**. Preliminary investigations indicated that a possible candidate for the second catalyst was the neutral species $[Rh(PCy_3)_2Cl]_2$, formed by recombination of chloride, present in low concentrations in the solvent (1,2-$C_6H_4F_2$), with the cationic species. Sodium chloride was a likely candidate in the catalyst mixture, due to the use of $Na[BAr^F{}_4]$ to abstract the chloride for the *in situ* generation of $\{Rh(PCy_3)_2L_n\}^+$. $[Rh(PCy_3)_2Cl]_2$ is rapidly hydrogenated to form $Rh(H)_2(PCy_3)_2Cl$, which does not readily lose dihydrogen,[1] and as such $Rh(H)_2(PCy_3)_2Cl$ is likely to be the true catalyst under the conditions of catalysis. In this chapter we explore the likely mechanism by which $Rh(H)_2(PCy_3)_2Cl$ dehydrogenates **A**, and also investigate the organometallic species that could be present in the cationic system when both the neutral and cationic fragments are present. Additionally, we investigate the stoichiometric reactivity of amine-boranes at the Rh(I) centre of $[Rh(PCy_3)_2Cl]_2$.

Related to this work, Manners and co-workers have reported the synthesis of the neutral Rh(I) complex, $Rh(PHCy_2)_3Cl$, which dehydrogenates **A** in a homogeneous manner.[2] The addition of the strong Lewis acid, $B(C_6F_5)_3$, aids dissociation of a PCy_2H

ligand[3] (Scheme 4.1) and resulted in a significant increase in the rate of dehydrocoupling; 100% conversion was observed after 10 hours *versus* 65% conversion in the absence of the added borane. The *bis*-phosphine complex that is assumed to form on removal of the phosphine is similar to our proposed catalyst, *i.e.* $[Rh(PCy_3)_2Cl]_2$.



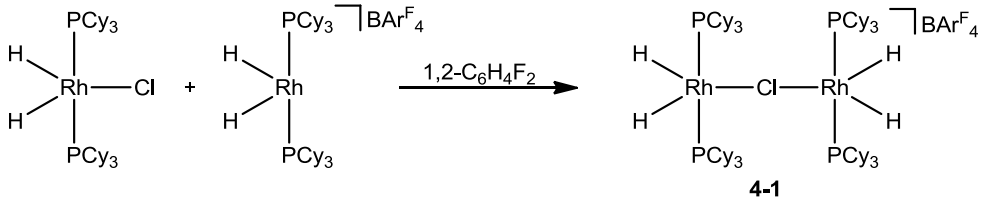
Scheme 4.1 Reaction of the Lewis acid $B(C_6F_5)_3$ with Manners' neutral *tris*-phosphine catalyst.

4.2 Chloride-bridged adduct

4.2.1 Synthesis and characterisation

For the dehydrocoupling of **A** catalysed by the cationic system (5 mol%, $[\mathbf{A}]_0$ = 0.072 M), the resting state was observed by $^{31}P\{^1H\}$ NMR spectroscopy to be the Rh(III) dihydride complex, $[Rh(H)_2(PCy_3)_2(\eta^2\text{-}H_3B{\cdot}NMe_2H)][BAr^F{}_4]$ (**3-4-Cy**) (Scheme 3.7). Under these conditions of catalysis, a detection limit of ~10% of the total phosphorus containing material by $^{31}P\{^1H\}$ NMR spectroscopy is plausible and, as such, if the co-catalyst was present in a low concentration (0.5 mol% or less) it would be difficult to observe. Intrigued as to the likely form of the co-catalyst when present with the cationic system we added one equivalent of $Rh(H)_2(PCy_3)_2Cl$ to one equivalent of $\{Rh(H)_2(PCy_3)_2L_n\}^+$ (L = solvent or agostic interaction) generated by degassing a 1,2-$C_6H_4F_2$ solution of $[Rh(H)_2(PCy_3)_2(\eta^2\text{-}H_2)_2][BAr^F{}_4]$ (**i-20**). The immediate and clean formation of the new chloride-bridged complex $[(PCy_3)_2(H)_2Rh(\mu\text{-}Cl)Rh(H)_2(PCy_3)_2][BAr^F{}_4]$ (**4-1**) was observed by ^1H and $^{31}P\{^1H\}$ NMR spectroscopy

(Scheme 4.2). **4-1**, which can additionally be formed by the addition of half an equivalent of $Na[BAr^F{}_4]$ to $Rh(H)_2(PCy_3)_2Cl$, has been characterised by a combination of NMR spectroscopy, ESI-MS, single crystal X-ray diffraction and elemental microanalysis (CHN).



Scheme 4.2 Synthesis of the new chloride-bridged complex $[(PCy_3)_2(H)_2Rh(\mu\text{-}Cl)Rh(H)_2(PCy_3)_2][BAr^F{}_4]$ (**4-1**).

Crystals of **4-1** suitable for single crystal X-ray diffraction were grown from a concentrated C_6H_5F solution at room temperature. The solid-state structure of **4-1** is shown in Figure 4.1, which demonstrates the Rh-Cl-Rh core. The chloride sits on a special position in the unit cell, resulting in one half of the molecule being generated by crystallographically-imposed symmetry. The solid-state structure of the related complexes $Rh(H)_2(PCy_3)_2Cl$ and $[Rh(PCy_3)_2(\mu\text{-}Cl)]_2$ have not been reported; instead the P^iPr_3 analogues have been used for comparison. The Rh-P distances (Rh1-P1, 2.3258(8) Å; Rh1-P2, 2.3295(7) Å) are comparable to, although marginally larger, than those observed for $Rh(H)_2(P^iPr_3)_2Cl$ (Rh1-P1 2.307(1) Å; Rh1-P2 2.303(2) Å)[4] and $[Rh(P^iPr_3)_2(\mu\text{-}Cl)]_2$ (Rh1-P1 2.262(2) Å; Rh1-P2 2.246 (2) Å)[5] complexes. Likewise the Rh-Cl distance is also slightly greater (Rh1-Cl1, 2.4813(3) Å) (*viz.* $Rh(H)_2(P^iPr_3)_2Cl$, 2.413(1) Å; $[Rh(P^iPr_3)_2(\mu\text{-}Cl)]_2$, 2.435(2) Å and 2.425(2) Å), which could be attributed to the greater steric bulk of the tricyclohexylphosphine *versus* triisopropylphosphine. The significantly smaller Rh1-Cl1-Rh1' angle of 103.0(1)° in

$[Rh(P^iPr_3)_2(\mu\text{-}Cl)]_2$ (*viz.* **4-1**, 153.61(5)°) reflects the constrained Rh-Cl-Rh-Cl square in $[Rh(P^iPr_3)_2(\mu\text{-}Cl)]_2$.

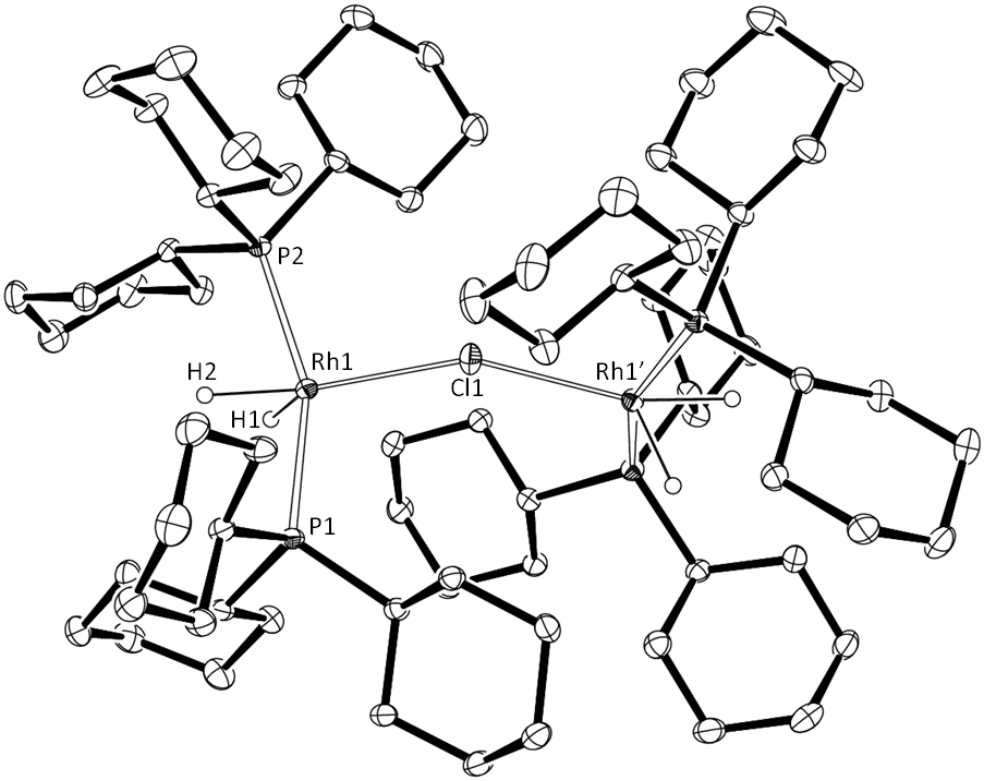


Figure 4.1 Solid-state structure of **4-1**. Displacement ellipsoids are given at the 30% probability level. The crystallographically equivalent atoms are generated by the operation –x, y, -z+½. $[BAr^F_4]^-$ anion and most hydrogen atoms omitted for clarity. Selected bond distances and angles: Rh1-P1, 2.3258(8) Å; Rh1-P2, 2.3295(7) Å; Rh1-H1, 1.51(3) Å; Rh1-H2, 1.51(3) Å; Rh1-Cl1, 2.4813(3) Å; Rh1-Rh1', 4.831(8) Å; P1-Rh1-P2, 156.75(3)°; Rh1-Cl1-Rh1', 153.61(5)°.

The room temperature (298 K) ^1H and $^{31}P\{^1H\}$ NMR spectra of **4-1** in CD_2Cl_2 display broad signals. A broad signal observed at δ -24.2 ppm in the ^1H NMR spectrum is assigned to the rhodium hydrides. A single broad environment at δ 49.6 ppm is observed in the $^{31}P\{^1H\}$ NMR spectrum (Figure 4.2). Cooling the sample to 200 K resolved these signals into those assignable to three separate, but similar, species whose individual shifts correspond well with the weighted average signal at 298 K, suggesting that at 298 K there is rapid interconversion between the three (Figure 4.2,

left). The $^{31}P\{^{1}H\}$ NMR data of the two minor species [δ 47.5 ppm (d, $^{1}J_{RhP}$ = 113 Hz, ~10%); δ 49.7 ppm (d, $^{1}J_{RhP}$ = 115 Hz, ~10%)] correspond well with that independently recorded for $Rh(H)_2(PCy_3)_2Cl$ [δ 49.4 ppm ($^{1}J_{RhP}$ = 114 Hz)] and $\{Rh(H)_2(PCy_3)_2L_n\}^+$ [δ 47.0 ppm ($^{1}J_{RhP}$ = 111 Hz)] at 200 K. The third species observed [δ 46.1 ppm (d, $^{1}J_{RhP}$ = 113 Hz, 80%)] is assigned to **4-1**. Three resonances are observed in the hydridic region of the ^{1}H NMR spectrum at 200 K, whose relative integrals and shifts correlate well with the assignments made from the $^{31}P\{^{1}H\}$ NMR data: δ -22.42 ppm (br, 0.31H, ~10%, $\{Rh(H)_2(PCy_3)_2L_n\}^+$); δ -23.44 ppm (br, 0.47H, ~10%, $Rh(H)_2(PCy_3)_2Cl$); δ -25.20 ppm (br, 3.22H, 80%, **4-1**) (Figure 4.2, right). Thus, we suggest that the three species observed at 200 K are **4-1** and $Rh(H)_2(PCy_3)_2Cl$ and $\{Rh(H)_2(PCy_3)_2L_n\}^+$ resulting from cleavage of the chloride bridge in **4-1**.

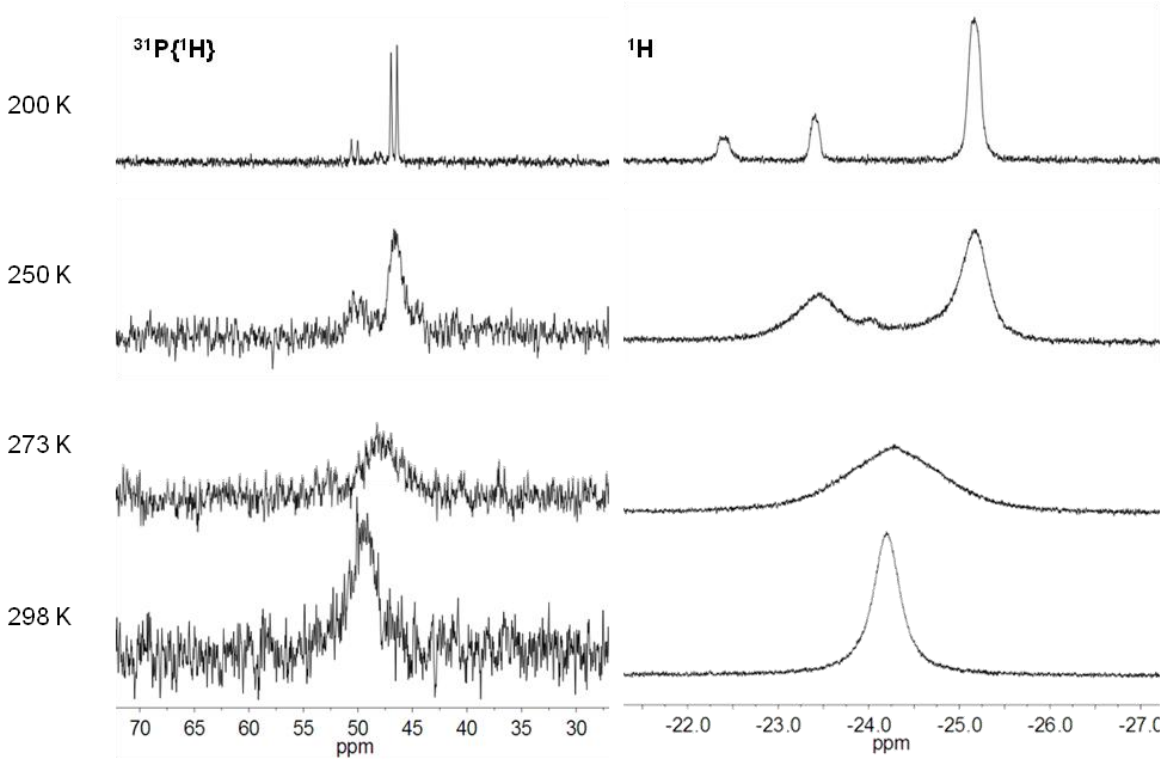
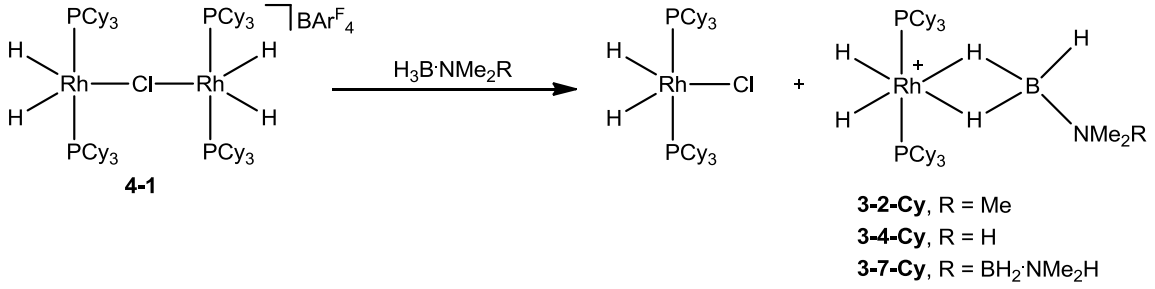


Figure 4.2 $^{31}P\{^{1}H\}$ and ^{1}H (hydridic region) NMR spectra of a sample of **4-1** in CD_2Cl_2 over a range of temperatures.

Analysis of complex **4-1** by ESI-MS revealed $\{[Rh(H)_2(PCy_3)_2]_2Cl\}^+$ to be present as a trace species (< 5%), *m/z* 1365.75 [M^+] (calc. 1365.74). The major species present was $\{Rh(H)_2(PCy_3)_2\}^+$, *m/z* 665.38 (calc. 665.38), generated by cleavage of the chloride bridge. The observed isotopic patterns were fully consistent with the molecular formulae.

4.2.2 Reactivity of 4-1

Initial reactivity studies on **4-1** focused on its stoichiometric reactivity with amine-boranes. Addition of **A** to **4-1** generated $Rh(H)_2(PCy_3)_2Cl$ and the cationic Rh(III) dihydride complex with **A** coordinated, **3-4-Cy** (Scheme 4.3). This reactivity revealed that although **4-1** is likely to form in the presence of excess $\{Rh(H)_2(PCy_3)_2L_n\}^+$ by combination of $\{Rh(H)_2(PCy_3)_2L_n\}^+$ and $Rh(H)_2(PCy_3)_2Cl$, at high concentrations of **A** (*i.e.* conditions at the start of catalysis) it is cleaved. At lower concentrations of **A** (*i.e.* towards the end of catalysis) it is possible that **4-1** reforms. **4-1** is also cleaved in the presence of TMAB and **B** to form $Rh(H)_2(PCy_3)_2Cl$ and the respective cationic amine-borane complexes (TMAB, **3-2-Cy**; **B**, **3-7-Cy**) (Scheme 4.3).



Scheme 4.3 Cleavage of the chloride-bridge in **4-1** in the presence of various amine-boranes. $[BAr^F_4]^-$ anions not shown.

Having examined the stoichiometric reactivity of **4-1** with amine-boranes the ability of **4-1** to act as a catalyst in amine-borane dehydrogenation was next investigated. Complex **4-1** (0.5 mol% $Rh(H)_2(PCy_3)_2Cl$, total Rh 1 mol% *i.e.* $Rh(H)_2(PCy_3)_2Cl$ and

$\{Rh(H)_2(PCy_3)_2L_n\}^+$) is a competent catalyst for the dehydrocoupling of **A** to ultimately afford the cyclic dimer **C** under the standard catalytic conditions ($[\mathbf{A}]_0$ = 0.072 M, 1,2-$C_6H_4F_2$, 298 K, open to a low flow of Ar). Complete conversion to **C** is observed after 360 minutes, although **A** had been fully consumed after 160 minutes. Monitoring the reaction by ^{11}B NMR spectroscopy and subsequent integration of the ^{11}B NMR data, as in Chapter 3, generated the time-concentration plot in Figure 4.3. **B** and **Z** were observed as intermediates, and the diaminoborane, $HB(NMe_2)_2$,[6] was also observed. As noted in Chapter 3, addition of NMe_2H to **Z** has been shown to lead to the formation of $HB(NMe_2)_2$,[7] and as such it is possible that the concentration of the diaminoborane has been artificially increased due to the decomposition of the highly reactive **Z** during sampling and analysis. Hence the absolute integrals of **Z** are likely to be unreliable.

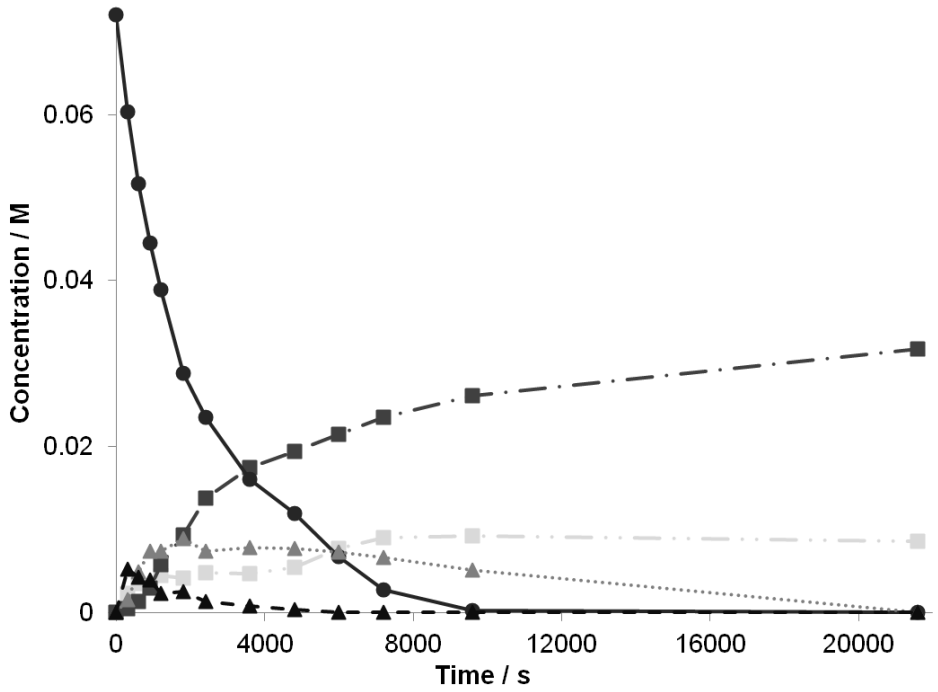


Figure 4.3 Plot of ^{11}B concentration for the dehydrocoupling of $H_3B{\cdot}NMe_2H$ (initial concentration = 0.072 M) using **4-1** (0.5 mol%). 0.1 mL aliquots diluted with 1,2-$C_6H_4F_2$ (0.25 mL). ●, $H_3B{\cdot}NMe_2H$ (**A**); ▲, $H_3B{\cdot}NMe_2BH_2{\cdot}NMe_2H$ (**B**); ■, $[H_2BNMe_2]_2$ (**C**); ▲, $H_2B{=}NMe_2$ (**Z**); ■, $HB(NMe_2)_2$.

The dehydrogenation of **A** follows a pseudo first order profile with a rate constant, k, of (0.37 ± 0.01) x 10^{-3} s^{-1} (Figure 4.4). This behaviour is consistent with that observed for the cationic catalyst system at 5 mol% ([**A**]$_0$ = 0.072 M) in which a second catalyst is proposed to operate in parallel (at 0.5 mol% or less), which also follows a pseudo first order decay of **A**. Kinetic simulations suggested a rate constant, k, of (0.58 ± 0.01) x 10^{-3} s^{-1} for this catalyst, which is similar to that observed for **4-1** (0.5 mol%). A comparison of these rate constants allows us to suggest that, in the cationic system, *ca.* 0.5 mol% of $Rh(H)_2(PCy_3)_2Cl$ could be present, acting in parallel with the cationic system to dehydrogenate **A**. This correlates with the detection limit of ~90% in $^{31}P\{^1H\}$ NMR spectroscopy, where 0.5 mol% or less of a second catalyst would be difficult to observe.

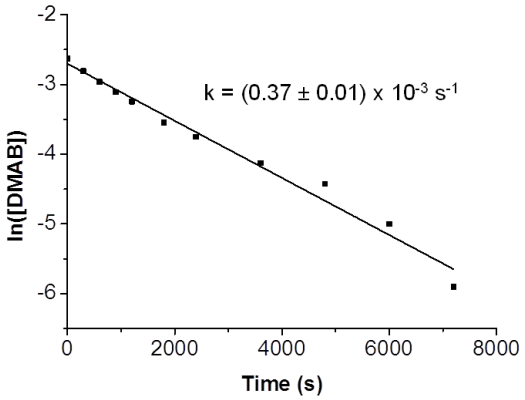


Figure 4.4 Pseudo first order kinetics for the consumption of **A**, catalysed by **4-1** (0.5 mol%).

4.3 Neutral rhodium(III) complex

As **4-1** is cleaved to form **3-4-Cy** and $Rh(H)_2(PCy_3)_2Cl$ in the presence of excess **A**, we turned our attention to the neutral species to probe its likely role in catalysis.

4.3.1 Catalysis

4.3.1.1 Catalytic dehydrocoupling of $H_3B{\cdot}NMe_2H$ (A)

$Rh(H)_2(PCy_3)_2Cl$ was tested as a catalyst for the dehydrocoupling of **A** under our standard conditions ($[\mathbf{A}]_0$ = 0.072 M, 1,2-$C_6H_4F_2$, 298 K, open to a low flow or argon). Although the results of the catalytic trial using **4-1** suggested that $Rh(H)_2(PCy_3)_2Cl$ was present in *ca.* 0.5 mol% concentrations in the cationic system, we chose to perform our detailed catalytic studies at 2 mol% due to the extremely low quantities of catalyst required for runs at 0.5 mol%, and the attendant issues with reproducibility that subsequently arise. The use of 2 mol% catalyst allows for the identification of likely organometallic species by NMR spectroscopy. Catalysis was monitored by ^{11}B NMR spectroscopy and subsequent integration of the ^{11}B NMR data generated the time-concentration plot shown in Figure 4.5, from which it is clear that $Rh(H)_2(PCy_3)_2Cl$ is a competent catalyst for the dehydrogenation of **A**. 95% conversion is achieved after 100 minutes (TON = 47.5). By comparison, the Wilkinson's catalyst analogue used by Manners and co-workers, $Rh(PHCy_2)_3Cl$ (1 mol%, in the presence of $B(C_6F_5)_3$ to promote dissociation of a phosphine), mediated complete conversion after 600 minutes.[2] A significant concentration of the intermediate amino-borane **Z**,[i] which dimerises to give the final product **C** was observed, along with smaller amounts of the intermediate linear diborazane, **B**.

[i] The concentration of **Z** appears to fall much more rapidly than expected for a simple second order process. This might suggest that dimerisation to **C** is metal promoted in this system.

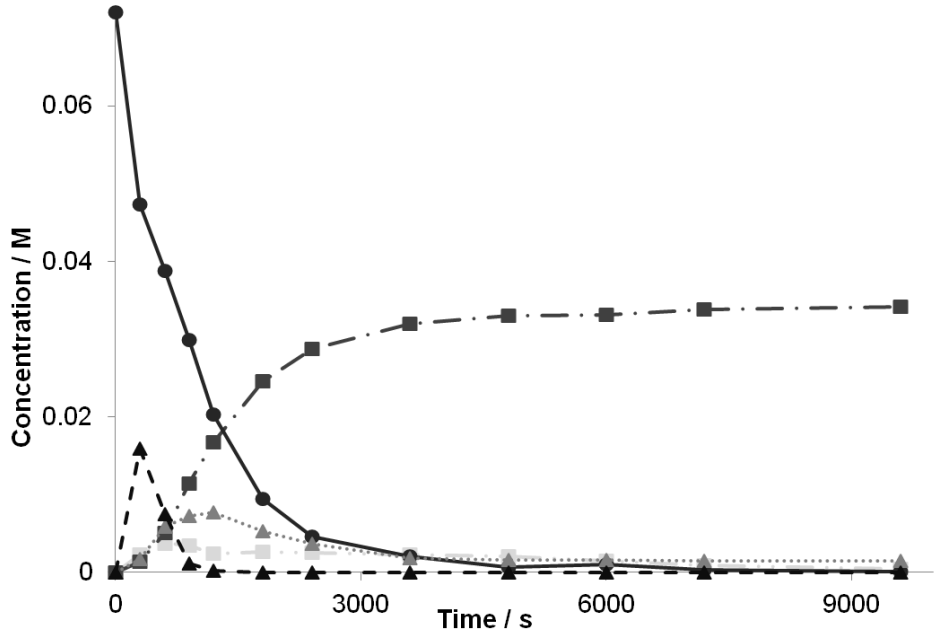


Figure 4.5 Plot of ^{11}B concentration for the dehydrocoupling of $H_3B{\cdot}NMe_2H$ (initial concentration = 0.072 M) using $Rh(H)_2(PCy_3)_2Cl$ (2 mol%). 0.1 mL aliquots diluted with 1,2-$C_6H_4F_2$ (0.25 mL). ●, $H_3B{\cdot}NMe_2H$ (**A**); ▲, $H_3B{\cdot}NMe_2BH_2{\cdot}NMe_2H$ (**B**); ■, $[H_2BNMe_2]_2$ (**C**); ▲, $H_2B{=}NMe_2$ (**Z**); ■, $HB(NMe_2)_2$.

The consumption of **A** is observed to follow pseudo first order kinetics, with a rate constant, k, of (1.03 ± 0.05) x 10^{-3} s^{-1} (Figure 4.6). As with **4-1**, this behaviour is consistent with the cationic catalyst system at 5 mol% ($[\mathbf{A}]_0$ = 0.072 M) with a second catalyst operating in parallel (0.5 mol% or less), which has a simulated pseudo first order decay of **A** (k = (0.58 ± 0.01) x 10^{-3} s^{-1}).

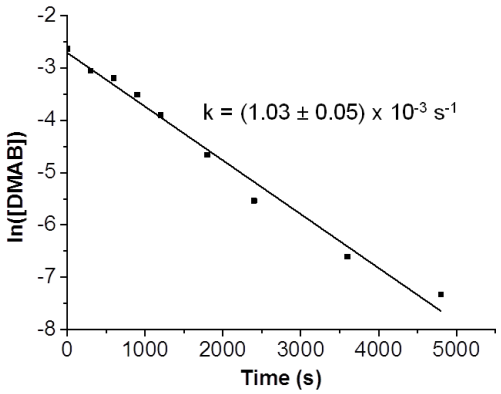


Figure 4.6 Pseudo first order kinetics for the consumption of **A**, catalysed by $Rh(H)_2(PCy_3)_2Cl$ (2 mol%).

At catalyst loadings below 2 mol%, the dehydrogenation of **A** does not go to completion: 0.5 mol%, ~65% **A** consumed; 0.1 mol%, ~15% **A** consumed. A time-concentration plot for 0.5 mol% $Rh(H)_2(PCy_3)_2Cl$ is shown in Figure 4.7. We suggest that the reduced consumption is due to irreversible catalyst deactivation. Consistent with the proposed irreversible deactivation, addition of further **A** did not restart catalysis to any significant level (a further ~5% **A** is consumed). The incomplete conversion is in contrast to that observed when **4-1** is utilised as a catalyst, yielding 100% conversion at the same catalyst loading of 0.5 mol% (Figure 4.3). It would appear that the cationic fragment, $\{Rh(H)_2(PCy_3)_2L_n\}^+$ present in **4-1** acts to stabilise the neutral fragment, $Rh(H)_2(PCy_3)_2Cl$, towards deactivation. The mechanism by which this occurs has not been investigated.

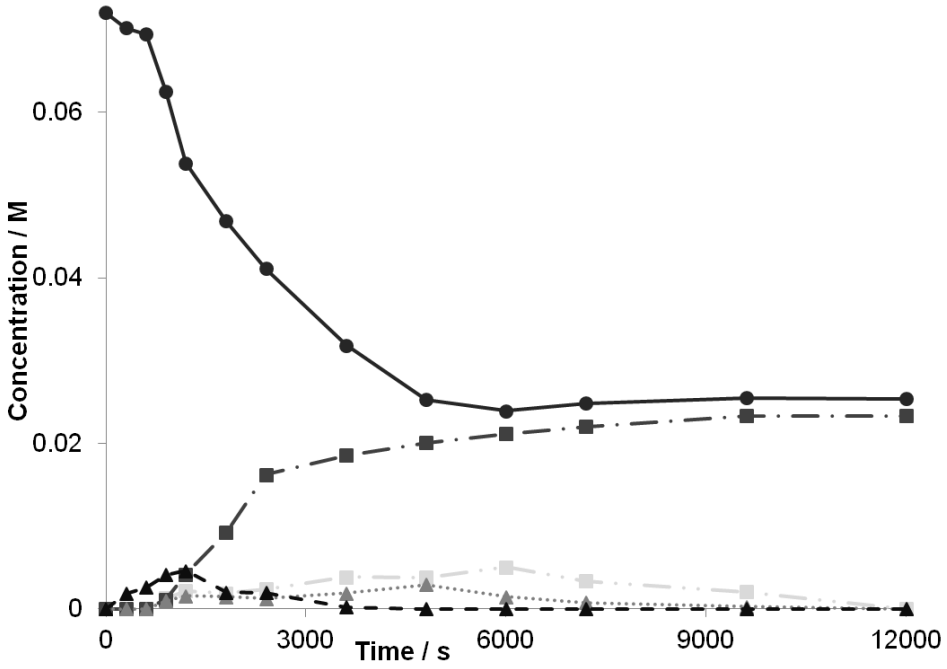
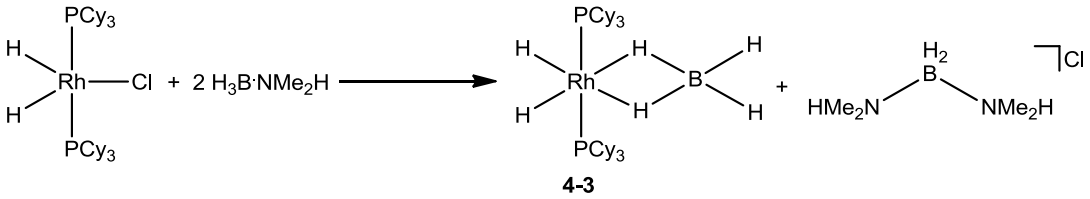


Figure 4.7 Plot of ^{11}B concentration for the dehydrocoupling of $H_3B{\cdot}NMe_2H$ (initial concentration = 0.072 M) using $Rh(H)_2(PCy_3)_2Cl$ (0.5 mol%). 0.1 mL aliquots diluted with 1,2-$C_6H_4F_2$ (0.25 mL). ●, $H_3B{\cdot}NMe_2H$ (**A**); ▲, $H_3B{\cdot}NMe_2BH_2{\cdot}NMe_2H$ (**B**); ■, $[H_2BNMe_2]_2$ (**C**); ▲, $H_2B{=}NMe_2$ (**Z**); ■, $HB(NMe_2)_2$.

Recent work in the Weller group by Molly Dickinson (Part II, 2011 - 2012) investigated the behaviour of the iridium analogue, $Ir(H)_2(PCy_3)_2Cl$ with **A**. Catalysis at 20 mol% in a sealed system (NMR tube) revealed the slow consumption of **A**, which halted after two equivalents of **A** had been consumed. The final product formed was not **C**, but the salt $[H_2B(NMe_2H)_2]Cl$. The major organometallic product observed by NMR spectroscopy was the borohydride complex, $Ir(H)_2(PCy_3)_2(\eta^2\text{-}BH_4)$ (**4-2**). **4-2** was independently synthesised *via* the addition of $Na[BH_4]$ to $Ir(H)_2(PCy_3)_2Cl$, in a method analogous to that reported for $Ir(H)_2(P^tBu_3)_2(\eta^2\text{-}BH_4)$,[8] and was shown to be inactive for the dehydrogenation of **A**. We postulated that the equivalent rhodium complex, $Rh(H)_2(PCy_3)_2(\eta^2\text{-}BH_4)$ (**4-3**),[9] might also be formed at low catalyst loadings (Scheme 4.4). To demonstrate this, **4-3** was synthesised independently in a method analogous to the iridium congener, and shown to be inactive for the dehydrogenation of **A**, demonstrating the plausibility of the proposed deactivation pathway. Further support for this proposal comes from analysis of the catalytic solution (0.5 mol%) by $^{31}P\{^1H\}$ NMR spectroscopy, which after 160 minutes revealed the major organometallic species present to be $Rh(H)_2(PCy_3)_2(\eta^2\text{-}BH_4)$ (~95%) [δ 54.6 ppm ($^1J_{RhP}$ = 109 Hz)] with trace amounts of $Rh(H)_2(PCy_3)_2Cl$ (~5%). The presence of trace amounts of $Rh(H)_2(PCy_3)_2Cl$ correlates with the small amount of dehydrocoupling observed on addition of further **A** (*vide supra*). Heinekey and co-workers have noted the formation of a catalytically dormant borohydride-like species during the dehydrogenation of ammonia-borane catalysed by $Ir(H)_2(POCOP)$ (POCOP = κ^3-1,3-$(OP^tBu_2)_2C_6H_3$) (**i-77**),[10, 11] although this compound is more accurately described as a $\sigma\text{-}BH_3$ compound of the parent dihydride, $Ir(H)_2(POCOP)(\eta^2\text{-}BH_3)$.[12]



Scheme 4.4 Likely deactivation pathway for $Rh(H)_2(PCy_3)_2Cl$ with **A**, at low catalyst loadings.

Figure 4.7 also shows that there is an induction period of 10 minutes before catalysis starts. A similar period of reduced activity is also observed at the beginning of catalysis using 0.1 mol% $Rh(H)_2(PCy_3)_2Cl$. The origin of this induction period has not been determined. Such a period of reduced activity can be characteristic of metal nano-particle formation[13-15] but the catalytic mixture retained its homogeneous appearance throughout catalysis with no black film or rhodium mirror observed. The addition of mercury, which can poison colloids *via* the formation of an amalgam,[16] did not significantly affect the rate of catalysis, although a slightly lower conversion was achieved (55% **A** consumed *versus* 65% at 2 mol%). A recent report by Finke and co-workers, however, demonstrates the need for caution when using Hg(0) poisoning to determine between homogeneous and heterogeneous catalysts.[17] The Wilkinson's complex analogue reported by Manners and co-workers was found to dehydrocouple **A** in a homogeneous manner.[2]

In a closed system (sealed high pressure NMR tube, 298 K, 1,2-$C_6H_4F_2$, $[\mathbf{A}]_0$ = 0.072 M) $Rh(H)_2(PCy_3)_2Cl$ (2 mol%) is also a competent catalyst for the dehydrogenation of **A**. However, in contrast to the open system, in which essentially complete conversion is observed using 2 mol% $Rh(H)_2(PCy_3)_2Cl$, only ~70% of **A** is consumed in the closed system. A time-concentration plot is shown in Figure 4.8. Addition of more **A** restarted catalysis, indicating that the catalyst remains active and is not undergoing irreversible deactivation under these conditions. Consistent with this, analysis of the

reaction mixture after 12 hours by $^{31}P\{^{1}H\}$ NMR spectroscopy revealed the major (~90%) organometallic species present to be $Rh(H)_2(PCy_3)_2Cl$ with **4-3** present only as a minor (~10%) component. Therefore, we propose that the incomplete conversion is due to hydrogen inhibition, as was observed for the cationic $\{Rh(PR_3)_2L_n\}^+$ systems in Chapter 3.[18-20] However, in contrast to the cationic system H_2 inhibition can be considered to be reversible for the neutral system, as removal of the H_2 atmosphere allows catalysis to restart, indicating that the effect of exogenous H_2 on the catalyst is reversible. This does not occur for the cationic system, with H_2 keeping the catalyst in the less active Rh(III) manifold.

In an attempt to probe how hydrogen inhibits dehydrocoupling for this system a 1,2-$C_6H_4F_2$ solution of $Rh(H)_2(PCy_3)_2Cl$ was placed under 4 atm of H_2. Jensen and co-workers have reported the η^2 coordination of dihydrogen when the iridium analogues $Ir(H)_2(PR_3)_2Cl$ (R = ^{i}Pr, Cy, ^{t}Bu) are placed under an atmosphere of H_2, generating $Ir(H)_2(PR_3)_2Cl(\eta^2\text{-}H_2)$.[21, 22] To the best of our knowledge, the Rh congeners have not been reported. For $Ir(H)_2(P^{i}Pr_3)_2Cl(\eta^2\text{-}H_2)$, the ^{1}H NMR spectrum shows a broad singlet at ~ δ -17 ppm, which sharpens and shifts upfield to δ -33.0 ppm upon removal of the hydrogen atmosphere, indicative of a dynamic equilibrium. However, for our system, no change in chemical shift or broadening was observed for the hydridic resonance at δ -22.86 ppm upon addition of 4 atm of hydrogen, implying that coordination of H_2 does not occur to $Rh(H)_2(PCy_3)_2Cl$. Therefore, we propose that the hydrogen atmosphere in a closed system inhibits H_2 loss (or turnover) from a species on the catalytic cycle after the addition of **A**.

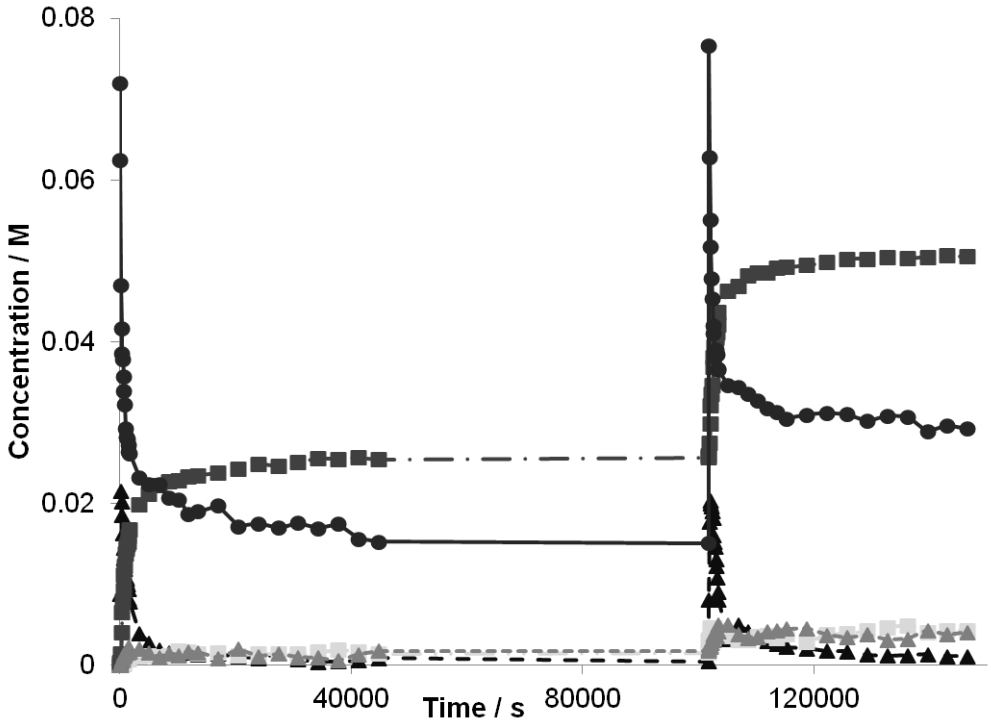


Figure 4.8 Plot of ^{11}B concentration for the dehydrocoupling of $H_3B{\cdot}NMe_2H$ (initial concentration = 0.072 M) using $Rh(H)_2(PCy_3)_2Cl$ (2 mol%) in a sealed high pressure NMR tube. Additional $H_3B{\cdot}NMe_2H$ added after 101840 seconds. ●, $H_3B{\cdot}NMe_2H$ (**A**); ▲, $H_3B{\cdot}NMe_2BH_2{\cdot}NMe_2H$ (**B**); ■, $[H_2BNMe_2]_2$ (**C**); ▲, $H_2B{=}NMe_2$ (**Z**); ■, $HB(NMe_2)_2$.

A significantly lower concentration of **B** is observed in the sealed system *versus* that in an open system (Figure 4.5), although the concentration of amino-borane **Z** in both is comparable. **B** could be formed by the combination of 2 **A** at a metal centre with the concomitant loss of H_2 as for $[TiCp_2]$ systems[23] or from the metal mediated combination of **A** and **Z**.[24, 25] Both of these require the approach of a second molecule of amine-borane (or amino-borane) to the metal centre presumably as a sigma complex. Under an atmosphere of hydrogen (closed system), it is possible that this approach is prevented by the coordination of dihydrogen which blocks the vacant site, preventing the formation of **B**.

4.3.1.2 Catalytic dehydrocoupling of $H_3B{\cdot}NMe_2BH_2{\cdot}NMe_2H$ (B)

As mentioned in Chapter 3, the intermediate linear diborazane **B**, which has previously been observed as an intermediate during the dehydrocoupling of **A** with other catalyst systems,[19, 23, 24, 26-29] can be independently synthesised.[26] As **B** was observed during the dehydrocoupling of **A** catalysed by $Rh(H)_2(PCy_3)_2Cl$ (Figure 4.5), we tested the ability of $Rh(H)_2(PCy_3)_2Cl$ to catalyse the dehydrocoupling of **B**. In a closed system ($[\mathbf{A}]_0$ = 0.072 M, 298 K, 1,2-$C_6H_4F_2$) $Rh(H)_2(PCy_3)_2Cl$ (4 mol% *i.e.* 2 mol% with respect to B-N units) catalyses the dehydrocoupling of **B**, with significant quantities of the amino-borane **Z** observed resulting from the B-N bond cleavage[24] of **C** (Figure 4.9). Very little **A** is detected by ^{11}B NMR spectroscopy; presumably it is dehydrogenated rapidly on formation. As well as B-N bond cleavage, **B** could also be consumed by dehydrocyclisation,[23] however we have not investigated this possibility, and the observation of significant quantities of **A** and **Z** mitigate against this.

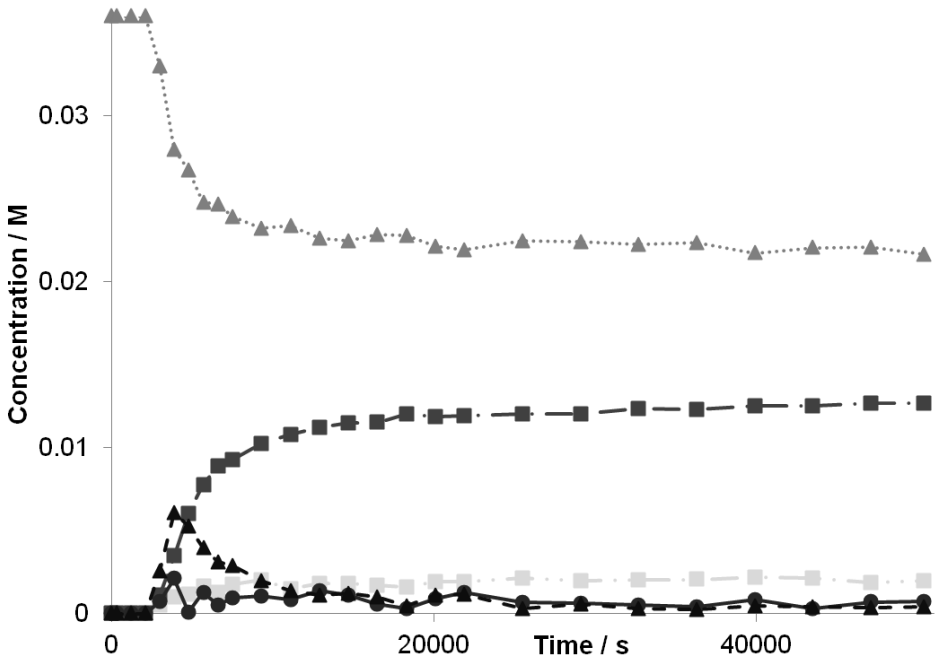


Figure 4.9 Plot of ^{11}B concentration for the dehydrocoupling of $H_3B{\cdot}NMe_2BH_2{\cdot}NMe_2H$ (initial concentration = 0.036 M) using $Rh(H)_2(PCy_3)_2Cl$ (2 mol% with respect to B-N units) in a sealed high pressure NMR tube. ●, $H_3B{\cdot}NMe_2H$ (**A**); ▲, $H_3B{\cdot}NMe_2BH_2{\cdot}NMe_2H$ (**B**); ■, $[H_2BNMe_2]_2$ (**C**); ▲, $H_2B{=}NMe_2$ (**Z**); ■, $HB(NMe_2)_2$.

Interestingly, dehydrocoupling only occurs after an induction period of 50 minutes. The origin of this induction period has not been investigated, but we speculate that it might arise from the slow generation of the active species. As we demonstrate later the active species is a monomer that is in equilibrium with an inactive dimer. The added steric bulk of **B** *versus* **A** may prevent **B** interacting with the dimer, resulting in slower formation of the active species. Consistent with this, as we show later, $Rh(H)_2(PCy_3)_2Cl$ does not undergo reversible B-H activation with the more sterically bulky TMAB. A similar induction period is observed under stoichiometric conditions.

4.3.1.3 Initial rates

Given the potentially complex nature of the overall kinetics, we chose to investigate the mechanism of dehydrocoupling using initial rates,[30] combined with isotopic labelling to determine the order of the reaction in **A** and $Rh(H)_2(PCy_3)_2Cl$, and also the

rate limiting process. Initial rate experiments were conducted in a sealed high pressure NMR tube under our standard conditions (298 K, 1,2-$C_6H_4F_2$). Catalysis was monitored by ^{11}B NMR spectroscopy and revealed **A** to be consumed, **B** and **Z** were observed as intermediates and **C** accumulated as the final product. The ^{11}B NMR data were subsequently integrated and the data from the first 180 seconds of catalysis were fitted to a pseudo zero order region of **A** consumption. A sample plot, using 2 mol% $Rh(H)_2(PCy_3)_2Cl$ with $[\mathbf{A}]_0$ = 0.072 M is shown in Figure 4.10.

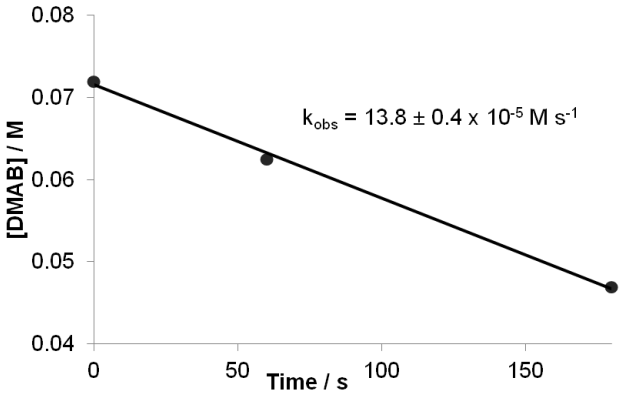


Figure 4.10 Sample initial rate plot for the dehydrocoupling of **A** (initial concentration = 0.072 M) using $Rh(H)_2(PCy_3)_2Cl$ (2 mol%) in 1,2-$C_6H_4F_2$ in a closed system.

These initial rate experiments were conducted at several different concentrations of [**A**] (Entries 1 – 3) and [Rh] (Entries 1, 4 and 5), and with varying levels of deuteration in **A** (Entries 6 – 8), generating the data shown in Table 4.1. Entry 9 contained exogenous **C** to test for the possibility of autocatalysis, as observed for the cationic system in Chapter 3.

Table 4.1 Initial rates for the dehydrocoupling of **A** using $Rh(H)_2(PCy_3)_2Cl$ in a sealed system (high pressure NMR tube) in 1,2-$C_6H_4F_2$. Catalysis does not go to completion under these conditions. **d_3-A** = $D_3B{\cdot}NMe_2H$, **d_1-A** = $H_3B{\cdot}NMe_2D$, **d_4-A** = $D_3B{\cdot}NMe_2D$. *25 equivalents of exogenous **C** (initial concentration of 0.036 M) added at start. Error given is the intrinsic error.

Entry	[Rh] / M	[A] / M	[d_3-A] / M	[d_1-A] / M	[d_4-A] / M	Initial Rate x 10^{-5}/ M s^{-1}
1	0.00144	0.072	-	-	-	13.8 ± 0.4
2	0.00144	0.036	-	-	-	5.5 ± 0.4
3	0.00144	0.144	-	-	-	26.6 ± 0.4
4	0.00072	0.072	-	-	-	9.9 ± 0.4
5	0.00288	0.072	-	-	-	19.5 ± 0.4
6	0.00144	-	0.072	-	-	11.5 ± 0.4
7	0.00144	-	-	0.072	-	2.6 ± 0.4
8	0.00144	-	-	-	0.072	2.7 ± 0.4
9	0.00144	0.072	-	-	-	14.0 ± 0.4*

Entries 1 – 3 show the reaction to be first order in **A**, which is shown graphically in Figure 4.11 (upper). Entries 1, 4 and 5 indicate that the reaction has a half order dependence on $Rh(H)_2(PCy_3)_2Cl$ (Figure 4.11, lower). The half order dependence on [Rh] indicates the presence of a rapid monomer-dimer equilibrium during catalysis, where the monomeric species is the active catalyst. The dimeric species is strongly favoured but is positioned outside of the catalytic cycle. This observation correlates with an earlier report by Duckett and co-workers, which assigned $Rh(H)_2(PCy_3)_2Cl$ as a chloride bridged dimer in solution on the basis of DOSY experiments, with a similar diffusion coefficient observed for $Rh(H)_2(PCy_3)_2Cl$ as for the known dimer $(PPh_3)_2(H)_2Rh(\mu\text{-}Cl)_2Rh(PPh_3)_2$.[31] The related species, $Rh(H)_2(P^iPr_3)_2Cl$, is monomeric in the solid-state, but this does not eliminate the possibility of a dimeric formulation in solution.[4] Monomer-dimer equilibria and a half order dependence on catalyst have

previously been reported for a variety of catalytic processes. These include Pd-catalysed reactions such as: arylation of alkenes,[32] hydrolysis of methylparathion[33] and Heck coupling reactions.[34] The kinetics by which Shvo's catalyst (**i-125**) catalyses hydrogen transfer reactions[35, 36] and notably the dehydrogenation of amine-boranes[37] has additionally been investigated and found to have such an order dependence. As mentioned previously, $Rh(H)_2(PCy_3)_2Cl$ does not lose H_2 under vacuum[1] and in line with this we see no evidence for the formation of mixed valence dimers such as $(PR_3)_2(H)_2Rh(\mu\text{-}Cl)_2Rh(PR_3)_2$. Such dimers have previously been reported to exist in an equilibrium with the Rh(I) chloride bridged dimers *via* loss of H_2 (R = Phephos, *p*-tolyl)[38, 39] (Phephos = 1,2-*bis*(diphenylphosphino)-1-phenylethane).[40]

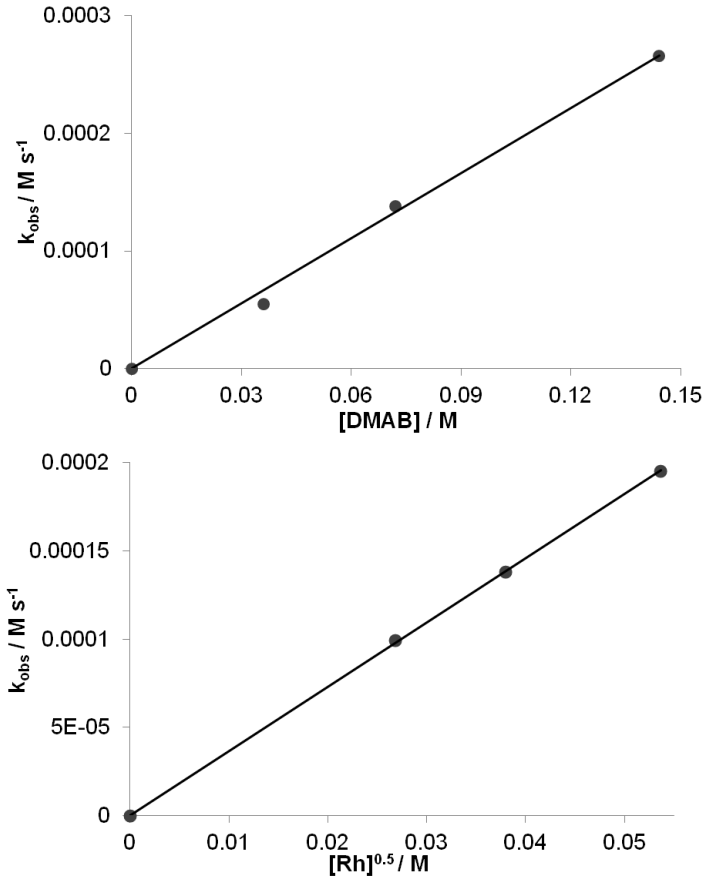
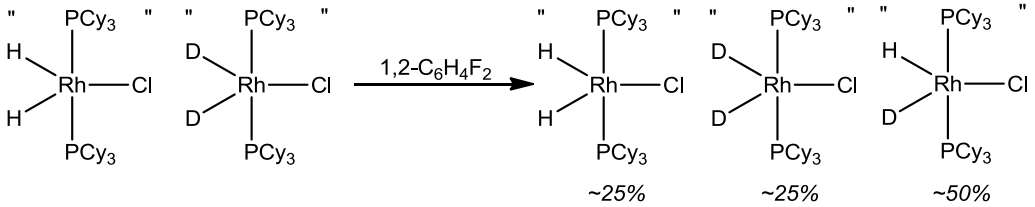


Figure 4.11 Plot of initial rate *versus* concentration for [DMAB] (upper) and $[Rh]^{0.5}$ (lower).

A half order dependence on the catalyst can also arise from ligand dissociation.[41] We suggest that this is unlikely to be the case for this system, as no evidence is observed for the dissociation of tricyclohexylphosphine *i.e.* no free PCy_3 is seen by $^{31}P\{^1H\}$ NMR spectroscopy. H_2 loss is another possibility, however this can be eliminated due to the need for ligand dissociation to be a reversible process: H_2 loss does not appear to occur, and if it did H_2 would be irreversibly lost to the headspace of the NMR tube due to its low solubility in 1,2-$C_6H_4F_2$.

Additional evidence for the formation of a dimer of $Rh(H)_2(PCy_3)_2Cl$ in solution comes from the reaction of $Rh(H)_2(PCy_3)_2Cl$ with $Rh(D)_2(PCy_3)_2Cl$[42] (Scheme 4.5). Analysis by $^{31}P\{^1H\}$ NMR spectroscopy revealed the formation of a third species, with a chemical shift intermittent between that of the starting materials [δ 51.1 ppm (d, $^1J_{RhP}$ = 116 Hz, $Rh(H)_2(PCy_3)_2Cl$); δ 51.2 ppm (d, $^1J_{RhP}$ = 117 Hz, new species); δ 51.3 ppm (d, $^1J_{RhP}$ = 117 Hz, $Rh(D)_2(PCy_3)_2Cl$)] (Figure 4.12, left). After 48 hours at room temperature, equilibrium is reached, with ~25% of each of the starting materials and ~50% of the new species.



Scheme 4.5 Reaction of $Rh(H)_2(PCy_3)_2Cl$ and $Rh(D)_2(PCy_3)_2Cl$ in 1,2-$C_6H_4F_2$. " " denotes likely dimeric formulation in solution.

We assign this new species as $RhHD(PCy_3)_2Cl$. In line with this assignment, two overlapping rhodium hydride signals are observed in the ^1H NMR spectrum at ~δ -23 ppm (Figure 4.12, right), at a chemical shift consistent with Rh-H species rather than a Rh-H-Rh species (*e.g.* a resonance for the bridging hydride in $[(PPh_3)_2Rh(H)(\mu\text{-}H)(\mu\text{-}$

$Cl(H)Rh(PPh_3)_2]^+$ is observed at δ -11 ppm).[43] Decoupling ^{31}P resolves the signals into two separate doublets [δ -22.86 ppm (d, $^1J_{RhH}$ = 27.7 Hz, $Rh(H)_2(PCy_3)_2Cl$); δ -22.96 ppm (d, $^1J_{RhH}$ = 27.7 Hz, $RhHD(PCy_3)_2Cl$)]. The relative integrals of these two species is *ca.* 1:1, which is consistent with their formulation as Rh-HD and Rh-$(H)_2$ species and their expected statistical distribution on reaching equilibrium (50% and 25% respectively). Two signals should also be present in the ^2H NMR spectrum, however only one very broad signal is observed. Although it is assumed that the dimeric form of $Rh(H)_2(PCy_3)_2Cl$ would be halide-bridged, the above reaction indicates that a H-bridged form is also accessible, which allows for H/D exchange, but in a low concentration as no evidence is observed for a bridging hydride. It should also be noted here that while the starting materials and products are likely dimeric, we draw them in monomeric form for simplicity, and consistency with the rest of this chapter.

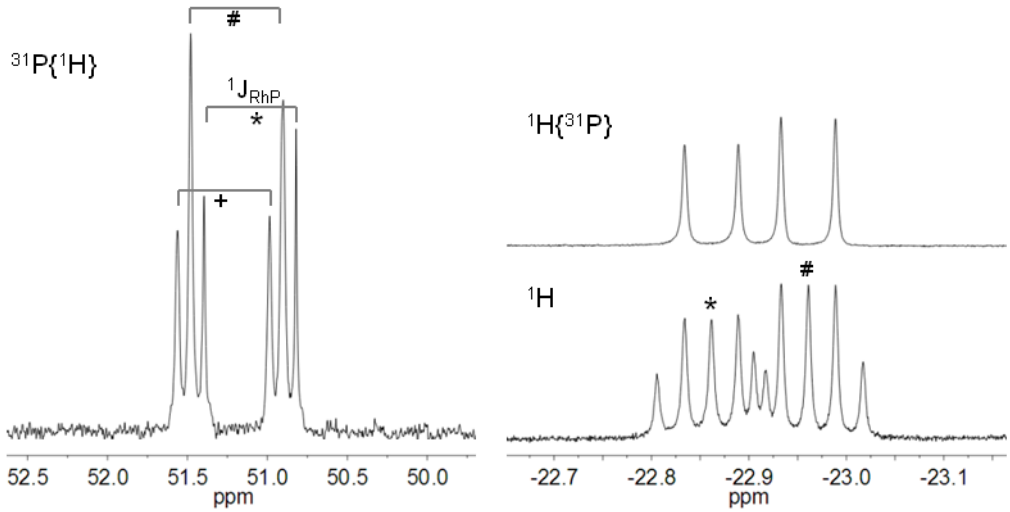


Figure 4.12 $^{31}P\{^1H\}$ and hydridic region of ^1H and $^1H\{^{31}P\}$ NMR spectra of the reaction between $Rh(H)_2(PCy_3)_2Cl$ and $Rh(D)_2(PCy_3)_2Cl$. * = $Rh(H)_2(PCy_3)_2Cl$, # = $RhHD(PCy_3)_2Cl$, + = $Rh(D)_2(PCy_3)_2Cl$.

The observation of separate rhodium hydride signals in the ^1H NMR spectrum for $Rh(H)_2(PCy_3)_2Cl$ and $RhHD(PCy_3)_2Cl$ is a result of isotopic perturbation of resonance. Secondary deuterium isotope effects also result in changes in the chemical shift in the

phosphorus NMR data (left, Figure 4.12), as observed for **2-8** in Chapter 2.[44] The difference in chemical shift of 0.08 ppm between the isotopologues in the $^{31}P\{^{1}H\}$ NMR spectrum is in line with those previously observed for **2-8** (0.14 ppm) and other reported systems.[44-46]

Having determined the order of the reaction in both Rh and **A**, we utilised isotopic labelling to identify the rate limiting process. Entries 6, 7 and 8 in Table 4.1 show the initial rates for deuteration in different positions of **A**, with the calculated kinetic isotope effects shown in Table 4.2. The use of $H_3B{\cdot}NMe_2D$ (**d_1-A**) shows a strong primary KIE (5.3 ± 1.2), indicating that irreversible N-H transfer is involved in the rate limiting process. A similar KIE was calculated for the dehydrocoupling of amine-boranes by a [$TiCp_2$] system.[23] For $D_3B{\cdot}NMe_2H$ (**d_3-A**), a much smaller KIE of 1.2 ± 0.1 is observed indicating that irreversible B-H activation is not involved in the rate determining step. A KIE of 5.1 ± 1.2 when $D_3B{\cdot}NMe_2D$ (**d_4-A**) is used is consistent with the values obtained for isotopic labelling of the hydrogen atoms at either the boron or nitrogen position.

Table 4.2 Kinetic isotope effects for the dehydrocoupling of $H_3B{\cdot}NMe_2H$ (initial concentration = 0.072 M) using $Rh(H)_2(PCy_3)_2Cl$ (2 mol%).

	k_H/k_D
d_1-A	5.3 ± 1.2
d_3-A	1.2 ± 0.1
d_4-A	5.1 ± 1.2

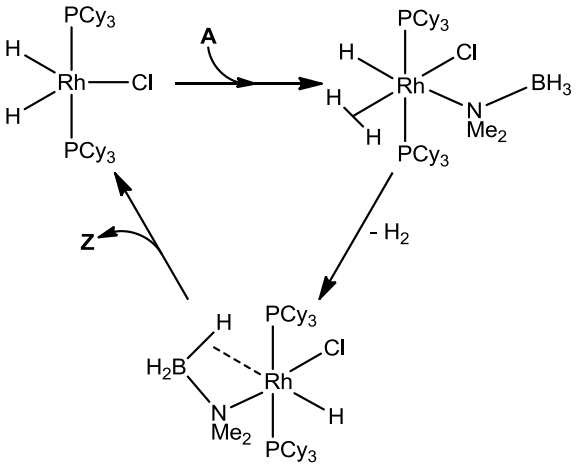
In an attempt to probe inhibition by hydrogen we repeated Entry 1 (Table 4.1) under an atmosphere of hydrogen. However, there was no significant difference in the initial rates, or conversion (both reached ~70% conversion of **A**). We attribute this to the

low solubility of H_2 in 1,2-$C_6H_4F_2$.[47] As such, hydrogen will only act as a modifier in catalysis at low [**A**], potentially through the formation of a sigma H_2 complex. We discuss this in more detail in Section 4.3.2.

The addition of 25 equivalents of exogenous **C** (Entry 9, Table 4.1) resulted in no change in the initial rate [(14.0 ± 0.4) x 10^{-5} M s^{-1} *c.f.* Entry 1 (13.8 ± 0.4) x 10^{-5} M s^{-1}]. This contrasts the cationic system for which **C** acted in an autocatalytic role, promoting the reductive elimination of dihydrogen from Rh(III) dihydride species to return to the more active Rh(I) species. Stoichiometric reactions of $Rh(H)_2(PCy_3)_2Cl$ with **C** confirmed this lack of reaction.

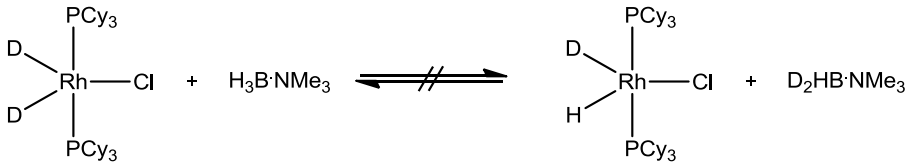
4.3.1.4 Probing B-H and N-H activation

Having determined the order of the reaction in **A** and catalyst, and in order to provide further insight into the mechanism, we next turned our attention to determining the relative order of B-H and N-H activation. N-H activation in cationic M(III)-dihydride systems has been calculated to be rate determining, which H/D exchange experiments support.[25, 28] We initially postulated that the neutral system may have a lower barrier to N-H activation, due the protic nature of H atom on the nitrogen, $N^{\delta-}$-$H^{\delta+}$, and could potentially occur first *via* protonation of the metal hydride (Scheme 4.6). This could then be followed β-H B-H elimination to release the amino-borane **Z** and regenerate the catalyst. This mechanism would be related to that discussed for neutral d^0 main group systems (Scheme 1.53).[48, 49]



Scheme 4.6 Potential mechanism for the dehydrogenation of **A** catalysed by $Rh(H)_2(PCy_3)_2Cl$, where N-H activation precedes B-H transfer.

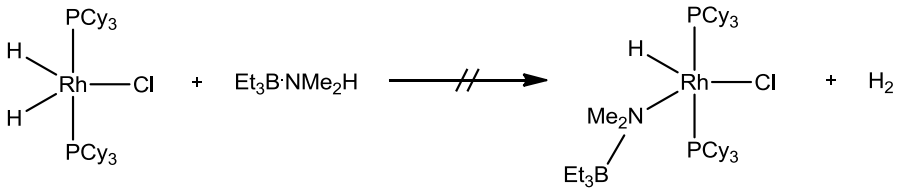
As discussed in Chapter 2, TMAB is a model amine-borane which can be used to study how an amine-borane interacts/coordinates to a catalyst. The addition of TMAB to $Rh(H)_2(PCy_3)_2Cl$ resulted in no reaction by NMR spectroscopy. This contrasts the cationic $\{Rh(H)_2(PR_3)_2L_n\}^+$ systems, which form σ-complexes with TMAB through 3-centre 2-electron Rh-H-B interactions.[18, 19, 28] To test if reversible B-H activation was happening, TMAB was added to $Rh(D)_2(PCy_3)_2Cl$ and the reaction monitored for signs of B-D and Rh-H by ^2H and ^1H NMR spectroscopy respectively. No H/D exchange was observed over the timescale of catalysis (1 hour, Scheme 4.7). For other related cationic systems,[50, 51] reversible B-H activation does occur, with exchange postulated to occur *via* a B-H/M-H σ-CAM process[52] that invokes a boryl intermediate. Although the lack of reactivity might suggest that reversible B-H activation does not occur during catalysis, it cannot definitively be ruled out as TMAB is not a perfect model for DMAB due the added steric bulk resulting from the additional N-methyl group.



Scheme 4.7 Possible reaction between TMAB and $Rh(D)_2(PCy_3)_2Cl$ resulting in incorporation of deuterium into TMAB through reversible B-H activation.

Likewise, no reactivity was observed between $Rh(H)_2(PCy_3)_2Cl$ (or $Rh(D)_2(PCy_3)_2Cl$) and the final product, the dimeric amino-borane **C**. Specifically, reductive elimination of dihydrogen to reform $[Rh(PCy_3)_2Cl]_2$ was not promoted. This supports the conclusions drawn from the initial rate calculated when exogenous **C** was present, which ruled out an autocatalytic rule for **C**, as had been observed for the cationic system in Chapter 3.

To probe the possibility of initial N-H activation, we synthesised the amine-borane, $Et_3B{\cdot}NMe_2H$,[53] which, due to the lack of B-H, cannot undergo dehydrogenation and therefore, like TMAB, could be considered to be a model amine-borane. Treatment of $Rh(H)_2(PCy_3)_2Cl$ with a solution of $Et_3B{\cdot}NMe_2H$ in 1,2-$C_6H_4F_2$ resulted in no reaction, and no observation of an amido-borane species by NMR spectroscopy (Scheme 4.8). However as for TMAB, $Et_3B{\cdot}NMe_2H$ is not a perfect model due to the added steric bulk resulting from the ethyl groups. The synthesis of the less bulky $Me_3B{\cdot}NMe_2H$ was not attempted due to the prohibitive cost of trimethylboron.[54] Reactivity studies with model amine-boranes were not conducted with the Wilkinson's complex analogue reported by Manners and co-workers.[2]



Scheme 4.8 Potential reactivity between $Rh(H)_2(PCy_3)_2Cl$ and $Et_3B{\cdot}NMe_2H$ to probe N-H activation.

As the above reactions did not provide definitive insight into the order and reversibility of B-H and N-H activation, we devised an alternative experiment. The dehydrocoupling of $D_3B{\cdot}NMe_2D$ (**d_4-A**) catalysed by $Rh(H)_2(PCy_3)_2Cl$ under *ca.* 4 atm of hydrogen was monitored by ^1H and ^{11}B NMR spectroscopy for signals corresponding to B-H or N-H, which would indicate reversible B-H(D) or N-H(D) activation processes respectively. Reversible B-D activation *via* a σ-CAM process would involve the formation of a boryl species, which could undergo exchange with exogenous H_2 (Figure 4.13, left) resulting in incorporation of H into BD_3 and the observation of B-H coupling in the ^{11}B NMR spectrum. Conversely, reversible N-D activation *via* protonation of a metal hydride would involve the formation of an amido deuteride species, which could undergo exchange with exogenous H_2 (Figure 4.13, right) leading to incorporation of H into the N-D position and the observation of N-H in the ^1H NMR spectrum.

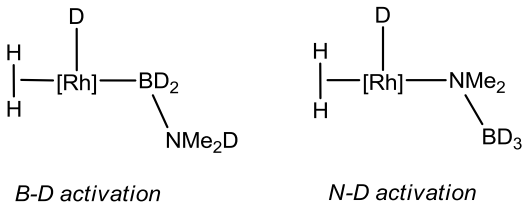
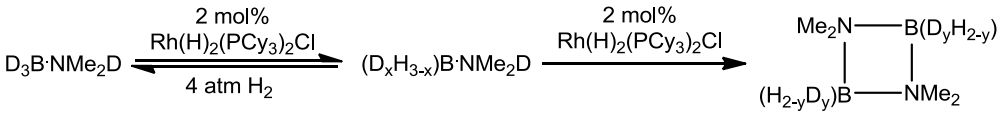


Figure 4.13 Potential B-D or N-D activation of **d_4-A** at $Rh(H)_2(PCy_3)_2Cl$ and exchange with exogenous H_2. [Rh] = $Rh(PCy_3)_2Cl$.

To the detection limits of ^1H NMR spectroscopy, no N-H was observed during dehydrocoupling, indicating that N-H activation is not reversible for this catalyst

system as indicated by initial rate KIE experiments. However, the formation of HD [δ 4.56 ppm, (t, $^{1}J_{HD}$ = 43 Hz)] was observed in the ^{1}H NMR spectra. In the ^{11}B NMR spectrum B-H coupling was evident in the amine-borane starting material signalling the formation of $(D_xH_{3-x})B{\cdot}NMe_2D$ (Scheme 4.9 and Figure 4.14). B-H coupling was also seen in the final product, $[(H_{2-y}D_yBNMe_2)]_2$. The blank reaction of **d_4-A** in 1,2-$C_6H_4F_2$ under 4 atm H_2 resulted in no H/D exchange at boron or nitrogen.



Scheme 4.9 Dehydrocoupling of **d_4-A** catalysed by $Rh(H)_2(PCy_3)_2Cl$ under 4 atm of dihydrogen provided evidence for rapid and reversible B-H activation.

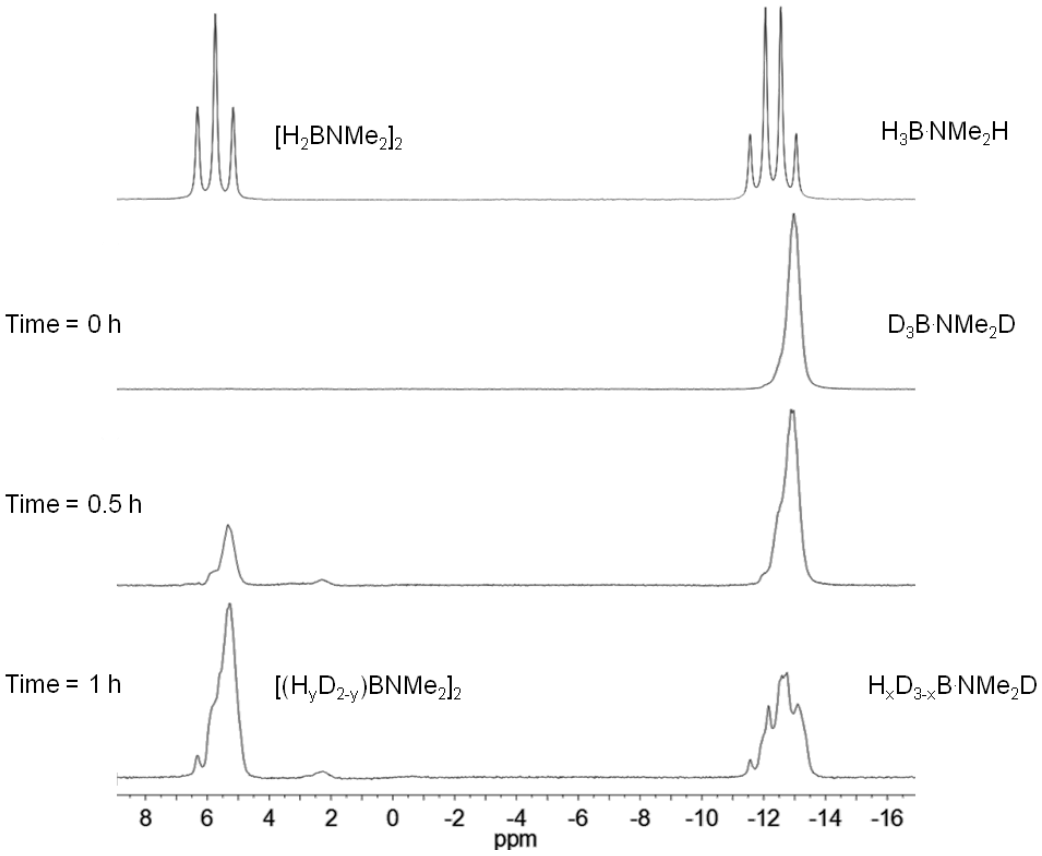


Figure 4.14 ^{11}B NMR spectra at various time intervals for the reaction between **d_4-A** and $Rh(H)_2(PCy_3)_2Cl$ (2 mol%) under *ca.* 4 atm of H_2. Top spectrum shows $H_3B{\cdot}NMe_2H$ and $[H_2BNMe_2]_2$.

The observation of B-H coupling and the formation of HD indicated that B-H activation of **A** is reversible and rapid in comparison to irreversible dehydrogenation. The observation of B-H coupling in free **A**, but not H/D exchange at nitrogen, reveals that, for this system, B-H activation must precede N-H activation in one of the possible cycles. A similar observation was made for the dehydrocoupling of **A** by Chirik and co-workers for the dimeric *bis*(cyclopentadienyl) titanium dinitrogen complexes under a deuterium atmosphere.[55] However, for the titanium system the possibility of incorporation of D into N-H could not be eliminated due to peak overlap with the protio isotopologue. From this data, the possibilty of a second cycle involving irreversible N-H activation followed by β-H B-H elimination cannot be discounted.

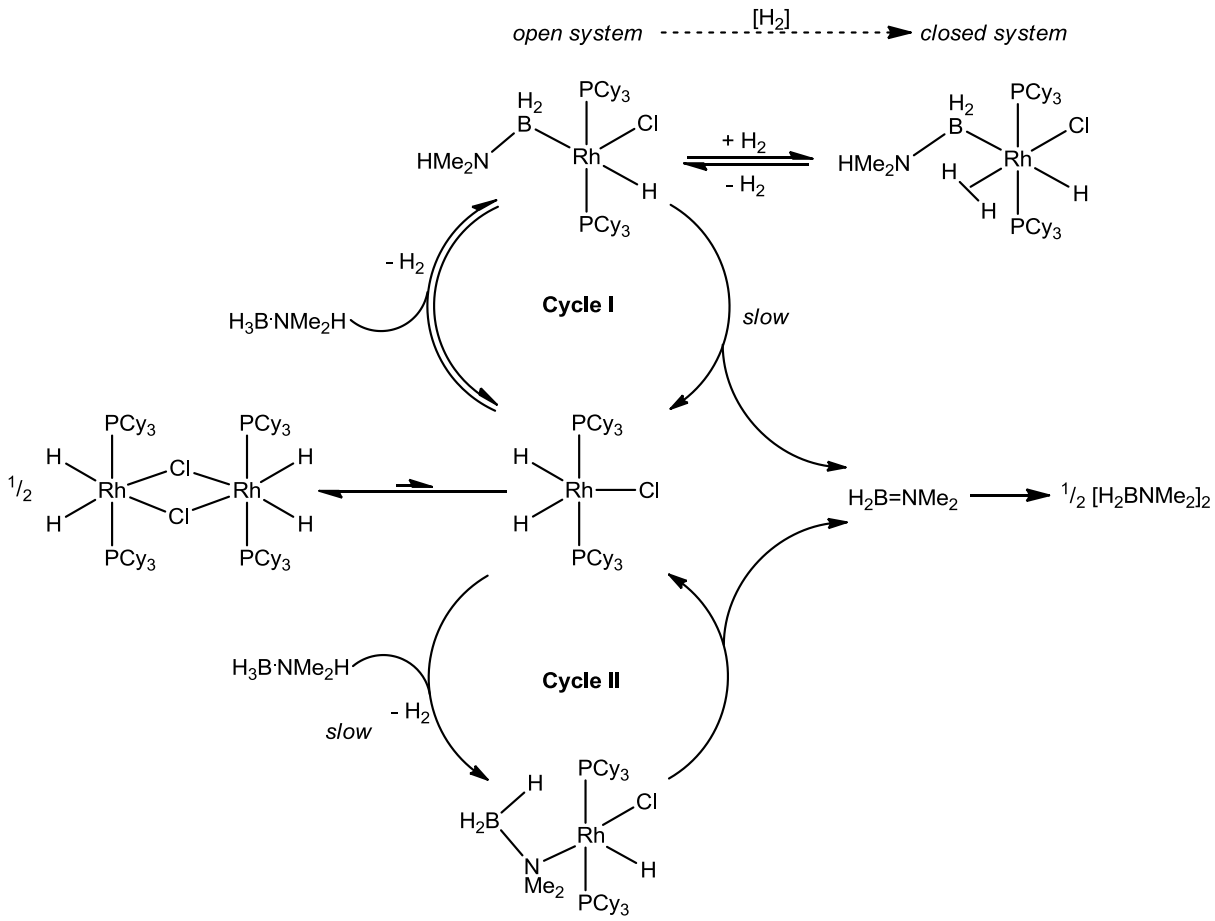
Although the above result indicates that TMAB might be expected to undergo reversible B-H activation at $Rh(H)_2(PCy_3)_2Cl$, the lack of reactivity could be attributed to the added steric bulk of TMAB *versus* **A**, as also suggested in the early phases of reaction with **B** (Section 4.3.1.1). An additional contributing factor could be TMAB's inability to form N-H···Cl-Rh interactions, which may remove a lower energy pathway for the approach of the amine-borane to rhodium resulting in a larger energy barrier to B-H activation. Such interactions have been proposed in related ruthenium *bis*(trimethylsilyl)amino complexes for the dehydrogenation of ammonia-borane.[56]

4.3.2 Proposed catalytic cycle

The above observations have led us to propose the catalytic cycle shown in Scheme 4.10 for the dehydrogenation of **A** as catalysed by $Rh(H)_2(PCy_3)_2Cl$. There exists a rapid monomer-dimer equilibrium for the catalyst, which strongly favours the inactive dimeric species, $[Rh(H)_2(PCy_3)_2(\mu\text{-}Cl)]_2$ which is positioned outside of the catalytic cycle. The active monomer, $Rh(H)_2(PCy_3)_2Cl$, can then undergo either

reversible B-H activation with **A** (Cycle I) or irreversible N-H activation (Cycle II). B-H activation in Cycle I presumably occurs *via* a constant oxidation state σ-CAM type process[52] as both B-H activation to form a Rh(V) species and H_2 loss from $Rh(H)_2(PCy_3)_2Cl$ to form a Rh(I) species prior to B-H activation are considered unlikely.[1] Related to this, H/D exchange at $Rh(H)_2(PCy_3)_2Cl$ to form $Rh(D)_2(PCy_3)_2Cl$ is postulated to proceed *via* a sigma bound intermediate such $Rh(H)_2(PCy_3)_2Cl(\eta^2\text{-}D_2)$, which then undergoes a σ-CAM exchange process. The boryl intermediate resulting from B-H activation then undergoes an irreversible N-H β-H transfer in the rate determining step for Cycle I to eliminate **Z** and regenerate the active catalyst. This captures the significant KIE associated with NH/ND while the small KIE associated with BH/BD is presumably the result of an equilibrium isotope effect. Cycle II proceeds *via* irreversible N-H activation (protonation) to generate an amido-borane intermediate, followed by β-H B-H elimination to generate **Z**. The small KIE observed for BH/BD could be due to a secondary isotope effect or B-H activation becoming synchronous with N-H activation. As mentioned previously, although the experimental data provides strong evidence for the occurrence of Cycle I, it does not allow us to discount the presence of Cycle II.

The proposed mechanism is similar to the constant oxidation state Rh(III) manifold suggested for the cationic catalyst in Chapter 3.[20] The related iridium system, $\{Ir(H)_2(PCy_3)_2L_n\}^+$ has also been proposed to operate in a constant oxidation state mechanism, with B-H activation preceding N-H transfer.[25] There are also similarities to the mechanism suggested by Chirik and co-workers for titanium sandwich complexes, with the main difference the change in oxidation state proposed for Ti.[55] Mechanisms proposed for Cr[57] and main-group systems[49] are also broadly similar.



Scheme 4.10 Suggested mechanism for the dehydrogenation of **A** to form the amino-borane, **Z**, catalysed by $Rh(H)_2(PCy_3)_2Cl$.

The proposed model also allows for H_2 inhibition in a closed system. Under high [H_2] (closed system), H_2 could coordinate to the boryl intermediate in Cycle I, attenuating the rate of the subsequent β-H N-H transfer. In an open system, under a low flow of argon, H_2 would be unlikely to coordinate allowing onward reactivity. The mechanism does not include the formation or consumption of the intermediate **B**, which has not been investigated in detail.

4.4 Neutral rhodium(I) complex

Having investigated the mechanism by which $Rh(H)_2(PCy_3)_2Cl$ catalyses the dehydrogenation of **A**, we next turned out attention to the reactivity of the neutral rhodium(I) complex, $[Rh(PCy_3)_2Cl]_2$, with amine-boranes.

4.4.1 Catalysis

The dehydrocoupling of **A** catalysed by $[Rh(PCy_3)_2Cl]_2$ could be anticipated to ultimately show the same reactivity as when $Rh(H)_2(PCy_3)_2Cl$ is the catalyst, as $[Rh(PCy_3)_2Cl]_2$ rapidly adds H_2 to generate $Rh(H)_2(PCy_3)_2Cl$, which does not lose hydrogen easily.[1] As expected, under our standard conditions ($[\mathbf{A}]_0$ = 0.072 M, 1,2-$C_6H_4F_2$, 298 K, open to a low flow of argon) $[Rh(PCy_3)_2Cl]_2$ (1 mol%, but effectively 2 mol% Rh) is a competent catalyst for the dehydrocoupling of **A** to ultimately afford **C** as the final product and 95% conversion was achieved after 100 minutes (TON = 47.5) (*viz*. TON of 47.5 for $Rh(H)_2(PCy_3)_2Cl$). The concentrations of the ^{11}B containing species were monitored by ^{11}B NMR spectroscopy. Subsequent integration generated the time-concentration plot in Figure 4.15. A significant concentration of the intermediate amino-borane **Z** was observed, along with the intermediate linear diborazane **B**.

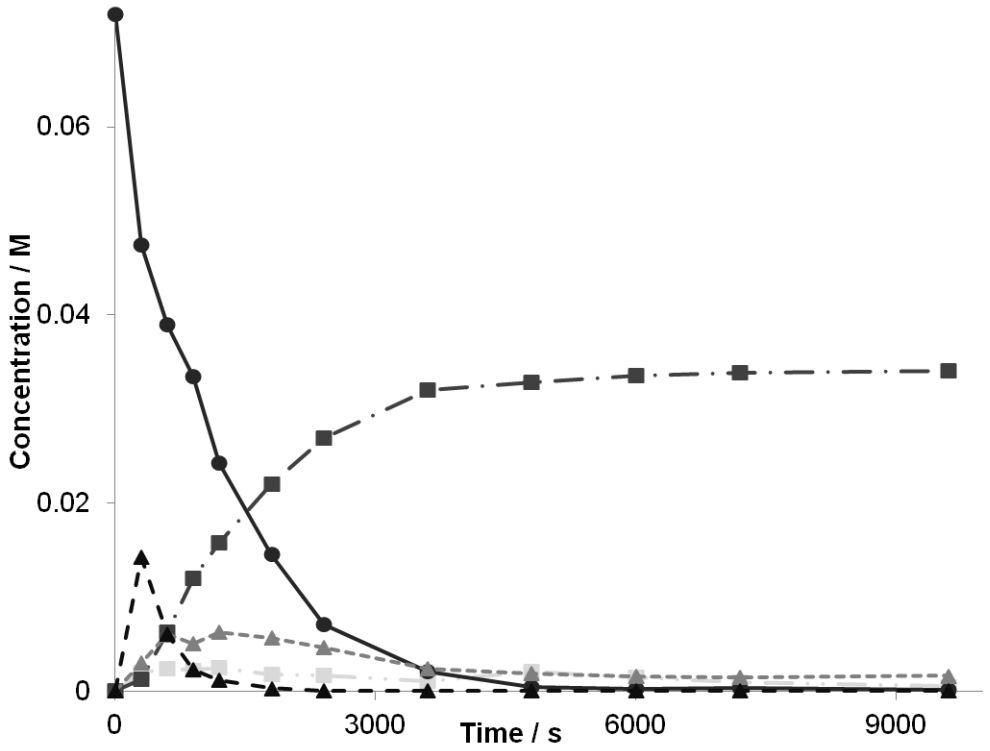


Figure 4.15 Plot of ^{11}B concentration for the dehydrocoupling of $H_3B{\cdot}NMe_2H$ (initial concentration = 0.072 M) using $[Rh(PCy_3)_2Cl]_2$ (2 mol%). 0.1 mL aliquots diluted with 1,2-$C_6H_4F_2$ (0.25 mL). ●, $H_3B{\cdot}NMe_2H$ (**A**); ▲, $H_3B{\cdot}NMe_2BH_2{\cdot}NMe_2H$ (**B**); ■, $[H_2BNMe_2]_2$ (**C**); ▲, $H_2B{=}NMe_2$ (**Z**); ■, $HB(NMe_2)_2$.

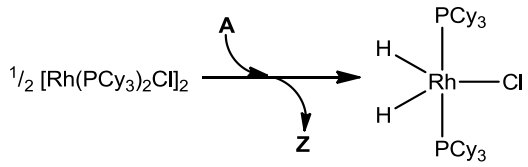
As with $Rh(H)_2(PCy_3)_2Cl$, the consumption of **A** follows pseudo first order kinetics, with a rate constant, k, of (1.05 ± 0.04) x 10^{-3} s^{-1} (*viz*. k = (1.03 ± 0.05) x 10^{-3} s^{-1} for $Rh(H)_2(PCy_3)_2Cl$). This adds further weight to our postulated theory that traces of chloride present in 1,2-$C_6H_4F_2$ in the cationic system, $\{Rh(PCy_3)_2L_n\}^+$ recombine with the cationic catalyst to form $[Rh(PCy_3)_2Cl]_2$, which is then rapidly hydrogenated to form $Rh(H)_2(PCy_3)_2Cl$.[5, 42]

4.4.2 Stoichiometric reactivity

Although stoichiometric reactions of $Rh(H)_2(PCy_3)_2Cl$ with **C** and TMAB showed a lack of reactivity, the more accessible rhodium(I) centre of $[Rh(PCy_3)_2Cl]_2$ might be expected to show different reactivity. As such, we carried out a series of stoichiometric reactions of $[Rh(PCy_3)_2Cl]_2$ with various amine-boranes.

4.4.2.1 Reactivity with $H_3B{\cdot}NMe_2H$ (A)

Initial investigations began with the substrate **A**. Addition of two equivalents of **A** to a 1,2-$C_6H_4F_2$ solution of $[Rh(PCy_3)_2Cl]_2$ forms $Rh(H)_2(PCy_3)_2Cl$ on time of mixing as the sole organometallic complex (^1H and $^{31}P\{^1H\}$ NMR spectroscopy) while significant quantities of the amino-borane **Z** are observed in the ^{11}B NMR spectrum (Scheme 4.11). Subsequent dimerisation of **Z** to form the dimeric amino-borane **C** was seen. A small quantity of **B** was also observed. No other intermediate organometallic species could be observed by NMR spectroscopy for the duration of catalysis. This contrasts the cationic system in Chapter 3 for which Rh(III) σ-complexes of **A** (**3-4-Cy**), and later **Z** (**3-5-Cy**), are seen.



Scheme 4.11 Reactivity of $[Rh(PCy_3)_2Cl]_2$ with $H_3B{\cdot}NMe_2H$.

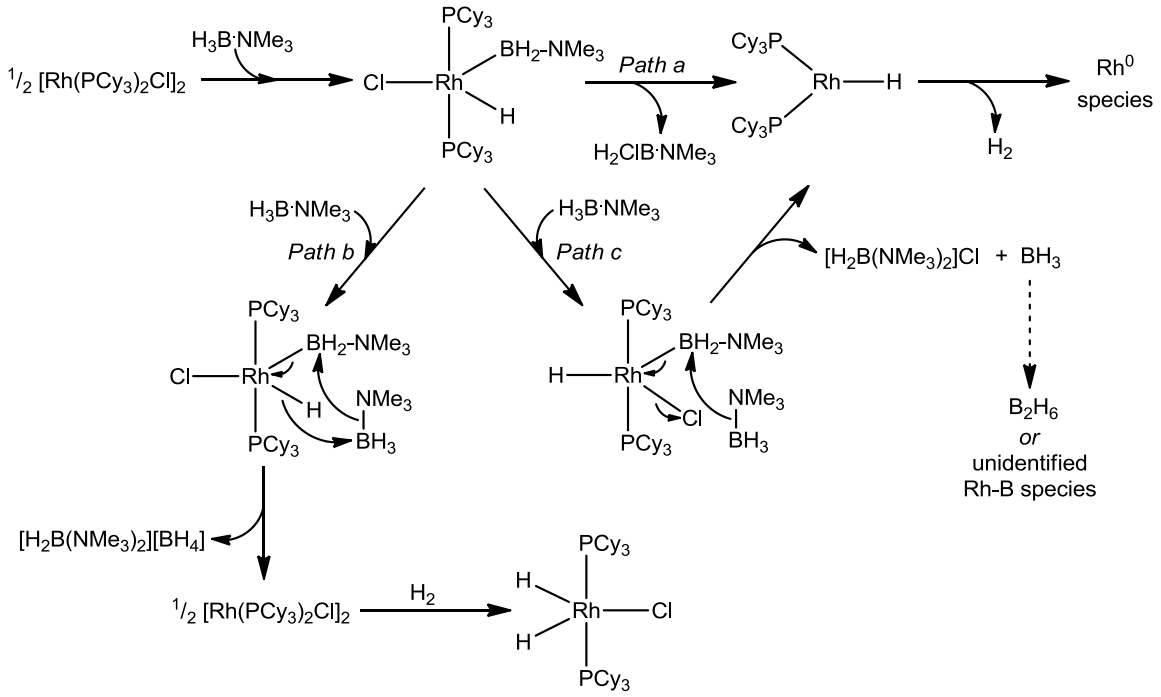
4.4.2.2 Reactivity with TMAB

Next, we investigated the reaction between $[Rh(PCy_3)_2Cl]_2$ and TMAB. Addition of an excess of TMAB to $[Rh(PCy_3)_2Cl]_2$ in 1,2-$C_6H_4F_2$ resulted in a colour change from purple to dark brown, perhaps indicative of the formation of Rh(0) species, over the course of 24 hours. Analysis by $^{31}P\{^1H\}$ NMR spectroscopy revealed the disappearance of $[Rh(PCy_3)_2Cl]_2$ and the formation of $Rh(H)_2(PCy_3)_2Cl$ as the major organometallic product visible by NMR spectroscopy. Two other unidentified species were observed to be present in minor amounts (<10% of $Rh(H)_2(PCy_3)_2Cl$) in the $^{31}P\{^1H\}$ NMR spectrum: δ 33.2 ppm (d, $^1J_{RhP}$ = 108 Hz) and δ 29.9 ppm (br). Besides those resulting from $Rh(H)_2(PCy_3)_2Cl$, two new signals were observed in the hydridic

region of the ^{1}H NMR spectrum: δ -13.33 ppm (m, J = 13.9 Hz,) and δ -20.25 ppm (dd, J = 38.6 and 14.4 Hz), whose relative integrals correlate with the two species observed in the $^{31}P\{^{1}H\}$ NMR spectrum. In the ^{11}B NMR spectrum, the formation of $Me_3N{\cdot}BH_2Cl$ [δ 0.2 ppm (t, $^{1}J_{HB}$ = 122 Hz); lit. -0.5 ppm (t, $^{1}J_{HB}$ = 121 Hz)][58] is observed along with unreacted TMAB. A third species is observed at [δ -4.6 ppm (t, $^{1}J_{HB}$ = 103 Hz, BH_2)], which is suggested to be $[(Me_3N)_2BH_2]^+$ [lit. -2.9 ppm (anion, signal multiplicity and solvent are not given)].[59, 60] A signal at δ -42.8 ppm (m) is assigned to BH_4^-, a possible counterion for $[(Me_3N)_2BH_2]^+$. However the relative ratio of $[(Me_3N)_2BH_2]^+$ to BH_4^- is not 1:1, but *ca.* 3:2. This could be accounted for by the formation of $[(Me_3N)_2BH_2]^+$ with an alternative counterion, Cl^-. The approximate ratio of $[(Me_3N)_2BH_2]^+$ to $Me_3N{\cdot}BH_2Cl$ is 2:1.

We suggest a reaction scheme to account for these observations where TMAB undergoes B-H activation at the Rh(I) centre to generate the boryl intermediate in Scheme 4.12. From here, reductive elimination of the observed $Me_3N{\cdot}BH_2Cl$ can occur to generate $Rh(H)(PCy_3)_2$ (Path a). $Rh(H)(PCy_3)_2$ could react with another equivalent of itself to generate Rh(0) species and hydrogen. The reduction of a Rh(I) species by TMAB has been previously observed; Manners and co-workers noted the formation of colloidal Rh upon the reaction of $[Rh(1,5\text{-}COD)(\mu\text{-}Cl)]_2$ with TMAB with the concomitant formation of $Me_3N{\cdot}BH_2Cl$.[61] No black film is observed for our system, but the dark brown solution could be indicative of the formation of Rh(0) species. Alternatively this boryl intermediate could react with a second equivalent of TMAB (Path b) and undergo a rearrangement as shown in Scheme 4.12 to produce $[(Me_3N)_2BH_2][BH_4]$ and regenerate $[Rh(PCy_3)_2Cl]_2$. A third option (Path c) also involves the rearrangement of this boryl intermediate with a second equivalent of

TMAB, but in contrast to Path b, $Rh(H)(PCy_3)_2$ is formed (as for Path a) along with $[(Me_3N)_2BH_2]Cl$. An additional BH_3 is unaccounted for by Path c, but it is plausible that this could react with Rh to form a Rh-B species, which would likely be broad and therefore unobservable in small quantities by ^{11}B NMR spectroscopy, or alternatively lost to the headspace of the NMR tube as B_2H_6. The formation of $Rh(H)_2(PCy_3)_2Cl$ as the major organometallic species visible by NMR spectroscopy is proposed to result from the reaction of $[Rh(PCy_3)_2Cl]_2$ with the dihydrogen produced during the reduction of $Rh(H)(PCy_3)_2$.



Scheme 4.12 Proposed reaction of $[Rh(PCy_3)_2Cl]_2$ with TMAB.

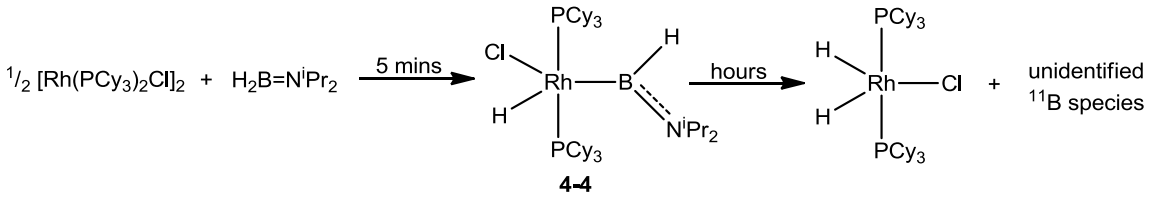
The difference in reactivity of TMAB with $[Rh(PCy_3)_2Cl]_2$ and $Rh(H)_2(PCy_3)_2Cl$ can be attributed to the reduced coordination number of $[Rh(PCy_3)_2Cl]_2$ with the presence of vacant coordination sites allowing facile B-H activation. The reactivity also contrasts that observed for cationic $\{Rh(PR_3)_2L_n\}^+$ systems, which form Rh(I) σ-complexes of the general formula $[Rh(PR_3)_2(\eta^2\text{-}H_3B{\cdot}NMe_3)][BAr^F{}_4]$ (R = ^{i}Bu, ^{i}Pr and Cy) *e.g.* **3-1-Cy**,

which undergo reversible B-H activation.[18-20, 28] Other catalyst systems have also been observed to form σ-complexes with TMAB.[25, 62-64]

4.4.2.3 Reactivity with $H_2B{=}N^iPr_2$

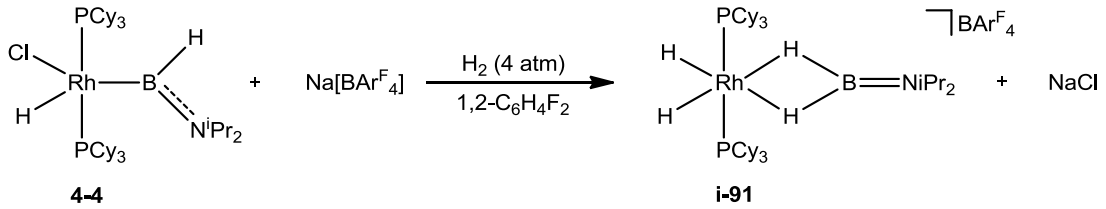
As the reaction with TMAB demonstrated the ability of $[Rh(PCy_3)_2Cl]_2$ to B-H activate amine-boranes, we investigated whether the stable amino-borane $H_2B{=}N^iPr_2$[65] could also undergo B-H activation at the Rh(I) centre to possibly generate a hydrido-boryl species. Aldridge and co-workers have reported precedent for this; addition of an amino-borane, $H_2B{=}NR_2$ (R = ^{i}Pr, Cy), to the electron rich iridium(I) precursor $Ir(PMe_3)_2(COE)Cl$ leads to the formation of the hydrido-boryl species $Ir(PMe_3)_3(H)Cl\{B(H)N^iPr_2\}$ (**i-75**) (Scheme 1.22).[66]

The addition of $H_2B{=}N^iPr_2$ to $[Rh(PCy_3)_2Cl]_2$ led to the formation of a complex that we have identified by spectroscopic methods as the hydridorhodium(hydrido-boryl) complex $Rh(H)(PCy_3)_2Cl\{B(H)N^iPr_2\}$ (**4-4**) (Scheme 4.13). **4-4** was characterised by a combination of NMR spectroscopy and elemental microanalysis. The ^{11}B NMR spectrum of **4-4** shows a broad downfield shifted resonance at δ 50 ppm, similar to that observed for other aminoboryl complexes *e.g.* $Ir(PMe_3)_3(H)Cl\{B(H)N^iPr_2\}$ (**i-75**) (δ 46 ppm),[66] $Rh(H)(IMes)_2\{B(H)NMe_2\}$ (**i-98**) (δ 53 ppm)[67] and $CpFe(CO)_2\{B(Cl)NMe_2\}$ (δ 57 ppm).[68] Key features in the ^{1}H NMR spectrum include an overlapping doublet of triplets at δ -16.22 ppm ($^1J_{RhH}$ = 28.4 Hz, $^2J_{PH}$ = 15.1 Hz) assigned to the rhodium hydride and a broad signal at δ 8.32 ppm, which sharpens in the $^1H\{^{11}B\}$ NMR spectrum and is therefore attributed to the B-H. In **i-75**, a similarly downfield shifted resonance at δ 7.18 ppm is assigned to the terminal B-H. A single phosphorus environment is observed in the $^{31}P\{^1H\}$ NMR spectrum (δ 39.8 ppm) with Rh-P coupling indicative of a Rh(III) centre ($^1J_{RhP}$ = 128 Hz).[69]



Scheme 4.13 Reaction between $[Rh(PCy_3)_2Cl]_2$ and $H_2B{=}N^iPr_2$ to form the boryl **4-4** and its onward reactivity to generate $Rh(H)_2(PCy_3)_2Cl$.

In solution, **4-4** is unstable, forming $Rh(H)_2(PCy_3)_2Cl$ with time (hours) and an unidentified boron containing species ($\delta^{11}B$ 27.1 ppm). The cause of this instability has not been determined, although the presence of trace H_2O in the solvents is a possibility, yet it has prevented, in various solvents, the characterisation of **4-4** by X-ray crystallography. Further characterisation data for **4-4** was obtained by the addition of $Na[BAr^F{}_4]$ to a 1,2-$C_6H_4F_2$ solution of **4-4** under a hydrogen atmosphere (4 atm) (Scheme 4.14). Analysis by NMR spectroscopy revealed the formation of the known Rh(III) amino-borane compound $[Rh(H)_2(PCy_3)_2(\eta^2\text{-}H_2B{=}N^iPr_2)][BAr^F{}_4]$ (**i-91**) as the sole organometallic product.[70]



Scheme 4.14 Reaction of **4-4** with $Na[BAr^F{}_4]$ under a hydrogen atmosphere to form the known amino-borane complex **i-91**.

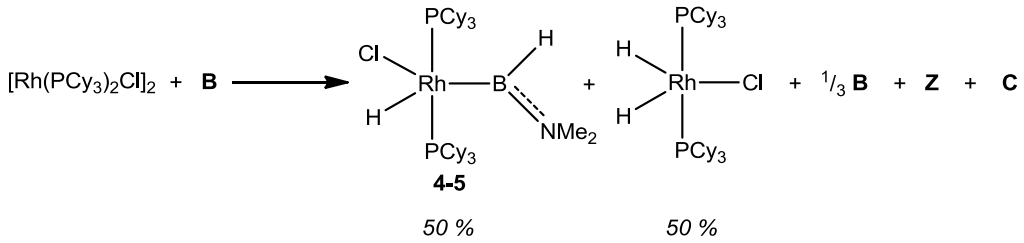
The equivalent reaction between $Rh(H)_2(PCy_3)_2Cl$ and $H_2B{=}N^iPr_2$ resulted in the observation of a trace (< 1%) of **4-4** after 24 hours at room temperature. Presumably the slower reaction rate is due to the difference in oxidation state [Rh(I) *versus* Rh(III)] and the relative ease at which they undergo oxidative addition. Suggested

additional factors include the more sterically congested rhodium centre, and also the instability of the resulting aminoboryl towards regeneration of the starting material.

4.4.2.4 Reactivity with $H_3B{\cdot}NMe_2BH_2{\cdot}NMe_2H$ (B)

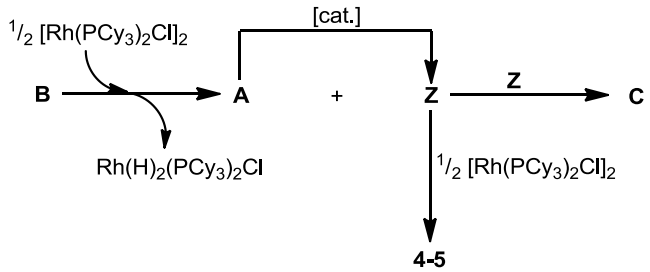
The intermediate linear diborazane, **B**, was observed during the catalytic dehydrocoupling of **A** with $[Rh(PCy_3)_2Cl]_2$ (Figure 4.15). The reactivity of $Rh(H)_2(PCy_3)_2Cl$ with **B** (stoichiometric and catalytic) has been discussed in Section 4.3.1.2, and displayed an induction period, which we postulated was due to the slow generation of the active monomeric species, from the inactive dimer. However as $[Rh(PCy_3)_2Cl]_2$ has been shown to react differently to $Rh(H)_2(PCy_3)_2Cl$ with TMAB (Section 4.4.2.2), we also chose to investigate the stoichiometric reactivity of $[Rh(PCy_3)_2Cl]_2$ with **B**.

The addition of one equivalent of **B** to $[Rh(PCy_3)_2Cl]_2$ rapidly (within 5 minutes) forms, in equal amounts by $^{31}P\{^1H\}$ NMR spectroscopy, $Rh(H)_2(PCy_3)_2Cl$ and a new species at δ 39.9 ppm (d, $^1J_{RhP}$ = 121 Hz). In the ^{11}B NMR spectrum a broad resonance was observed at δ 54 ppm, while in the ^1H NMR spectrum a resonance at δ -17.05 ppm (overlapping dt, $^1J_{RhH}$ = 30.5 Hz, $^2J_{PH}$ = 14.5 Hz) indicated the presence of a rhodium hydride. A comparison of the NMR data with **4-4** led us to assign this new species to the closely related hydridorhodium(hydrido-boryl) complex $Rh(H)(PCy_3)_2Cl\{B(H)NMe_2\}$ (**4-5**) (Scheme 4.15). As with **4-4**, **4-5** is unstable in solution forming $Rh(H)_2(PCy_3)_2Cl$. Also visible in the ^{11}B NMR spectrum is unreacted **B** (~1/3 remaining by ^1H NMR integrals) and the amino-borane **Z**. Over time **C** is observed to grow in, resulting from the dimerisation of **Z**.[25, 51]



Scheme 4.15 The formation of the aminoboryl **4-5** and $Rh(H)_2(PCy_3)_2Cl$ by the addition of **B** to $[Rh(PCy_3)_2Cl]_2$.

We propose that **B** undergoes B-N bond cleavage, mediated by $[Rh(PCy_3)_2Cl]_2$, to generate **A** and **Z** (Scheme 4.16). As mentioned in Section 4.4.2.1, **A** is rapidly dehydrogenated by $[Rh(PCy_3)_2Cl]_2$ to generate **Z** and $Rh(H)_2(PCy_3)_2Cl$, and the small quantity of **A** generated here is likely to experience the same fate, accounting for the lack of observation of **A**. The **Z** formed can either undergo B-H activation at $[Rh(PCy_3)_2Cl]_2$ to form the aminoboryl **4-5** or dimerise to form **C**. The observation of unreacted **B** despite the 1:1 reaction ratio suggests that **Z** reacts more rapidly with $[Rh(PCy_3)_2Cl]_2$, forming **4-5**, than **B**. The concentration of **B** remains constant for the next hour, consistent with the induction period observed for its catalytic dehydrocoupling by $Rh(H)_2(PCy_3)_2Cl$ (Section 4.3.1.2).



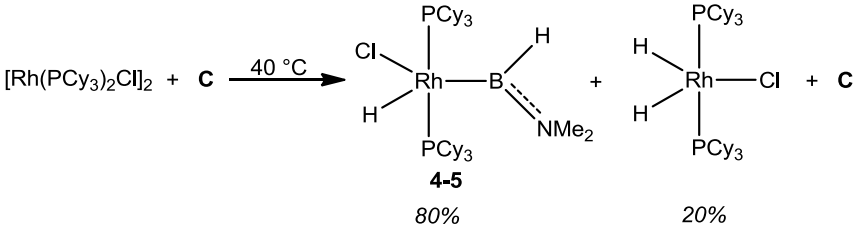
Scheme 4.16 Proposed reaction scheme for the reaction of **B** with $[Rh(PCy_3)_2Cl]_2$. [cat.] = $Rh(H)_2(PCy_3)_2Cl$ or $[Rh(PCy_3)_2Cl]_2$.

This reactivity provides insight into how $[Rh(PCy_3)_2Cl]_2$ promotes the consumption of **B**. Here, **B** is predominantly consumed *via* B-N bond cleavage[20, 24] rather than

dehydrocyclisation to generate the final product **C** as observed for [$TiCp_2$] systems.[20, 23]

4.4.2.5 Reactivity with cyclic dimer (C)

The final product **C** can be used as a source of the monomer **Z** due to the equilibrium which exists between them, although the equilibrium lies vastly in favour of **C** at room temperature.[25, 51] In an attempt to produce the aminoboryl **4-5** cleanly, **C** was added to $[Rh(PCy_3)_2Cl]_2$ in 1,2-$C_6H_4F_2$. After 12 hours at room temperature, analysis by $^{31}P\{^1H\}$ and ^1H NMR spectroscopy indicated the partial formation of **4-5**, along with a minor amount of $Rh(H)_2(PCy_3)_2Cl$. The major (~90%) organometallic species present was unreacted $[Rh(PCy_3)_2Cl]_2$. Heating the reactants to 40 °C drove the reaction forward to yield **4-5** (80%) and $Rh(H)_2(PCy_3)_2Cl$ (20%) (^1H NMR data) (Scheme 4.17). The separation of the two organometallic products was not attempted as like **4-4**, **4-5** is unstable in solution and forms $Rh(H)_2(PCy_3)_2Cl$ with time. The onward reactivity of **4-5** and the position of the equilibrium between **Z** and **C** are likely to prevent its clean formation.



Scheme 4.17 Reaction between $[Rh(PCy_3)_2Cl]_2$ and **C** in an attempt to cleanly produce **4-3**.

The formation of $Rh(H)_2(PCy_3)_2Cl$ in the presence of **C** contrasts the cationic system in Chapter 3 where **C** promoted the loss of dihydrogen from Rh(III)-dihydride species and the return to the Rh(I) oxidation state.[20] It is, however, consistent with earlier results which indicated a lack of reactivity between $Rh(H)_2(PCy_3)_2Cl$ and **C**; no

autocatalytic effect was seen for the dehydrocoupling of **A** in the presence of exogenous **C** and no B-H/D exchange was observed between $Rh(D)_2(PCy_3)_2Cl$ and **C**.

4.5 Conclusions and future work

The synthesis and full characterisation of the halide-bridged species **4-1**, which could be present in the cationic system at low concentrations of **A**, has been detailed. Although **4-1** is a competent catalyst for the dehydrocoupling of **A**, reactivity studies demonstrated that at high concentrations of **A** (at the start of catalysis), **4-1** is cleaved to generate the cationic σ-amine-borane complex **3-4-Cy** and $Rh(H)_2(PCy_3)_2Cl$. The mechanism by which the neutral rhodium species, $Rh(H)_2(PCy_3)_2Cl$, catalyses the dehydrogenation of **A** has been studied through initial rates and H/D exchange experiments, allowing the proposal of the mechanism shown in Scheme 4.10. Key features include the existence of a rapid monomer-dimer equilibrium in the catalyst, where the strongly favoured dimeric species is inactive and lies outside of the catalytic cycle. B-H activation of **A** at the active monomer is reversible and rapid (in relation to the irreversible dehydrogenation) and occurs prior to β-H N-H transfer. Monitoring catalysis by ^{11}B NMR spectroscopy indicated that the dehydrogenation of **A** followed pseudo first order kinetics, which correlated with the pseudo first order consumption of **A** observed in the cationic system in Chapter 3, where the neutral catalyst was proposed to be present acting in parallel. Subtleties of the system include the irreversible deactivation of the catalyst at low catalyst loadings to form the inactive borohydride complex **4-3**, while H_2 inhibition is observed in a sealed system, potentially through coordination of dihydrogen at the boryl intermediate preventing subsequent β-H N-H transfer. Additionally, the understanding of the mechanism by

which the neutral species operates allows full insight into the overall mechanism in the cationic system.

The catalytic dehydrocoupling of **A** by $[Rh(PCy_3)_2Cl]_2$ also followed pseudo first order kinetics, with the same rate constant (within error) as for $Rh(H)_2(PCy_3)_2Cl$. This correlates with the stoichiometric reactivity of $[Rh(PCy_3)_2Cl]_2$ with **A**, where complete conversion to $Rh(H)_2(PCy_3)_2Cl$ is observed. The reactivity studies of $[Rh(PCy_3)_2Cl]_2$ with amine-boranes served to demonstrate its more reactive nature relative to $Rh(H)_2(PCy_3)_2Cl$ allowing the formation of rhodiumhydrido(hydrido-boryl) species, **4-4** and **4-5**.

Future work in this area could explore the faster catalysis demonstrated by the neutral catalysts *versus* the cationic rhodium catalysts, more traditionally used in the Weller group. Currently one of the fastest catalysts for the dehydrocoupling of **A** is the cationic rhodium *bis*-chelating phosphine systems, $[Rh(Ph_2P(CH_2)_nPPh_2)][BAr^F{}_4]$ (n = 3-5) (**i-78**) due to their strong preference for the Rh(I) oxidation state.[71, 72] Potentially, the neutral version may offer enhanced activity. The ability of the neutral catalysts to facilitate the dehydrocoupling of primary amine-boranes such as $H_3B{\cdot}NMeH_2$, potentially yielding polymeric $[H_2BNMeH]_n$ is also of interest.

4.6 References

1. H. Itagaki, H. Murayama and Y. Saito, *Bull. Chem. Soc. Jpn.*, 1994, **67**, 1254-1257.
2. M. E. Sloan, T. J. Clark and I. Manners, *Inorg. Chem.*, 2009, **48**, 2429-2435.
3. G. Erker, *Dalton Trans.*, 2005, 1883-1890.
4. R. L. Harlow, D. L. Thorn, R. T. Baker and N. L. Jones, *Inorg. Chem.*, 1992, **31**, 993-997.
5. P. Binger, J. Haas, G. Glaser, R. Goddard and C. Kruger, *Chem. Ber.*, 1994, **127**, 1927-1929.
6. H. Noth and H. Vahrenka, *Chem. Ber. Recl.*, 1966, **99**, 1049-1050.
7. A. B. Burg and C. L. Randolph, *J. Am. Chem. Soc.*, 1951, **73**, 953-957.
8. H. D. Empsall, E. Mentzer and B. L. Shaw, *J. Chem. Soc. Chem. Commun.*, 1975, 861-862.
9. H. L. M. Vangaal, J. M. J. Verlaak and T. Posno, *Inorg. Chim. Acta*, 1977, **23**, 43-51.

10. M. C. Denney, V. Pons, T. J. Hebden, D. M. Heinekey and K. I. Goldberg, *J. Am. Chem. Soc.*, 2006, **128**, 12048-12049.
11. I. Gottker-Schnetmann, P. S. White and M. Brookhart, *Organometallics*, 2004, **23**, 1766-1776.
12. T. J. Hebden, M. C. Denney, V. Pons, P. M. B. Piccoli, T. F. Koetzle, A. J. Schultz, W. Kaminsky, K. I. Goldberg and D. M. Heinekey, *J. Am. Chem. Soc.*, 2008, **130**, 10812-10820.
13. J. A. Widegren, M. A. Bennett and R. G. Finke, *J. Am. Chem. Soc.*, 2003, **125**, 10301-10310.
14. M. A. Watzky and R. G. Finke, *J. Am. Chem. Soc.*, 1997, **119**, 10382-10400.
15. K. S. Weddle, J. D. Aiken and R. G. Finke, *J. Am. Chem. Soc.*, 1998, **120**, 5653-5666.
16. C. Paal and W. Hartmann, *Chem. Ber.*, 1918, **51**, 711-712.
17. E. Bayram, J. C. Linehan, J. L. Fulton, J. A. S. Roberts, N. K. Szymczak, T. D. Smurthwaite, S. Ozkar, M. Balasubramanian and R. G. Finke, *J. Am. Chem. Soc.*, 2011, **133**, 18889-18902.
18. T. M. Douglas, A. B. Chaplin and A. S. Weller, *J. Am. Chem. Soc.*, 2008, **130**, 14432-14433.
19. A. B. Chaplin and A. S. Weller, *Inorg. Chem.*, 2010, **49**, 1111-1121.
20. L. J. Sewell, G. C. Lloyd-Jones and A. S. Weller, *J. Am. Chem. Soc.*, 2012, **134**, 3598-3610.
21. M. Mediati, G. N. Tachibana and C. M. Jensen, *Inorg. Chem.*, 1992, **31**, 1827-1832.
22. D. W. Lee and C. M. Jensen, *J. Am. Chem. Soc.*, 1996, **118**, 8749-8750.
23. M. E. Sloan, A. Staubitz, T. J. Clark, C. A. Russell, G. C. Lloyd-Jones and I. Manners, *J. Am. Chem. Soc.*, 2010, **132**, 3831-3841.
24. A. Friedrich, M. Drees and S. Schneider, *Chem. Eur. J.*, 2009, **15**, 10339-10342.
25. C. J. Stevens, R. Dallanegra, A. B. Chaplin, A. S. Weller, S. A. Macgregor, B. Ward, D. McKay, G. Alcaraz and S. Sabo-Etienne, *Chem. Eur. J.*, 2011, **17**, 3011-3020.
26. C. A. Jaska, K. Temple, A. J. Lough and I. Manners, *J. Am. Chem. Soc.*, 2003, **125**, 9424-9434.
27. M. Vogt, B. de Bruin, H. Berke, M. Trincado and H. Grutzmacher, *Chem. Sci.*, 2011, **2**, 723-727.
28. T. M. Douglas, A. B. Chaplin, A. S. Weller, X. Z. Yang and M. B. Hall, *J. Am. Chem. Soc.*, 2009, **131**, 15440-15456.
29. R. Dallanegra, A. B. Chaplin, J. Tsim and A. S. Weller, *Chem. Commun.*, 2010, **46**, 3092-3094.
30. R. B. Jordan, *Reaction Mechanisms of Inorganic and Organometallic Systems*, Oxford University Press, Oxford, 2007.
31. R. R. Zhou, J. A. Aguilar, A. Charlton, S. B. Duckett, P. I. P. Elliott and R. Kandiah, *Dalton Trans.*, 2005, 3773-3779.
32. G. P. F. van Strijdonck, M. D. K. Boele, P. C. J. Kamer, J. G. de Vries and P. W. N. M. van Leeuwen, *Eur. J. Inorg. Chem.*, 1999, 1073-1076.
33. M. Kim, A. Picot and F. P. Gabbai, *Inorg. Chem.*, 2006, **45**, 5600-5606.
34. T. Rosner, J. Le Bars, A. Pfaltz and D. G. Blackmond, *J. Am. Chem. Soc.*, 2001, **123**, 1848-1855.
35. J. B. Johnson and J. E. Backvall, *J. Org. Chem.*, 2003, **68**, 7681-7684.
36. M. K. Thorson, K. L. Klinkel, J. M. Wang and T. J. Williams, *Eur. J. Inorg. Chem.*, 2009, 295-302.
37. Z. Lu, B. L. Conley and T. J. Williams, *Organometallics*, 2012, **31**, 6705-6714.
38. C. A. Tolman, P. Z. Meakin, D. L. Lindner and J. P. Jesson, *J. Am. Chem. Soc.*, 1974, **96**, 2762-2774.
39. P. Krüger and H. Werner, *Eur. J. Inorg. Chem.*, 2004, **2004**, 481-491.
40. R. B. King, J. Bakos, C. D. Hoff and L. Marko, *J. Org. Chem.*, 1979, **44**, 1729-1731.
41. J. E. Marshall, J. B. Keister and S. T. Diver, *Organometallics*, 2011, **30**, 1319-1321.
42. B. R. James, M. Preece and S. D. Robinson, *Inorg. Chim. Acta*, 1979, **34**, L219-L221.

43. A. Rifat, N. J. Patmore, M. F. Mahon and A. S. Weller, *Organometallics*, 2002, **21**, 2856-2865.
44. A. K. Jameson and C. J. Jameson, *J. Magn. Reson.*, 1978, **32**, 455-457.
45. J. C. Christofides and D. B. Davies, *J. Am. Chem. Soc.*, 1983, **105**, 5099-5105.
46. P. Vujanić, E. Gacs-Baitz, Z. Meić, T. Šuste and V. Smrečki, *Magn. Reson. Chem.*, 1995, **33**, 426-430.
47. M. B. Kruger, C. Selle, D. Heller and W. Baumann, *J. Chem. Eng. Data*, 2012, **57**, 1737-1744.
48. M. S. Hill, M. Hodgson, D. J. Liptrot and M. F. Mahon, *Dalton Trans.*, 2011, **40**, 7783-7790.
49. D. J. Liptrot, M. S. Hill, M. F. Mahon and D. J. MacDougall, *Chem. Eur. J.*, 2010, **16**, 8508-8515.
50. H. C. Johnson, A. P. M. Robertson, A. B. Chaplin, L. J. Sewell, A. L. Thompson, M. F. Haddow, I. Manners and A. S. Weller, *J. Am. Chem. Soc.*, 2011, **133**, 11076-11079.
51. E. M. Leitao, N. E. Stubbs, A. P. M. Robertson, H. Helten, R. J. Cox, G. C. Lloyd-Jones and I. Manners, *J. Am. Chem. Soc.*, 2012, **134**, 16805-16816.
52. R. N. Perutz and S. Sabo-Etienne, *Angew. Chem. Int. Ed.*, 2007, **46**, 2578-2592.
53. H. Landesman and R. E. Williams, *J. Am. Chem. Soc.*, 1961, **83**, 2663-2666.
54. Sigma-Aldrich, 5 g of trimethylboron £895.00 14/12/2012.
55. D. Pun, E. Lobkovsky and P. J. Chirik, *Chem. Commun.*, 2007, 3297-3299.
56. M. C. MacInnis, R. McDonald, M. J. Ferguson, S. Tobisch and L. Turculet, *J. Am. Chem. Soc.*, 2011, **133**, 13622-13633.
57. Y. Kawano, M. Uruichi, M. Shimoi, S. Taki, T. Kawaguchi, T. Kakizawa and H. Ogino, *J. Am. Chem. Soc.*, 2009, **131**, 14946-14957.
58. M. L. Denniston, M. A. Chiusano and D. R. Martin, *J. Inorg. Nucl. Chem.*, 1976, **38**, 979-981.
59. J. M. Purser and B. F. Spielvog, *Inorg. Chem.*, 1968, **7**, 2156-2157.
60. N. E. Miller and E. L. Muetterties, *J. Am. Chem. Soc.*, 1964, **86**, 1033-1036.
61. C. A. Jaska and I. Manners, *J. Am. Chem. Soc.*, 2004, **126**, 9776-9785.
62. M. Shimoi, S.-i. Nagai, M. Ichikawa, Y. Kawano, K. Katoh, M. Uruichi and H. Ogino, *J. Am. Chem. Soc.*, 1999, **121**, 11704-11712.
63. T. Kakizawa, Y. Kawano and M. Shimoi, *Organometallics*, 2001, **20**, 3211-3213.
64. Y. Kawano, M. Hashiva and M. Shimoi, *Organometallics*, 2006, **25**, 4420-4426.
65. L. Euzenat, D. Horhant, Y. Ribourdouille, C. Duriez, G. Alcaraz and M. Vaultier, *Chem. Commun.*, 2003, 2280-2281.
66. M. O'Neill, D. A. Addy, I. Riddlestone, M. Kelly, N. Phillips and S. Aldridge, *J. Am. Chem. Soc.*, 2011, **133**, 11500-11503.
67. C. Y. Tang, N. Phillips, J. I. Bates, A. L. Thompson, M. J. Gutmann and S. Aldridge, *Chem. Commun.*, 2012, **48**, 8096-8098.
68. H. Braunschweig, C. Kollann and U. Englert, *Eur. J. Inorg. Chem.*, 1998, 465-468.
69. R. W. Kunz and P. S. Pregosin, *^{31}P and ^{13}C NMR of transition metal phosphine complexes*, Springer-Verlag, Berlin ; New York, 1979.
70. G. Alcaraz, A. B. Chaplin, C. J. Stevens, E. Clot, L. Vendier, A. S. Weller and S. Sabo-Etienne, *Organometallics*, 2010, **29**, 5591-5595.
71. R. Dallanegra, A. P. M. Robertson, A. B. Chaplin, I. Manners and A. S. Weller, *Chem. Commun.*, 2011, **47**, 3763-3765.
72. A. D. Wilson, A. J. M. Miller, D. L. DuBois, J. A. Labinger and J. E. Bercaw, *Inorg. Chem.*, 2010, **49**, 3918-3926.

5 Experimental

5.1 Experimental techniques

5.1.1 General

All manipulations, unless otherwise stated, were performed under an atmosphere of argon, using standard Schlenk-line and glove-box techniques. Glassware was oven dried at 130 °C overnight and flamed under vacuum prior to use. CH_2Cl_2, THF, MeCN, Et_2O, pentane, hexane and toluene were dried using a Grubbs type solvent purification system (MBraun SPS-800) and degassed by successive freeze-pump-thaw cycles.[1] Ethanol was degassed *via* saturation with argon. *Tert*-butylethylene (TBE) and C_6D_6 were dried over sodium, vacuum distilled and stored over 3 Å molecular sieves. CD_2Cl_2, C_6H_5F and 1,2-$C_6H_4F_2$ were dried over CaH_2, vacuum distilled and stored over 3 Å molecular sieves. $CDCl_3$ was degassed by successive freeze-pump-thaw cycles and stored over 3 Å molecular sieves. $H_3B{\cdot}NMe_3$ was sublimed once and $H_2B{\cdot}NMe_2H$ twice prior to use (5×10^{-2} mbar, 298 K). Microanalyses were performed by Elemental Microanalysis Ltd and Stephen Boyer at London Metropolitan University.

5.1.2 Hydrogenation

The sample was freeze-pump-thaw degassed twice and backfilled with H_2. When the flask was filled and sealed at 298 K, the resulting H_2 pressure was 1 atm. When the flask was filled and sealed while in liquid N_2 (77 K), the internal H_2 pressure upon warming to 298 K was *ca.* 4 atm (298/77 = 3.9).

5.1.3 Nuclear Magnetic Resonance spectroscopy

NMR spectra were recorded on a Varian Mercury VX 300 MHz, Varian Unity Plus 500 MHz spectrometer, Bruker AVD 500 MHz or a Bruker AVC 500 MHz spectrometer at room temperature unless otherwise stated. Residual protio solvent was used as a reference for ^{1}H and ^{13}C NMR spectra. In 1,2-$C_6H_4F_2$ and C_6H_5F, ^{1}H NMR spectra were referenced to the centre of the downfield solvent multiplet (δ = 7.07 and 7.11 ppm respectively). ^{31}P and ^{11}B NMR spectra were referenced externally against 85% H_3PO_4 and $F_3B{\cdot}OEt_2$ respectively. Chemical shifts are quoted in ppm. Coupling constants are quoted in Hz.

5.1.4 Mass Spectrometry

Electrospray Ionisation Mass Spectrometry (ESI-MS) was recorded using a Bruker MicrOTOF instrument directly connected to a modified Innovative Technology glove box.[2] The mass spectrometer was calibrated in positive ion mode using a 10 ng/ mL mixture of tetraalkylammonium bromides $[N(C_n\text{-}H_{2n+1})_4]Br$ (n = 2, 3, 4, 5, 6, 7, 8, 12, 16, 18) in CH_2Cl_2. Typical acquisition parameters were; sample flow rate 4 μL/ min; nebuliser gas pressure 0.4 bar, drying gas (argon at 60 °C, flowing at 4L/ min), capillary voltage 4.5 kV, funnel voltage 200 Vpp; and the solvent, CH_2Cl_2, C_6H_5F or 1,2-$C_6H_4F_2$). MS samples were diluted to a concentration of ~1 x 10^{-6} M before running. Neutral samples were analysed by the EPSRC National Mass Spectrometry Service Centre in Swansea.

5.1.5 X-Ray crystallography

Structure determinations were carried out by either Dr. Adrian B. Chaplin or Dr. Miguel A. Huertos. Relevant crystallographic data for complexes **2-3, 2-4**, **3-1-^{c}Pr** and

4-1 can be found in Tables 6.1 and 6.2 (Appendix 6.1). Data were acquired on a Nonius Kappa CCD diffractometer using graphite monochromated Mo Kα radiation (λ = 0.71073 Å) and a low-temperature device.[3] All non-hydrogen atoms were refined anisotropically. Data deposited in CCDC and can be obtained free of charge *via* www.ccdc.cam.ac.uk/data_request/cif. Graphical representations of X-ray structures were made using ORTEP3.[4]

5.2 Synthesis and characterisation

5.2.1 Starting materials

The starting materials $H_3B{\cdot}NMe_2BH_2{\cdot}NMe_2H$,[5] $[H_2BNMe_2]_2$,[5] $H_3B{\cdot}NMe_2D$,[6] $D_3B{\cdot}NMe_2H$,[6] $D_3B{\cdot}NMe_2D$,[6] $Na[BAr^F{}_4]$,[7] $Na[BAr^{Cl}{}_4]$,[8] $[Rh(P^iPr_3)_2(\eta^6\text{-}C_6H_5F)][BAr^F{}_4]$,[9] $[Rh(P^iPr_3)_2Cl]_2$,[10] $[Rh(P^cPr_3)_2Cl]_2$,[11] $[Rh(PCy_3)_2Cl]_2$,[12] $[Rh(COE)_2Cl]_2$,[13] $[Rh(NBD)Cl]_2$,[14] $[Rh(PCy_3)_2(NBD)][BAr^F{}_4]$,[15] $Ir(H)_2(PCy_3)_2Cl$,[16] $[Ir(H)\{PCy_2(\eta^2\text{-}C_6H_9)\}\{PCy_2(\eta^3\text{-}C_6H_8)\}][BAr^F{}_4]$[16] and $[Ir(H)_2(PCy_3)_2(\eta^2\text{-}H_3B{\cdot}NMe_3)][BAr^F{}_4]$[17] were prepared by literature methods or variations thereof. $H_2B{=}N^iPr_2$ was prepared by Dr. Gilles Alcaraz (CNRS, Toulouse).[18] All other chemicals are commercial products and were used as received from Sigma-Aldrich, Acros, Fisher, Fluka, Fluorochem or Strem Chemicals.

5.2.2 Synthesis of new complexes

$P^tBu^iBu_2$

Iso-butyl lithium (31.4 ml, 50.3 mmol) was added to 30 mL of Et_2O, in a large Schlenk equipped with a reflux condenser. The contents of the flask were cooled to 0 °C in an ice bath. A solution of P^tBuCl_2 (2.00 g, 12.6 mmol) in Et_2O (25 mL) was prepared and

added to the *iso*-butyl lithium solution dropwise over 15 minutes. An off-white suspension was formed, and the reaction mixture heated under reflux for 3 hours. The reaction mixture was cooled to room temperature and hydrolysed with 20 mL of degassed, deionised water. The Et_2O layer was separated and dried over anhydrous magnesium sulphate. The solution was filtered and the solvent removed *in vacuo*. The resulting pale yellow liquid was purified by vacuum distillation; a colourless, viscous liquid was collected. Yield: 1.76 g (69%).

^{1}H NMR (300 MHz, $CDCl_3$): δ 1.70 – 1.55 (m, 2H, ^{i}Bu{CH}), 1.20 (dd, 2H, $^2J_{HH}$ = 13.8, J = 8.0, ^{i}Bu{CH_2}), 1.11 (doublet of apparent triplets, 2H, $^2J_{HH}$ = 13.8, J = 5.8, ^{i}Bu{CH_2}), 0.98 (dd, J = 6.5, J = 3.9, 12H, ^{i}Bu{Me}), 0.97 (d, $^3J_{PH}$ = 11.3, 9H, ^{t}Bu{Me}).

^{31}P {^{1}H} NMR (122 MHz, $CDCl_3$): δ -12.7 (s).

$Rh(H)_2(P^tBu^iBu_2)_2Cl$ (2-2)

To a Young's flask charged with $[Rh(COE)_2Cl]_2$ (0.115 g, 0.16 mmol) was added a solution of $P^tBu^iBu_2$ (0.146 g, 0.72 mmol) in CH_2Cl_2 (5 mL) at -78 °C. The flask was sealed and immediately frozen in liquid nitrogen. The argon atmosphere was removed and replaced with hydrogen (4 atm). The solution was stirred at room temperature for 30 minutes before removal of the solvent *in vacuo*. Recrystallisation from pentane at -80 °C yielded the product as yellow crystals. Yield: 0.122 g (70%).

^{1}H NMR (CD_2Cl_2, 500 MHz): δ 2.10 (apparent nonet, 4H, J = 6, ^{i}Bu{CH}), 1.83 – 1.77 (m, 4H, ^{i}Bu{CH_2}), 1.64 – 1.59 (m, 4H, ^{i}Bu{CH_2}), 1.17 (apparent t, 18H, J = 6, ^{t}Bu{Me}), 1.03 (d, $^3J_{HH}$ = 1.2, 12H, ^{i}Bu{Me}) ,1.02 (d, $^3J_{HH}$ = 1.2, 12H, ^{i}Bu{Me}), -22.84 (dt, 2H, $^1J_{RhH}$ = 27.7, $^2J_{PH}$ = 15.5, RhH).

^{1}H {^{31}P} NMR (CD_2Cl_2, 500 MHz): δ 2.10 (nonet, 4H, $^3J_{HH}$ = 6.4, ^{i}Bu{CH}), 1.79 (dd, $^2J_{HH}$ = 14.3, $^3J_{HH}$ = 5.7, 4H, ^{i}Bu{CH_2}), 1.61 (dd, $^2J_{HH}$ = 14.3, $^3J_{HH}$ = 7.0, 4H, ^{i}Bu{CH_2}), 1.17 (s,

18, ^{t}Bu{Me}), 1.03, (d, $^{3}J_{HH}$ = 1.2, 12H, ^{i}Bu{Me}),1.02, (d, $^{3}J_{HH}$ = 1.2, 12H, ^{i}Bu{Me}), -22.84 (d, 2H, $^{1}J_{RhH}$ = 27.9, RhH).

^{31}P {^{1}H} NMR (CD_2Cl_2, 202 MHz): δ 44.9 (d, $^{1}J_{RhP}$ = 115).

^{13}C {^{1}H} NMR (CD_2Cl_2, 126 MHz): δ 34.9 (apparent t, J = 10, ^{i}Bu{CH_2}), 31.8 (apparent td, J = 13, J = 1, ^{t}Bu{C}), 28.1 (apparent t, J = 3, ^{t}Bu{Me}), 26.5 (s, ^{i}Bu{CH}), 26.0 (apparent t, J = 4, ^{i}Bu{Me}), 25.6 (apparent t, J = 3, ^{i}Bu{Me}).

Anal. Calcd. for $C_{24}H_{56}ClP_2Rh$ (545.01 gmol^{-1}): C, 52.89; H, 10.36. Found: C, 52.88; H, 10.35.

[Rh(H)$_2$(P^{t}Bu^{i}Bu$_2$)$_2$][BAr$^{F}_4$] (2-3)

To a Young's flask charged with Rh(H)$_2$(P^{t}Bu^{i}Bu$_2$)$_2$Cl (0.015 g, 0.028 mmol) and Na[BAr$^{F}_4$] (0.026 g, 0.029 mmol) was added CH_2Cl_2 (1 mL). The solution was sonnicated for 10 minutes and then filtered in to a Young's crystallisation tube. The solution was layered with pentane and held at 5 °C for several days affording the product as pale yellow crystals. Yield: 0.027 g (71%).

^{1}H NMR (CD_2Cl_2, 500 MHz): δ 7.72 (br, 8H, BAr$^{F}_4$), 7.56 (br, 4H, BAr$^{F}_4$), 1.95 – 1.79 (m, 8H, ^{i}Bu{CH/CH_2}), 1.73 – 1.67 (m, 4H, ^{i}Bu{CH_2}), 1.16 (apparent t, 18H, J = 7, ^{t}Bu{Me}), 0.89 (d, 12H, $^{3}J_{HH}$ = 6.5, ^{i}Bu{Me}), 0.81 (d, 12H, $^{3}J_{HH}$ = 6.5, ^{i}Bu{Me}), -22.03 (dt, 2H, $^{1}J_{RhH}$ = 47.1, $^{2}J_{PH}$ = 13.3, RhH).

^{1}H {^{31}P} NMR (CD_2Cl_2, 500 MHz): δ 7.72 (br, 8H, BAr$^{F}_4$), 7.56 (br, 4H, BAr$^{F}_4$), 1.95 – 1.79 (m, 8H, ^{i}Bu{CH/CH_2}), 1.69 (dd, 4H, J = 6.9, J = 14.5, ^{i}Bu{CH_2}), 1.16 (s, 18H, ^{t}Bu{Me}), 0.89 (d, 12H, $^{3}J_{HH}$ = 6.5, ^{i}Bu{Me}), 0.81 (d, 12H, $^{3}J_{HH}$ = 6.5, ^{i}Bu{Me}), -22.03 (d, 2H, $^{1}J_{RhH}$ = 47.3, RhH).

^{31}P {^{1}H} NMR (CD_2Cl_2, 202 MHz): δ 56.9 (d, $^{1}J_{RhP}$ = 109).

^{13}C {^{1}H} NMR (CD_2Cl_2, 126 MHz): δ 162.3 (q, $^{1}J_{BC}$ = 50, BAr^F_4), 135.4 (s, BAr^F_4), 129.4 (qq, $^{2}J_{FC}$ = 32, $^{3}J_{BC}$ = 3, BAr^F_4), 125.2 (q, $^{1}J_{FC}$ = 272, BAr^F_4), 118.0 (sept, $^{3}J_{FC}$ = 4, BAr^F_4), 35.7 (apparent t, J = 11, ^{i}Bu{CH_2}), 31.3 (apparent td, J = 15, J = 2, ^{t}Bu{C}), 28.0 (apparent t, J = 2, ^{i}Bu{CH}), 27.5 (apparent t, J = 3, ^{t}Bu{Me}), 25.2 (apparent t, J = 2, ^{i}Bu{Me}), 24.9 (apparent t, J = 3, ^{i}Bu{Me}).

^{1}H NMR (CD_2Cl_2, 500 MHz, 190 K): δ 7.71 (br, 8H, BAr^F_4), 7.53 (br, 4H, BAr^F_4), 1.76 (br, 8H, ^{i}Bu{CH_2}), 1.54 (br, 4H, ^{i}Bu{CH}), 1.04 (br, 18H, ^{t}Bu{Me}), 0.75 (d, J = 4.6, 12H, ^{i}Bu{Me}), 0.67 (d, $^{3}J_{HH}$ = 4.2, 12H, ^{i}Bu{Me}), -21.48 (dt (br), $^{1}J_{RhH}$ = 44.9, $^{2}J_{PH}$ = 11.7, 2H, RhH).

^{31}P {^{1}H} NMR (CD_2Cl_2, 202 MHz, 190 K): δ 57.2 (br d, $^{1}J_{RhP}$ = 105).

Anal. Calcd. for $C_{56}H_{68}BF_{24}P_2Rh$ (1372.77 $gmol^{-1}$): C, 49.00; H, 4.99. Found: C, 48.87; H, 4.92.

ESI-MS (C_6H_5F, 60 °C) positive ion: m/z, 509.29 [M^+] (calc. 509.29). The observed isotopic pattern (3 lines) was fully consistent with the molecular formula.

IR (CH_2Cl_2, cm^{-1}): ν($CH_{agostic}$) 2671 (br).

[Rh(P^{t}Bu^{i}Bu$_2$)$_2$][BAr$^F_4$] (2-4)

To a Young's flask charged with Rh(H)$_2$(P^{t}Bu^{i}Bu$_2$)$_2$Cl (0.015 g, 0.028 mmol) and Na[BAr^F_4] (0.026 g, 0.029 mmol) was added CH_2Cl_2 (1 mL). The solution was sonnicated for 10 minutes and then filtered before the addition of TBE (9 μL, 0.069 mmol). The solution was left for 1 hour before layering with pentane and then held at 5 °C for several days affording the product as yellow crystals. Yield: 0.021 g (56%).

^{1}H NMR (CD_2Cl_2, 500 MHz): δ 7.73 (br, 8H, BAr^F_4), 7.57 (br, 4H, BAr^F_4), 1.90 – 1.74 (m, 8H, ^{i}Bu{CH/CH_2}), 1.72 – 1.63 (m, 4H, ^{i}Bu{CH_2}), 1.14 (dd, 18H, J = 7.5, J = 7.3, ^{t}Bu{Me}), 1.00 – (–0.80) (br, 24H, ^{i}Bu{Me}).

^{1}H {^{31}P} NMR (CD_2Cl_2, 500 MHz): δ 7.73 (br, 8H, BAr^F_4), 7.57 (br, 4H, BAr^F_4),), 1.89 – 1.76 (m, 8H, ^{i}Bu{CH/CH_2}), 1.67 (dd, 4H, J = 14, J = 7, ^{i}Bu{CH/CH_2}), 1.14 (s, 18H, ^{t}Bu{Me}), 1.00 – (-0.80) (br, 24H, ^{i}Bu{Me}).

^{13}C {^{1}H} NMR (CD_2Cl_2, 126 MHz): δ 162.3 (q, $^{1}J_{BC}$ = 50, BAr^F_4), 135.4 (s, BAr^F_4), 129.4 (qq, $^{2}J_{FC}$ = 32, $^{3}J_{BC}$ = 3, BAr^F_4), 125.2 (q, $^{1}J_{FC}$ = 272, BAr^F_4), 118.0 (sept, $^{3}J_{FC}$ = 4, BAr^F_4), 32.5 (vbr, ^{i}Bu{CH_2}), 31.7 (vbr, ^{i}Bu{CH}), 31.4 (apparent t, J = 14, ^{t}Bu{C}), 27.2 (apparent t, J = 2, ^{t}Bu{Me}), 26.6 – 26.0 (vbr overlapping multiplet, ^{i}Bu{Me}).

^{31}P {^{1}H} NMR (CD_2Cl_2, 202 MHz): δ 64.5 (br).

^{1}H NMR (CD_2Cl_2, 500 MHz, 173 K): δ 7.74 (br, 8H, BAr^F_4), 7.55 (br, 4H, BAr^F_4), 2.39 – 1.30 (multiple peaks, 12H, ^{i}Bu{CH/CH_2}), 1.21 - 0.30 (multiple peaks, 35H, ^{i}Bu/^{t}Bu{Me}), 0.25 – (-0.38) (several broad peaks, 6H, ^{i}Bu{Me-agostic}), -22.00 (br d, J = 54.4, 0.63H, RhH), -22.15 (br d, J ~ 50, 0.03H, RhH), -22.83 (br d, J = 55.8, 0.06H, RhH), -23.04 (br d, J = 56.9, 0.28H, RhH).

^{1}H {^{31}P} NMR (CD_2Cl_2, 500 MHz, 173 K): δ 7.74 (br, 8H, BAr^F_4), 7.55 (br, 4H, BAr^F_4), 2.39 – 1.30 (multiple peaks, 12H, ^{i}Bu{CH/ CH_2}), 1.21 - 0.30 (multiple peaks, 35H, ^{i}Bu/^{t}Bu{Me}), 0.25 – (-0.38) (several broad peaks, 6H, ^{i}Bu{Me-agostic}), -22.00 (d, J = 54.6, 0.63H, RhH), -22.15 (d, J ~ 50, 0.03H, RhH), -22.83 (d, J = 55.7, 0.06H, RhH), -23.04 (d, J = 56.9, 0.28H, RhH).

^{31}P {^{1}H} NMR (CD_2Cl_2, 202 MHz, 173 K): δ 85.7 (dd, $^{2}J_{PP}$ = 295, $^{1}J_{RhP}$ = 115, C-H activated P -isomer 1), 83.9 (dd, $^{2}J_{PP}$ = 296, $^{1}J_{RhP}$ = 114, C-H activated P - isomer 2), 78.6 (dd, $^{2}J_{PP}$ = 299, $^{1}J_{RhP}$ = 114, C-H activated P – isomer 3), 69.8 (dd, $^{2}J_{PP}$ = 298, $^{1}J_{RhP}$ = 116, C-H activated P - isomer 4), 56.2 2 (dd, $^{2}J_{PP}$ = 295, $^{1}J_{RhP}$ = 115, non C-H activated P – isomer 4), ~49.8 (assumed dd, obscured by isomers 2 and 3, only outer lines visible, non C-H activated P – isomer 3), 49.2 (dd, $^{2}J_{PP}$ = 296, $^{1}J_{RhP}$ = 114, non C-H activated P – isomer 2), 48.9 (dd, $^{2}J_{PP}$ = 296, $^{1}J_{RhP}$ = 116, non C-H activated P – isomer 1).

Peaks assigned by relative integrals and coupling constants. Approximate percentage of the 4 isomers by relative ^{31}P integrals; 1, 55%; 2, 34%; 3, 8%; 4, 3%.

Anal. Calcd. for $C_{56}H_{66}BF_{24}P_2Rh$ (1370.75 $gmol^{-1}$): C, 49.07; H, 4.85. Found: C, 48.99 H, 4.80.

ESI-MS (C_6H_5F, 60 °C,) positive ion: m/z, 507.28 [M^+] (calc. 507.28). The observed isotopic pattern (3 lines) was fully consistent with the molecular formula.

IR (CH_2Cl_2, cm^{-1}): $\nu(CH_{agostic})$ 2684 (vbr).

[Rh(P^{t}Bu^{i}Bu$_2$)$_2$][BAr$^{Cl}_4$]

Same procedure as for [Rh(P^{t}Bu^{i}Bu$_2$)$_2$][BAr$^F_4$] substituting Na[BAr$^F_4$] with Na[BAr$^{Cl}_4$] (Ar^{Cl}= 3,5-$C_6H_5Cl_2$). Yield: 65%.

^{1}H NMR (CD_2Cl_2, 500 MHz): δ 7.04 – 6.99 (m, 12H, BAr$^{Cl}_4$), 1.90 – 1.74 (m, 8H, ^{i}Bu{CH/CH_2}), 1.72 – 1.63 (m, 4H, ^{i}Bu{CH_2}), 1.14 (dd, 18H, J = 7.5, J = 7.3, ^{t}Bu{Me}), 1.00 – –0.80 (br, 24H, ^{i}Bu{Me}).

^{31}P {^{1}H} NMR (CD_2Cl_2, 202 MHz): δ 64.2 (br).

[Rh(P^{t}Bu^{i}Bu$_2$)$_2$(MeCN)$_2$][BAr$^F_4$] (2-5-)

MeCN (4 μL, 0.073 mmol) was added to a solution of [Rh(P^{t}Bu^{i}Bu$_2$)$_2$][BAr$^F_4$] (0.010 g, 0.0073 mmol) in CH_2Cl_2 (1 mL). The yellow solution was layered with pentane and held at 5 °C for several days yielding the product as yellow crystals. Yield: 0.006 g (56%).

^{1}H NMR (CD_2Cl_2, 500 MHz): δ 7.72 (br, 8H, BAr$^F_4$), 7.56 (br, 4H, BAr$^F_4$), 2.21 (td, $^4J_{PH}$ = 1.6, $^5J_{RhH}$ = 0.6, 6H, MeCN), 2.07 (br, 4H, ^{i}Bu{CH}), 1.67 – 1.62 (m, 4H, ^{i}Bu{CH_2}), 1.58 – 1.52 (m, 4H, ^{i}Bu{CH_2}), 1.25 (apparent t, J = 7, 18H, ^{t}Bu{Me}), 1.21 (d, $^3J_{HH}$ = 6.6, 12H, ^{i}Bu{Me}), 1.14 (d, $^3J_{HH}$ = 6.6, 12H, ^{i}Bu{Me}).

^{1}H {^{31}P} NMR (CD_2Cl_2, 500 MHz): δ 7.72 (br, 8H, BAr^F_4), 7.56 (br, 4H, BAr^F_4), 2.21 (d, $^{4}J_{RhH}$ = 0.6, 6H, MeCN), 2.07 (nonet, $^{3}J_{HH}$ = 6.6, 4H, ^{i}Bu{CH}), 1.64 (dd, $^{2}J_{HH}$ = 14.6, $^{3}J_{HH}$ = 5.6, 4H, ^{i}Bu{CH2}), 1.55 (dd, $^{2}J_{HH}$ = 14.6, $^{3}J_{HH}$ = 8.0, 4H, ^{i}Bu{CH_2}), 1.25 (s, 18H, ^{t}Bu{Me}), 1.21 (d, $^{3}J_{HH}$ = 6.7, 12H, ^{i}Bu{Me}), 1.14 (d, $^{3}J_{HH}$ = 6.6, 12H, ^{i}Bu{Me}).

^{31}P {^{1}H} NMR (CD_2Cl_2, 202 MHz): δ 21.9 (d, $^{1}J_{RhP}$ = 128).

^{13}C {^{1}H} NMR (CD_2Cl_2, 126 MHz): δ 162.3 (q, $^{1}J_{BC}$ = 50, BAr^F_4), 135.4 (s, BAr^F_4), 129.4 (qq, $^{2}J_{FC}$ = 32, $^{3}J_{BC}$ = 3, BAr^F_4), 125.1 (q, $^{1}J_{FC}$ = 272, BAr^F_4), 125.1 (d, J = 14, Me<u>C</u>N), 118.0 (sept, $^{3}J_{FC}$ = 4, BAr^F_4), 33.6 (apparent t, J = 11, ^{t}Bu{C}), 31.3 (apparent t, J = 8, ^{i}Bu{CH_2}), 28.2 (apparent t, J = 3, ^{t}Bu{Me}), 26.3 (apparent t, J = 4, ^{i}Bu{Me}), 25.9 (s, ^{i}Bu{CH}), 25.4 (apparent t, J = 3, ^{i}Bu{Me}), 4.99 (s, <u>Me</u>CN).

Anal. Calcd. for $C_{60}H_{72}BF_{24}N_2P_2Rh$ (1452.85 gmol^{-1}): C, 49.60; H, 5.00; N, 1.93. Found: C, 49.48; H, 4.95; N, 1.77.

ESI-MS (1,2-$C_6H_4F_2$, 60 °C) positive ion: m/z, 589.33 [M^+] (calc. 589.33). The observed isotopic pattern (3 lines) was fully consistent with the molecular formula.

[Rh($P^tBu^iBu_2$)$_2$(η^2-$H_3B{\cdot}NMe_3$)][BAr^F_4] (2-6)

1,2-$C_6H_4F_2$ (1 mL) was added to a Young's crystallisation tube containing [Rh($P^tBu^iBu_2$)$_2$][BAr^F_4] (0.017 g, 0.012 mmol) and $H_3B{\cdot}NMe_3$ (0.0009 g, 0.012 mmol). The resulting inky blue solution was layered with pentane and held at 5 °C for several days yielding the product as blue crystals. Yield: 0.009 g (50%).

^{1}H NMR (1,2-$C_6H_4F_2$, 500 MHz): δ 8.34 (br, 8H, BAr^F_4), 7.69 (br, 4H, BAr^F_4), 2.88 (s, 9H, NMe_3), 2.17 (m, 4H, ^{i}Bu{CH}), 1.95 (m, 4H, ^{i}Bu{CH_2}), 1.72 (m, 4H, ^{i}Bu{CH_2}), 1.35 (apparent t, J = 7, 18H, ^{t}Bu{Me}), 1.27 (d, $^{3}J_{HH}$ = 6.5, 12H, ^{i}Bu{Me}), 1.23 (d, $^{3}J_{HH}$ = 6.7, 12H, ^{i}Bu{Me}), -2.80 (br, 3H, BH_3).

^{31}P {^{1}H} NMR (1,2-$C_6H_4F_2$, 202 MHz): δ 56.2 (d, $^{1}J_{RhP}$ = 183).

^{11}B NMR (1,2-$C_6H_4F_2$, 160 MHz): δ 26.8 (br, BH_3), -6.1 (s, BAr^F_4).

Anal. Calcd. for $C_{59}H_{78}B_2F_{24}NP_2Rh.2(SiOMe_2)$ (1592.00 $gmol^{-1}$): C, 47.53; H, 5.70; N, 0.88. Found: C, 47.26; H, 5.29; N, 0.84.

ESI-MS (1,2-$C_6H_4F_2$, 60 °C) positive ion: m/z, 580.38 [M^+] (calc. 580.38), 507.27 [M^+ - $H_3B{\cdot}NMe_3$] (calc. 507.28). The observed isotopic patterns (5 lines and 3 lines) were fully consistent with the molecular formulae.

[Rh(H)$_2$($P^tBu^iBu_2$)$_2$(η^2-$H_3B{\cdot}NMe_3$)][BAr^F_4] (2-7)

Addition of hydrogen (4 atm) to a 1,2-$C_6H_4F_2$ (0.4 mL) solution of [Rh($P^tBu^iBu_2$)$_2$(η^2-$H_3B{\cdot}NMe_3$)][BAr^F_4] (0.008g, 0.006 mmol) resulted in a rapid colour change from deep blue to colourless. *In situ* analysis by NMR spectroscopy revealed the quantitative formation of [Rh(H)$_2$($P^tBu^iBu_2$)$_2$(η^2-$H_3B{\cdot}NMe_3$)][BAr^F_4].

^{1}H NMR (1,2-$C_6H_4F_2$, 500 MHz): δ 8.34 (br, 8H, BAr^F_4), 7.69 (br, 4H, BAr^F_4), 2.86 (s, 9H, NMe_3), 2.11 (m, 4H, ^{i}Bu{CH}), 1.90 (m, 4H, ^{i}Bu{CH_2}), 1.67 (m, 4H, ^{i}Bu{CH_2}), 1.23 (apparent t, J =7.0, 18H, ^{t}Bu{Me}), 1.13 (d, $^3J_{HH}$ = 6.6, 12H, ^{i}Bu{Me}), 1.08 (d, $^3J_{HH}$ = 6.6, 12H, ^{i}Bu{Me}), -0.15 (br d, $^1J_{BH}$ = 95, 3H, BH_3), -19.92 (br, 2H, RhH_2).

^{31}P {^{1}H} NMR (1,2-$C_6H_4F_2$, 202 MHz): δ 46.9 (d, $^1J_{RhP}$ = 110).

^{11}B NMR (1,2-$C_6H_4F_2$, 160 MHz): δ 2.7 (br, BH_3), -6.1 (s, BAr^F_4).

ESI-MS (1,2-$C_6H_4F_2$, 60 °C) positive ion: *m/z* 509.28 [M^+ - $H_3B{\cdot}NMe_3$] (calc. 509.29). The observed isotopic pattern (3 lines) was fully consistent with the molecular formula.

[Rh($P^tBu^iBu_2$)$_2$(η^2-$Me_3N{\cdot}H_2BCH_2CH_2CMe_3$)][$BAr^F_4$] (2-8)

1,2-$C_6H_4F_2$ (1 mL) was added to a Young's crystallisation tube containing [Rh($P^tBu^iBu_2$)$_2$][BAr^F_4] (0.050 g, 0.037 mmol) and $H_3B{\cdot}NMe_3$ (0.0027 g, 0.037 mmol).

TBE (24 μL, 0.183 mmol) was then added and the tube sealed. After 5 days the purple solution was layered with pentane and held at 5 °C for several days yielding the product as deep purple crystals. Yield: 0.042 g (72%). Crystals suitable for single crystal X-ray diffraction were grown by using $[Rh(P^tBu^iBu_2)_2][BAr^{Cl}_4]$ in place of $[Rh(P^tBu^iBu_2)_2][BAr^F_4]$.

^{1}H NMR (1,2-$C_6H_4F_2$, 500 MHz): δ 8.34 (s, 8H, BAr^F_4), 7.69 (s, 4H, BAr^F_4), 2.94 (s, 9H, NMe_3), 2.18 (br, 4H, ^{i}Bu{CH}), 1.97 – 1.79 (m, 8H, ^{i}Bu{CH_2}), 1.73 - 1.70 (m, 2H, CH_2), 1.34 – 1.20 (m, 44H, ^{i}Bu{Me}, ^{t}Bu{Me}, CH_2), 1.02 (s, 9H, C{Me}), -7.07 (br, 2H, BH_2).

^{1}H {^{11}B} NMR (1,2-$C_6H_4F_2$, 500 MHz): δ 8.34 (s, 8H, BAr^F_4), 7.69 (s, 4H, BAr^F_4), 2.93 (s, 9H, NMe_3), 2.18 (br, 4H, ^{i}Bu{CH}), 1.97 – 1.79 (m, 8H, ^{i}Bu{CH_2}), 1.72 - 1.70 (m, 2H, CH_2), 1.34 – 1.20 (m, 44H, ^{i}Bu{Me}, ^{t}Bu{Me}, CH_2), 1.02 (s, 9H, C{Me}), -7.07 (apparent triplet, 2H, $^2J_{HP}$ = 32 and $^1J_{RhH}$ = 32, BH_2).

^{31}P {^{1}H} NMR (1,2-$C_6H_4F_2$, 202 MHz): δ 53.8 (d, $^1J_{RhP}$ = 182).

^{11}B NMR (1,2-$C_6H_4F_2$, 160 MHz): δ 37.9 (br, BH_2), -6.1 (s, BAr^F_4).

Anal. Calcd. for $C_{65}H_{90}B_2F_{24}NP_2Rh$ (1527.85 gmol^{-1}): C, 51.10; H, 5.94; N, 0.92. Found: C, 51.51; H, 5.86; N, 0.97.

ESI-MS (1,2-$C_6H_4F_2$, 60 °C) positive ion: *m/z* 664.48 [M^+] (calc. 664.48). The observed isotopic pattern (5 lines) was fully consistent with the molecular formula.

$Me_3N{\cdot}H_2B(CH_2CH_2CMe_3)$ (I)

1,2-$C_6H_4F_2$ (435 μL) and TBE (15 μL, 0.117 mmol) were added to a high pressure NMR tube containing $[Rh(P^tBu^iBu_2)_2][BAr^F_4]$ (0.0080 g, 0.006 mmol) and $H_3B{\cdot}NMe_3$ (0.0085 g, 0.117 mmol). The tube was sealed and *in situ* analysis by ^{1}H and ^{11}B NMR spectroscopy indicated the formation of $Me_3N{\cdot}H_2B(CH_2CH_2CMe_3)$. Only ~70% conversion was achieved with ~ 30% unreacted $H_3B{\cdot}NMe_3$ remaining.

^{1}H NMR (1,2-$C_6H_4F_2$, 500 MHz): δ 2.51 (s, 9H, NMe_3), 2.40 – 1.93 (m, 2H, BH_2), 1.43 – 1.40 (m, 2H, $CH_2C\underline{H}_2CMe_3$), 1.02 (s, 9H, CMe_3), 0.55 (br, 2H, $C\underline{H}_2CH_2CMe_3$).

^{11}B NMR (1,2-$C_6H_4F_2$, 160 MHz): δ -0.83 (t, $^{1}J_{HB}$ = 96).

[Rh(P^cPr_3)$_2$(η^6-C_6H_5F)][BAr^F_4]

C_6H_5F (2.5 mL) was added to a Schlenk containing [Rh(P^cPr_3)$_2$Cl]$_2$ (0.100 g, 0.112 mmol) and Na[BAr^F_4] (0.203 g, 0.229 mmol). The resulting solution was stirred for 30 minutes and then filtered. Layering with pentane (15 mL) yielded the product as brown crystals. Yield: 0.200 g (65%).

^{1}H NMR (C_6H_5F, 500 MHz): δ 8.38 (s, 8H, BAr^F_4), 7.69 (s, 4H, BAr^F_4), 6.20 (m, 2H, C_6H_5F), 6.12 (m, 2H, C_6H_5F), 5.68 (m, 1H, C_6H_5F), 0.60 (br m, 24H, ^{c}Pr CH_2), 0.36 (br m, 6H, ^{c}Pr CH).

^{31}P {^{1}H} NMR (C_6H_5F, 202 MHz): δ 42.4 (d, $^{1}J_{RhP}$ = 211).

Anal. Calcd. for $C_{56}H_{47}BF_{25}P_2Rh$ (1370.5965 gmol^{-1}): C, 49.07; H, 3.46. Found: 48.84; 3.39.

ESI-MS (C_6H_5F, 60 °C) positive ion: *m/z* 507.12 [M^+] (calc. 507.12). The observed isotopic pattern (3 lines) was fully consistent with the molecular formula.

[Rh(P^cPr)$_2$(η^2-$H_3B{\cdot}NMe_3$)][BAr^F_4] (3-1-^{c}Pr)

1,2-$C_6H_4F_2$ (~1 mL) was added to a Young's crystallisation tube containing [Rh(P^cPr_3)$_2$(η^6-C_6H_5F)][BAr^F_4] (0.030 g, 0.0219 mmol) and $H_3B{\cdot}NMe_3$ (0.0016 g, 0.0219 mmol). The deep purple solution was layered with pentane and held at 2 °C for several days yielding the product as deep purple crystals. Yield: 0.023 g (78%).

^{1}H NMR (1,2-$C_6H_4F_2$, 500 MHz): δ 8.33 (s, 8H, BAr^F_4), 7.68 (s, 4H, BAr^F_4), 2.86 (s, 9H, NMe_3), 0.86 – 0.77 (m, 30H, ^{c}Pr), -2.38 (br, 3H, BH_3).

^{31}P {^{1}H} NMR (1,2-$C_6H_4F_2$, 202 MHz): δ 64.0 (d, $^{1}J_{RhP}$ = 179).

^{11}B NMR (1,2-$C_6H_4F_2$, 160 MHz): δ 24.3 (br, BH_3), -6.0 (s, BAr^F_4).

Anal. Calcd. for $C_{53}H_{54}B_2F_{24}NP_2Rh$ (1347.4393 $gmol^{-1}$): C, 47.24; H, 4.04; N, 1.04. Found: C, 46.98; H, 3.99; N, 1.11.

ESI-MS (1,2-$C_6H_4F_2$, 60 °C) positive ion: *m/z* 484.19 [M^+] (calc. 484.19). The observed isotopic pattern (4 lines) was fully consistent with the molecular formula.

[Rh(H)$_2$(P^{c}Pr)$_2$(η^2-H$_3$B·NMe$_3$)][BAr$^F_4$] (3-2-^{c}Pr)

Addition of hydrogen (4 atm) to a 1,2-$C_6H_4F_2$ (0.4 mL) solution of [Rh(P^{c}Pr$_3$)$_2$(η^2-$H_3B{\cdot}NMe_3$)][BAr^F_4] (0.008g, 0.006 mmol) resulted in a rapid colour change from deep purple to colourless. *In situ* analysis by NMR spectroscopy revealed the quantitative formation of [Rh(H)$_2$(P^{c}Pr$_3$)$_2$(η^2-$H_3B{\cdot}NMe_3$)][BAr^F_4].

^{1}H NMR (1,2-$C_6H_4F_2$, 500 MHz): δ 8.33 (s, 8H, BAr^F_4), 7.68 (s, 4H, BAr^F_4), 2.90 (s, 9H, NMe_3), 0.87 – 0.70 (m, 30H, ^{c}Pr), -0.78 (br, 3H, BH_3), -19.20 (overlapping dt, 2H, $^{1}J_{RhH}$ = 18.2, $^{2}J_{RhP}$ = 13.9, RhH).

^{31}P {^{1}H} NMR (1,2-$C_6H_4F_2$, 202 MHz): δ 52.8 (d, $^{1}J_{RhP}$ = 114).

^{11}B NMR (1,2-$C_6H_4F_2$, 160 MHz): δ 9.5 (br, BH_3), -6.1 (s, BAr^F_4).

ESI-MS (1,2-$C_6H_4F_2$, 60 °C) positive ion: *m/z* 484.18 [M^+ - H_2] (calc. 484.19). The observed isotopic pattern (5 lines) was fully consistent with the molecular formula.

[Rh(PCy$_3$)$_2$(η^2-H$_3$B·NMe$_3$)][BAr$^F_4$] (3-1-Cy)

1,2-$C_6H_4F_2$ (1 mL) was added to a Young's flask containing [Rh(PCy$_3$)$_2$Cl]$_2$ (0.020 g, 0.014 mmol), Na[BAr^F_4] (0.027 g, 0.030 mmol) and $H_3B{\cdot}NMe_3$ (0.0022 g, 0.030 mmol). The resulting inky blue solution was filtered. Removal of the solvent *in vacuo* and washing with pentane (3 x 2 mL) yielded a lilac powder. Yield: 0.029 g (63%). Despite

repeated attempts, crystalline material suitable for microanalysis could not be obtained.

^{1}H NMR (1,2-$C_6H_4F_2$, 500 MHz): δ 8.34 (s, 8H, BAr^F_4), 7.68 (s, 4H, BAr^F_4), 2.96 (s, 9H, NMe_3), 2.22 – 1.37 (m, 66H, Cy), -2.87 (br, 3H, BH_3).

^{31}P {^{1}H} NMR (1,2-$C_6H_4F_2$, 202 MHz): δ 60.7 (d, $^{1}J_{RhP}$ = 175).

^{11}B NMR (1,2-$C_6H_4F_2$, 160 MHz): δ 27.1 (br, BH_3), -6.0 (s, BAr^F_4).

ESI-MS (1,2-$C_6H_4F_2$, 60 °C) positive ion: *m/z* 736.48 [M^+] (calc. 736.48). The observed isotopic pattern (5 lines) was fully consistent with the molecular formula.

[Rh(H)$_2$(PCy$_3$)$_2$(η^2-H$_3$B·NMe$_3$)][BAr$^F_4$] (3-2-Cy)

Addition of hydrogen (4 atm) to a 1,2-$C_6H_4F_2$ (0.4 mL) solution of [Rh(PCy$_3$)$_2$(η^2-H$_3$B·NMe$_3$)][BAr^F_4] (0.008 g, 0.005 mmol) resulted in a rapid colour change from blue to colourless. *In situ* analysis by NMR spectroscopy revealed the quantitative formation of [Rh(H)$_2$(PCy$_3$)$_2$(η^2-H$_3$B·NMe$_3$)][BAr^F_4].

^{1}H NMR (1,2-$C_6H_4F_2$, 500 MHz): δ 8.34 (s, 8H, BAr^F_4), 7.68 (s, 4H, BAr^F_4), 2.93 (s, 9H, NMe_3), 2.14 – 1.31 (m, 66H, Cy), -0.28 (br, 3H, BH_3), -19.62 (overlapping dt, 2H, $^{1}J_{RhH}$ = 22.1, $^{2}J_{RhP}$ = 15.1, RhH).

^{31}P {^{1}H} NMR (1,2-$C_6H_4F_2$, 202 MHz): δ 53.0 (d, $^{1}J_{RhP}$ = 108).

^{11}B NMR (1,2-$C_6H_4F_2$, 160 MHz): δ 4.7 (br, BH_3), -6.1 (s, BAr^F_4).

ESI-MS (1,2-$C_6H_4F_2$, 60 °C) positive ion: *m/z* 736.48 [M^+ - H_2] (calc. 736.48). The observed isotopic pattern (5 lines) was fully consistent with the molecular formula.

[Rh(PCy$_3$)$_2$(η^2-H$_3$B·NMe$_2$H)][BAr$^F_4$] (3-3-Cy)

$H_3B{\cdot}NMe_2H$ (0.021M in 1,2-$C_6H_4F_2$, 0.4 mL, 8.6 x 10^{-3} mmol) was added to [Rh(PCy$_3$)$_2$Cl]$_2$ (6.0 mg, 4.3 x 10^{-3} mmol) and Na[BAr^F_4] (7.6 mg, 8.6 x 10^{-3} mmol).

Immediate *in situ* characterisation by NMR spectroscopy showed a mixture of products; $[Rh(H)_2(PCy_3)_2(\eta^2\text{-}H_3B{\cdot}NMe_2H)][BAr^F{}_4]$, $[Rh(H)_2(PCy_3)_2(\eta^2\text{-}H_2B{=}NMe_2)][BAr^F{}_4]$, an unknown species {δ ^{31}P 47.8 ($^1J_{RhP}$ = 118)} and a species postulated to be $[Rh(PCy_3)_2(\eta^2\text{-}H_3B{\cdot}NMe_2H)][BAr^F{}_4]$.

^{1}H NMR (1,2-$C_6H_4F_2$, 500 MHz): δ 8.32 (s, 8H, $BAr^F{}_4$), 7.67 (s, 4H, $BAr^F{}_4$), 4.63 (br, 1H, $NMe_2\underline{H}$), 2.92 (d, 6H, J = 5.6, $N\underline{Me}_2H$), 2.19 – 1.30 (m, 66H, Cy), -2.85 (br, 3H, BH_3).

^{31}P {^{1}H} NMR (1,2-$C_6H_4F_2$, 202 MHz): δ 61.8 (d, $^1J_{RhP}$ = 178).

^{11}B NMR (1,2-$C_6H_4F_2$, 160 MHz): δ 23.3 (br, BH_3), -6.1 (s, $BAr^F{}_4$).

$[Rh(H)_2(PCy_3)_2(\eta^2\text{-}H_3B{\cdot}NMe_2H)][BAr^F{}_4]$ (3-4-Cy)

Addition of $H_3B{\cdot}NMe_2H$ (0.021M in 1,2-$C_6H_4F_2$, 0.4 mL, 8.6 x 10^{-3} mmol) to $\{Rh(H)_2(PCy_3)_2\}^+$ [formed *in situ* by placing a 1,2-$C_6H_4F_2$ (0.1 mL) solution of $[Rh(PCy_3)_2Cl]_2$ (6.0 mg, 4.3 x 10^{-3} mmol) and $Na[BAr^F{}_4]$ (7.6 mg, 8.6 x 10^{-3} mmol) under 4 atm of H_2, and subsequent degassing] gave $[Rh(H)_2(PCy_3)_2(\eta^2\text{-}H_3B{\cdot}NMe_2H)][BAr^F{}_4]$ as a pale yellow solution, which was characterised *in situ* by NMR spectroscopy and ESI-MS.

^{1}H NMR (1,2-$C_6H_4F_2$, 500 MHz): δ 8.33 (s, 8H, $BAr^F{}_4$), 7.68 (s, 4H, $BAr^F{}_4$), 3.81 (br, 1H, $NMe_2\underline{H}$), 2.89 (d, 6H, J = 5.4, $N\underline{Me}_2H$), 2.11 – 1.28 (m, 66H, Cy), -0.80 (br, 3H, BH_3), -18.03 (overlapping dt, 2H, J = 20.8 and 13.8, RhH_2).

^{31}P {^{1}H} NMR (1,2-$C_6H_4F_2$, 202 MHz): δ 55.9 (d, $^1J_{RhP}$ = 110).

^{11}B NMR (1,2-$C_6H_4F_2$, 160 MHz): δ 2.7 (br, BH_3), -6.1 (s, $BAr^F{}_4$).

ESI-MS (1,2-$C_6H_4F_2$, 60 °C) positive ion: *m/z* 724.47 [M^+] (calc. 724.48). The observed isotopic pattern (5 lines) was fully consistent with the molecular formula.

[Rh(PCy$_3$)$_2$(η^2-H$_3$B·NMe$_2$BH$_2$·NMe$_2$H)][BAr$^F_4$] (3-6-Cy)

Addition of H$_3$B·NMe$_2$BH$_2$·NMe$_2$H (0.021M in 1,2-C$_6$H$_4$F$_2$, 0.4 mL, 8.6 x 10^{-3} mmol) to [Rh(PCy$_3$)$_2$Cl]$_2$ (6.0 mg, 4.3 x 10^{-3} mmol) and Na[BAr$^F_4$] (7.6 mg, 8.6 x 10^{-3} mmol) resulted in the formation of the deep purple complex [Rh(PCy$_3$)$_2$(η^2-H$_3$B·NMe$_2$BH$_2$·NMe$_2$H)][BAr$^F_4$] which was characterised *in situ* by NMR spectroscopy and ESI-MS.

^{1}H NMR (1,2-C$_6$H$_4$F$_2$, 500 MHz): δ 8.32 (s, 8H, BAr$^F_4$), 7.67 (s, 4H, BAr$^F_4$), 4.31 (br, 1H, NMe$_2$<u>H</u>), 2.73 (d, 6H, J = 5.5, N<u>Me</u>$_2$H), 2.69 (s, 6H, NMe$_2$), 2.19 – 1.30 (m, 66H, Cy), -3.05 (br, 3H, BH$_3$). Remaining BH$_2$ signal could not be assigned, presumably obscured by aliphatic peaks.

^{31}P {^{1}H} NMR (1,2-C$_6$H$_4$F$_2$, 202 MHz): δ 61.4 (d, $^1J_{RhP}$ = 178).

^{11}B NMR (1,2-C$_6$H$_4$F$_2$, 160 MHz): δ 28.1 (br, 1B, BH$_3$), 2.4 (br, 1B, BH$_2$), -6.1 (s, BAr$^F_4$).

ESI-MS (1,2-C$_6$H$_4$F$_2$, 60 °C) positive ion: *m/z* 779.54 [M$^+$] (calc. 779.54). The observed isotopic pattern (6 lines) was fully consistent with the molecular formula.

[Rh(H)$_2$(PCy$_3$)$_2$(η^2-H$_3$B·NMe$_2$BH$_2$·NMe$_2$H)][BAr$^F_4$] (3-7-Cy)

Addition of H$_3$B·NMe$_2$BH$_2$·NMe$_2$H (0.021M in 1,2-C$_6$H$_4$F$_2$, 0.4 mL, 8.6 x 10^{-3} mmol) to {Rh(H)$_2$(PCy$_3$)$_2$}$^+$ (8.6 x 10^{-3} mmol) gave [Rh(H)$_2$(PCy$_3$)$_2$(η^2-H$_3$B·NMe$_2$BH$_2$·NMe$_2$H)][BAr$^F_4$] as a pale yellow solution, which was characterised *in situ* by NMR spectroscopy and ESI-MS.

^{1}H NMR (1,2-C$_6$H$_4$F$_2$, 500 MHz): δ 8.33 (s, 8H, BAr$^F_4$), 7.68 (s, 4H, BAr$^F_4$), 4.26 (br, 1H, NMe$_2$<u>H</u>), 2.80 (d, 6H, J = 6.2, N<u>Me</u>$_2$H), 2.64 (s, 6H, NMe$_2$), 2.14 – 1.30 (m, 66H, Cy), -0.54 (br, 3H, BH$_3$), -19.46 (overlapping dt, 2H, J = 19.4 and 16.0, RhH$_2$). Remaining BH$_2$ signal could not be assigned, presumably obscured by aliphatic peaks.

^{31}P {^{1}H} NMR (1,2-C$_6$H$_4$F$_2$, 202 MHz): δ 53.3 (d, $^1J_{RhP}$ = 111).

^{11}B NMR (1,2-$C_6H_4F_2$, 160 MHz): δ 2.9 (br, 2B, BH_2 and BH_3), -6.1 (s, BAr^F_4).

ESI-MS (1,2-$C_6H_4F_2$, 60 °C) positive ion: *m/z* 781.55 [M^+] (calc. 781.55). The observed isotopic pattern (6 lines) was fully consistent with the molecular formula.

[Rh(PCy$_3$)$_2${η^2-(H$_2$BNMe$_2$)$_2$}][BAr$^F_4$] (3-8-Cy)

Addition of $[H_2BNMe_2]_2$ (0.021M in 1,2-$C_6H_4F_2$, 0.4 mL, 8.6 x 10^{-3} mmol) to $[Rh(PCy_3)_2Cl]_2$ (6.0 mg, 4.3 x 10^{-3} mmol) and Na[BAr^F_4] (7.6 mg, 8.6 x 10^{-3} mmol) resulted in the formation of a deep purple complex [Rh(PCy$_3$)$_2${η^2-(H$_2$BNMe$_2$)$_2$}][BAr^F_4] which was characterised *in situ* by NMR spectroscopy.

^{1}H NMR (1,2-$C_6H_4F_2$, 500 MHz): δ 8.33 (s, 8H, BAr^F_4), 7.69 (s, 4H, BAr^F_4), 2.88 (v br, 2H, BH_2), 2.74 (s, 12H, NMe_2), 2.30 – 1.40 (m, 66H, Cy), -6.33 (br, 2H, Rh-H_2B).

^{31}P {^{1}H} NMR (1,2-$C_6H_4F_2$, 202 MHz): δ 55.2 (d, $^1J_{RhP}$ = 177).

^{11}B NMR (1,2-$C_6H_4F_2$, 160 MHz): δ 33.3 (t, J = 90, Rh-H_2B), 5.4 (v br, BH_2), -6.1 (s, BAr^F_4).

ESI-MS could not be obtained, presumably due to the sensitivity of the complex.

[(PCy$_3$)$_2$(H)$_2$Rh(μ-Cl)Rh(H)$_2$(PCy$_3$)$_2$][BAr$^F_4$] (4-1)

C_6H_5F (1 mL) was added to a Young's flask containing $Rh(H)_2(PCy_3)_2Cl$ (0.030 g, 0.043 mmol) and Na[BAr^F_4] (0.038 g, 0.043 mmol). The mixture was filtered in to a crystallisation tube containing $Rh(H)_2(PCy_3)_2Cl$ (0.030 g, 0.043 mmol) yielding a dark yellow solution. The solution was layered with pentane and held at 2 °C for several days yielding the product as yellow crystals. Yield: 0.063 g (66%). Crystals suitable for crystallographic characterisation were grown from a concentrated C_6H_5F solution at room temperature.

^{1}H NMR (CD_2Cl_2, 500 MHz): δ 7.73 (s, 8H, BAr^F_4), 7.57 (s, 4H, BAr^F_4), 2.10 – 1.24 (m, 132H, Cy), -24.18 (br, 4H, RhH).

^{31}P {^{1}H} NMR (CD_2Cl_2, 202 MHz): δ 49.6 (br).

^{1}H NMR (CD_2Cl_2, 500 MHz, 200 K): δ 7.73 (s, 8H, BAr^F_4), 7.57 (s, 4H, BAr^F_4), 2.00 – 1.08 (m, 132H, Cy), -22.42 (br, ~0.4H, RhH, $\{Rh(H)_2(PCy_3)_2L_n\}^+$), -23.44 (br, ~0.4H, RhH, $Rh(H)_2(PCy_3)_2Cl$), -25.20 (br, 3.2H, RhH, **4-1**).

^{31}P {^{1}H} NMR (CD_2Cl_2, 202 MHz, 200 K): δ 49.7 (d, $^1J_{RhP}$ = 115, ~10%, $Rh(H)_2(PCy_3)_2Cl$), 47.5 (d, $^1J_{RhP}$ = 114, ~10%, $\{Rh(H)_2(PCy_3)_2L_n\}^+$), 46.1 (d, $^1J_{RhP}$ = 113, ~80%, **4-1**).

Anal. Calcd for $C_{104}H_{148}BClF_{24}P_4Rh_2$ (2230.2196 g mol^{-1}): C, 56.01; H, 6.69. Found: C, 56.12; H, 6.75.

ESI-MS (1.2-$C_6H_4F_2$, 60 °C) positive ion: *m/z* 1365.83 [M^+, minor] (calc. 1365.74), 665.38 [M^+ - $Rh(H)_2(PCy_3)_2Cl$, major] (calc. 665.38). The observed isotopic patterns (7 lines and 3 lines) were fully consistent with the molecular formulae.

$Rh(H)_2(PCy_3)_2(\eta^2\text{-}BH_4)$ (4-3)

Although a known compound[19], $Rh(H)_2(PCy_3)_2(\eta^2\text{-}BH_4)$ was synthesised *via* an alternative method to that reported in the literature. Degassed ethanol (5 mL) was added to a Schlenk containing $Rh(H)_2(PCy_3)_2Cl$ (0.050 g, 0.071 mmol) and $Na[BH_4]$ (0.013g, 0.357 mmol). The mixture was sonnicated for 3 hours before filtration. The cream solid was washed with ethanol (2 x 5 mL) and dried *in vacuo*. Yield 64%. NMR data was as reported in the literature.

$Rh(H)Cl(PCy_3)_2\{B(H)N^iPr_2\}$ (4-4)

A solution of $H_2B{=}N^iPr_2$ (0.030 g, 0.08 mmol) in C_6H_5F (2 mL) was added to a Young's flask containing $[Rh(PCy_3)_2Cl]_2$ (0.030 g, 0.021 mmol). The mixture was stirred for 2 minutes during which a colour change from purple to pale yellow was observed. The solvent was removed and the resulting pale yellow solid was washed with pentane (3 x 5 mL). The compound was dried yielding a cream solid. Yield: 0.022 g (63%). Attempts to grow crystalline material suitable for crystallographic characterisation resulted in the onward reaction to $Rh(H)_2(PCy_3)_2Cl$.

^{1}H NMR (C_6H_5F, 500 MHz): δ 8.32 (br, 1H, BH), 4.31 (br, 1H, ^{i}Pr CH), 3.23 (sept, $^3J_{HH}$ = 6.9, 1H, ^{i}Pr CH), 2.44 – 1.24 (m, 66H, Cy), 1.36 (d, 6H, $^3J_{HH}$ = 6.9, ^{i}Pr CH_3), 1.15 (d, 6H, $^3J_{HH}$ = 6.9, ^{i}Pr CH_3), -16.22 (overlapping dt, 1H, $^1J_{RhH}$ = 28.4, $^2J_{PH}$ = 15.1, RhH).

^{1}H {^{31}P} NMR (C_6H_5F, 500 MHz, selected data): δ -16.22 (d, 1H, $^1J_{RhH}$ = 28.4, RhH).

^{31}P {^{1}H} NMR (C_6H_5F, 202 MHz): δ 39.8 (d, $^1J_{RhP}$ = 128).

^{11}B NMR (C_6H_5F, 160 MHz): δ 50.3 (br, Rh-B).

Anal. Calcd for $C_{42}H_{82}BClNP_2Rh$ (812.2242 g mol^{-1}): C, 62.11; H, 10.18; N, 1.72. Found: C, 61.92; H, 9.99; N, 1.84.

5.3 Catalysis

5.3.1 Hydroboration

5.3.1.1 General method for TMAB

1,2-$C_6H_4F_2$ (435 μL) and TBE (15 μL, 0.117 mmol) were added to a high pressure NMR tube containing $[Rh(P^tBu^iBu_2)_2][BAr^F{}_4]$ (0.0080 g, 0.006 mmol) and $H_3B{\cdot}NMe_3$ (0.0085 g, 0.117 mmol). The sample was mixed twice and then immediately followed

by ^{11}B NMR spectroscopy. Kinetic plots gave the initial rate over the first 1900 seconds. Errors were calculated assuming a 10% error in the ^{11}B integrations.

Oxidation of $Me_3N{\cdot}H_2B(CH_2CH_2CMe_3)$

The catalytic mixture was transferred to a round bottomed flask and THF (2 mL), EtOH (2 mL), NaOH (2M, 2 mL) and H_2O_2 (35 % aq. solution, 3 mL) were added. The solution was stirred at 40 °C for 16 hours to ensure complete oxidation. The reaction mixture was extracted with Et_2O (3 x 20 mL), and the organic phase washed with a 2M aq. NaOH solution (20 mL), H_2O (20 mL) and finally brine (20 mL). The organic layer was dried over $MgSO_4$, filtered and concentrated to yield $HOCH_2CH_2CMe_3$ as the only product (^1H NMR spectroscopy).

5.3.2 Dehydrocoupling

5.3.2.1 General method, open system

To a 3-necked Schlenk flask, connected to an external oil bubbler and charged with a magnetic stirrer bar and the catalytic precursor, was added a solution of $H_3B{\cdot}NMe_2H$ (0.072 M, 5.0 mL, 0.36 mmol) in 1,2-$C_6H_4F_2$. Catalysis was monitored by analyzing regular aliquots of the reaction solution (0.1 mL; quenched with 0.25 mL MeCN or diluted with 0.25 mL 1,2-$C_6H_4F_2$ under argon) by ^{11}B NMR spectroscopy.

5.3.2.2 General method, sealed system (cationic)

To a high pressure NMR tube containing the catalyst precursor was added a solution of $H_3B{\cdot}NMe_2H$ in 1,2-$C_6H_4F_2$ (0.072 M, 0.4 mL, 28.8 x 10^{-3} mmol). The reaction was followed *in situ* by ^{11}B NMR spectroscopy.

5.3.2.3 General method, sealed system (neutral)

To a high pressure NMR tube was added a solution of the catalyst precursor in 1,2-$C_6H_4F_2$ (100 μL). To this was added a solution of $H_3B{\cdot}NMe_2H$ in 1,2-$C_6H_4F_2$ (300 μL, 0.096 M, 28.8 x 10^{-3} mmol). The reaction was followed *in situ* by ^{11}B NMR spectroscopy.

5.4 Kinetic Simulations (Chapter 3)

5.4.1 General comments

In the discussion below, we present only our final model (Figure 5.1) that evolved from exploration of an extensive series of mechanistically diverse models. In this, and all models explored, numerous simplifications were made: many of the rate constants represent telescoped steps, some to termolecularity, and many have notional irreversibility. The model is intended *solely* to provide a *qualitative fit of temporal concentration data in support of the global mechanistic picture for the dehydrocoupling reaction, including autocatalysis and parallel catalysis*. The model and its associated rate constants (k_1 to k_6) should not be interpreted in isolation or indeed in any quantitative manner.

5.4.2 Procedure

For each of the five data sets (**I**, **II**, **III**, **IV** and **V**) shown below, temporal concentration data was explored using the model shown in Figure 5.1. Starting with approximate values for k_1, derived from linear regressions of $\ln([\mathbf{A}]_0/[\mathbf{A}]_t)$ versus t, preliminary fits were derived for datasets **I-III** by visual inspection of the output of computer-based simulations,[20-22] with repeated manual modulation of rate constants k_2 to k_6. There

was no inclusion of a depletion in [Rh(III)/Rh(I)] caused by generation of neutral "Rh(III)Cl" for parallel catalysis of **A** → **Z**, and k_1 is set up as a pseudo first order decay to represent the sum of both processes (k_1 = {(n (k_{RhCl} -k_{Rh+})) + (k_{Rh+}[Rh(III)]$_0$)}), where n = [Cl]$_0$. In the range of [Rh]$_0$ that was explored (0.036-0.075 M), near-identical fits are obtained using k' [Rh]$_0$ in place of k_1, where k' = (0.206-(20.23 × [Rh]$_0$)), indicative that turnover in the model is predominantly by Rh(III)Cl. With a preliminary fit in hand, dataset **I** was optimized by up to 1000 cycles of automated iteration. Using this as a start point, and locking rate constants k_{-3} and k_5 to give some stability between fits for individual datasets, rate constants k_1, k_2, k_3, k_4, k_{-4} and k_6 in each of the remaining datasets (**II**-**V**) were optimized as untethered variables, each through up to 1000 cycles of automated iteration. It soon became evident that the feedback loops in the interlinked cycles make the model sensitive to small changes in some of the rate constants and catalyst concentrations, and a unique fit for the entire dataset (**I**-**V**) would not be found. This is not surprising given the simplifications made in the model, the presence of unknown concentrations of activator and the possibility for secondary intermolecular NH and BH interactions causing changes in reactivity and rates. As emphasized above, *the model is intended solely to provide a qualitative fit of temporal concentration data in support of a global mechanistic picture for a complex catalytic process*. Nonetheless, within a moderate range of rate constants (Figure 5.1) a good *qualitative* fit of the datasets can be made. The key outcome is that the model can satisfactorily account for the complex curvature in the temporal evolution of both **B** and **C**.

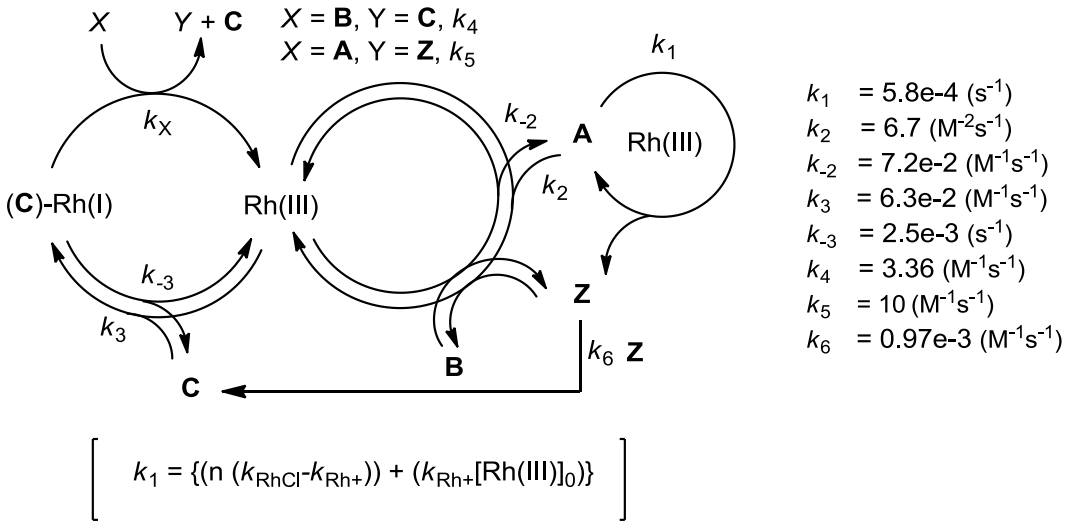


Figure 5.1 Model for the kinetics of dehydrocoupling of **A** to **C** *via* **B** and **Z**; rate constants shown are the average values used for sets **I**-**V**; the set-specific values and their standard deviation are shown below.

Table 5.1 Rate constants and their standard deviation in models employed to simulate datasets **I**-**V**.

	I	**II**	**III**	**IV**	**V**	Average	SD
k_1 / s^{-1}	5.1×10^{-4}	5.7×10^{-4}	4.2×10^{-4}	6.2×10^{-4}	7.9×10^{-4}	5.8×10^{-4}	1.4×10^{-4}
k_2 / $M^{-2}\,s^{-1}$	5.8	5.2	6.1	8.9	7.6	6.7	1.5
k_{-2} / $M^{-1}\,s^{-1}$	7.4×10^{-2}	6.2×10^{-2}	7.4×10^{-2}	8.8×10^{-2}	6.1×10^{-2}	7.2×10^{-2}	1.1×10^{-2}
k_3 / $M^{-1}\,s^{-1}$	11.8×10^{-2}	5.5×10^{-2}	3.5×10^{-2}	7.2×10^{-2}	3.5×10^{-2}	6.3×10^{-2}	3.4×10^{-2}
k_{-3} / s^{-1}	2.5×10^{-3}	2.5×10^{-3}	2.5×10^{-3}	2.5×10^{-3}	2.5×10^{-3}	2.5×10^{-3}	0
k_4 / $M^{-1}\,s^{-1}$	3.53	1.43	1.93	8.33	1.60	3.36	2.90
k_5 / $M^{-1}\,s^{-1}$	10	10	10	10	10	10	0
k_6 / $M^{-1}\,s^{-1}$	5.3×10^{-3}	6.8×10^{-3}	6.4×10^{-3}	2.5×10^{-3}	4.8×10^{-3}	0.97×10^{-3}	0.9×10^{-3}

Table 5.2 Starting conditions for models employed to simulate datasets **I**-**V**.

	I	**II**	**III**	**IV**	**V**
$[\mathbf{A}]_0$ / M	0.072	0.120	0.150	0.000	0.072
$[\mathbf{B}]_0$ / M	0.000	0.000	0.000	0.036	0.000
$[\mathbf{C}]_0$ / M	0.000	0.000	0.000	0.000	0.04
$[Rh(III)]_0$ / M	0.0036	0.006	0.0075	0.0036	0.0036
$[Rh(I)]_0$ / M	0.000	0.000	0.000	0.000	0.000

5.5 Computational (Chapter 2)

DFT calculations were run with Gaussian 09 and employed the BP86 functional. Ir and P were described with SDD pseudopotentials and the associated basis sets, with added polarisation functions on P (ζ = 0.387). 6-31g** basis sets were used for all other atoms.

5.6 References

1. A. B. Pangborn, M. A. Giardello, R. H. Grubbs, R. K. Rosen and F. J. Timmers, *Organometallics*, 1996, **15**, 1518-1520.
2. A. T. Lubben, J. S. McIndoe and A. S. Weller, *Organometallics*, 2008, **27**, 3303-3306.
3. J. Cosier and A. M. Glazer, *J. Appl. Crystallogr.*, 1986, **19**, 105-107.
4. L. J. Farrugia, *J. Appl. Crystallogr.*, 1997, **30**, 565.
5. C. A. Jaska, K. Temple, A. J. Lough and I. Manners, *J. Am. Chem. Soc.*, 2003, **125**, 9424-9434.
6. M. E. Sloan, A. Staubitz, T. J. Clark, C. A. Russell, G. C. Lloyd-Jones and I. Manners, *J. Am. Chem. Soc.*, 2010, **132**, 3831-3841.
7. W. E. Buschmann and J. S. Miller, *Inorg. Synth.*, 2002, **33**, 83-91.
8. A. B. Chaplin and A. S. Weller, *Eur. J. Inorg. Chem.*, 2010, 5124-5128.
9. A. B. Chaplin, A. I. Poblador-Bahamonde, H. A. Sparkes, J. A. K. Howard, S. A. Macgregor and A. S. Weller, *Chem. Commun.*, 2009, 244-246.
10. H. Werner, J. Wolf and A. Hohn, *J. Organomet. Chem.*, 1985, **287**, 395-407.
11. K. Wang, M. E. Goldman, T. J. Emge and A. S. Goldman, *J. Organomet. Chem.*, 1996, **518**, 55-68.
12. P. Binger, J. Haas, G. Glaser, R. Goddard and C. Kruger, *Chem. Ber.*, 1994, **127**, 1927-1929.
13. A. Vanderent and A. L. Onderdelinden, *Inorg. Synth.*, 1990, **28**, 90-92.
14. E. W. Abel, M. A. Bennett and G. Wilkinson, *J. Chem. Soc.*, 1959, 3178-3182.
15. M. J. Ingleson, S. K. Brayshaw, M. F. Mahon, G. D. Ruggiero and A. S. Weller, *Inorg. Chem.*, 2005, **44**, 3162-3171.
16. G. Alcaraz, A. B. Chaplin, C. J. Stevens, E. Clot, L. Vendier, A. S. Weller and S. Sabo-Etienne, *Organometallics*, 2010, **29**, 5591-5595.
17. C. J. Stevens, R. Dallanegra, A. B. Chaplin, A. S. Weller, S. A. Macgregor, B. Ward, D. McKay, G. Alcaraz and S. Sabo-Etienne, *Chem. Eur. J.*, 2011, **17**, 3011-3020.
18. L. Euzenat, D. Horhant, Y. Ribourdouille, C. Duriez, G. Alcaraz and M. Vaultier, *Chem. Commun.*, 2003, 2280-2281.
19. H. L. M. Vangaal, J. M. J. Verlaak and T. Posno, *Inorg. Chim. Acta*, 1977, **23**, 43-51.
20. F. J. Weigert, *Comput. Chem.*, 1987, **11**, 273-280.
21. R. N. Stabler and J. P. Chesick, *Int. J. Chem. Kinet.*, 1978, **10**, 461-469.
22. R. J. McKinney and F. J. Weigert, *Quantum Chemistry, Program Exchange, program No. QCMP022.*, Simulations were conducted using commercially available software (MacKinetics, Leipold Associates, USA) on an Apple Mac Power PC under OS9.

6 Appendices

6.1 Crystallographic data

Table 6.1 Crystallographic data for **2-3**, **2-4** and **3-1-^{c}Pr**.

	2-3	**2-4**	**3-1-^{c}Pr**
CCDC number	776219	776220	-
Formula	$C_{56}H_{68}BF_{24}P_2Rh$	$C_{56}H_{66}BF_{24}P_2Rh$	$C_{53}H_{54}B_2F_{24}NP_2Rh$
M	1372.76	1370.75	1347.44
Crystal System	Triclinic	Triclinic	Monoclinic
Space group	*P-1*	*P-1*	*P2(1)/c*
T [K]	150(2)	150(2)	150(2)
a [Å]	12.88050(10)	12.9373(2)	19.1226(2)
b [Å]	13.05280(10)	13.0919(2)	16.7830(2)
c [Å]	22.3154(2)	22.2056(3)	19.2658(2)
α [deg]	103.1981(3)	72.9625(7)	90
β [deg]	94.4213(4)	85.6901(6)	108.2608(5)
γ [deg]	118.4125(4)	60.4717(6)	90
V [Å^3]	3136.24(4)	3118.05(8)	5871.68(11)
Z	2	2	4
Density [gcm^{-3}]	1.454	1.460	1.524
μ [mm^{-1}]	0.430	0.432	0.458
θ range [deg]	$5.11 \leq \theta \geq 27.88$	$5.11 \leq \theta \geq 26.37$	$5.10 \leq \theta \geq 26.37$
Refl^{n}s collected	26387	22967	21300
R_{int}	0.0193	0.0252	0.0220
No. of data/restr/ param	14829 / 1704 /1244	12605 / 1802 / 1214	11887 / 841 / 946
R_1 [I > 2σ(I)]	0.0560	0.0722	0.0457
wR_2 [all data]	0.1669	0.2276	0.1177
GoF	1.032	1.042	1.027
Largest diff. pk and hole [eÅ^{-3}]	1.236 and -0.550	0.857 and -0.605	0.843 and -0.505

Table 6.2 Crystallographic data for **4-1**.

	4-1
CCDC number	915250
Formula	$C_{58}H_{73}B_{0.50}Cl_{0.50}F_{13}P_2Rh$
M	1205.14
Crystal System	Monoclinic
Space group	*P* 2/c
T [K]	150(2)
a [Å]	17.1205(2)
b [Å]	16.9183(2)
c [Å]	21.4057(3)
α [deg]	90
β [deg]	109.2920(10)
γ [deg]	90
V [Å^3]	5852.00(13)
Z	4
Density [gcm^{-3}]	1.368
μ [mm^{-1}]	0.447
θ range [deg]	$5.10 \leq \theta \geq 27.45$
Refl^{n}s collected	25647
R_{int}	0.0503
No. of data/restr/ param	13278 / 198 / 734
R_1 [I > 2σ(I)]	0.0468
wR_2 [all data]	0.1199
GoF	1.021
Largest diff. pk and hole [eÅ^{-3}]	0.814 and -0.872

6.2 Publications

L.J. Sewell, M.A. Huertos, M.E. Dickinson, G.C. Lloyd-Jones, A.S. Weller, Dehydrocoupling of Dimethylamine Borane Catalysed by $Rh(H)_2(PCy_3)_2Cl$, *Inorganic Chemistry*, 2013, DOI: 10.1021/ic302804d.

L.J. Sewell, G.C. Lloyd-Jones, A.S. Weller, Development of a Generic Mechanism for the Dehydrocoupling of Amine-Boranes: A Stoichiometric, Catalytic, and Kinetic Study of $H_3B{\cdot}NMe_2H$ using the $[Rh(PCy_3)_2]^+$ Fragment, *Journal of the American Chemical Society*, 2012, **134**, 3598-3610.

H.C. Johnson, A.P.M. Robertson, A.B. Chaplin, L.J. Sewell, A.L. Thompson, M.F. Haddow, I. Manners, A.S. Weller, Catching the First Oligomerization Event in the Catalytic Formation of Polyaminoboranes: $H_3B{\cdot}NMeHBH_2{\cdot}NMeH_2$ Bound to Iridium, *Journal of the American Chemical Society*, 2011, **133**, 11076-11079.

L.J. Sewell, A.B. Chaplin, A.S. Weller, Hydroboration of an alkene by amine-boranes catalysed by a $[Rh(PR_3)_2]^+$ fragment. Mechanistic insight and tandem hydroboration/dehydrogenation, *Dalton Transactions*, 2011, **40**, 7499-7501.

L.J. Sewell, A.B. Chaplin, J.A.B. Abdalla, A.S. Weller, Reversible C-H activation of a $P^tBu^iBu_2$ ligand to revealed a masked 12 electron $[Rh(PR_3)_2]^+$ cation, *Dalton Transactions*, 2010, **39**, 7437-7439.